



# **EXAMINATION OF THE SPATIAL RESOLUTION AND DISCRIMINATION CAPABILITY OF VARIOUS ACOUSTIC SEAFLOOR CLASSIFICATION TECHNIQUES BASED ON MBES BACKSCATTER DATA**

## **Dissertation**

zur Erlangung des Doktorgrades (Dr. rer. nat.)  
an der Mathematisch-Naturwissenschaftlichen Fakultät  
der Christian-Albrechts-Universität zu Kiel

vorgelegt von

**Evangelos Alevizos (M.Res.)**

Kiel, October 2017

Erster Gutachter: Prof. Dr. Jens Greinert, (GEOMAR Helmholtz Centre for Ocean Research, Kiel)

Zweiter Gutachter: Dr. Mirjam Snellen ( TU Delft)

Tag der mündlichen Prüfung: 17 November 2017

## Erklärung

Hiermit erkläre ich, dass ich die vorliegende Doktorarbeit selbständig und ohne unerlaubte Hilfe erstellt habe. Weder diese noch eine ähnliche Arbeit wurde an einer anderen Abteilung oder Hochschule im Rahmen eines Prüfungsverfahrens vorgelegt, veröffentlicht oder zur Veröffentlichung vorgelegt. Ferner versichere ich, dass die Arbeit unter Einhaltung der Regeln guter wissenschaftlicher Praxis der Deutschen Forschungsgemeinschaft entstanden ist.

Kiel, den 05.10.2017

Evangelos Alevizos

**TABLE OF CONTENTS**

<b>Abbreviations</b>	<b>4</b>
<b>Zusammenfassung</b>	<b>6</b>
<b>Abstract</b>	<b>7</b>
<b>1. INTRODUCTION</b>	<b>8</b>
1.1 Rationale for the study	8
1.2 Research questions	13
1.3 Case studies overview	14
<b>2. RESEARCH BACKGROUND - ACOUSTIC REMOTE SENSING OF THE SEAFLOOR</b>	<b>16</b>
2.1 MBES principles and state-of-the-art	16
2.2 Principles of seafloor acoustic backscatter	21
2.2.1 Ensonified area on the seafloor	22
2.2.2 Seafloor surface scattering	23
2.2.3 Sediment volume scattering	25
2.2.4 Angular dependence of seafloor backscatter	25
2.2.5 Frequency dependence of seafloor backscatter	27
2.2.6 Backscatter data corrections	28
2.3 Acoustic Seafloor Classification approaches	29
2.3.1 The importance of angular dependence	29
2.3.2 Geophysical and empirical ARA models	30
2.3.3 Backscatter classification based on image analysis	34
2.4 Ground-truth sampling and analysis	40
<b>3. ACOUSTIC DISCRIMINATION OF RELATIVELY HOMOGENEOUS FINE SEDIMENTS USING BAYESIAN CLASSIFICATION ON MBES DATA</b>	<b>43</b>
3.1 Introduction	45
3.2 Methodology	48
3.3 Results	50
3.4 Discussion	54



---

3.5 Conclusions	61
<b>4. MULTI-ANGLE BACKSCATTER CLASSIFICATION AND SUB-BOTTOM PROFILING FOR IMPROVED SEAFLOOR CHARACTERIZATION</b>	<b>62</b>
4.1 Introduction	64
4.2 Methodology	65
4.3 Results	71
4.4 Discussion	78
4.5 Conclusions	81
<b>5. QUANTIFICATION OF THE FINE-SCALE DISTRIBUTION OF MN-NODULES: INSIGHTS FROM AUV MULTI-BEAM AND OPTICAL IMAGERY DATA FUSION</b>	<b>83</b>
5.1 Introduction	85
5.2 Methodology	88
5.3 Results	94
5.4 Discussion	98
5.5 Conclusions	103
<b>6. THE HYPER-ANGULAR CUBE CONCEPT FOR IMPROVING THE SPATIAL AND ACOUSTIC RESOLUTION OF MBES BACKSCATTER ANGULAR RESPONSE ANALYSIS</b>	<b>105</b>
6.1 Introduction	107
6.2 Methodology	108
6.3 Results	113
6.4 Discussion	117
6.5 Conclusions	119

<b>7. CONCLUSIONS</b>	<b>121</b>
7.1 Acoustic class separation	121
7.1.1 Quantification of class separation – coupling of Bayesian method with ARA	121
7.1.2 The concept of geo-acoustic resolution	123
7.2 Improvements of angular response analysis	124
7.2.1 The hyper-angular cube matrix:spatial resolution, class separation, machine learning	124
<b>REFERENCES</b>	<b>127</b>
<b>APPENDICES</b>	<b>137</b>
<b>APPENDIX OF CHAPTER 3</b>	<b>137</b>
<b>APPENDIX OF CHAPTER 4</b>	<b>138</b>
<b>APPENDIX OF CHAPTER 5</b>	<b>140</b>
<b>APPENDIX OF CHAPTER 6</b>	<b>142</b>

## Abbreviations

AC	Acoustic class
ASC	Acoustic seafloor classification
ANOVA	Analysis of variance
ARA	Angular response analysis
APL	Applied physics laboratory
ANN	Artificial neural network
AUV	Autonomous underwater vehicle
BS	Backscattering strength
BORIS-SSA	Bottom Reverberation from Inhomogeneities and Surfaces-Small-Slope Approximation
CCD	Calcium compensation depth
CH	Calinski & Harabazsr
CTD	Conductivity temperature depth
DISCOL	Disturbance and Recolonization
GSAB	Generic seafloor acoustic backscatter
GIS	Geographical information system
GPS	Global positioning system
GLCM	Grey-Level Co-occurrence Matrices
HAC	Hyper-angular cube
IMS	Inertial motion sensor
ISA	International seabed authority
iHAC	Interpolated Hyper-Angular Cube
ISODATA	Iterative self-organizing data analysis
JPIO	Joint Programming Initiative Healthy and Productive Seas and Oceans
LAT	Latitude
LED	Light-emitting diode
LBL	Long baseline
LON	Longitude
MCK	Map comparison kit
MGET	Marine geospatial ecology toolbox
MLC	Maximum likelihood classification
MBES	Multi-beam echo-sounder
OBIA	Object-based image analysis
OFOS	Ocean floor observation system
OOB	Out-of-Bag Error
PCA	Principal components analysis
PDF	Probability density function
RF	Random forest
ROV	Remotely operated vehicle
SSS	Side-scan sonar
SCI	Site of Community Importance
SBP	Sub-bottom profiling
SAD	Sum of Absolute Differences
SVM	Support vector machine
USBL	Ultra-short baseline

## Acknowledgements

This work has been supported technically and intellectually by several persons who I would like to deeply thank. First of all, I would like to thank my promotor Prof Jens Greinert and my co-supervisor Dr. Mirjam Snellen for arranging and providing everything needed for my research work. Particularly, Prof Jens Greinert provided access to the datasets used in this thesis, assisted in allocation of resources (including hardware and ship-time) and assisted in establishing a fruitful collaboration with researchers from TU Delft. Additionally, Prof Jens Greinert supported my doctoral training by providing funding for participation in international conferences and the SMART summer School (2014, Ireland). Prof Jens Greinert offered me the opportunity to teach GIS modules to his Master's students, fact that increased my teaching experience.

An important part of my doctoral training included participation in seminars and workshops provided by the Integrated School of Ocean Science (ISOS, CAU Kiel). Dr Mirjam Snellen and Prof Dick G. Simons provided access to their in-house software and assisted in having a productive time during my visits at their group (ANCE group, TU Delft, the Netherlands). Regarding my collaboration with the ANCE group I would like to thank Jeroen Janmaat and Dr Kerstin Siemes for their valuable discussions and software support throughout my visits at their group.

In addition, I would like to thank all the captains and crew of RV Littorina and RV Polarfuchs for their valuable support at field expeditions. Sediment sampling for the needs of the study described in chapter 3 was coordinated by Dr Filip Maysman (NIOZ) and supported by Eduard Fabrizio (GEOMAR). Especially, I would like to thank the captain and crew of RV Sonne and the AUV team of GEOMAR for pre-processing of the AUV hydro-acoustic data used in chapter 5. In addition the AUV team of GEOMAR provided significant support that assisted me in analyzing the AUV hydro-acoustic data used in chapter 5. Continuing, I am particularly thankful to Prof Armin Freund for providing access and assistance with the laser particle analyzer from his department at GEOMAR. He provided me with valuable information about the use of the instrument and how to present the measurement data. Bettina Domeyer and Anke Bleyer from GEOMAR offered to me drills on laboratory use and access to their laboratory and consumables for performing sediment grain size analyses.

I would like to especially thank Dr Markus Diesing (NGU) for his support in collaborating with CEFAS (UK). This collaboration took place during January 2016 where I participated the research team of Dr Markus Diesing for working on OBIA applications. Dr Markus Diesing arranged my stay in the UK and provided valuable insights on image analysis during our collaboration.

Anne Peukert and Dr Inken Preuss from the DeepSea Monitoring group (GEOMAR) supported me in proof-reading and reviewing my manuscripts prior to submission. Their support is particularly recognized and appreciated. Dr Inken Preuss as well as Anne Volsch and Christine Utecht assisted me greatly with administrative tasks within GEOMAR that made my studies smoother, thus I am very thankful to them.

Finally, I would like to express my gratitude to the DeepSea Monitoring group (GEOMAR) for their generous support all the time of my PhD studies. Last but not least, a big "thanks" to my family and friends for supporting my efforts in their own, special way!

## Zusammenfassung

Die vorliegende Dissertation beschäftigt sich mit zwei Hauptthemen der akustischen Meeresbodenklassifizierungstechniken. Im Fokus des ersten Teils steht die Separierung von akustischen Klassen, die die Diskriminierungsfähigkeit der Klassifizierungstechniken und die Qualität ihrer Ergebnisse beeinflusst. Der zweite Teil befasst sich mit der räumlichen Auflösung von akustischen Karten des Meeresbodens, die mit der akustischen Klassenseparierung in wesentlicher Verbindung steht. Die Themenbereiche werden mithilfe eines integrierten Ansatzes untersucht, der a) eine fortgeschrittene unüberwachte Klassifizierungstechnik benutzt und b) deren Auswirkungen auf die "angular response analysis" (ARA) analysiert. Darüber hinaus wird ein neuartiger Ansatz zur Verbesserung der ARA-Technik beschrieben. Durch die Anwendung einer unüberwachten Technik auf der Grundlage der Bayesschen Statistik, die einen internen Cluster-Validierungstest durchführt, wurde eine objektive Klassifizierung der gesamten Rückstreuungsdaten erlangt. Diese Technik nutzt Rückstreuungsmessungen der einzelnen Winkel aus dem zentralen Bereich des Sonar Fächers und bietet dadurch eine bessere Diskriminierung von akustischen Klassen.

Die grössten Vorteile der Bayesschen Technik sind, dass keine Sonarkalibrierung erforderlich ist, sie innerhalb des Fächers Variationen des Meeresbodens unterscheidet und ordinale kategorische Werte für akustische Klassen ausgibt. Letzteres hilft bei der Korrelation von akustischen Klassen mit Daten von Sedimentproben. Die Kapitel dieser Studie basieren auf drei Studien der Bayesschen Technik für die Diskriminierung von: ähnlichen Typen von weichen Sedimenten, unterschiedlichen Sedimenttypen von Schluff bis Kies sowie verschiedenen Dichten von Mn-Knollen (Knollen  $m^{-2}$ ). Die Klassifizierungsergebnisse werden pro Strahl zugewiesen und ermöglichen eine hohe räumliche Auflösung der Meeresboden-Klassen. Insbesondere ein spezieller hydroakustischer Datensatz mit stark überlappenden Fächern in Verbindung mit empirischer ARA unterstützte die Untersuchung der Bayesschen Ergebnisse. Es wurde festgestellt, dass die Bayessche Technik die dominanten Winkelresonanzen aus den gesamten Rückstreuungsdaten objektiv klassifizieren kann. In Anbetracht dessen, dass die ARA-Technik auf den physikalischen Zuständen des Meeresbodens basiert und dass sie durch akustische Klassenhomogenitätsprobleme und fehlende räumliche Auflösung begrenzt ist, schlagen wir einen neuen Ansatz zur Verbesserung dieser Probleme vor. Hierfür wird das Konzept des Hyper-Angular Cube (HAC) angewendet und seine Ergebnisse mit den Bayesschen Klassifizierungsergebnissen verglichen. Der HAC wird durch mehrere Rückstreuungsschichten aufgebaut, die entweder durch die Interpolation von dichten Echomessungen oder durch die Normalisierung der Rückstreu- Mosaik bei unterschiedlichen Einfallswinkeln resultieren können. Die letztgenannte Methode minimiert die Kosten für den Erwerb von dichten hydroakustischen Daten und wurde bisher noch nicht vorgestellt. Die hochdimensionale Datenstruktur des HAC ist geeignet für die überwachte Klassifizierung mit maschinellen Lerntechniken und einer eingeschränkten Menge an Sedimentproben. Der Ansatz betrachtet die Winkelabhängigkeit der Rückstreuung und nutzt hydroakustische- und Probandaten effizienter als es bisher möglich war.

## Abstract

This thesis focuses on two major topics regarding acoustic seafloor classification techniques. The first topic is that of acoustic class separation which affects the discriminative power of classification techniques and the quality of final results. The second topic is the spatial resolution of seafloor acoustic maps that is fundamentally coupled with acoustic class separation. These topics are examined through an integrated approach which, a) employs an advanced unsupervised classification technique and b) analyzes its implications on the angular response analysis (ARA) of acoustic backscatter. Moreover, a novel approach for improving the ARA technique is described. Applying an unsupervised technique (based on Bayesian statistics) that performs an internal cluster validation test, we obtain objective classification of the entire backscatter dataset. This technique utilizes single-angle backscatter measurements from the middle range of the sonar swath offering better discrimination of acoustic classes. The main advantages of the Bayesian technique are that it does not require sonar calibration, it resolves along-swath seafloor variations and that it outputs ordinal categorical values for acoustic classes. The latter advantage assists in correlating acoustic classes with ground truth information. The Bayesian technique was applied in three studies for discriminating: similar types of soft sediments, a wide range of sediment types from silt to gravel and various densities of Mn-nodules (nodules  $m^{-2}$ ) respectively. The classification results are assigned per beam providing high spatial resolution of the seafloor classes. In particular, a special hydro-acoustic dataset with high swath overlap assisted the examination of Bayesian results in conjunction with empirical ARA. It was found that the Bayesian technique can objectively classify the dominant angular responses from the entire backscatter dataset. Considering that the ARA technique, is based on the physical properties of the seafloor and that it is limited by acoustic class homogeneity issues and lack of spatial resolution, we suggest a new approach for improving these issues. Therefore, the concept of the Hyper-Angular Cube (HAC) is applied and its results are compared with the Bayesian classification results. The HAC is built by several angular backscatter layers which can result either by interpolation of dense soundings or by normalization of backscatter mosaics at different incidence angles. The latter method minimizes the cost of acquiring dense hydro-acoustic data and has not been presented formerly. The high dimensional data of the HAC is suitable for supervised classification using machine learning techniques and restricted amount of ground truth information. This approach takes angular dependence of backscatter into consideration and utilizes hydro-acoustic and ground truth data in a more efficient way than it was possible until now.

## 1. INTRODUCTION

### 1.1 Rationale for the study

In recent decades the world ocean-floor faces significantly increased anthropogenic pressure related to climate/ocean change, coastal population/infrastructure growth and considerable demand for marine resources (fish, minerals). As a consequence, a number of efforts have been initiated in order to better evaluate and monitor marine areas that are affected by these pressures. These efforts primarily use seafloor mapping as a tool helping to interpret, analyze, and predict numerous seafloor-types at different spatial scales and their change over time. The development of multi-beam echo-sounders (MBES) has played a key role in seafloor mapping. The strongly expanding use of MBES technology in recent years has significantly increased the availability of hydro-acoustic data at various spatial scales. The main advantage of MBES systems is that they provide co-registered, motion-compensated bathymetric and backscatter data covering relatively large areas on the seafloor. Bathymetric data are used primarily for precise bathymetric mapping while backscatter data provide important information about the seafloor type. The ever-increasing volume of MBES data has triggered the need for methods towards more efficient and detailed mapping of the seafloor. This occurs because the solution for a variety of research and marine spatial planning and management problems relies on input of geo-information about the seafloor and its associated habitats. Thus there is a fundamental requirement to transform hydro-acoustic data into meaningful seafloor maps that carry useful information at appropriate spatial scale. To achieve this, the scientific field of Acoustic Seafloor Classification (ASC) (Anderson et al., 2008) that incorporates different kinds of methods and approaches has been developed. Essentially the main objective of ASC is to identify discrete parts in the hydro-acoustic data (bathymetry and/or backscatter) that are characterized by individual homogeneity that reflects physical seafloor properties (i.e.: sediment grain size, porosity, etc.). A robust way to perform ASC is through statistical analysis and parallel involvement of the acoustic properties of the seafloor (see ASC methodologies box, section 2.3). Parts of the seafloor with unique acoustic features and properties are then compiled to create seafloor classification maps which can be validated by means of ground-truth data (e.g. physical sampling, visual observations, section 2.4). Seafloor classification maps comprise valuable input information to various marine spatial projects such as for sediment characterization, benthic habitat mapping, seafloor resource exploration and evaluation and even for geochemical studies.

#### **ASC METHODOLOGIES**

*There are several ASC approaches available in literature which can be generally divided in three categories according to the following criteria:*

*a) The type of hydro-acoustic data that they are applied to: meaning that MBES data can be processed either as acoustic signal by utilizing seafloor acoustic parameters and theoretical models (signal processing) or as processed gridded data such as bathymetric surfaces and backscatter mosaics which can be processed using image analysis techniques.*

b) The type of processing outcomes, which could be i) categorical variables representing seafloor types (qualitative, semi-quantitative results) or ii) continuous variables representing seafloor properties or quantitative sedimentary features such as grain size, percentage of gravel etc,

c) The employment of ground-truth information in the classification process. Classification methods that require a priori input of ground-truth information for determining the number of classes are called supervised methods while methods that only use ground-truth data for validation of results are called unsupervised. In this regard if there is a substantial amount of ground-truth data then supervised classification can be applied whereas in case of lack or limited ground-truth data an unsupervised approach should be preferred instead. As with any remote sensing technique, a minimum amount of ground-truth information is required for validating the classification results regardless the method used to process the data. This is because remotely sensed data provide only indirect information about the seafloor; since they do not represent actual seafloor samples.

A) Processing style	B) Results type	C) Ground-truth data input
signal processing (angular responses)	quantitative (continuous)	Supervised (a priori)
image processing (grids)	qualitative (categorical)	Unsupervised (not required)

Using the categories mentioned above, one can efficiently describe the nature of any ASC method. In literature a number of ASC methods have been widely studied and some of them became established as standard approaches in some cases. The ASC approaches that have been studied in this thesis include:

- **Angular Response Analysis (ARA)**. This is a signal-based approach that provides semi-quantitative and quantitative information about the seafloor. It has been established by experimental and in-situ hydro-acoustic studies on various sediment types. These studies yielded a number of acoustic parameters which determine the absolute acoustic backscatter values of sediments for certain frequencies and incidence angles of ensonification. Geophysical models of seafloor backscatter (section 2.3.2) make use of these acoustic parameters for predicting the angular responses of certain seafloor types and vice-versa. ARA inversion uses measured MBES backscatter values for adjusting the appropriate model parameters and thus predicting seafloor sediments. ARA is part of the Geocoder software that runs in some commercial MBES processing suites (FMGT, Caris HIPS). Apart from model-based ARA there is also the empirically-derived ARA. In this case the relative backscatter intensity values (Chapter 4) are extracted from each incidence angle and compared with ground truth information.

- **Unsupervised classification combining Principal Components Analysis (PCA) and k-means clustering**.

PCA has been extensively applied in several classification studies in literature. The main advantage of PCA is that it can combine information from a high dimension feature space and output less features (the principal components) that possess more descriptive properties. The principal components can then be clustered using a k-means approach and produce a representation of seafloor classes. However the number of clusters needs to be



defined by the user. In this respect, many unsupervised methods require some sort of cluster validation test in order to identify the optimum number of clusters in which the dataset can be divided into. PCA can be applied either on tables or grids and it can include numerous MBES bathymetric and/or backscatter features (variables). As for example, Huang et al. (2013) applied PCA on tables with backscatter angular response features (e.g.: slope, minimum, maximum) and produced principal components for each incident angle. Another example of PCA application is the QTC Multiview software that is based on Preston 2009 implementation. Preston 2009 developed a PCA approach for classifying MBES backscatter data using a large number of backscatter gridded features (1<sup>st</sup> order statistics, textural analysis statistics) along with bathymetric gridded data.

- **Unsupervised classification using Bayesian probability.** This method has been in the core of this thesis being applied in diverse MBES datasets and compared to other ASC approaches. It is a relatively new method implemented by Simons and Snellen (2009). The method is based on the central limit theorem interpreted for MBES backscatter data. According to this theorem, the backscatter values resulted from the beam footprint of a particular incidence angle should follow normal distribution for a specific seafloor type (section 2.3.3). The Bayesian method has some important advantages over more commonly used unsupervised methods. First it assigns acoustic classes to each beam and so it resolves across-track seafloor type changes on a footprint scale. One of the most important features of the Bayesian method is that it calculates statistically the optimum number of classes, thus offering more objective results.

- **Supervised methods (traditional and machine learning algorithms).** In contrast to unsupervised methods the supervised ones require pre-definition of the seafloor classes. Therefore, ground-truth data of adequate quality and quantity should be employed in this kind of classification approach. One of the most commonly-used supervised methods is the Maximum Likelihood Classification (MLC). It has been applied in satellite image classification and also in studies using MBES data. The MLC method requires that hydro-acoustic data values of a particular seafloor type have a normal distribution. In practice this is not always valid hence this assumption can be a drawback of the method. In addition MLC becomes problematic with high dimensional data (i.e.: large number of MBES grids). In contrast, recent developments of machine learning algorithms provide supervised classification in a more robust way, meaning that they do not require normal distributions of the data and they can identify non-linear relationships between the MBES features and seafloor types (Chapter 6). Moreover, machine learning algorithms can deal with high dimension data and relatively small amount of ground-truth information.

An important feature that affects the usefulness of ASC maps is spatial resolution. A seafloor classification map should be at a scale comparable with that of ground-truth samples/the natural heterogeneity in order to provide useful geo-information to the end-users (Reid 2007; Anderson et al., 2008; McGonigle et al., 2009). Reid (2007) incorporated the beam footprint (i.e.: the ensonified area on the seafloor, section 2.2.1) in the notion of seafloor habitat scales, implying that seafloor features greater than the beam footprint can be mapped and thus classified by means of ASC (Greene et al., 1999). Regarding seafloor mapping in shallow water or at low altitude from the seafloor (10-1000 m range between sonar and seafloor) the beam footprint diameter ranges on average from 0.4 to 1.4m in 10

m depth (incidence angles from 0° to 60°) to 3.5 to 14m in 100 m depth. These beam footprint sizes are comparable to the scale of ground-truth observations and support the assumption that the seafloor type is mostly homogeneous within these footprints. Consequently it is inferred that effective ASC should be carried out on a per beam footprint basis so that seafloor maps represent natural seafloor variability and can be correctly compared with ground-truth data.

ASC maps with high spatial resolution can be used for example, in support of quantitative resource evaluation of certain minerals on the seafloor (i.e.: Mn-nodules, sulfides etc). Margolis & Burns (1976) were among the first to discover that Mn-nodule densities, sizes and shapes vary significantly over distances of few tens of meters. However they note that Mn-nodule spatial variability could not be resolved by the acoustic means that were available at the time of their study. Mn-nodules not only represent a potential resource for exploitation but also they serve as an important hard substrate habitat for deep-sea sessile fauna (Vanreussel et al., 2016; Purser et al., 2016). Thus they can be used as habitat surrogate for particular species and ASC maps of Mn-nodules with sufficient spatial resolution can support better fauna abundance estimates and spatial heterogeneities of nodule-related species over wider areas.

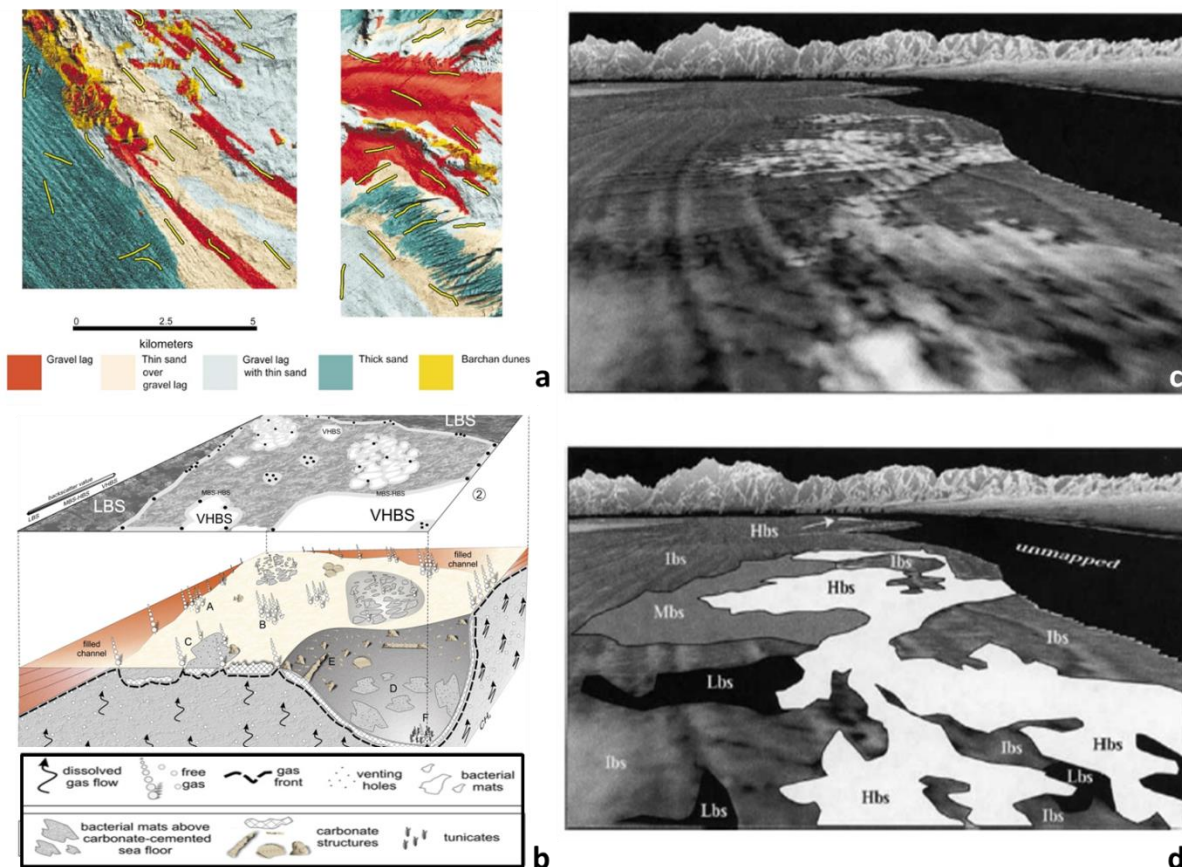


**Figure 1.1:** A) Fine scale acoustic classification map of scallop habitats (from Kostylev et al., 2003) B) Seafloor areas with very high (VHBS) and low backscatter values (LBS) indicating geological features related to methane seeps (from Naudts et al., 2008) C) & D) Seafloor areas with, low (Lbs), medium (Mbs) and high (Hbs) backscatter values representing various geomorphological features (Gardner et al., 2003).

Another important parameter of ASC methods is class separation. Class separation refers to the degree at which hydro-acoustic data exhibit unique properties so that an ASC method can distinguish one seafloor type from another. The significance of identifying acoustically homogeneous areas on the seafloor has been highlighted by Hughes-Clarke (1994), Parnum (2007) and Fonseca et al. (2009). However, due to method restrictions, results from traditional ASC methods (Fonseca and Mayer, 2007; Che-Hasan et al., 2014) cannot resolve the across-track seafloor changes as they do not hold sufficient spatial resolution (section 2.3.1). To overcome these drawbacks, alternative ways have been investigated for improving acoustic class separation (Fonseca et al., 2009). Another approach is the concept of angle-cube which was originally developed by Parnum (2007) and is further utilized in this study (chapters 4, 6).

Since seafloor sediments or substrate types are often being used as surrogates for various benthic habitats (Greene et al., 1999) the need for ASC with improved spatial resolution and sediment discrimination capability is even more important. An important example of MBES backscatter mapping is the study of Kostylev et al. (2003) which focuses on acoustic mapping of sediments related to the commercial species of scallop *Placopecten magellanicus*. Their study concludes, that precise seafloor classification maps that are able to capture fine scale sediment variability, can assist sustainable scallop fishing activity and improve fishery and dredging management (Fig.1.1 A). Another study that highlights the significance of high resolution hydro-acoustic data in habitat mapping is that of Summers-Morris et al. (2004) where they combined bathymetric analysis with underwater video data for delineating hard substrates, serving as rock-fish habitats in inshore waters. Gardner et al. (2003) studied the geomorphology of Santa Monica bay considering high resolution MBES backscatter data. Accordingly, they linked physiographic features (of tectonic, sea-level and sedimentary origin) with generic categories (high/low) of acoustic backscatter values (Fig.1.1 C&D). Their study is a useful example regarding the role of backscatter data in interdisciplinary mapping approaches. Moreover, Naudts et al. (2008) utilized MBES backscatter data for mapping fine-scale geological features related to methane seeps (e.g.: methane-derived authigenic carbonate structures) (Fig.1.1 B). Similarly, Greinert et al. (2010) utilized MBES backscatter measurements for establishing a relation between these and the number of methane seeps which then was applied for extrapolation (of the number of seeps) in a wider area. The last two studies demonstrate the value of MBES backscatter data, through the diversity of scientific problems which they can apply to.

Ideally, an ASC should be able to differentiate the minimum seafloor heterogeneity which exists at a scale comparable to that of the sonar footprint. Considering that the sonar footprint at shallow waters (<<100 m water depth) is at a scale of a few square meters, the ability of ASC methods to acoustically resolve similar seafloor types becomes a challenging task. This thesis focuses on ASC strategies that provide sufficient class differentiation and produce results with spatial resolution comparable to that of the sonar footprint for relatively short ranges (10-100 m) between the sonar and the seafloor. For improving class separation and spatial resolution in ASC, we examine two different strategies of analyzing acoustic backscatter from MBES data: one that is based on a particular methodology which can be applied on any kind of sonar data and one that is based on a particular data structure which can be analyzed with advanced ASC methodologies.

### Method-based strategy

Initially a novel ASC method based on Bayesian probability is applied on various MBES datasets covering different seafloor types and it is compared to other ASC approaches (PCA with k-means clustering, empirical Angular Response Analysis, machine learning algorithms). This method analyzes the backscatter variability within selected beams (of certain incidence angles) and assigns classes to each beam footprint according to Bayesian probability criteria. By applying the Bayesian approach on different MBES datasets collected from diverse study areas (section 1.3) we aim at evaluating the performance of the method in producing high resolution ASC results showing sufficiently separated acoustic classes that correspond to ground-truth information.

### Data-structure strategy

Alternatively, improved spatial resolution and class separation can be achieved by constructing and analyzing a particular data matrix. Multiple backscatter layers can be produced for each beam incidence angle (chapter 6) and stacking of all layers produces the so-called Hyper-Angular Cube (HAC) matrix which is similar to the angle-cube model developed by Parnum (2007). The main advantage of this approach is that each cell of the cube holds substantial acoustic information which can be exploited by traditional ASC methods (i.e. ARA) for providing acoustically meaningful, high resolution classification results. Such a data matrix has not been reported widely in the literature, although it has been pointed out that it is a crucial tool for improving class separation in ASC (Rzhanhov et al., 2012; Che-Hasan et al., 2014; Huang et al., 2013).

## 1.2 Research questions

This thesis was primarily driven by the following scientific questions about improving spatial resolution and class separation in ASC using MBES backscatter data.

- *What is the minimum difference between sediment types that can be discerned by ASC methods?*

To answer this question we employed the Bayesian method and compared its performance with other methods that are commonly applied for ASC (PCA with k-means clustering, empirical Angular Response Analysis, machine learning algorithms). For better constraining the application towards the scientific question, we applied the Bayesian method to MBES data from an area with high seafloor sediment homogeneity and an area with broad range of sediment types (section 1.3). In this way, the Bayesian method was tested for producing useful ASC results that sufficiently distinguish a variety of sediment types.

- *How can acoustic class separation be quantified?*

This question led to the comparison of Bayesian method results with angular response information extracted from the HAC. The cells of the HAC include information at high spatial

resolution about the angular dependence of backscatter values. Angular dependence is a fundamental acoustic property of the seafloor and it forms an essential component of many ASC methods (section 2.3.1). The HAC information in conjunction with Bayesian results provide a useful framework for evaluating class separation and how the Bayesian method contributes in separating dominant angular responses representing major seafloor types. In addition we examine the suitability of the HAC as a specific data structure for producing adequate ASC results using novel ASC methods (pattern recognition and machine learning algorithms) and utilizing a small amount of ground-truth data as a priori information.

- *Is the Bayesian method suitable for ASC of hard substrates such as Mn-nodules fields?*  
Mapping of Mn-nodule fields comprises an active field of research with important implications in resource evaluation, deep sea benthic habitat mapping and deep sea mining impact assessment. Therefore in this study we compare the Bayesian method with predictive mapping (random forests) using sufficient quantitative ground-truth data for acoustic class validation. High resolution AUV MBES data provide an excellent opportunity to map the Mn-nodule coverage at the scale of the sonar footprint.

### 1.3 Case studies overview

This thesis was based on analysis of high resolution (meters scale) hydro-acoustic data-sets from MBES surveys in three different study areas. Each study area comprises a unique seafloor environment with all of them covering a wide range of seafloor variability. The diversity of seafloor types incorporated in the study, assisted in evaluating the scientific questions set in the previous paragraph.

#### - Grevelingen

The Grevelingen study area (chapter 3) is a dammed estuary in the Netherlands, formerly exposed to the North Sea. The seafloor of the Grevelingen is covered by sediments ranging from silt and clay to medium sand with shell fragments. The main bathymetric features of the area include relict tidal bed-forms (sand ripples), as well as steep channel slopes and rugged terrain created during sediment dredging in recent years. Underwater video data provide evidence for localized epi-benthic cover with various densities of pebbles. MBES data from this area are suitable to test the ability of the Bayesian method to discriminate very similar sediment types. The study based on this data compares the Bayesian method with PCA and k-means classification and validates their results with grain size analysis information.

#### - Eckernförde Bay

The seafloor of the Eckernförde Bay study area shows a smooth bathymetry with various sediment types (chapters 4, 5). The seafloor sediments range from (anoxic) silt and clay to gravel and pebbles. Areas covered by fine sand were found to be colonized by diverse benthic epi-fauna and infauna. In addition a large part of the bay has been surveyed with more than 100% swath overlap resulting in high density ensonification of the seafloor.

This allowed the calculation of several backscatter layers building up the Hyper-Angular Cube. Backscatter angular response information from each cell of the HAC assisted in identifying homogeneous acoustic areas that contain ground-truth information. Angular responses were then combined with Bayesian method results for quantifying acoustic class separation. Furthermore, the HAC data were used in unsupervised and supervised ASC algorithms. The performance of ASC algorithms was evaluated using sediment grain size information and the Bayesian classification results for comparison.

- **DISCOL**

Hydro-acoustic data from the DISCOL area (chapter 5) assist in mapping of Mn-nodules and testing the Bayesian method in classifying a hard seafloor substrate. The seafloor in the study area generally shows a smooth bathymetry and is almost entirely covered by Mn-nodules. According to AUV optical data the coverage of nodules varies significantly over short distances (10s-100s meters), forming sparse and dense patterns. Therefore, nodule variability that is captured by hydro-acoustic data allows testing the Bayesian and predictive mapping methods in quantifying this hard substratum that serves as important potential mineral resource and as a fragile deep sea ecosystem.

## 2. RESEARCH BACKGROUND - ACOUSTIC REMOTE SENSING OF THE SEAFLOOR

### 2.1 MBES principles and state-of-the-art

Analogous to airborne and space-borne radars which are based on electromagnetic signals, active sonars transmit acoustic pulses underwater and record their response travel-time (bathymetry) and intensity (backscatter). In this way, collection of underwater 3D imaging data is possible, having particular implications in seafloor mapping studies. Apart from valuable information about the range (which is transformed to depth measurement) sonars provide also intensity records, which are influenced by the physical properties of the seafloor in a complex way. Modern seafloor mapping pays particular attention to acoustic intensity (recorded by multi-beam echo-sounders (MBES) as a robust mean for characterizing the seafloor (Brown and Blondel, 2009). In literature, these MBES records are referred as acoustic backscatter, or backscattering strength (BS, for absolute values).

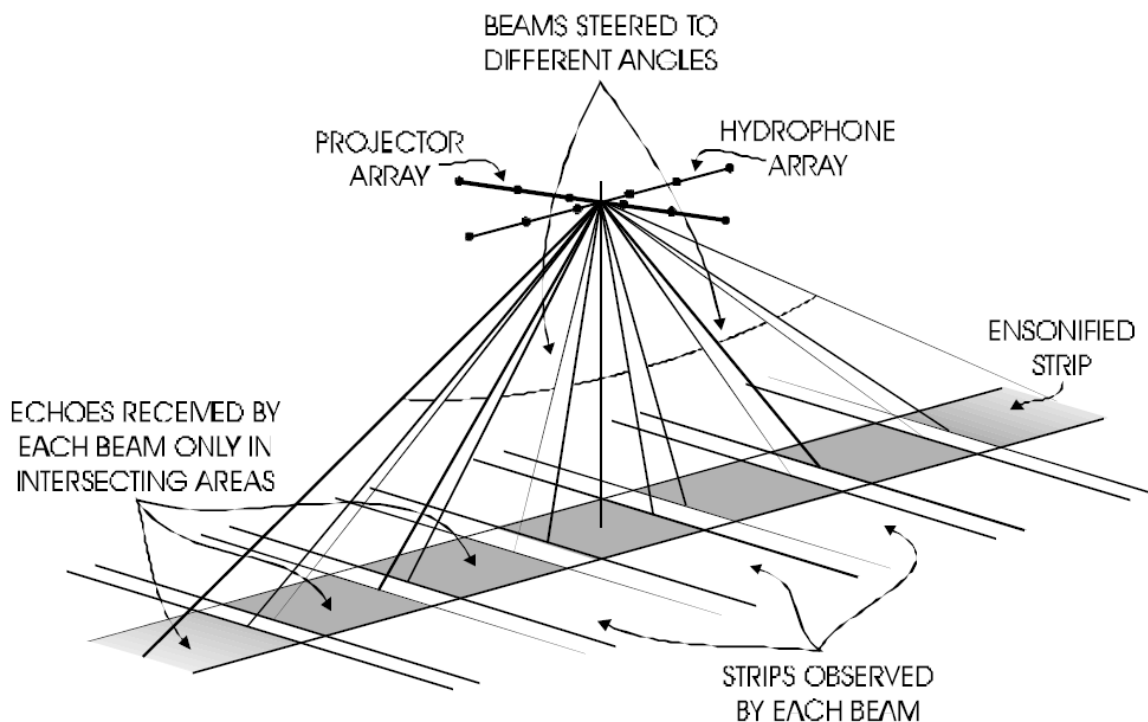


**Figure 2.1:** Diagram showing the geometry of a MBES sonar transmission. Each ensonified strip (grey rectangles) accounts for a portion of seafloor area that is defined as beam-footprint. (source: <http://www3.mbari.org/products/mbsystem/sonarfunction/SeaBeamMultibeamTheoryOperation.pdf>)

The acoustic signal is projected through a *beam-forming* process from the *transmitter* onto the seafloor (Lurton, 2002). Beam forming is a technique for projecting several acoustic signals (beams) so they are steered on specific azimuthal directions (de Moustier, 1988). The acoustic signal is characterized by a *swath* of acoustic beams which exhibit fan-shape geometry (Fig.2.1). Consequently, each projected beam ensonifies an area on the seafloor at



a certain *incidence angle*. The area encompassed by each beam is called the *beam footprint*. The beam footprint is proportional to the *pulse length* (duration), the *across and along track opening* of each beam, the incidence angle and the distance from the sonar to the seafloor (Fig.2.2) (Lurton, 2010). The beam footprint is quantifiable not only as area but also as the time at which, the acoustic pulse with particular duration interacts with the seafloor (Parnum, 2007; Simons and Snellen, 2009). The temporal dimension of the footprint is exploited by some sonar types in order to record individual backscatter values from within each footprint (*time-series*, snippets, section 2.2.1) instead of providing only an average value of the backscatter for each beam (Innanghi et al., 2015). It is implied that beams having a greater footprint size would carry more backscatter measurements. After interaction with the seafloor the acoustic signal is reflected backwards in some or any direction (depending on the seafloor roughness, section 2.2.2), and the *receiver* (hydrophone) captures the intensity of the signal at each receiving beam angle (Urick, 1983). The sonar system software then, amplifies and processes the recorded backscatter data which is co-registered with each depth measurement resulted from each beam (Lamarche et al., 2011). Measurements of depth and backscatter from each beam are also termed *soundings*. A single, full-swath transmission is called *ping* and usually involves more than one hundred beams with incidence angles from 0 to maximum 80 degrees, resulting in equal number of soundings (as the number of beams). Typically, most MBES systems trigger multiple pings per second, providing increased along track coverage which is also affected by the survey speed of the vessel (de Moustier, 1988; Lurton and Lamarche, 2015). Regarding the across track coverage, it depends on the degree of overlap between adjacent survey tracks and the maximum angle of the swath (de Moustier, 1988). Sounding coverage (or density) is a crucial factor in MBES mapping once it influences the spatial resolution of the final maps and also it affects the applicability and performance of ARA method (Hughes-Clarke et al., 1994; Huang et al., 2013). MBES surveys with high overlap provide increased sounding coverage at increased survey time and cost. However the resulting data density allows for improved backscatter analyses with unprecedented accuracy (Chapters 4, 6, Alevizos, 2017).

The ensonification area directly underneath the sonar transmitter is called the *nadir* and the beams steered at this direction have normal incidence angle (i.e.: perpendicular to the seafloor). This area has particular interest regarding the backscatter behavior and is going to be analyzed further in the next paragraphs. Beams away from nadir are called *oblique* whereas beams at the boundaries of swath are called outer beams (section 2.2.4).

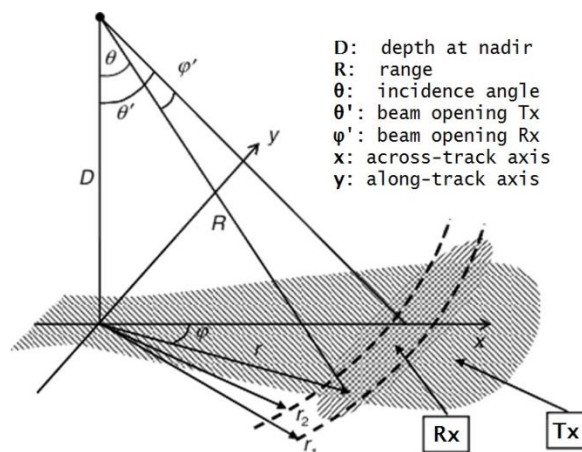


**Figure 2.2:** Intersection of beam opening in the along-track (receiver beam: Rx) and the across-track (transmitter beam Tx) directions forming the beam footprint (ellipse) on the seafloor (modified from Parnum and Gavrilov 2011).



Functionality of MBES systems depends upon a number of appropriate parameters, so they are able to provide accurate measurements of depth and backscatter values. Accurate depth and backscatter values are required as input data to any ASC method for valid classification results. Several MBES parameters need to be adjusted prior to MBES data acquisition and during post-processing. For collection of MBES data of adequate quality the sonar system has to be provided with external information regarding the following parameters:

- ***Accurate above- and under-water positioning***

Spatial accuracy is of great importance in MBES mapping and its level is dictated by the specific objectives of the project. Ship-based MBES surveys rely on GPS antennas in conjunction with motion information (explained below) for accurate positioning and georeferencing of sounding measurements (Mayer, 1999; Blondel, 2009). Autonomous Underwater Vehicle (AUV), Remotely Operated Vehicle (ROV) or other underwater platforms rely on acoustic Ultra-Short Base-Line (USBL) or Long Base-Line (LBL) systems for accurate underwater positioning (Blondel, 2009). USBL systems consist of pairs of acoustic transponders between the underwater platform and the surface vessel that provide relative distance and direction of the underwater platform with reference to the vessel. This information is then combined with GPS data in order to obtain underwater navigation and MBES data georeferencing. LBL systems are used for underwater navigation of AUVs and they are fixed transponders, placed on the seafloor. LBL systems transmit acoustic signals that are received by the AUV which uses them to triangulate its position and to georeference the MBES data using USBL communication with the surface vessel.

- ***Inertial motion compensation***

Vessels and underwater platforms are dynamic even when they are not moving, meaning that their position is susceptible to motion induced by the constantly changing conditions of water masses. Vessel motion introduces artifacts in the MBES data records which need to be compensated for (Blondel, 2009). Inertial motion sensors (IMS) measure the motion of vessel or underwater platforms in three dimensions. The main motion components being measured by an IMS system are: roll, pitch, yaw and heave (Fig.2.3). Motion information is then combined with GPS data allowing the MBES system to perform real-time motion compensation of the hydro-acoustic data (Hughes–Clarke et al., 1997). Because in practice the MBES system and the motion sensor/-s cannot be perfectly aligned there are a number of tests required prior to MBES data acquisition so that the MBES applies the correct motion parameters. Application of these parameters is based on matching of timestamps between the IMS and the MBES sonar, thus accurate time between these is crucial for achieving good quality hydro-acoustic data (Blondel, 2009). The tests required prior to MBES data acquisition, are called the “patch test” and they assist in measuring the fine-scale misalignments (of angles) relative to the IMS and the MBES system. The patch test consists of:

- a) A *roll test*: this is to identify the difference in angle between the MBES and the IMS that introduces bias in the motion about the y-axis. To perform this test the vessel should run 2 lines in opposite directions with half swath overlap over flat seafloor. In an ideal sensor configuration swath data from these lines should perfectly overlap but this is not the case. The dipping angle of flat seafloor should be measured for port and starboard sides and provided to the MBES software as roll bias value.
- b) A *pitch test*: this is to identify the difference in angle between the MBES and the IMS that introduces bias in the motion about the x-axis. To perform this test the vessel should run 2 lines in opposite directions with half swath overlap over seafloor with slope and parallel to the slope. Measurement of the along-swath angle difference of seafloor slope in the two swaths should be provided to the MBES software as pitch bias value.
- c) A *yaw (or heading) test*: this is to identify the difference in angle between the MBES and the IMS that introduces bias in the motion about the z-axis. To perform this test the vessel should run 2 lines in opposite directions with half swath overlap over seafloor with slope, perpendicular to the slope or over flat seafloor with some distinct target (e.g.: shipwreck). Measurement of the across-swath angle difference of the target or seafloor slope in the two swaths should be provided to the MBES software as pitch bias value.

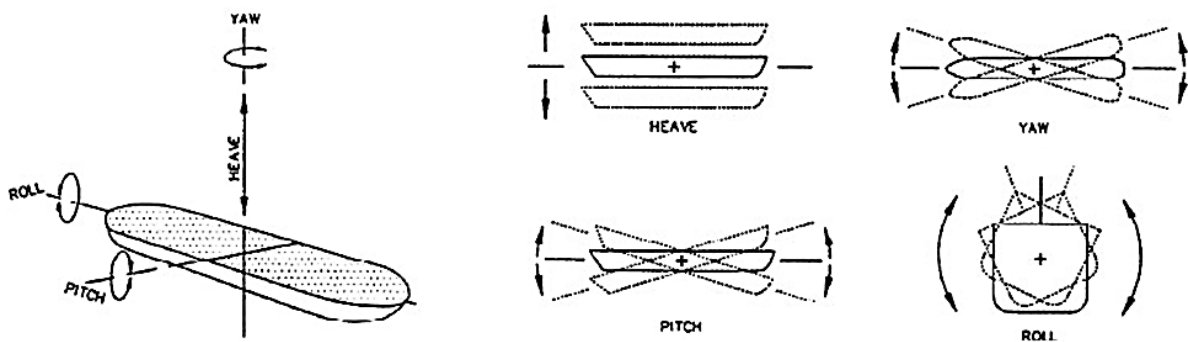


**Figure 2.3:** Sketch illustrating the inertial motion components of a vessel (modified from: <http://coastalhydraulicslaboratoryfact.tpub.com/chetn-ix-1/chetn-ix-10004im.jpg>).

- **Static offsets and time differences between the sensors**

The survey components (antennas, sensors) are not all placed at the same point, therefore the MBES accuracy depends on the so called static offsets between these components. The relative position of the MBES sensor to the GPS antennas and the IMS sensor has to be measured and inserted in the MBES software prior to data acquisition so MBES data receive position and motion information that is spatially corrected (Lurton and Lamarche, 2015). In addition to the spatial offsets, time differences between the survey components must be taken into account. Time differences can cause the so called “latency errors” which are related to erroneous application of motion bias compensation on the data.

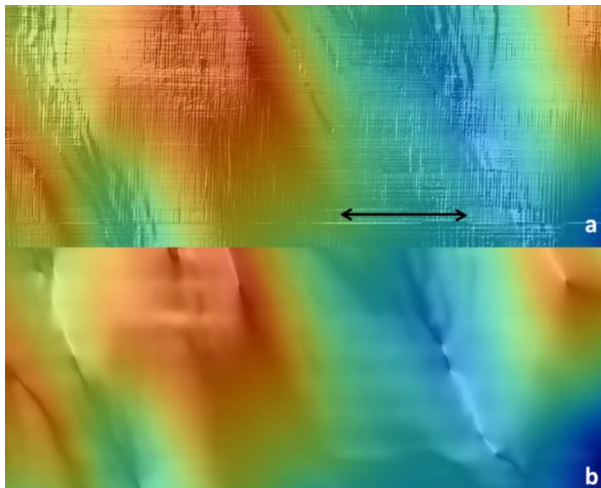


**Figure 2.4:** a) AUV bathymetry grid (3 m x 3 m cell size) with motion (roll bias) artefacts due to varying time difference between the IMS and the MBES sonar (latency error). Black arrows indicate the along-track direction. b) Filtered AUV bathymetry grid (3 m x 3 m cell size) using a Gaussian filter for images.

This occurs because time is the parameter that interconnects the components of a MBES system and even a small time delay can have a great impact on data quality (Fig.2.4 a). Such an effect was encountered in AUV bathymetry data in chapter 5 where it was not possible to account for a varying time difference and a Gaussian filter for images was applied instead (Fig.2.4 b). Time-related offsets can be measured via a latency test. The vessel needs to run two overlapping lines in the same direction over a target on the seafloor at two different speeds (one twice as fast as the other). The target will appear in different positions if a latency error exists. The time difference can be given by the following formula when the apparent distance of the target on the seafloor is measured:

$$t = D / (V_{\text{fast}} - V_{\text{slow}}) \quad [2.1]$$

where:  $t$  = time delay in seconds,  $D$  = apparent along-track displacement of target between the two lines in meters,  $V$  = the vessel speed for fast and slow lines respectively (in meters/second).

#### - **Sound velocity data**

Propagation of sound under water is affected by the physical properties of the water column and primarily by water density. Layers of water masses with different densities cause refraction of the acoustic signal in the same way that different transparent materials refract light (Fig.2.5). As a result, varying sound velocities can produce artifacts in the hydro-acoustic data in the sense that refracted signals are received in wrong positions and that faster/slower sound velocities may be incorrectly converted to shallower/deeper depth measurements. Lurton et al. (1994) derived a sound speed profile from measured water column properties for correcting the MBES depth measurements. This method is currently an essential part in every MBES survey.

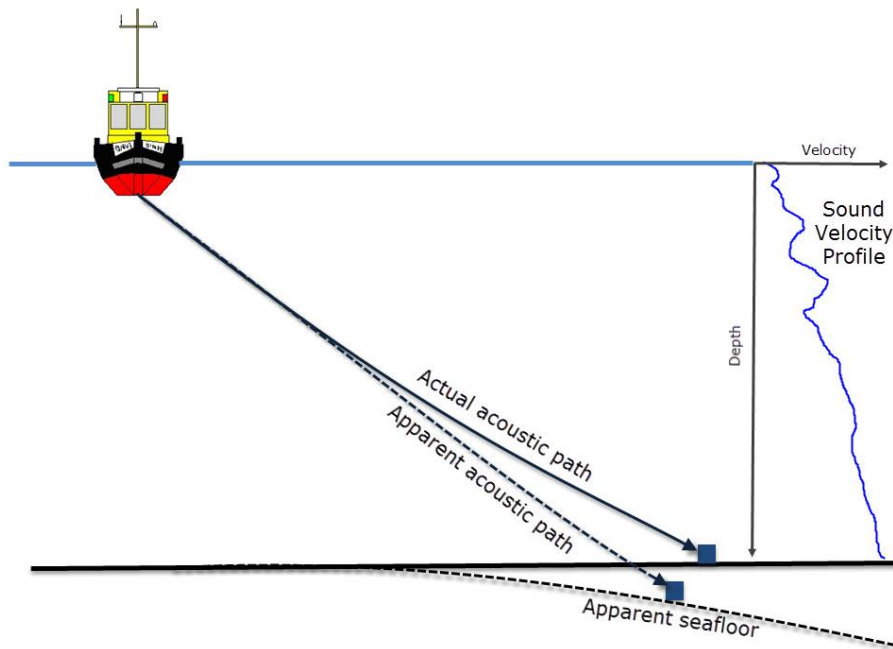


**Figure 2.5:** Diagram representing the effect of water column sound properties on the hydro-acoustic signal. (source: <https://confluence.qps.nl>).

### - Vertical motion

Tidal information with reference to a vertical datum local to the study area should be obtained and applied to the MBES data either prior to the survey or in post-processing of the data. Additionally, measurement of the relative draft of the vessel along with draft change (due to bulge, fuel consumption) should be taken into consideration for correcting the vertical motion effects on the MBES bathymetry data.

Once the above parameters are tuned, then the MBES survey can yield reliable hydro-acoustic data without positional or motion artefacts. However other kinds of artifacts might be present on the data (bubbles, fish, turbulence) and post-processing of bathymetry is required in order to obtain clean bathymetric data. Bathymetric data of high quality are needed to improve the quality of backscatter data as well, but the backscatter data require particular post-processing steps in order to be used for ASC. The corrections of backscatter measurements are analyzed in the following section along with the various factors that influence backscatter from the seafloor.

## 2.2 Principles of seafloor acoustic backscatter

The interaction between the incident acoustic signal and the seafloor is a complex, stochastic physical process. Its complexity is due to the fact that a large number of factors affect backscattering of the seafloor. In order to obtain a solid view about the acoustic behaviour of the seafloor in a practical way one should consider the following.

Kinsler et al. (1999) demonstrated that seafloor backscattering is primarily dependent on the difference between the acoustic impedances of the water and the seafloor material, while it is also affected by seafloor surface roughness (relative to signal wavelength), sediment volume heterogeneity and angle of ensonification (Lurton and Lamarche, 2015). It has to be noted that interaction between the acoustic signal and the seafloor surface roughness or sediment volume depends on the frequency of the transmitted signal as well (Jackson et al., 1986). In a simplified example where seafloor surface is considered as flat

and smooth and the incident acoustic pulse is perpendicular to the seafloor surface, backscatter can be estimated simply by the reflection coefficient between the two media; i.e.: water and seafloor cover. The reflection coefficient is derived by the ratio of transmitted to the reflected acoustic pressures which at normal incidence angles is only dependent on the acoustic impedance of the material that covers the seafloor (Eq.2.2). In contrast, at oblique angles of ensonification the reflection coefficient also depends on the incidence angle (Kinsler et al., 1999).

Reflection coefficient for normal incidence angles:

$$V = (Z_2 - Z_1) / (Z_2 + Z_1) = (\rho c_2 - \rho c_1) / (\rho c_2 + \rho c_1) \quad [2.2]$$

where:  $Z$ = acoustic susceptibility of the media,  $\rho$ = bulk density of the media,  $c$ =speed of sound through the media

Natural seafloor not only includes a large variety of sedimentary/benthic cover types but also it occurs in a variety of forms including slopes in any aspect, various scales of surface irregularity and volume inhomogeneity. The following sections describe the effects of seafloor surface and volume characteristics on acoustic backscatter.

### 2.2.1 Ensonified area on the seafloor

The acoustic signal is projected as an array of beams (swath) on the seafloor at various incidence angles, ensonifying a particular area on the seafloor, that is dependent on pulse length (duration) and angle of ensonification (Lurton, 2010). It has been shown that a large seafloor surface is ensonified at incidence angles close to nadir and when long pulses are transmitted, whereas a small seafloor surface is ensonified at incidence angles towards the outer range of the swath and when short pulses are transmitted (Lurton, 2010). The ensonified area can be expressed as a function of time (that is the duration of the pulse length) implying that each ensonified area yields a number of acoustic time series values that depends on the footprint size (Hammerstad, 2000). These backscatter time series values are called snippet data (or snippets, or scatter-pixels) and can either be logged by the MBES separately or they are combined for measuring the mean backscatter from each beam (Fig.2.6).

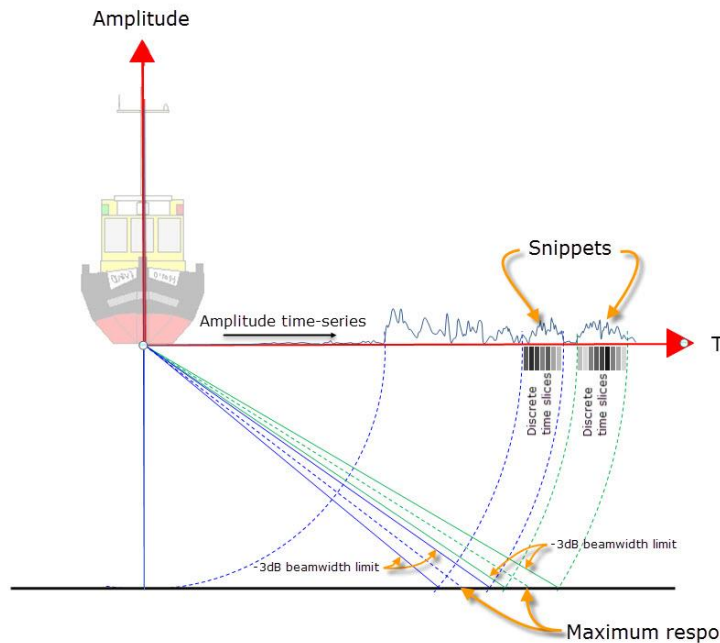


**Figure 2.6:**  
Diagram representing the time-series/snippets of backscatter measurements within a single footprint (ensonified area)  
(source: <https://confluence.qps.n>)

The snippets are involved in the theory of the Bayesian method (chapter 3) where it is suggested that the values of a large number of individual snippet data within a single incidence angle footprint would have a normal distribution when a homogenous seafloor type is considered (Simons and Snellen, 2009).

## 2.2.2 Seafloor surface scattering

When the acoustic pressure wave hits the seafloor, initially it interacts with the seafloor surface. A smooth and flat seafloor surface will reflect the incident acoustic signal opposite but along to the direction of ensonification (Fig.2.7 d) (Jackson and Richardson, 2007). This is called the specular reflection and its backscattering strength depends on the angle of ensonification and the acoustic impedance of the seafloor cover (Urlick, 1983). However, in practice this does not occur in its absolute sense. Seafloor surface is known for having irregular relief hence it reflects acoustic energy in any direction with part of it being reflected directly back to the sonar sensor (Fig.2.7 d). The relief of seafloor surface can be described by different statistical expressions, including the variance of seabed heights, the root mean square residuals of an average fitted seafloor bathymetry (Fig.2.7 b) and power spectra analysis (Ferrini and Flood, 2006; Eleftherakis, 2013; Lurton and Lamarche, 2015).

The seafloor surface can be characterized as smooth or rough when compared to the wavelength of the incident acoustic signal (Table 2.1). Thus, surfaces with seafloor height variations greater than the signal wavelength are considered rough, whereas surfaces with height variations smaller than the signal wavelength are considered smooth (Lurton and Lamarche, 2015). In the case of smooth surfaces, the incident acoustic signal is highly subjective to specular reflection for normal incidence angles and backscattering is affected by angular dependence for oblique angles (Fig.2.8 d). When a rough surface is ensonified, it scatters the acoustic energy in all directions hence the effect of angular dependence decreases and backscattering is similar for all incidence angles (Fig.2.8 f).

Table 2.1: Frequency and acoustic wavelength for given sound speed underwater (1500 m/s).

Frequency (kHz)	$\lambda$ (mm)
50	32
180	9
400	4
700	2

Considering the above, it is understood that the frequency of the acoustic signal (that controls signal's wavelength) plays a very important role in acoustic backscatter (Table 2.1). It is implied that seafloor roughness which is at a scale similar to the acoustic wavelength will have a prominent impact on backscatter signal, meaning that, depending on the operating sonar frequency the same seafloor may appear rough or smooth.

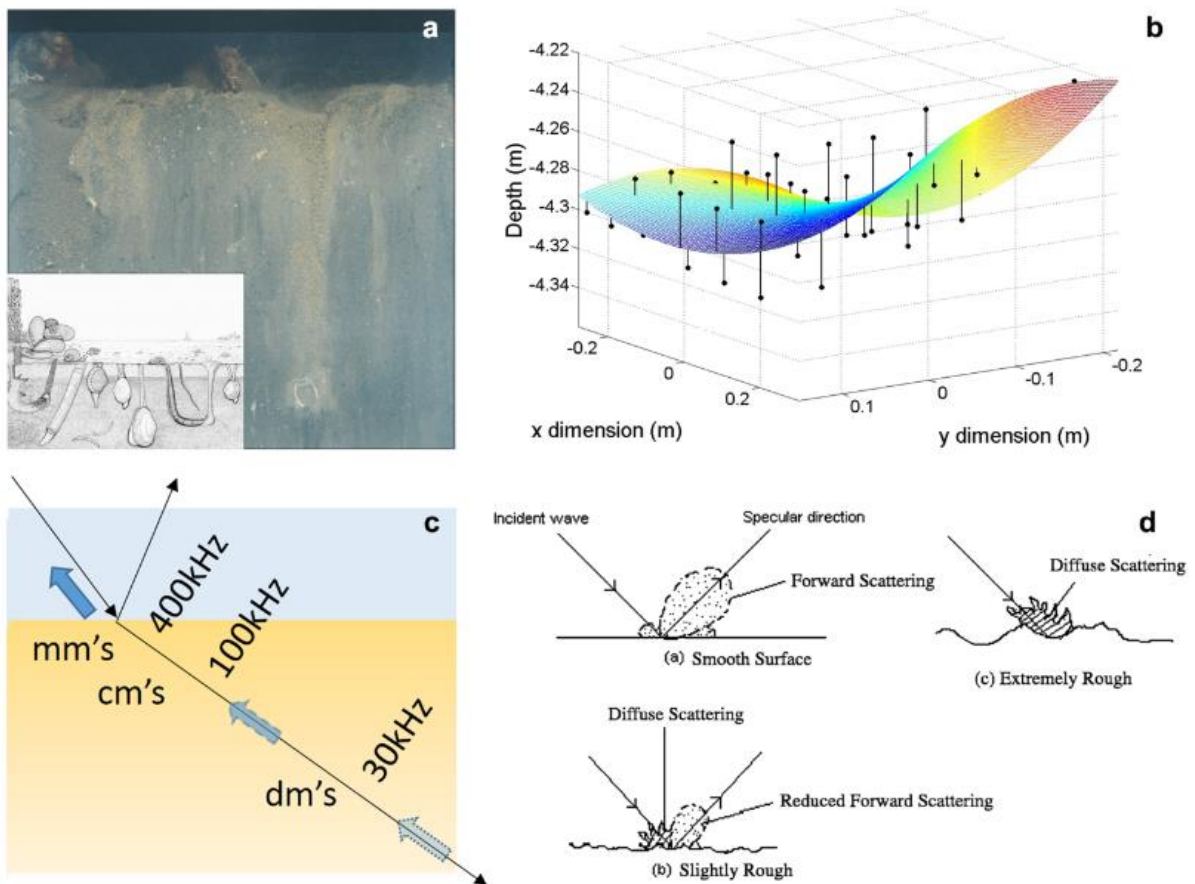


**Figure 2.7:** a) Sediment Profile Imager photo displaying volume inhomogeneity and bioturbation effects (illustrated in minor image, source: Senckenberg Institute) in the upper 30 cm of surface sediments. b) Root mean square residuals (black dots) from fitted bathymetric surface, as an example of seafloor roughness measure (from Eleftherakis, 2013). c) Sketch of acoustic signal penetration at different frequencies for a middle range incidence angle (Beaudoin et al., 2015). d) effect of seafloor roughness on the directivity of the specular reflection of backscatter (Lurton and Lamarche, 2015).



### 2.2.3 Sediment volume scattering

Part of the acoustic wave energy is transmitted through the seafloor to some extent. The extent of acoustic penetration is determined by the sonar frequency (i.e.: the wavelength of the acoustic signal), the density of seafloor material and the angle of ensonification (Fig.2.7) (Urlick, 1983; Jackson and Briggs, 1992).

Seafloor sediments with low impedance (sediments with low bulk density) allow transmission of acoustic energy through their volume deeper than sediments with higher impedance. In addition, acoustic signals with short wavelengths (i.e.: high frequency sonar, >100 kHz) are more susceptible to absorption by the seafloor sediments than signals with larger wavelengths (i.e.: low frequency sonar) (APL, 1994; Ferrini and Flood, 2006; Fonseca and Mayer, 2007). Thus large wavelength signals penetrate deeper into the sediments for given sediment impedance. In nature, the sediment volume is not necessarily homogeneous in all cases; therefore backscatter includes a contribution from individual scatterers such as, infauna, sub-surface layering, gas bubbles or concavities due to bioturbation (Fig.2.7. a) (Novarini and Caruthers, 1998). In case of smooth and flat seafloor surface, intermediate oblique incidence angles (from the middle range) show greater penetration potential than normal incidence and greater oblique angles at the outer swath range (Fig.2.7 c). At normal incidence angles, the specular reflection counteracts the penetration of the acoustic signal into the seafloor and at greater oblique angles the acoustic signal produces a weak backscattering because most of its energy is entirely reflected (Lamarche et al., 2011).

Apart from the concepts described previously, two major parameters that constitute acoustic properties of the seafloor influence the acoustic backscatter. These are the angular and frequency dependences of backscatter strength, the features of which provide valuable insights in the task of seafloor characterization.

### 2.2.4 Angular dependence of seafloor backscatter

Angular dependence refers to the influence that the ensonification angle exerts on seafloor backscatter measurements. This phenomenon has been observed in experiments, in situ and also it has been predicted by geo-acoustic models. Angular dependence is a physical property of the seafloor (Jackson and Briggs 1992; Fonseca and Mayer, 2007) meaning that a certain seafloor type yields a unique set of angular responses.

This set is also referred to as acoustic signature of a particular seafloor type (Alevizos 2017) and it contains information about seafloor roughness and volume heterogeneity. In angular response analysis, the angular responses are divided in parts of the incidence angles domain (normal, intermediate oblique and very oblique) (Fonseca and Mayer, 2007; Huang et al., 2013). These domains can also be expressed in terms of increasing distance from the sonar nadir as near, middle and outer ranges respectively (Fig.2.8 b).

A smooth seafloor composed of soft sediments (with low impedance) would yield high backscatter values at the near nadir domain (specular reflection effect) followed by lower values at middle range angles and even lower values at outer range angles (Fig.2.8 c,d). The smoother the surface it is, the greater the effect of specular backscatter at the near range leading to greater contrast between the backscatter values of the near and middle ranges. The backscatter at the middle range includes contribution from the seafloor volume (as



penetration is optimal for these angles, section 2.2.3) whereas in the outer range backscatter gets weaker since the acoustic energy is distributed at a larger ensonification area (Lamarche et al., 2011). A seafloor of harder material produces more uniform angular responses along all angular domains with a clear decrease in backscatter values in the outer range (Fig.2.8 e,f). Furthermore, it has been found that smooth seafloor with soft sediments would result in high backscatter values at normal incidence angles, appearing as hard seafloor. In contrast, backscatter values from the middle range angles differ substantially for each seafloor type, making them an ideal tool in seafloor acoustic classification (section 2.3.1) (Lamarche et al., 2011).

Although angular dependence is a valuable property for acoustic investigations of the seafloor, it rather complicates the appearance of acoustic imagery. When considering acoustic backscatter maps of the seafloor, the angular dependence is removed from the data so they only represent backscatter variations as if the entire survey took place with single incidence angle beams (Fonseca et al., 2009; Lamarche et al., 2011).

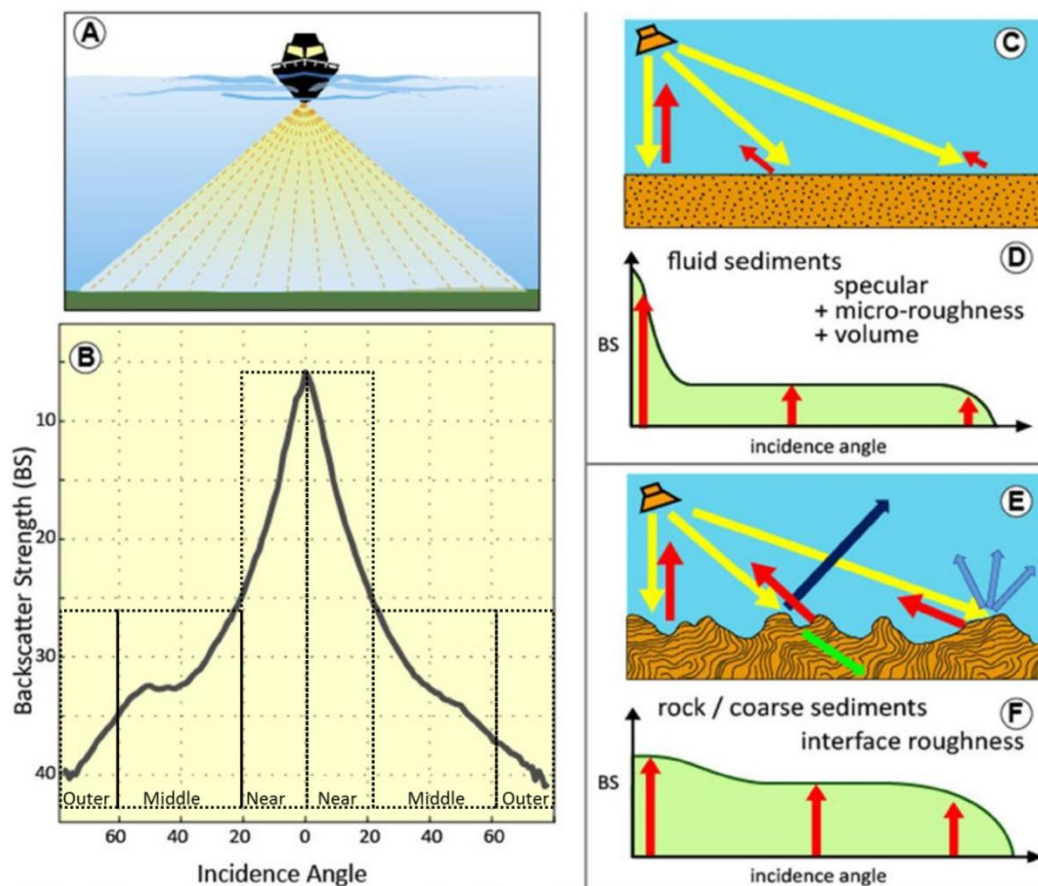


**Figure 2.8:** **A)** Sketch showing across-track MBES swath. **B)** Example port and starboard backscatter responses of incidence angles corresponding graphically with beam angles in figure A. The dotted rectangles indicate the angular regimes relatively to the nadir (zero). **C)** Schematic representation of backscattering geometry of a smooth seafloor regarding the three regimes (arrows) described in figure B. **D)** Schematic representation of angular responses from a smooth seafloor with red arrows indicating the BS at each angular regime. **E)** Schematic representation of backscattering geometry of a rough seafloor. Red and yellow arrows indicate the acoustic energy directed back to the receiver, whereas the rest of the arrows indicate the diffused paths of acoustic energy. **F)** Schematic representation of angular responses from a rough seafloor with red arrows indicating the BS level at each angular regime. (modified from Lurton and Lamarche 2015).

The preferable incidence angles for backscatter image normalization are in the middle range (40-45 degrees) of the swath and the backscatter of these incidence angles is considered as a robust single parameter suitable for geological interpretations (Lamarche et al., 2011). By normalizing the backscatter intensity for a certain incidence angle, the backscatter mosaic can be obtained. The mosaic is a georeferenced image analogous to the bathymetric grid which contains co-registered backscatter intensity information. Backscatter mosaics along with their neighbourhood statistics can be utilized by image-based techniques for ASC (section 2.3.3).

Every seafloor type has unique geological and morphological characteristics (on its surface and volume) that influence backscatter, thus producing a broad spectrum of angular responses depending on several seafloor physical variables (such as surface roughness, grain sizes, sediment porosity) and sonar parameters (incidence angle and frequency) (Williams and Jackson, 1998). It has been further demonstrated that angular dependence varies with sonar frequency as well, adding supplementary information about the seafloor properties (Hughes-Clarke, 2015). In order to describe more accurately the angular dependence, geophysical and empirical models have been developed and they are described in section 2.3.2.

## 2.2.5 Frequency dependence of seafloor backscatter

Considering the optics theory, each material absorbs and emits radiation at certain wavelengths suggesting that a certain type of material would show a unique variability in reflectance depending on the wavelength of the incoming radiation (Campbell, 1996). A comparable concept also accounts in hydro-acoustics, meaning that backscatter intensity (analogous to reflectivity) of a particular seafloor type would express a distinct response when signals of different frequencies are used. This is owing to the interaction between the signal wavelength (which is frequency dependent) and the magnitude of seafloor roughness and sediment grain size (Table 2.1) (Jackson and Richardson, 2007). It is expected that seafloor types with a particular roughness magnitude would yield maximum backscatter intensity for certain signal wavelengths, providing valuable information about seafloor roughness or sediment grain sizes (Ferrini and Flood, 2006). In practice, there is not a continuous dataset for backscatter values over a wide range of acoustic wavelengths as it is true for optical data (Fig.2.9). However, recent studies based on multi-frequency (or multi-spectral) MBES hydro-acoustic mapping support the use of more than one sonar frequency, either simultaneously or repeatedly over the same study area (Hughes-Clarke et al., 2015; Beaudoin et al., 2016). As it has already been stated, sonar frequency determines the wavelength of the acoustic signal and therefore it controls the penetration of the signal through the seafloor and its interaction with surface roughness (Jackson and Richardson, 2007). The exploitation of multiple frequencies is of great potential in studying the acoustic behaviour of seafloor. One way to achieve this is by comparing the angular responses of various seafloor types resulted from different frequencies (Lurton and Lamarche, 2015). Angular domains with contrasting backscatter values may be exploited for advanced seafloor classification approaches. Until now, geophysical models such as the APL have investigated lower sonar frequencies (10-100 kHz) so more recent studies focus on examination of seafloor backscatter from higher frequencies (Bajor, 2013).

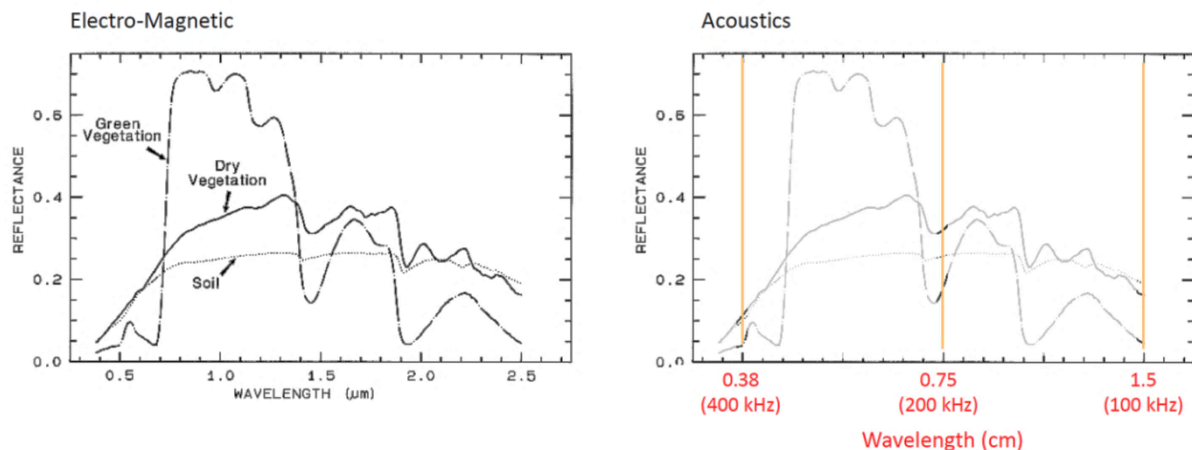


**Figure 2.9:** Left: Example of continuous spectral responses of terrestrial land cover. Right: Graphical example of multi-frequency acoustic responses relatively to spectral ones. (source: Beaudoin et al., 2016, GEOHAB)

Although from a theoretical perspective the frequency dependence provides a multitude of opportunities for seafloor characterization, in technical terms it is not much developed due to associated high cost of instrumentation and multiplication of ship-time for achieving good coverage using multiple frequency sonars. Recent developments in sonar technology allow for ensonification using three different frequencies (200, 300 and 400 kHz) simultaneously. This type of sonars is going to offer more opportunities in the field of seafloor classification.

## 2.2.6 Backscatter data corrections

Before any useful information about the seafloor can be extracted from backscatter measurements using ASC methods, it is necessary that the received acoustic signal is filtered appropriately in such a way so backscatter variability reflects only changes in seafloor type. A standard procedure should be followed for providing geometric (ensonified area, seafloor slope) and radiometric (beam pattern, absorption, gain) corrections in the received acoustic signal (Beaudoin et al., 2002; Hellequin et al., 2003). The following corrections are applied by the majority of commercial software for backscatter processing and considered as standard good practice for backscatter data processing.

### Geometric and radiometric corrections

Seafloor topography influences the ensonified area and alters the angle of the incident beams. As a result, backscatter values may contain variations related to bathymetric surface variability. These effects produce backscatter artefacts and must be compensated for. Consequently, backscatter values need to be corrected for seafloor slope and orientation, and the actual footprint area of each beam (Beaudoin, 2002; Fonseca and Calder, 2006).

Seafloor backscatter also includes artefacts due to the dynamic way that the sonar system treats the received acoustic signal (Fonseca and Mayer, 2007). These artefacts are related to transmission power, beam pattern, receiver gain, and pulse length parameters and

require appropriate corrections. As an example, changes in the transmission power can alter backscatter intensities unequally within the same seafloor type. The beam pattern can also influence the responses of certain beams making them appear with higher or lower intensities than their adjacent beams responses (Beaudoin, 2002; Lurton and Lamarche, 2015). The received signal is often amplified by applying different gains which obscure the actual seafloor backscatter. Finally, pulse length changes influence the extent of the ensonified area on the seafloor hence altering backscatter intensity for a given seafloor surface (Lurton and Lamarche, 2015).

### Sonar calibration

The above compensations for the backscatter values are usually applied on a single dataset resulted from single sonar configuration on a given study area. Additional issues may be introduced by: i) different sonar/survey configurations or processing software, ii) varying oceanographic conditions and iii) repeated surveys over the same area (Lurton and Lamarche, 2015). Case studies have demonstrated that the above factors can considerably affect backscatter measurements over a range of 3 to 10 dB.

In order to achieve comparable results when different sonars, sonar configurations and settings, and repeated surveys take place, MBES sensors should ideally be calibrated. Calibration of MBES sensors includes internal (industry standardized) and field calibration procedures (still in experimental stage). Internal calibration takes place at the manufacturing stage and assures that the acoustic signal is transmitted and received within a certain range of acoustic energy (dB values). Field calibration is considered as the ultimate tuning of the sensor though this method faces significant operational restrictions. The purpose of field calibration is to reduce the backscatter measurements to absolute dB values which are representative of reference seafloor types and comparable to values from experimental measurements (Mopin et al., 2012; Welton et al., 2013). It is understood that for successful field calibration a reference seafloor area with appropriate physical properties is required (Sutherland et al., 2007; Lurton and Lamarche, 2015). The issue of field calibration is not trivial and requires a combination of laboratory and field work along with commonly acceptable seafloor reference areas in order to be effectively applied.

However the absence of sensor calibration does not prohibit adequate backscatter processing up to a certain level. The only requirement is that the MBES acquires backscatter in a stable, linear and repeatable way (Preston, 2009; Alevizos et al., 2017). Then even when the backscatter values are not absolute, it is possible to identify differences in hydro-acoustic data due to seafloor type variations (Chapters 4, 6).

## **2.3 Acoustic Seafloor Classification approaches**

### **2.3.1 The importance of angular dependence**

Seafloor backscatter variability due to the angle of ensonification has led to the development of several types of signal-based seafloor classification techniques generally called Angular Response Analysis (ARA). This approach has extensive applications in MBES backscatter interpretation, providing results which exhibit high correlation with seafloor

properties such as: grain size ( $\phi$ ), porosity and roughness (Fig.2.10, Fonseca and Mayer, 2007; Fonseca et al., 2009).

On this basis, the concept of angular dependence of seafloor backscatter can be exploited in order to accurately characterize parts of the seafloor that have been ensonified from multiple angles. To achieve accurately absolute and universally comparable results, it is required that the MBES sonar is calibrated. However, it is also possible to derive empirical angular response signatures from uncalibrated sonars as long as the signatures hold sufficiently distinguishable geometry for each seafloor type (Beyer et al., 2007; Lurton and Lamarche, 2015; Alevizos et al., 2017). A particular problem with ARA is that in most instances it accounts for a wide patch on the seafloor, hence decreasing the spatial resolution of the resulted classification map and masking out along-swath sediment variability or simply, sedimentary features that are smaller than the analysing patch. This is caused because in most cases it is common to utilize half of the MBES swath to derive the angular signatures. Some strategies to improve the spatial resolution of ARA have been developed and they are based on initial segmentation of the backscatter mosaic in homogeneous objects assuming that they hold similar angular responses (Fonseca et al., 2009; Rzhhanov et al., 2012; Che-Hasan et al., 2014). Ultimately, the spatial resolution issue of the ARA, would be effectively solved if MBES surveys for seafloor characterization were designed in such a way in order to achieve high density of multi-angle soundings per seafloor unit (Augustin and Lamarche, 2015; Alevizos et al., 2017). This would allow for extraction of angular response signatures from a much finer part of the seafloor, drastically improving the classification map resolution and maximizing the discrimination of various seafloor types.

### 2.3.2 Geophysical and empirical ARA models

In literature several geophysical or empirical models have been applied for predicting acoustic backscatter as a function of incidence (or grazing) angle for a given sonar frequency. Usually these models are based on a set of parameters regarding each seafloor type, and by varying these parameters (as model inputs) the model outputs the backscatter response as a function of angle. Inversely, when field hydro-acoustic data exist, the model can be used for predicting the seafloor parameters and finally the seafloor type. Next we consider three of the most-implemented models that have been used in various studies.

The first model is the APL based on a study from Jackson et al. (1986) and described in detail in APL-UW TR9407 (1994) report. This model uses the Kirchhoff approximation at near normal incidence angles combined with Lambert's law away from normal incidence to fit experimental observations of absolute backscatter values of soft sediments obtained by relatively low frequency sonar systems (10-100 kHz). The APL model considers the seafloor as homogenous fluid with isotropic surface roughness and applies empirical parameters for surface roughness and volume backscatter to simulate more complex seafloor types. The APL model is valid for a given number of sediment types (Fig.2.10) and its outputs help to understand the backscatter behaviour as a function of angle for a given sonar frequency.

In general it is a widely accepted and implemented model particularly in research, which lacks in describing complex seafloor types such as those with discrete scatterers,

volume inhomogeneity, gravel beds and benthic cover such as submerged vegetation and coral reefs.

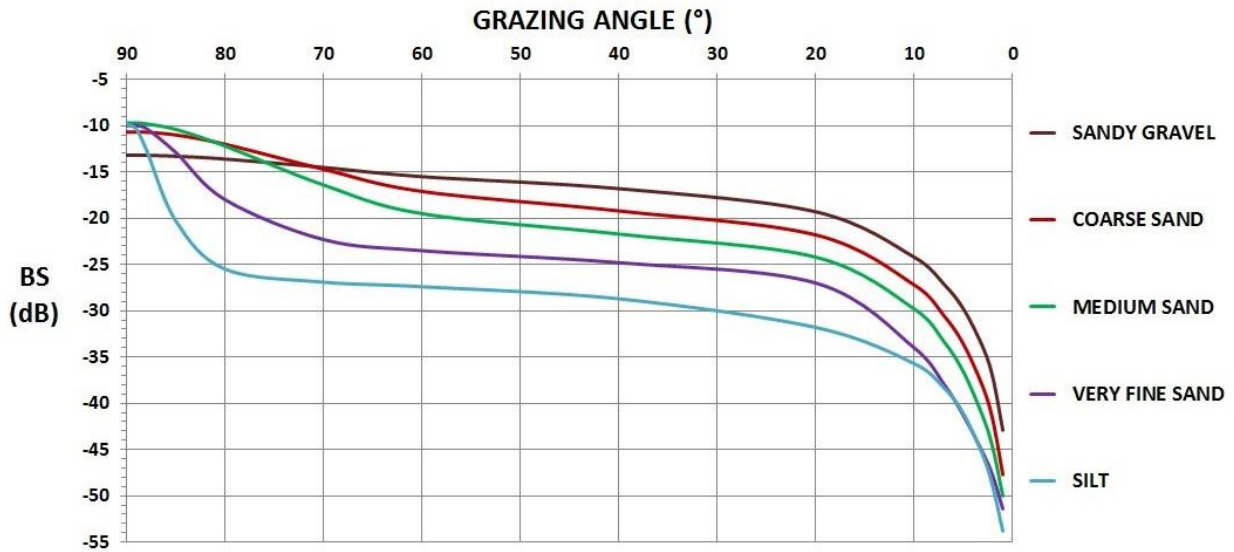


**Figure 2.10:** Prediction of angular response values of general sediment types using the APL model for 100 kHz frequency. (source: Lurton and Lamarche, 2015).

In general the outputs of the APL model (as those shown in Fig.2.10) are based on the target strength (TS) equation:

$$TS = BS + 10\log_{10} A = 10\log_{10}(\sigma_r + \sigma_v) + 10\log_{10} A \quad [2.3]$$

Where: BS is the recorded backscattering strength (absolute values), A is the ensonified area and  $\sigma_r$  and  $\sigma_v$  are the roughness and volume backscatter coefficients respectively.

Another geophysical model was developed through laboratory work of Pouliquen et al. (1999), Bergem et al. (1999) and Canepa et al. (2005) which simulates the effects of volume inhomogeneity and micro-roughness more effectively. In the so called BORIS-SSA model sediment volume inhomogeneity is modelled by assuming spheres with variable radii and elasticity within the sediment matrix. In addition the BORIS-SSA model accounts for small (cm scale) seafloor surface roughness by incorporating a Gaussian power law spectral density stochastic surface. Model results have demonstrated that large scale surface roughness (greater than the pulse wavelength) affects the time of arrival and the dispersion of energy in directions other than the specular of the acoustic signal. In contrast, small-scale surface roughness influences the maximum amplitude of the backscatter response (Tesei et al., 2009). The model has been validated not only by experimental data but also by in situ measurements.

In addition to the physical models, empirical models have also been developed. One important empirical approach is the GSAB model (Lamarche et al., 2011). This model fits angular BS values using a nested function of the incidence angle with three components (Fig.2.11, Eq. 2.4). The components contain a limited amount of parameters (A-F) the tuning of which results in predictions of angular backscatter values. This model is generalizing well

any type of angular response and has shown agreement with physical model prediction results (Lamarche et al., 2011).

$$BS(\theta) = A \exp(-\theta^2/B) + C \cos^D \theta + E \exp(-\theta^2/F) \quad [2.4]$$

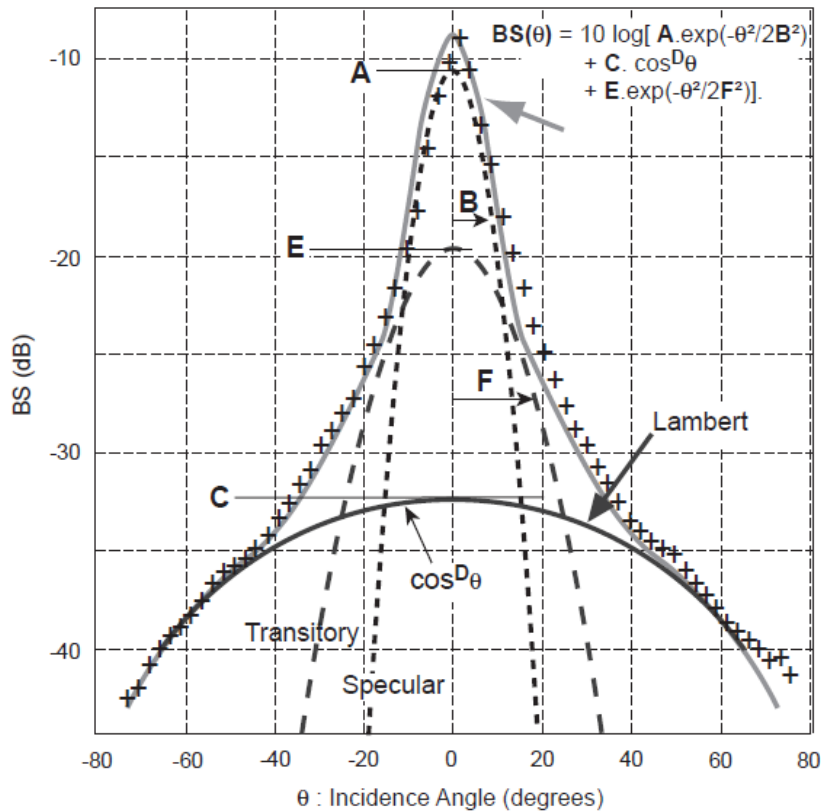


**Figure 2.11:** Example of the GSAB model fitting (grey line) of measured backscatter values (crosses) by combining exponential and Gaussian functions (dashed lines) using parameters A-F. The parameters are used to adjust the shape of functions until a successful fitting to the original measurements is achieved. (source: Lamarche et al., 2011).

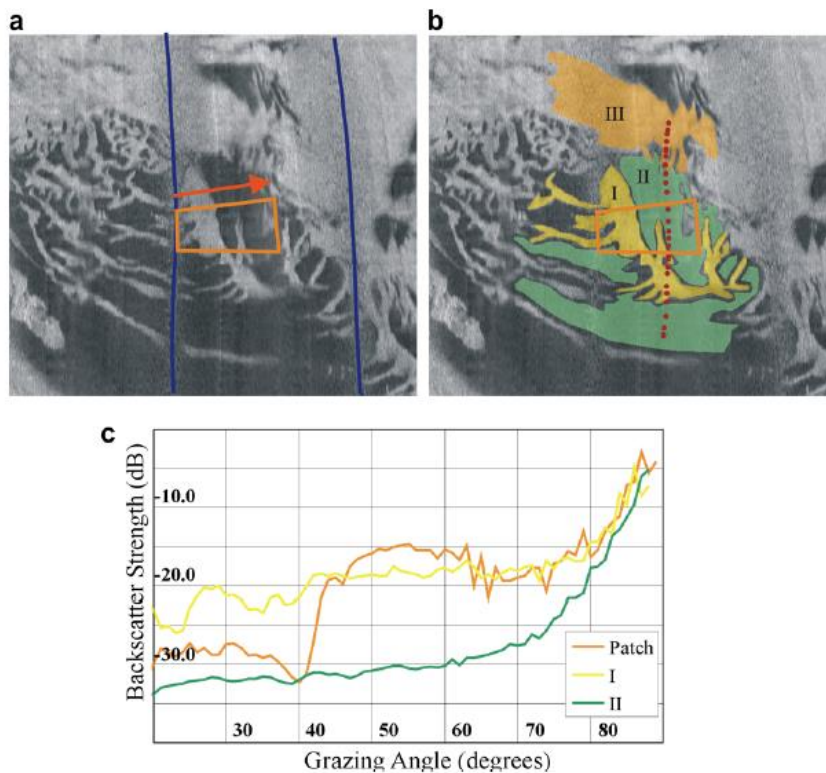
### Latest ARA implementations

ARA has also been combined with image-based techniques in an effort to maximize class separation. This occurred since initial ARA applications were based (and some still do) on an analysis window defined by half-swath and a few tens of consecutive pings (Fig. 2.13 A). This approach, yields sediment prediction maps with coarse spatial resolution that are unable to differentiate along swath sediment variability (Fig. 2.12). As a result new hybrid approaches that incorporate ARA made their appearance in more recent studies.

Fonseca & Mayer (2009) suggested an alternative approach according to which ARA should be based on soundings resulted from homogenous areas on the seafloor (Fig. 2.12, 2.13 B). The need for acoustic class homogeneity had just been born. To achieve this, they utilized the backscatter mosaic which they segmented into acoustic objects (i.e.: groups of grid-cells, see OBIA box). Each object is assumed to be acoustically homogeneous thus soundings from within discrete reference objects should produce more pronounced angular responses. Combination of ARA with backscatter mosaic segmentation was followed in other studies as well. Che-Hasan et al. (2014) applied backscatter mosaic segmentation for identifying homogeneous areas that yield distinct angular responses of benthic habitats (invertebrates, algae) and sediments. In their studies classification of acoustically homogenous areas was based on supervised classification algorithms such as the Random



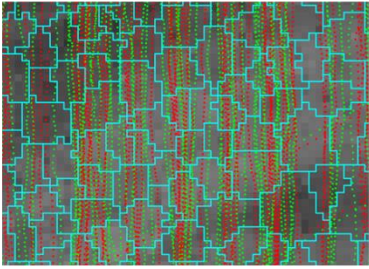
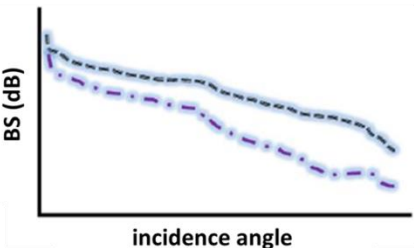
Forest (RF) and Maximum Likelihood Classification (MLC) using ARA variables and bathymetric derivatives as inputs. In another approach utilizing ARA, Rzhanov et al. (2012), enhanced the step of segmentation. They applied over-segmentation to the backscatter mosaic in order to identify as homogenous areas as possible. Then they extracted angular response curves from reference objects and applied pattern recognition concepts utilizing both angular response curves and object geometry.



**Figure 2.12:** The approach introduced by Fonseca et al. (2009) for improving the discriminating power of ARA, a) Patch (orange rectangle) of half swath width and few tens of pings long, the angular signature of which is shown in sub-plot c (orange curve), b) homogeneous objects resulted from mosaic segmentation (orange, green and yellow areas numbered as I, II and III), c) Distinct angular signatures of object I (yellow) and object II (green) in contrast to the mixed signature of the orange patch.

Furthermore some other studies consider ARA curves as geometric objects which can be classified directly (Fig.2.13 C). Hughes-Clarke et al. (1997) and Huang et al. (2013) extracted several geometrical ARA features by treating ARA curves as 2D vectors. These ARA features were used for classifying seafloor sediments. Their studies introduced new concepts in ARA but also highlighted the need for acoustic measurements from homogeneous seafloor areas that help differentiating better the angular responses. In a similar approach, Hamilton and Parnum (2011) applied unsupervised statistical clustering for 2D objects directly on ARA curves for sediment classification. Their approach, although it offers a new aspect on treating ARA curves it does not perform cluster validation meaning that the user has to define the number of clusters intuitively.



<b>ARA approaches</b>					
A) <u>Traditional</u> (acoustic patches)	<table style="width: 100%; border: none;"> <tr> <td style="width: 50%; border: none;"><b>Port</b></td> <td style="width: 50%; border: none;"><b>Starboard</b></td> </tr> <tr> <td style="border: none;">                     ○○○○○○○○○○○○○○○○○○○○○                      ○○○○○○○○○○○○○○○○○○○○○                      ○○○○○○○○○○○○○○○○○○○○○                      ○○○○○○○○○○○○○○○○○○○○○                      ○○○○○○○○○○○○○○○○○○○○○                      ○○○○○○○○○○○○○○○○○○○○○                      ○○○○○○○○○○○○○○○○○○○○○                      ○○○○○○○○○○○○○○○○○○○○○                      ○○○○○○○○○○○○○○○○○○○○○                      ○○○○○○○○○○○○○○○○○○○○○                      ○○○○○○○○○○○○○○○○○○○○○                      ○○○○○○○○○○○○○○○○○○○○○                 </td> <td style="border: none;">                     ○○○○○○○○○○○○○○○○○○○○○                      ○○○○○○○○○○○○○○○○○○○○○                      ○○○○○○○○○○○○○○○○○○○○○                      ○○○○○○○○○○○○○○○○○○○○○                      ○○○○○○○○○○○○○○○○○○○○○                      ○○○○○○○○○○○○○○○○○○○○○                      ○○○○○○○○○○○○○○○○○○○○○                      ○○○○○○○○○○○○○○○○○○○○○                      ○○○○○○○○○○○○○○○○○○○○○                      ○○○○○○○○○○○○○○○○○○○○○                      ○○○○○○○○○○○○○○○○○○○○○                      ○○○○○○○○○○○○○○○○○○○○○                 </td> </tr> </table>	<b>Port</b>	<b>Starboard</b>	○○○○○○○○○○○○○○○○○○○○○ ○○○○○○○○○○○○○○○○○○○○○ ○○○○○○○○○○○○○○○○○○○○○ ○○○○○○○○○○○○○○○○○○○○○ ○○○○○○○○○○○○○○○○○○○○○ ○○○○○○○○○○○○○○○○○○○○○ ○○○○○○○○○○○○○○○○○○○○○ ○○○○○○○○○○○○○○○○○○○○○ ○○○○○○○○○○○○○○○○○○○○○ ○○○○○○○○○○○○○○○○○○○○○ ○○○○○○○○○○○○○○○○○○○○○ ○○○○○○○○○○○○○○○○○○○○○	○○○○○○○○○○○○○○○○○○○○○ ○○○○○○○○○○○○○○○○○○○○○ ○○○○○○○○○○○○○○○○○○○○○ ○○○○○○○○○○○○○○○○○○○○○ ○○○○○○○○○○○○○○○○○○○○○ ○○○○○○○○○○○○○○○○○○○○○ ○○○○○○○○○○○○○○○○○○○○○ ○○○○○○○○○○○○○○○○○○○○○ ○○○○○○○○○○○○○○○○○○○○○ ○○○○○○○○○○○○○○○○○○○○○ ○○○○○○○○○○○○○○○○○○○○○ ○○○○○○○○○○○○○○○○○○○○○
<b>Port</b>	<b>Starboard</b>				
○○○○○○○○○○○○○○○○○○○○○ ○○○○○○○○○○○○○○○○○○○○○ ○○○○○○○○○○○○○○○○○○○○○ ○○○○○○○○○○○○○○○○○○○○○ ○○○○○○○○○○○○○○○○○○○○○ ○○○○○○○○○○○○○○○○○○○○○ ○○○○○○○○○○○○○○○○○○○○○ ○○○○○○○○○○○○○○○○○○○○○ ○○○○○○○○○○○○○○○○○○○○○ ○○○○○○○○○○○○○○○○○○○○○ ○○○○○○○○○○○○○○○○○○○○○ ○○○○○○○○○○○○○○○○○○○○○	○○○○○○○○○○○○○○○○○○○○○ ○○○○○○○○○○○○○○○○○○○○○ ○○○○○○○○○○○○○○○○○○○○○ ○○○○○○○○○○○○○○○○○○○○○ ○○○○○○○○○○○○○○○○○○○○○ ○○○○○○○○○○○○○○○○○○○○○ ○○○○○○○○○○○○○○○○○○○○○ ○○○○○○○○○○○○○○○○○○○○○ ○○○○○○○○○○○○○○○○○○○○○ ○○○○○○○○○○○○○○○○○○○○○ ○○○○○○○○○○○○○○○○○○○○○ ○○○○○○○○○○○○○○○○○○○○○				
B) <u>OBIA</u> BS mosaic segmentation (acoustic themes)					
C) <u>2D curves</u> Clustering of shapes					

**Figure 2.13:** The main ARA approaches found in recent literature and in commercial software: A) analysis on acoustic patches (FMGT software), B) applied on homogenous objects (Fonseca et al., 2009; Che-Hasan et al., 2014), C) shape analysis (Hamilton and Parnum 2011).

### 2.3.3 Backscatter classification based on image analysis

Apart from ARA-based studies there are others that employ backscatter mosaic and bathymetry layers (gridded data) for seafloor classification. As it has been discussed earlier, the angular dependence can be removed from the backscatter data for producing mosaics with angle-normalized backscatter values which are favourable for visual analysis (either by expert users or image processing algorithms). Backscatter mosaics show variations of backscatter intensity (for single incidence angle) reflecting changes according to seafloor types. Usually the backscatter mosaic and bathymetry grids are used for producing several other grids such as backscatter statistics and bathymetric derivatives (Table 2.2). The list of derivable bathymetric and statistical backscatter products is extensive and Table 2.2 presents the most-frequently used examples in literature. Bathymetric derivative such as the Bathymetric Position Index (BPI), rugosity, complexity, curvature and aspect have shown close relation with benthic ecosystem processes such as shelter availability and species abundance (Wilson et al., 2007; Dunn and Halpin, 2009; Ferrari et al., 2016) as well as with seafloor substrate type (Lundblad et al., 2006, chapter 5) and local hydrodynamic regime (Dolan et al., 2008; Rengstorf, 2013; Peukert, 2015). Consequently, it is understood that bathymetric derivatives hold a major role as proxies in seafloor mapping. In addition backscatter neighborhood statistics have been effectively applied in classifying seafloor sediments according to textural information (Blondel et al., 2006; Preston, 2009). The bathymetric derivatives and backscatter statistics are calculated within a spatial neighborhood analysis window (circular or rectangular covering  $n \times n$  cells) or within objects which resulted from backscatter mosaic segmentation (see OBIA box). The backscatter

mosaic can be used for calculating not only the first order statistics (mean, median, mode, standard deviation, quantiles etc) but also: textural statistics using Grey Level Co-occurrence Matrices (GLCMs, Haralick, 1973) and 8-bit color transformations (HSI). ARA features (such as slope, skewness, kurtosis) can also be calculated for image-objects of backscatter mosaics and thus incorporated in image-based analysis (Che-Hasan et al., 2014). Following, the batch of bathymetric and backscatter grids is used as input to unsupervised or supervised image-classification algorithms. When the backscatter and bathymetry grids and their derivatives/statistics are used as input for modelling the ground-truth data (i.e.: with supervised classification algorithms) they called explanatory variables or descriptors, while the ground-truth data are called response variables.

*Table 2.2: List of the most-commonly used bathymetric derivatives, and backscatter statistics (textural and angular) in literature (modified from Stephens and Diesing, 2014 and Che-Hasan et al., 2014).*

<b>Bathymetric derivatives</b>	
slope	the first derivative of bathymetric surface, a measure of the rate of bathymetry change along a path (measured in degrees, percent or radians)
aspect	the azimuthal orientation of slope facets, measured in degrees
eastness	normalized aspect with regards to the east direction, measured in radians
northness	normalized aspect with regards to the north direction, measured in radians
standard deviation	dispersion from the mean depth of the spatial neighborhood
rugosity	It is a measure of the irregularity of a surface. Most commonly appearing as Terrain Ruggedness Index or Vector Ruggedness Measure
fractal dimension	It is the rate of complexity change as a function of scale.
mean curvature	It is the second derivative of a surface (Moore et al., 1991). Positive values indicate that the neighborhood surface is upward convex, negative values indicate tha it is upward concave and zero values indicate flat surface.
profile curvature	It is curvature perpendicular to the slope direction
planar curvature	It is curvature along the slope direction
Bathymetric Position Index	It calculates the relative topographic position of a central grid-cell to a spatial neighborhood defined by a rectangular or circular annulus with an inner and outer radius. (Weiss, 2001, Wright et al., 2005). Positive values indicate local elevations, negative values indicate local depressions and zero values indicate flat areas
complexity	is a 2D measure of surface roughness along a path
Moran's I	it measures the autocorrellation between the cell-values of a predifiend neighborhood
<b>Backscatter statistics</b>	
mean	It is the average backscatter value within a spatial neighborhood of cells
median	It is the median backscatter value within a spatial neighborhood of cells
mode	It is the most frequently occurred value within a spatial neighborhood of cells
standard deviation	It is the dispersion from the mean backscatter value of the spatial neighborhood

HSI	Hue-Saturation-Intensity cube for transforming RGB values (e.g.: of a backscatter mosaic) into a more intuitive geometrical color space
<b>GLCM textural statistics</b>	Grey-Level Co-Occurrence Matrices analyse the grey-level 8-bit cell-values of backscatter mosaics along pre-defined orientations (e.g.: NE) within a spatial neighborhood. They measure the frequency and numerical relation between the cell-values and output the textural statistics below:
GLCM entropy	It measures the level of randomness of cell-values within a spatial neighborhood
GLCM correlation	It measures the linear dependency of gray levels of neighboring pixels, (Kumar 2014)
GLCM contrast	It measures the differences between the cell-values within the spatial neighborhood.
GLCM standard deviation	Both measure the degree of dispersion of a cell-value around the mean value of the spatial neighborhood
GLCM variance	
GLCM homogeneity	It measures the similarity between the cell-values within the spatial neighborhood.
<b>ARA statistics</b>	These are calculated within certain domains of the angular response curves (i.e.: from incidence angle 10 to 30 degrees)
ARA mean	It is the average angular backscatter value of the entire angular curve
ARA slope	It is the rate of change of angular backscatter values at a certain part of the curve (between two incidence angles)
ARA skewness	It is a measure of curve symmetry with reference to a central incidence angle
ARA kurtosis	It is a measure of curve distortion from normal distribution

### Unsupervised ASC methods

Unsupervised methods employ statistical expressions for identification of natural groupings that may exist within hydro-acoustic datasets. Therefore these methods do not require input from ground-truth data. Unsupervised classification is considered as more objective and robust approach than the supervised ones, however many unsupervised techniques suffer from lack of estimating the optimum number of classes in the data (cluster validation).

Traditionally, the user selects the number of classes in which the data should be classified in and then the various classification results are correlated against ground-truth information. The minimum number of classes beyond which there is no statistically significant improvement of the correlation coefficient (between acoustic classes and ground-truth information) is usually considered optimal for final classification. The most common unsupervised techniques for data clustering include the k-means algorithm, the ISODATA algorithm (Chapter 5) and the principal component analysis (PCA) which typically is combined with the k-means algorithm. The k-means approach, clusters the data in k number of clusters (set by the user) by minimizing the within class Euclidian distances and maximizing the between class variances. Similarly the ISODATA algorithm clusters the data in a number of clusters by using a set of input parameters defined by the user. The user selects (intuitively) the minimum and maximum number of clusters along with thresholds about the within- and between-class standard deviation values that are considered acceptable for each cluster.

The ISODATA algorithm will merge together clusters that have lower between-class standard deviation than the one selected and it will divide clusters with greater within-class standard deviation (Memarsadeghi et al., 2006). In general, most of the unsupervised approaches require an external diagnostic test for cluster validation. Such diagnostic tests include the F-test, the gap statistic, the silhouette coefficient and the C-H criterion (Tibshirani et al., 2001). The role of diagnostic tests is to identify the minimum number of clusters that describe data variability effectively (i.e.: increasing number of clusters does not improve the score of the tests). In the studies included in this thesis we applied the silhouette coefficient (chapter 3) and the C-H criterion (chapter 4) tests. The silhouette coefficient examines how homogeneous are elements within a class. The coefficient can take values from -1 to 1. Values closer to 1 indicate high class homogeneity with majority of elements correctly assigned this class whereas values closer to -1 suggest that elements differ significantly from class mean value and thus should belong to another class. Values close to zero indicate that the elements are at the decision boundary between two classes hence they could be assigned any of these classes. The second tool is the Calinski-Harabaz (C-H) criterion that evaluates the optimal number of clusters. This method takes into account the between-class and the within-class differences at the same time for elements clustered in given number of classes. The number of classes that receives the highest C-H score is suggested as optimal for partitioning the data (Calinski and Harabazr, 1974).

### Supervised ASC methods

In supervised classification the input of ground-truth information assists in establishing a model or a rule-set according to which the data can be classified in. In that sense, classes are pre-defined. The ground-truth data used to inform the classification is called training set. Supervised algorithms can be simple or complex ranging from user-defined class values (e.g.: Benthic Terrain Modeller, Wright et al., 2012) to random forest models and artificial neural networks (Stephens and Diesing, 2014). In any case the supervised algorithm establishes a set of criteria (knowledge) from ground-truth data values and uses these criteria to classify unknown parts of the acoustic data.

#### **TRAINING & VALIDATION SETS**

*When a sufficient amount of ground-truth data is available, part of it can be used for algorithm training in supervised classification approaches. Depending on the algorithm, the training samples need to fulfil certain criteria. For example, in case of MLC the hydro-acoustic data belonging to training samples from each class should hold normal distribution. On the other hand, this is not required when machine learning algorithms are used (such as the RF or SVM). In general it is required that ground-truth samples represent all different types of seafloor from the study area and the corresponding hydro-acoustic data cover a broad range of values allowing for more robust training of the algorithm.*

*The part of the ground-truth data that is not used for algorithm training may be preserved for assessment of classification results. Assigning a ground-truth sample as for training or for validation should be done randomly and validation samples should be*

appropriately separated in space from the training samples in order to avoid introducing bias during classification assessment due to auto-correlation effects.

Assigning several times (the number of times depends on various characteristics of the data and it can be estimated by statistical tools such as the Monte Carlo test) different part of the ground-truth data as for training or validation is called bootstrapping and it assists in capturing the sensitivity of the algorithm to different input data. In addition bootstrapping aids cross-validation of the training data results. Thus cross-validation helps in quantifying the robustness of the supervised classification algorithm.

### Data exploration

When a large amount of explanatory variables exists, it is desirable to exploit only those that assist more in class separation. To identify which explanatory variables provide better class separation than others data exploration tools are applied. The most-common tools in data exploration include the probability density functions (PDFs) and box-plot diagrams. PDFs indicate the range of values (of an explanatory variable) within which each class occurs more frequently (Fig.2.14 A). This is a very informative way to evaluate how suitable an explanatory variable is in discriminating a set of classes. The box-plots designate also the range of explanatory variables values that the majority of training samples occur (2<sup>nd</sup> to 3<sup>rd</sup> quartile) along with the median value for each class (Fig.2.14 B). Both statistical tools provide useful semi-quantitative information that assists in decision-making on the selection of the most informative explanatory variables.

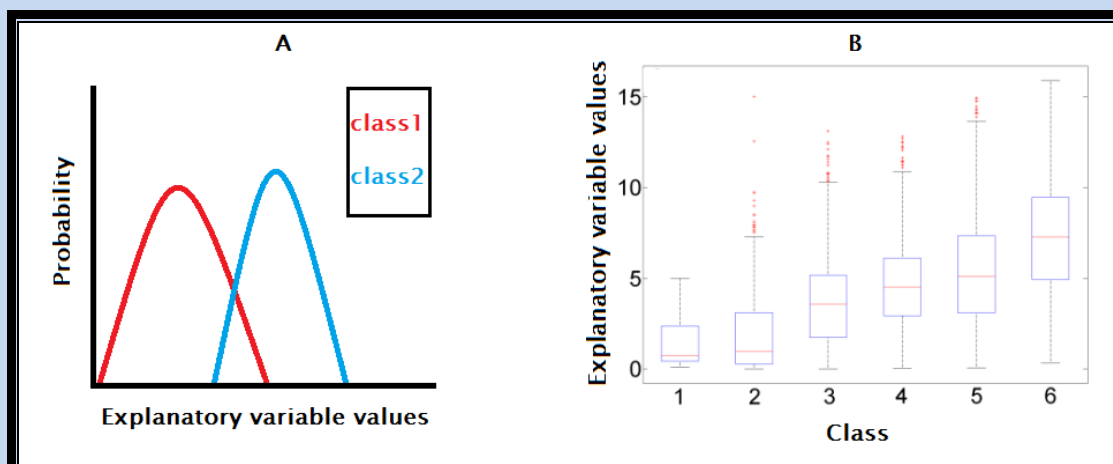


Figure 2.14: A) Example PDF plot using two classes. B) Example box-plot examining six classes.

### Studies on image-based ASC techniques

Either in supervised or unsupervised classification approaches the validity of results needs to be tested using part of the ground-truth data. Unsupervised classification results, are tested by correlating them to ground-truth information such as grain size distribution data or expert-defined categories of seafloor. If there is significant correlation between classes and ground-truth data then ground-truth is used to characterize each unsupervised class. Classes from supervised approaches are compared with ground-truth data via their

contingency (or confusion) matrices and using Cohen's kappa coefficient (chapter 4). Contingency matrices provide the accuracy percentages of modelled (or predicted) classes over the actual classes provided by the ground-truth. In addition the Cohen's kappa coefficient is used for testing the agreement between output and actual classes and thus evaluating the performance of the supervised classifier. Some indicative studies using image-based unsupervised or supervised approaches are presented below.

Backscatter and bathymetry grids (including their statistics and derivatives) have been commonly used in unsupervised classification algorithms such as the PCA (chapters 3, 4). The PCA applies an orthogonal transformation to a set of correlated variables for calculating a reduced amount of new, uncorrelated variables that account for the same data variability. The new variables are called principal components and they carry information from all initial variables. It is implied that some initial variables have a greater contribution than others in the principal components. Following, the first two or three principal components often account for most of the data variability and they can be clustered in feature space using a k-means algorithm. PCA using an extended set of backscatter textural statistics grids was introduced by Preston (2009). His study analyzes how the commercial ASC software QTC Multiview calculates three principal component vectors from a set of 123 backscatter textural and statistical variables (gridded). Other applications of PCA approach include that of Eleftherakis et al. (2013) for classifying riverbed sediments using a large set of bathymetric and backscatter statistics including bathymetry residuals.

Blondel et al. (2006) developed a classification scheme based on textural features of BS mosaics resulted from different frequency sonars. They applied grey level co-occurrence matrices (GLCMs) transformation to the BS mosaics for obtaining new grids (descriptors) with textural information. Then they processed them using unsupervised classification algorithms from the TexAn software. Since BS mosaics are represented as greyscale imagery, they are suitable for calculation of several textural statistics (Table 2.2). Textural statistics often contain valuable information about seafloor cover hence they can be useful descriptors in ASC tasks.

Ierodiaconnou et al. (2011) applied supervised classification (MLC, decision trees) on a set of bathymetric derivatives and backscatter mosaic derivatives (color-transformed cell values) using video data as ground-truth information for classifying macro-benthic organisms. Stephens and Diesing (2014) compared six supervised methods (Classification Trees, Support Vector Machines, k-Nearest Neighbour, Neural Networks, Random Forest and Naive Bayes) for classifying seafloor sediments using ground-truth information from an extensive collection of sediment samples. They propose that careful tuning of supervised classifiers and selection of appropriate bathymetry/backscatter descriptors is important to obtain accurate results. It has to be noted that k-Nearest Neighbor and Naive Bayes algorithms are considered simpler and with less computational requirements compared to the rest of the algorithms. The other supervised algorithms (Classification Trees, Support Vector Machines, Neural Networks and Random Forests) are extensively used in the field of machine learning providing the ability to better identify complex relations in the data but they are considered to be computational demanding. Moreover their settings need to be adjusted for each specific data application and usually this is done by trial and error since a variety of input data can be used in different cases. Lucieer and Lamarche (2011) employed supervised and unsupervised classification methods within the context of object-based image analysis (OBIA). They utilized textural variables extracted from BS mosaics and bathymetric derivatives in conjunction with fuzzy k-means clustering for producing

probability maps for different sediment contents (i.e.: silt, sand, gravel). In addition they used backscatter and bathymetry grids as inputs for segmenting the study area into homogeneous objects. Following, they applied the nearest neighbour algorithm for predicting the sediment contents of unknown objects based on objects corresponding to highest probability from the initial unsupervised classification results. In the same sense, Lucieer and Lucieer (2013) compared three supervised classification methods (KNN, RF and decision trees) for classifying seafloor morphology, benthos and substrate using AUV MBES data in conjunction with OBIA.

### **OBIA**

*The increasing volume and resolution of geo-spatial datasets has led to the development of more sophisticated methods for data processing and interpretation. The concept of OBIA was developed taking advantage of the high spatial resolution imagery and treating image elements not as grid-cells (pixels) but as objects. Objects are groups of pixels with similar geometric and other properties, which can be related to other objects and in essence they represent real world objects (i.e: lakes, roads, buildings etc).*

*OBIA is performed in two steps. The first step is called “segmentation” and it helps in grouping the image pixels for the production of objects. One or more grids can be used for segmentation and different segmentation algorithms/settings can yield various types of objects. In practice, segmentation involves expert knowledge provided by the user which should reflect the needs and particularities of the specific task. Segmentation is an automated and repeatable method for producing image objects the properties of which can be calculated as attributes table.*

*The second step is “classification” of the image objects. As with traditional pixel-based image classification the same with OBIA, objects need to be classified into an optimum number of classes or a predefined set of classes suggested by ground truth information. Thus unsupervised or supervised classification techniques can be applied on image objects in the same sense as if they were pixels.*

## **2.4 Ground-truth sampling and analysis**

As with any remote sensing technique so with hydro-acoustic mapping of the seafloor, backscatter measurements and their analytic results are not a direct representation of the real seafloor types, but they form an alternative source of information about the seafloor. Therefore results from ASC need to be linked somehow to the actual seafloor types that they describe (Sutherland et al., 2007). To achieve this, availability of an adequate amount and quality ground-truth data is necessary. Throughout backscatter analysis, ground-truth samples can be utilized in two major tasks: classification training and classification results validation (see training and validation tests box).

The most common types of ground-truth data include sediment samples and underwater video/images. Acquisition of sediment samples is usually made with grabs or multi-corers (Fig.2.15 A,B). These types of gear are capable of sampling a few tens of squared centimetres of sediment area from the upper half meter of the seafloor column.



Underwater stills or video can also be utilized for ground-truth once they have been carefully annotated/interpreted. It is implied that adequate positioning is provided during seafloor sampling (McGonigle et al., 2009). Positioning errors can affect the classification accuracy and artificially increase or decrease the performance of classification algorithms.

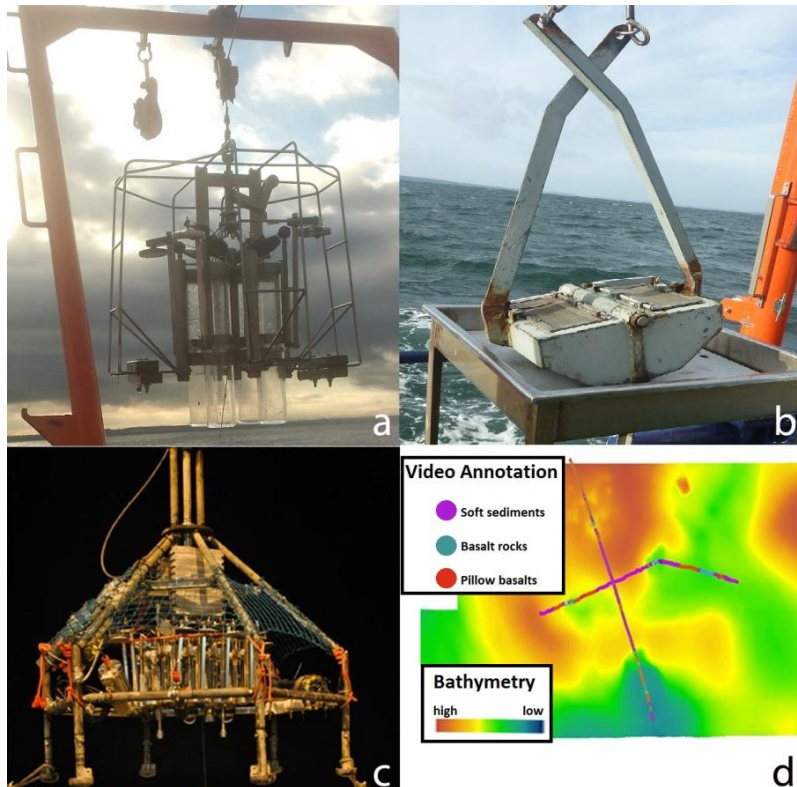


**Figure 2.15:** a) Multi-corer sampler for soft sediments, b) Van-Veen grab sampler for coarse (sand, gravel) sediments, c) Ocean Floor Observation System (OFOS) underwater video platform, d) example of video annotations overlaid on bathymetry map.

In some cases ground-truth sampling takes place prior to or during hydro-acoustic surveys, thus little or no involvement of acoustic data information is used for guiding the plan of ground-truth locations. When seafloor sampling takes place after the MBES survey it is recommended that acoustic information is taken into account in scheduling of ground-truth survey. Acoustic information may result from backscatter mosaic and/or combination of bathymetry through identification of particular acoustic/bathymetric features. Duplicates of sediment samples should be taken for each acoustic feature identified and samples should expand in the whole survey area. This is because due to sediment heterogeneity that can cause different seafloor types to express similar acoustic behaviour from place to place (chapter 4, Eleftherakis 2013).

Sediment samples are usually analysed for grain size distribution of the fine fraction (<500  $\mu\text{m}$ ) whereas the coarse fraction is separated with various sieves and each sub-fraction is weighted (Collier and Brown, 2005). Integration of grain size distribution and weights of sieved fractions provides grain size quantitative information (such as the mean, median and mode) for the whole sample which then can be used for comparison with acoustic data (chapter 4).

Underwater images and/or video provide recordings of seafloor surface type along transects of several tens or hundreds of meters (Fig.2.15 C,D). The recordings consist of multiple sample points with unique coordinates and timestamp. The most common analysis is expert (manual) annotation/interpretation of each image or video slice which normally is



time-consuming and results in subjectivity-related errors. On the other hand automated image analysis can save time and provide results in a more consistent way (chapter 5). The results (either from expert or automated analysis) can be quantitative or qualitative. Quantitative information may refer to sediment grain size, number of boulders and seafloor roughness, while qualitative information is related to sediment types (rock, sand, silt). Semi-quantitative results may also be provided referring to percentage of seafloor coverage or presence/absence of geological features (e.g.: boulders).

### 3. Acoustic discrimination of relatively homogeneous fine sediments using Bayesian classification on MBES data

This chapter was published in October 2015 in Marine Geology:

Alevizos E., Snellen M., Simons D. G. , Siemes K., Greinert J., 2015, Acoustic discrimination of relatively homogeneous fine sediments using Bayesian classification on MBES data, Marine Geology, Volume 370, Pages 31-42, ISSN 0025-3227, <http://dx.doi.org/10.1016/j.margeo.2015.10.007>

<b>Authors contributions (Elsevier standards)</b>	
Study conception and design:	Alevizos, Greinert
Acquisition of data:	Greinert
Analysis and interpretation of data:	a) classification software development: Snellen, Siemes, Simons b) classification analysis and interpretation: Alevizos
Drafting of manuscript:	Alevizos
Critical revision:	Alevizos, Greinert

## Abstract

Modern seafloor mapping is based on high resolution MBES systems that provide detailed bathymetric and acoustic intensity (backscatter) information. We examine and validate the performance of two unsupervised MBES classification techniques for discriminating acoustic classes of sedimentary units with small grain size variability. The first technique, based on a principal components analysis (PCA), is commonly used in literature and has been applied for comparison with the more recent approach of Bayesian statistics. By applying these techniques to a MBES dataset from an estuarine area in the Netherlands, we tested their ability to discriminate fine grained sediments (at least 70% silt) holding small percentages of coarser material such as sand, shell hash or shells. We focus on the Bayesian technique as it outputs acoustically significant classes related to backscatter values. This technique utilizes backscatter values averaged over scatter pixels (projected pulse lengths) inside the footprint of each beam. The originality of our application lies in the fact that, the optimal number of classes is derived by utilizing a number of beams simultaneously. It is assumed that the backscatter values per beam vary relatively to the varying seafloor types. By treating the beams separately, across track variation in the seafloor type can also be accounted for. Thereby the classification is guided by outer, more discriminative beams. Additionally we control the optimal number of classes by employing the quantitative criterion of goodness of fit ( $\chi^2$ ). The Bayesian acoustic classes show correlation with grain size parameters such as coarse fraction ( $>500\mu\text{m}$ ) percentage and mean of the grain size ( $<500\mu\text{m}$ ) when analysed with multiple linear regression. In order to examine the relative scale of the acoustic classification results we compare the Bayesian acoustic classes with underwater video interpretation. Our results reveal that the Bayesian approach enhances the sedimentological interpretation of MBES high resolution data, by providing classification on seascape scale (here meters to tens of meters). Hence we suggest that backscatter processing techniques are more commonly applied to produce classes that discriminate sediments with low grain size contrast. To describe this ability we introduce the term geoacoustic resolution. We want to encourage the use of the Bayesian technique also in deep sea applications, based on AUV data, where sediments express low variability but sampling would be time consuming and costly. The advantages of this method would favour mapping of macro-habitats which appear at meter-scale and require datasets of sufficient resolution in order to be quantitatively described.

### 3.1 Introduction

Acoustic remote sensing of the sea, river or lake floor provides a non-destructive and cost effective way to produce a variety of qualitative and quantitative maps of depth and sediment type. Multibeam echo-sounders (MBES) are the state-of-the-art tool commonly used for bathymetric and sediment property mapping that finally results in sediment classification or habitat maps. In this respect, the increasing amount of MBES specific information recorded (pulse length, gain, snippets) allows for an increasingly accurate and representative description. Many of the MBES acoustic classification techniques discriminate between sediment types as different acoustic classes. Assigning sediment properties to these acoustic classes requires expensive and time consuming ground truthing (Simons & Snellen, 2009; Holmes et al., 2008; Clements et al., 2010). Obtaining better/more predictive seafloor maps at less ground truth cost is one of the goals in modern seafloor mapping research. Therefore, significant effort has been made towards improving and developing methodologies for a more quantitative representation of the seafloor lithology through MBES data analyses (Collier & Brown, 2004; Lamarche et al., 2011; Fonseca et al., 2009).

#### Acoustic backscatter classification

Backscatter intensities registered by MBESs provide the most explanatory yet complex information regarding seafloor sediment properties (Hamilton & Parnum, 2010). Its complexity is the result of a number of factors including the sonar beam pattern characteristics, the sonar frequency, the incidence angle of the beam with the seafloor, the micro-roughness of the seafloor, the grain size of the sediments, coverage with epibenthic organisms and the volume scattering of the sediment (Hamilton & Parnum, 2010).

Before any reasonable analysis can take place, backscatter data have to be geometrically (e.g. beam pattern, incident angle) and radiometrically (pulse length, gain, receive band width) corrected and ideally the MBES sonar has to be calibrated to record real dB values for comparison with other systems as well as for time series studies (Lamarche et al., 2011; Eleftherakis et al., 2014). An important factor that characterizes unprocessed backscatter data is the dependence of the received backscatter signals on the swath/incident angle which comprises a physical property of the seafloor (de Moustier & Alexandrou, 1991; Fonseca & Mayer, 2007). Sediments of the same type will give a different backscatter response when ensonified from different angles. This effect can be the basis of further analyses or can be compensated for in order to obtain a normalized image of the backscatter intensities. McGonigle et al. (2014) divide the different methodologies for backscatter processing in two main groups, i.e. the signal-based and the image-based methodologies.

The signal-based methodologies include 1) the Angular Response Analysis (ARA), which makes use of the angular dependence (Fonseca et al., 2009; CheHasan et al., 2012; Huang et al., 2013; Rzhanozov et al., 2012) and 2) acoustic modelling (Lamarche et al., 2011; Simons & Snellen, 2009). The advantage of signal-based methods is that they, in theory, can provide sediment characteristics such as mean grain size with no or only very limited ground truth data. These methods require good calibration of the MBES backscatter measurements to be comparable. Their computational demands can be significant if

inversion is applied, where the match between the measured and modelled signal is maximized by searching for the unknown sediment parameters (e.g.: mean grain size, porosity, seabed roughness). Implementation of signal-based methods is often less straightforward compared to the image-based methods.

The image-based backscatter analyses include 1) supervised classification using underwater photos/videos (Summers-Morris, 2004; Rooper & Zimmerman, 2007; Ierodiakonou et al., 2011; Foubert et al., 2011; Neves et al., 2013; Marcon et al., 2013; Stephens & Diesing, 2014), 2) unsupervised classification based purely on statistical relationships and patterns of the data such as correlations and trends between their statistical derivatives (Hamilton & Parnum, 2010; Snellen and Simons, 2009; Lucieer & Lucieer, 2009; Amiri-Simkooei et al., 2009; Preston, 2009), and 3) combinations of supervised/unsupervised classification with Object Based Image Analyses (OBIA) of the backscatter mosaics (Lucieer & Lamarche et al., 2011; Estomata et al., 2012). These image-based methods are less dependent on the calibration of the MBES backscatter measurements and do not use inversion techniques. However, independent ground truthing is needed for assigning physical sediment properties to the resulting sediment classes.

All of the above-mentioned techniques for backscatter classification make use of at least some ground truth data in order to provide quantitative sediment property maps of the seafloor. In this study we focus on unsupervised classification algorithms and their ability to separate acoustic data in representative sedimentary classes. While in supervised techniques, the final classes are pre-defined according to the amount of ground truth data, in unsupervised techniques the natural meaning of the number of classes is being defined a posteriori.

## Rationale of the study

In this study we are testing two unsupervised techniques for producing acoustic classes and compare the results with ground truth data including sediment grain sizes and visual observations. The goal is to examine if the fine scale variability within sediments is resolved by the acoustic classification algorithms given that the seafloor consists of the same overall sediment type (i.e. at least 70% silt).

The ability to discriminate small differences in sediments is valuable in benthic habitat mapping of certain species (Kostylev et al., 2003) and potentially in seafloor exploration for aggregates extraction (dredging). For our MBES-based classification we propose an improved unsupervised acoustic classification of fine grained sediments. This technique is an advanced version of the Bayesian technique presented by Simons & Snellen (2009). The technique presented here does not require absolute sonar calibration, it is capable to resolve along swath sediment variations, makes use of the full backscatter record and most importantly, it provides statistical control for the optimum number of classes in contrast to other unsupervised techniques. A novelty of this study is that we utilize for the first time a combination of beams simultaneously in order to derive the optimal number of classes. The other unsupervised classification technique is based on MBES derivatives of backscatter or bathymetric measurements. By applying a principal component analysis, followed by a clustering of the most important principal components, acoustic classes are assigned to all data points.

## Study area

The MBES data were acquired in the Grevelingen (The Netherlands) which was cut off from the North Sea in 1971 when a dyke was built. The study area is a former estuary of the Rhine River but now it is mostly a brackish water lake with a depth ranging between 5 and 48 meters. After the severe flooding of 1953, the Grevelingen became disconnected from the North Sea in 1971 as part of the Delta Project, which included the development of several dams. Since 1978 the Grevelingen is connected with the North Sea again via a lock build in the dam structure west of the area (Fig. 3.1). The Delta project had also a post construction phase for monitoring the geomorphological and ecological response of the ebb tidal deltas of South-West Netherlands (Mulder et al., 1991).

The study site has received intense anthropogenic pressure in recent times as it has been used for sediment dredging to build the dam and as a dumping site for shell debris from locally farmed oysters. The sediment extraction has altered dramatically the area's bathymetry by introducing elongated deep channels and local depressions (visible as the dark areas in the inset of Fig. 3.1). After building the dam, tidal activity of the North Sea that shaped the seafloor ceased. The previously formed ripples became buried by lacustrine sedimentation. Due to the connection to the North Sea via the small outlet in the dam, the Grevelingen offers habitat for several marine species mainly algae, crustaceans and fish, which form the local biodiversity pattern (Mulder et al., 1991). The area consists of loose sediments with low contrast in grain sizes. The main variability exists due to the varying content of sand, shell fragments, coverage of epibenthic organisms and the local occurrence of pebbles. The ability of discriminating rather homogeneous sediments, as investigated in this contribution, is important for a better understanding of habitats and organisms that show a strong discrimination between a subtle variability of fine grained sediments not only in the shallow water of the Grevelingen, but also in the deep sea (Etter & Grassle, 1992).

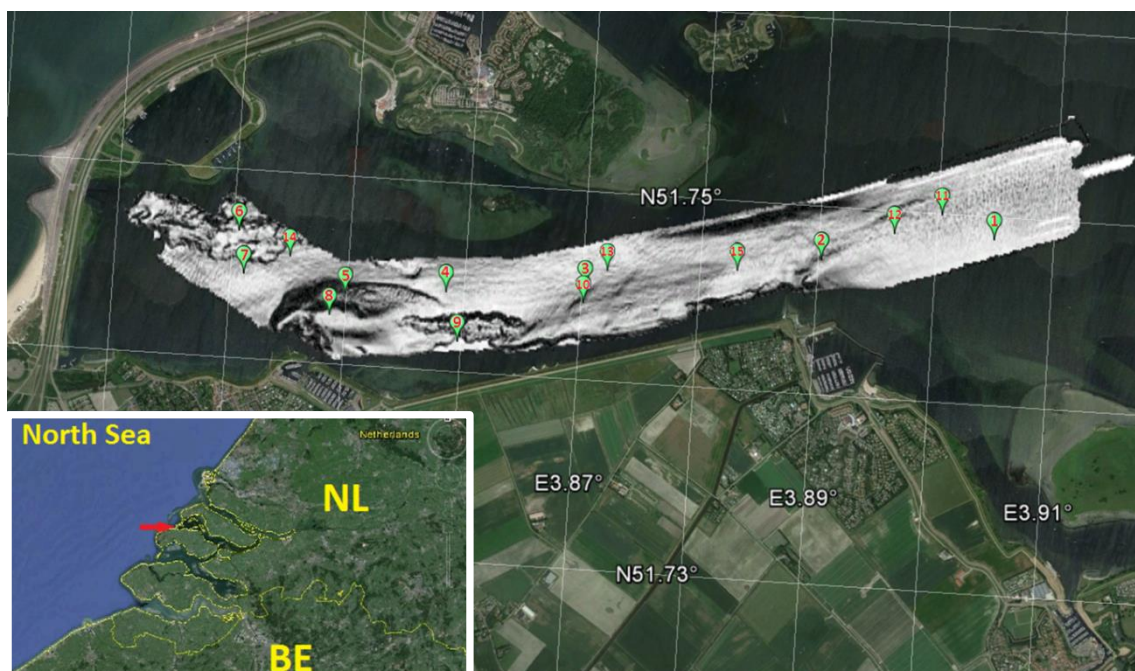


**Figure 3.1:** Shaded MBES bathymetry over a close-up of the area from Google Maps (red arrow in the lower left corner indicates the location). The green flags indicate micro-corer sample positions.

## 3.2 Methodology

### MBES survey and ground truth data

The MBES survey was carried out in April 2013 using a Seabeam 1180 sonar with 180 kHz and 1.5° across by 3° along track beam angles. Line spacing was 50 m with varying 50-100% overlap. Raw backscatter data were exported with the HDPPost software as ASCII files and then further processed in Matlab. Sediment was recovered as ground truth data from 15 micro-corer deployments and underwater video recording using GEOMARs Ocean Floor Observation System (OFOS) in December 2013 and July 2014. The upper 10 cm of the sediment were used for grain size analysis given that the MBES frequency of 180 kHz does not allow deeper penetration into the sediments.

*Table 3.1: Grain size statistics of the fine (<500 μm) and coarse (>500 μm) fractions of sediment samples with shell presence and Shepard class.*

No	Lon	Lat	Fine fraction				Coarse fraction	Shells (y/n)	Shepard class
			Mean (μm)	Median (μm)	Mode (μm)	W.%	W.%		
1	3.9049	51.7488	106.1	19.5	14.9	80.4	19.6	y	sandy Silt
2	3.8903	51.7472	31.9	10.7	9.4	100	0	n	clayey Silt
3	3.8703	51.7449	27.0	14.5	16.4	97.6	2.4	n	Silt
4	3.8585	51.7442	20.1	9.3	10.3	100	0	n	clayey Silt
5	3.8499	51.7437	18.2	8.2	8.5	100	0	n	clayey Silt
6	3.8405	51.7468	26.2	10.9	16.4	100	0	n	clayey Silt
7	3.8411	51.7445	27.7	12.0	16.4	98.3	1.7	n	clayey Silt
8	3.8487	51.7426	22.5	10.7	14.9	100	0	n	clayey Silt
9	3.8597	51.7416	24.4	10.2	11.3	98.9	1.1	n	clayey Silt
10	3.8702	51.7441	24.8	11.9	13.6	100	0	n	clayey Silt
11	3.9003	51.7499	222.0	230.0	272.0	91.7	8.3	y	Sand
12	3.8964	51.7488	9.0	7.9	14.8	100	0	n	Silt
13	3.8721	51.7459	77.7	12.9	221.0	73.4	26.6	y	sandy Silt
14	3.8450	51.7456	12.5	9.5	12.9	100	0	n	Silt
15	3.8832	51.7463	10.6	9.4	15.9	100	0	n	Silt

The coarse and fine fraction were split using a 500μm sieve. The finer fraction was analyzed with a Coulter Counter and the results are presented in Table 3.1. The underwater video footage was interpreted using the Ocean Floor Observation Protocol (OFOP) classification module and exported as an ASCII point file (Hütten & Greinert, 2008). The

annotation of the videos was based on the macroscopic qualitative description of seafloor surface coverage. Four main types of seafloor cover were discriminated; they include dense epifauna and/or pebbles, sparse epifauna and/or pebbles and no epifauna or pebbles. The fourth type represents a seafloor covered with phytodetritus in water depth greater than 20 meters.

## Classification algorithms

In this study we compare two unsupervised classification algorithms and their capabilities of discriminating different sediment types. As first method we apply a Principal Components Analysis (PCA) in conjunction with k-means clustering for the assignment of classes as applied to underwater sediment classification by Amiri-Simkooei et al. (2011) and Eleftherakis et al. (2013). The algorithm was implemented in Matlab and the resulting classes were imported in a GIS environment for further examination.

The PCA technique is using a numerous set of potentially moderately correlated variables in order to produce new, uncorrelated variables that fully describe the variability of the original dataset. For the variables we utilized five acoustic backscatter derivatives, including the mean BS, median BS, mode BS, min BS, and max BS (Eleftherakis et al., 2012). The first two principal components corresponding to the highest eigenvalues, which explain most of the data variation, were used for further classifications. Once the first two principal components are assigned, their coefficients can be plotted separately in GIS. These coefficients will show a gradual variation and will not indicate separate classes. In order to separate the PCA results into classes and combine the information contained in the two PCAs, we apply the k-means clustering algorithm. The k-means algorithm clusters the data by minimizing the distances of all points regarding to their class centroid (Eleftherakis et al., 2013). It has to be noted that the final classes are assigned to patches of 3 neighbouring beams and 3 consecutive pings. The second classification method applied is the Bayesian technique as defined by Simons & Snellen (2009), Amiri-Simkooei et al. (2009) and Siemes et al. (2010). By using the average BS value per beam footprint, a histogram of the different dB values is created per beam. Our method utilizes the backscatter (dB) value fluctuations in the histogram derived from all backscatter values at a certain beam angle and fits a number of Probability Density Functions (PDFs, Gaussian) to it. The number of PDFs needed for a good match between modelled and measured histogram represents the number of seafloor types that can be discriminated from the backscatter data. The assumption underlying the method is that the number of scatter pixels in a beam (its footprint; see appendix of chapter 3, Fig. 3.2, Fig. 3.3) is large and that consequently the backscatter per beam and seafloor type is distributed according to a normal distribution (Gaussian curve). Mathematically this assumption derives from the central limit theorem according to which the beam backscatter, as derived from a sufficient number of scatter pixels, will exhibit a Gaussian distribution for a single seafloor type. Consequently, the algorithm accounts for the ping-to-ping variability of the backscatter measurements. Variations in seafloor type can be approximated by summing a number of normal distributions with varying shape around a varying mean backscatter value. According to Amiri-Simkooei et al. (2009) the outer beams (beyond the middle range of the swath) are preferably utilized for fitting the Gaussians, and hence identifying the number of classes. This occurs because the outer beams encompass a larger area at the seafloor (due to larger grazing angles) hence include more scatter pixels, giving rise to a



lower standard deviation and consequently increased geo-acoustic resolution (more on this term in paragraph 5.3). The amount of Gaussian curves needed for obtaining a good fit with the measured histogram is determined by the  $\chi^2$  goodness of fit criterion. Fitting stops when adding Gaussians to the backscatter histogram does not lead to a further improvement of the  $\chi^2$  (as close to 1 as possible). This quantitative measure allows for determining the statistically significant number of classes. Applying the  $\chi^2$  criterion to a set of outer beams simultaneously, for identification of the optimum number of classes, makes the novelty in our processing approach. It has to be mentioned that the Bayesian technique assigns acoustic classes which correspond to certain dB ranges, thus resulting in acoustically meaningful clusters. Subsequently the grain size distribution parameters of the fine fraction and percentage of the coarse fraction can be plotted against their acoustic class for performing a linear regression. Finally, the outer beams are used to determine the distribution of BS measurements among the acoustic classes and the BS values at the remaining angles are assigned according to the same distribution. We then obtain a classification map of high spatial resolution with a 2x2m bin size. In our study the MBES used did not provide the actual amount of scatter pixels per beam, therefore we estimated this number by applying the formula used by Siemes et al. (2009) to each beam (see appendix for chapter 3, Eq. 3.1).

### 3.3 Results

#### PCA and k-means clustering

The first two principal components are derived from five backscatter properties (mean BS, median BS, mode BS, min BS, and max BS) which showed the highest correlation with these principal components. From the principal components that the PCA yielded we have chosen the first two as input for the k-means algorithm to cluster the geospatial patches according to their principal components values. The clustering results are shown as 2D plots using only the first two PCs (Fig. 3.4). Several quantitative measures are presented in the literature that aid determining the number of clusters. In order to evaluate the number of acoustic classes that can be discriminated, we applied two quantitative criteria apart from the comparison with ground truth data. The first criterion is the total sum of distances and the second criterion is the silhouette coefficient as considered by Eleftherakis et al. (2013). The total sum of distances is a metric related to the difference of all classified points with the value of the class centroid. It generally decreases with an increasing number of classes. The silhouette coefficient is a measure of dissimilarity of a point compared to the points of its cluster (Eleftherakis et al., 2013) ranging from 0 to 1. Values above 0.5 generally account for sufficient separation of classes whereas less than 0.5 represent misclassification of data (potential class overlap). When applying the PCA technique there is a good evaluation of the number of classes using the sum of distances and the silhouette coefficient for more than 4 classes; particularly for the 6 classes, the silhouette coefficient is 0.75. We have chosen to present the result for 6 classes for comparison with the Bayesian approach which also provides an optimal number of 6 classes (see next section). The resulting classes represent areas with similar values for the first two principal components (Fig. 3.4), hence a direct correlation with dB values cannot be established. This would have allowed further examinations with ground truth data. In order to visualize the PCA effectiveness in separating the classes, we added the mean grain size to classified patches (groups of beams

and pings) that are within a radius of 10 meters from each sampling location, assuming that they hold the same sediment type (Fig. 3.4). Finally the assigned classes of the k-means algorithm were plotted and gridded in GIS (Fig. 3.5). It can be seen that higher mean grain sizes correspond to the more negative values of PC1 and the lower mean grain sizes is corresponding to increasing PC1 values. Still, within an acoustic class the mean grain size shows significant variation, indicating that other parameters than mean grain size contribute to the variations in the PC1 values.

An important observation is that the PCA classes are separated by parallel “cuts” in the principal components space. This indicates that the initial features are highly correlated and even the first principal component alone would be enough to describe all of the data variation. In case of another data source is added, for example parameters derived from the bathymetric measurements, both PC1 and PC2 are expected to add to the method’s discriminating performance.

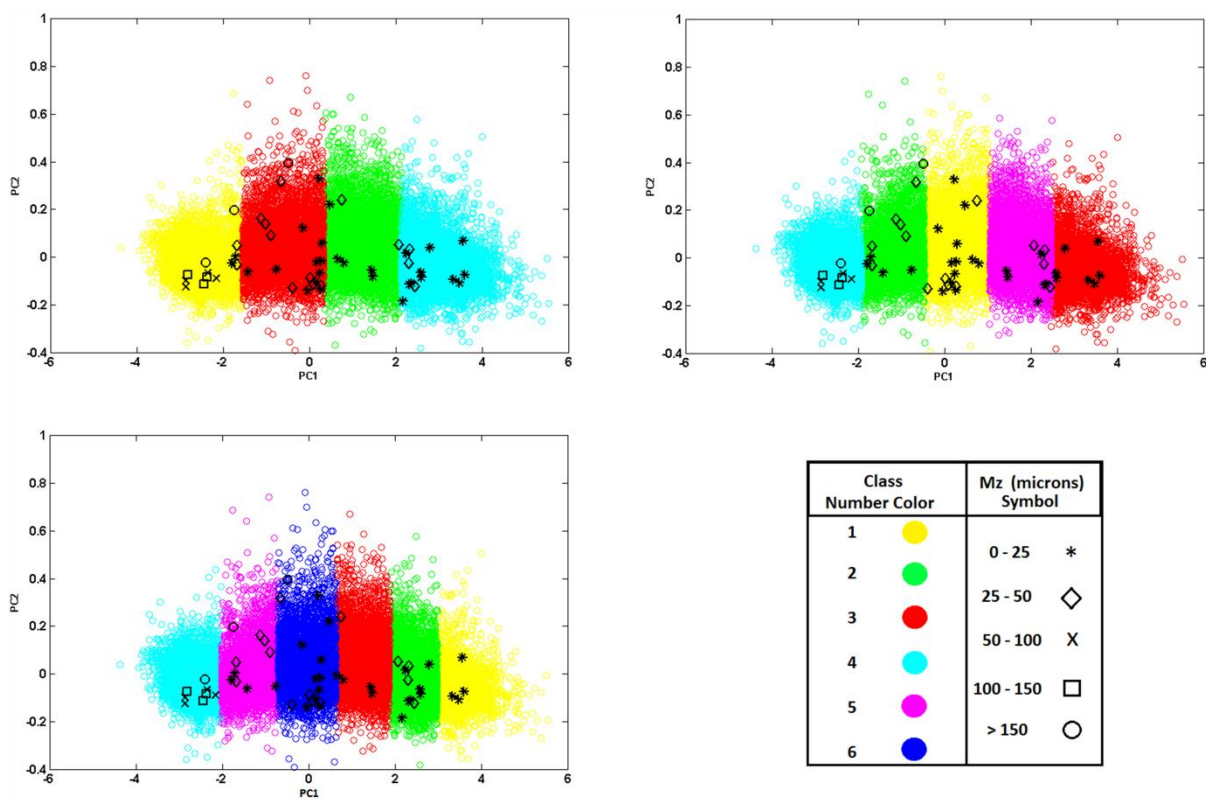


**Figure 3.4:** Plot of the first two principal components for three different acoustic classifications with 4, 5 and 6 classes (plot a, b, and c respectively). The black symbols refer to corresponding locations within a radius of 10m from each ground truth sample.

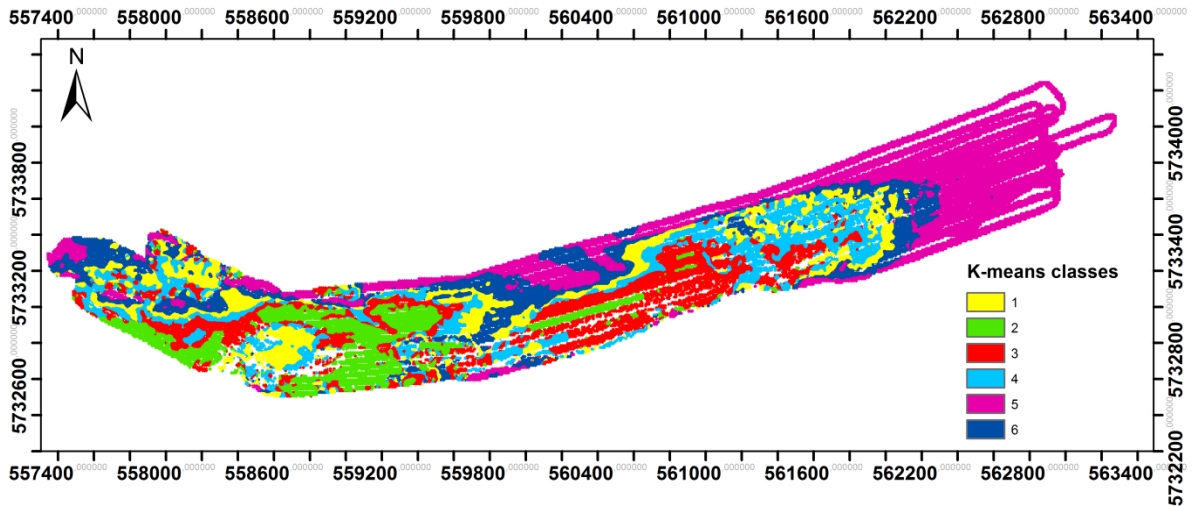


Figure 3.5: Classes resulting from combination of PC1 and PC2 using the k-means clustering method.

### Bayesian technique

The Bayesian technique consists of the steps: identification of the number of classes, fitting the histogram for the outer beams, relating neighboured beams, and assigning data to the classes.

In order to identify the optimal number of classes we used data from different beams from port and starboard sides. This happened in order to utilize the maximum of information provided by each side. For the port side we selected the beams that correspond to grazing angles of 50, 48 and 46 degrees, whereas for the starboard side we selected beams with grazing angle 44, 40 and 38 degrees (these beams were chosen as beam 50, 48 and 46 were quite noisy). Considering that the results of the selected sets of beams are consistent with regards to the number of classes, we present the results for six classes, which satisfy the  $\chi^2$  criterion for all of the selected beams. A number of six classes was also found to provide a maximum class separability with minor overlap of adjacent classes. This is evident from Fig. 3.6, which shows the fit of 6 PDFs for the three outer beams at port side. The class boundaries at these beams are extracted from the intersection points of the PDFs. Together, these PDFs provide an average distribution of BS values among the acoustic classes. The final assignment of classes was guided by the statistics of these outer beams and was based on the assumption that the remaining beams would express the same distribution.

Table 3.2: Correspondence of sediment classes from micro-corer locations that fall within each Bayesian class.

Class	Sediment type
1	clayey silt
2	Silt
3	clayey silt with 1-2% coarse material
4	clayey silt with >2% coarse material
5	sand with 2-10% shell fragments
6	sandy silt with 10-25% shell fragments

The derived classification was exported to GIS, the result of which is shown in Fig. 3.7. Each class represents a range around a central dB value. The classes 1-6 express a gradient from low to high backscatter intensities (Table 3.2) and therefore can be examined against physical properties of sediment samples, through linear regression. Once the final classes were assigned to the rest of the beams, we gridded the results using a 2x2 meter bin size. Regarding areas with overlapping classes we applied the maximum value given that there were no differences larger than 1 class. The Bayesian technique produced classes that show strong agreement between neighbouring beams and transects. It can be noticed that the geospatial distribution of PCA classes is relatively similar to that of the Bayesian classes (Fig 3.5 and Fig. 3.7).

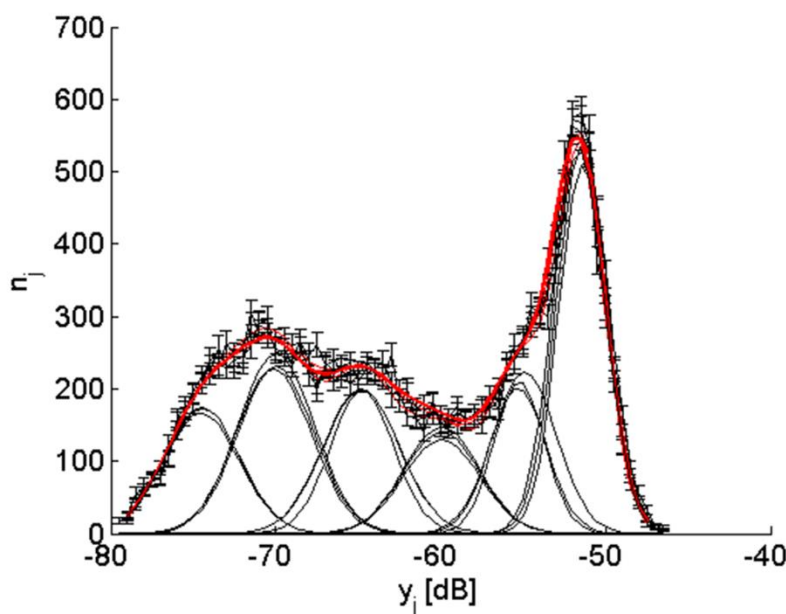


**Figure 3.6:** Example of the overall curve fitting (red line) of the histogram values and PDFs for 6 classes from the selected beams of 50, 48 and 46 degrees (port side). Note the fair agreement of each Gaussian (PDF) for the three adjacent beams.

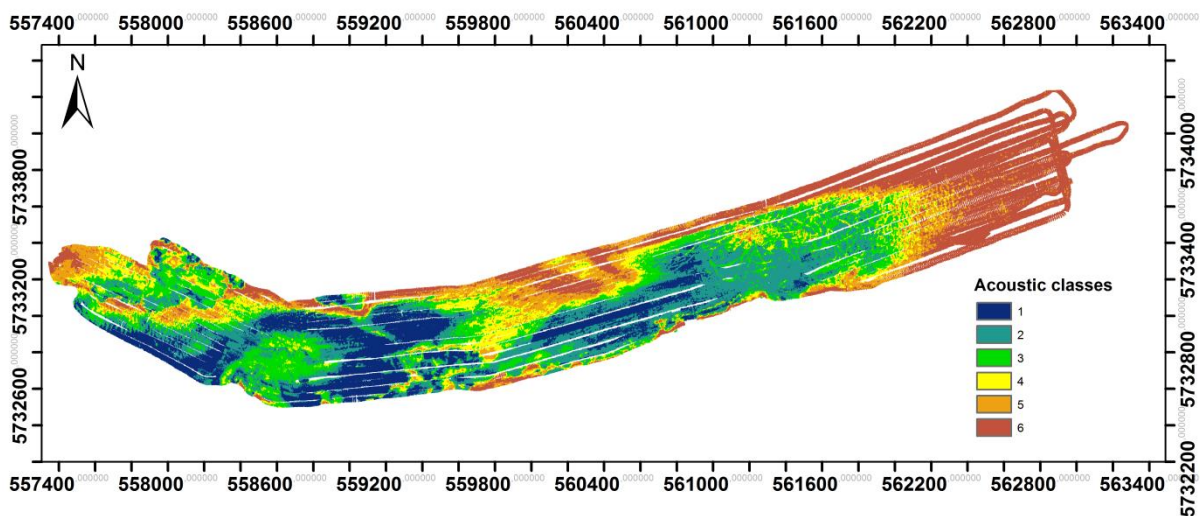


**Figure 3.7:** Acoustic classes resulting from combination of beams 20-60 from both port and starboard sides.

### 3.4 Discussion

#### Optimal number of classes

Finding the optimal number of clusters is a common problem in unsupervised classification techniques (Canty 2007). There are several algorithms to determine the optimal number of classes based on statistical criteria in addition to visual examination of the data (Dunn 1973, Calinski and Harabasz 1974). In this study the cluster validity rules include: a) the  $\chi^2$  goodness of the fit criterion for the Bayesian classification and b) the total sum of distances and the silhouette coefficient for the k-means classification (Eleftherakis, 2013). The  $\chi^2$  criterion allows determining the optimal number of classes prior to the classification whereas the latter validate the resulting clusters once classification is performed. To extend the validation process of the Bayesian technique we investigated the correspondence between its classification and the information from the sediment analyses.

Given that earlier studies have demonstrated the correlation of mean grain size and other statistics with backscatter values (Collier & Brown, 2005; Ferrini & Flood, 2006; McGonigle et al., 2014) we decided to perform a multivariate linear regression (Simons et al., 2007). The sample parameters considered in the multivariate correlation analysis are the mean grain size of the fine fraction (<500  $\mu\text{m}$ ), and the percentage of the coarse fraction (>500  $\mu\text{m}$ ) given that they yield better correlation coefficients (Table 3.3).

For this, we write

$$y = c_0 + c_1x_1 + c_2x_2 \quad [3.2]$$

with the coefficients describing the linear relationship between  $y$ , i.e. the acoustic class or corresponding backscatter value, and  $x_1$  and  $x_2$  the two sediment parameters under consideration.

Defining matrix  $\mathbf{A}$  as the matrix containing ones in the first column and in the remaining three columns all 15 measurements of  $x_1$  and  $x_2$  respectively, we have

$$\begin{matrix} \mathbf{u} \\ y \end{matrix} = \mathbf{A} \begin{matrix} \mathbf{c} \end{matrix} \quad [3.3]$$

where the column vector  $\begin{matrix} \mathbf{u} \\ y \end{matrix}$  contains the Bayesian classification result at the 15 micro-corer locations. Vector  $\begin{matrix} \mathbf{c} \end{matrix}$  contains the three coefficients. The least-squares solution to the above system equation is

$$\begin{matrix} \mathbf{r} \\ \mathbf{c} \end{matrix} = (\mathbf{A}^T \mathbf{A})^{-1} \mathbf{A}^T \begin{matrix} \mathbf{u} \\ y \end{matrix} \quad [3.4]$$

For  $\begin{matrix} \mathbf{r} \\ \mathbf{c} \end{matrix}$  we find [2.5, 0.16, 0.007] which results in:

$$\text{Acoustic class} = 2.5 + 0.16 * \text{coarse} + 0.007 * Mz \quad [3.5]$$

Where: *coarse* is the percentage of the coarse fraction and *Mz* is the mean grain size of the fine fraction (in  $\mu\text{m}$ ).

By using these estimates for the coefficients of the percentage of coarse-grained material and the mean grain size to predict the classification results and by correlating our modelled predictions with the real measurements, we find a linear correlation coefficient of 0.79 (Fig. 3.8). Another observation is that especially for the lower acoustic classes, the above equation predicts higher classes. Care has to be taken when drawing conclusions from the above presented comparison between acoustic classification results and the analysed sediment parameters. First of all, the number of samples is very limited as for some of the acoustic classes, only a single sediment sample is available. Secondly, many of the samples have been taken in areas that show variability with regards to the acoustic classes. Still, this good correlation supports our selection of 6 classes based on the outer beams and the application of the  $\chi^2$  criterion.

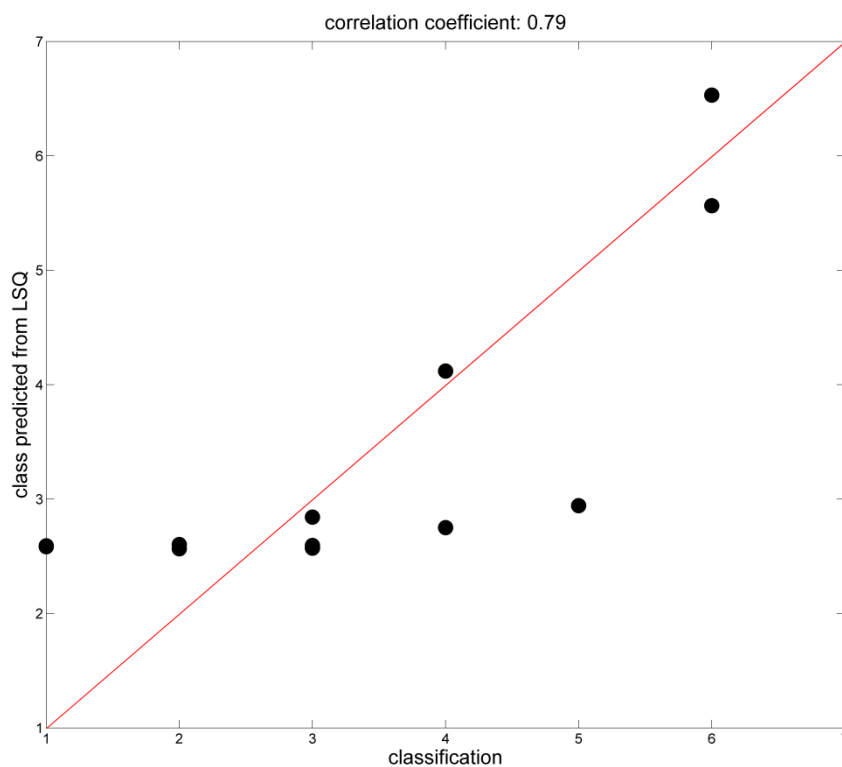


**Figure 3.8:** Class prediction results using a linear relationship between the percentage of coarse-grained material and the mean grain size of the fine fraction.

In the above described processing, a multivariate correlation was carried out. When considering univariate correlations with the acoustic classes, the highest correlation coefficient (see Table 3.3) is found for the correlation between the percentage of the coarse fraction and the acoustic classification results. This indicates that in relatively homogeneous fine sediments even small additions (1-20%) of coarse material is capable to alter the backscatter signal significantly (Fig. 3.9). It gives clear evidence for the sensitivity of backscattering with respect to volume scattering processes which cannot be derived from seafloor surface video data (Calvert et al., 2014). We infer that small variations of the coarse fraction create a gradient of sedimentary zones which at the end are detectable by our proposed classification. The lower correlation between acoustic class and sediment mean grain size indicates some insensitivity of backscatter on mean grain size for very fine grained sediments. In addition, the three classes derived from the visual examination of underwater video (sparse/dense epifauna and/or pebbles, uncovered mud Fig. 3.10) show a close

relationship with acoustic classes resulting from the Bayesian technique. We infer that different percentages of seafloor coverage by shells, shell hash and/or epi-benthic organisms can produce different acoustic classes. Also evident is that the high resolution achieved in our acoustic classification is comparable to the fine scale classification results from the video analyses. This is seen in the almost coinciding transition points in both the acoustic classes and video classes (Fig. 3.10). Based on the above we conclude that the number of acoustic classes can be affected by variable percentages of coarse grained material within generally fine-grained sediments. In addition, the percentage of seafloor coverage by epibenthic organisms and pebbles has an influence as well; often coarser sediment and benthos occur together.

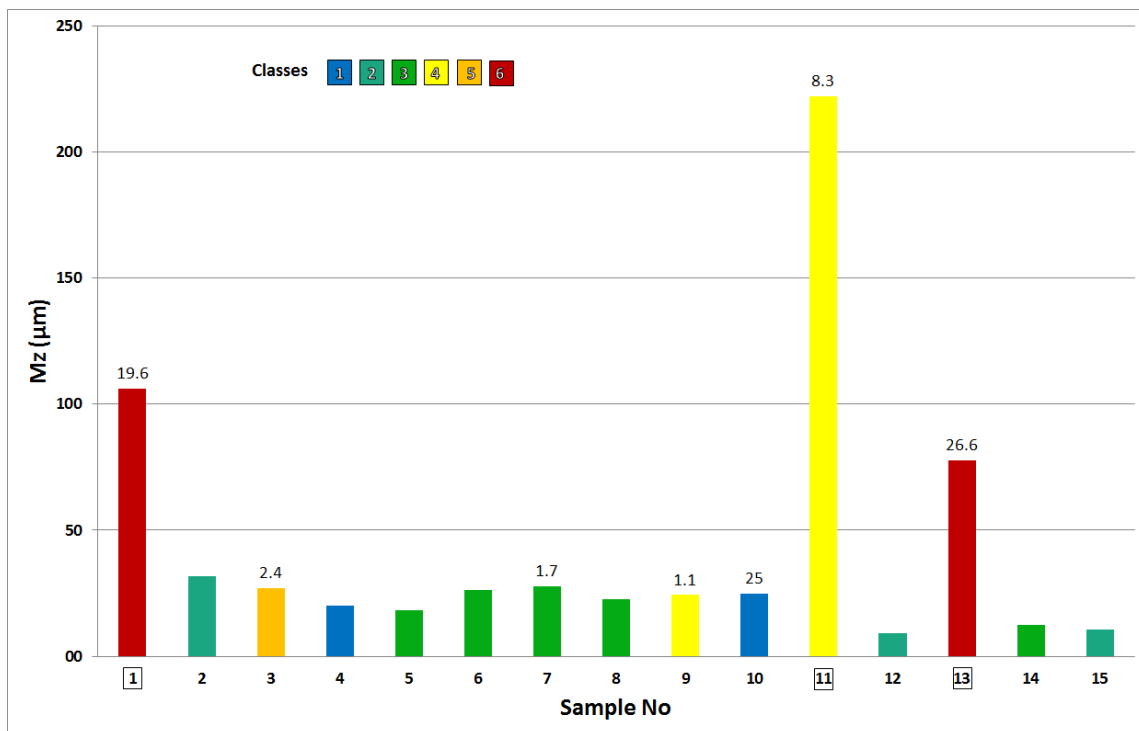


**Figure 3.9:** Color-coded class of each sediment sample against their mean grain size. The numbers above the bars indicate the percentage of the coarse fraction (>500 μm). Squares around sample numbers indicate the presence of shell fragments in these samples.



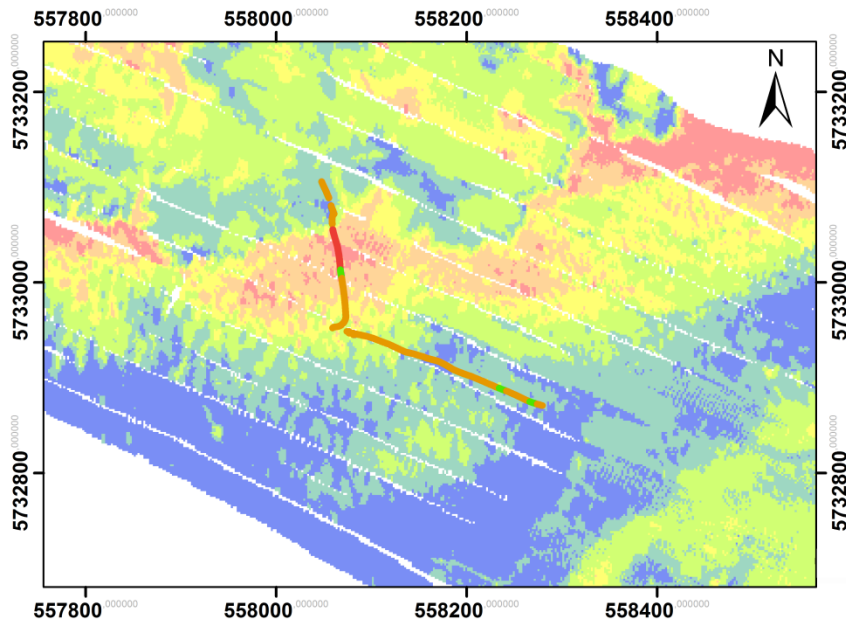


**Figure 3.10:** Color-coded macroscopic description of seafloor cover from underwater video plotted over the Bayesian acoustic classes. Video: orange: uncovered mud, red: dense epifauna/pebbles, green: sparse epifauna/pebbles.

## Advantages of the Bayesian technique and comparison with the PCA

By applying the Bayesian technique on data from an uncalibrated MBES we found that the method proved robust enough despite the missing sonar calibration. The method allowed identification of classes across the swath of the MBES. This is in contrast with techniques that are based on the full backscatter curve (Hamilton & Parnum 2010, Simons&Snellen 2008). Although these methods show high correlation with ground truth they are not able to resolve across swath sediment variations, which is the case for natural seafloors. As a result the Bayesian technique provides an acoustic discrimination of the seafloor in high resolution being able to resolve acoustic variations on the scale of the MBES footprint ideally.

A novel approach in this study is that the number of classes was determined by a combination of beams simultaneously. In previous applications of Amiri-Simkooei et al. (2009) and Simons & Snellen (2009) only one beam was utilized and in Siemes et al. (2010) three beams were used separately. The outer beams, which have the greatest discriminative potential, are used to determine both the number of classes and the distribution of BS measurements among these classes, i.e. the percentage of BS values assigned to each class. Relating the BS values at other, less discriminative beams (closer to nadir) to the distribution of classes found for the outer beams, increases their classification potential.

Although there was high correlation between ground truth and the Bayesian classes we recognize that the number of sediment samples per class is not sufficient to establish a thorough study of the relation between acoustic class and sediment parameters such as mean grain size or the abundance of a coarse sediment fraction. Sampling of ground truth sediments was based on bathymetry and backscatter mosaic evaluation and hence some samples fall along and close to the boundaries of acoustic classes. This has an effect on the correlation of ground truth with the classes. Ideally, future applications should include more



ground truth samples from each classified area. Regarding the performance of the two acoustic classification techniques, we examine it in terms of correlation with grain size statistics and overall description of class extent. As shown in Table 3.3, the classification based on the PCA features expressed lower class correlation with grain size parameters whereas the Bayesian technique classes appear to correlate better. It is also clear from Table 3.3 that hierarchically the percentage of coarse grains, the mean grain size and the mode (the most frequent grain size in the sediment sample) rank in a descending manner for both classification approaches. The better performance of the Bayesian technique is attributed to the fact that the dB values for each of the acoustic classes are derived with an approach that can be considered model-based. The model consists of a sum of Gaussians with a mean and standard deviation that are determined by maximizing the agreement between the modelled histogram and the measured histogram of backscatter values. No model underlies the derived dB ranges per acoustic class in the PCA approach; it is purely data driven. Despite the differences in correlation coefficients, the two methods yielded classes of similar spatial extent.

*Table 3.3: Correlation coefficients for each type of classification and major grain size parameters.*

Classes	Coarse	Mean	Median	Mode	Combined*
PCA	0.5	0.53	0.4	0.48	0.6
Bayes	0.8	0.47	0.18	0.44	0.8

\*Combined result takes into account only the highest values, i.e. excluding the median and mode in both instances.

## Implications on classification resolution and fine scale habitat mapping

An important aspect of our study is that the Bayesian technique allowed producing a classification map of high spatial resolution with a 2x2 meters bin size (Fig. 3.7). The issue of spatial resolution in seafloor mapping has been addressed by earlier studies (Greene et al., 1999; Greene et al., 2007; Le Bas & Huvenne, 2009; Brown et al., 2011). McGonigle et al. (2009) support that in order for a habitat map to be useful for real world applications the scale of the data used for classification should at least match the scale of the mapped features. Greene et al. (2007) discriminate seafloor habitats in 4 major groups according to their spatial scale (Table 3.4). Currently, techniques based on backscatter acoustic mapping are able to provide classes at a fine spatial scale (Siemes et al., 2009; Siemes et al., 2010). These, however, still have to find their way into the area of habitat mapping. For example, regarding the meso- and macro-habitat studies, only little has been done yet regarding high resolution acoustic classification on this scale level (Kostylev et al., 2003; Durand et al., 2006; Savini et al., 2014). Often use is made of image/video mapping instead of acoustic classification. However, this includes manual or supervised classification that might come with a subjective error (Brown et al., 2011). In addition, it is difficult and more time consuming to obtain 100% coverage of an area with visual mapping.

Although fine spatial resolution can nowadays be achieved in unsupervised classification, there are still a number of items to be resolved. These are related mainly to the transition zones between sedimentary classes (Kostylev et al., 2003; Lucieer & Lucieer, 2009). In addition to the spatial resolution, also the degree to which the method can discriminate between different sediment types is of importance.

A significant improvement bridging the gap between spatial resolution and acoustic discrimination capability was done by Fonseca et al. (2009). They combined the high correlation of the ARA technique and ground truth data, with backscatter mosaics in order to gain better spatial resolution. In their approach they relied on discrete homogeneous acoustic units in the mosaic which were characterised by the ARA analysis. This however, suffers from the assumption that fine scale sedimentological features should also exist in broader scales in order to be resolved by the ARA. This is not always the case; for example it is typical that sand ripples (Fig. 3.11) with a wavelength of 1-10 meters in shallow water (10-15 m) can hold various grain sizes depending on current direction or changes in sedimentation. Hence, sediment variations on a meter scale cannot be resolved by the ca. 50 meters swath footprint that the ARA relies on in 10-15m water depth. As a consequence the ARA method is ideally applied when mapping coarser scales e.g.: mega-habitats.

The finer the spatial scale becomes (e.g.: macro- and microhabitats) the less within-habitat sediment heterogeneity exists. This means that modern techniques should be able not only to fully exploit the MBES spatial resolution, but also to discriminate rather small acoustic contrasts of different sedimentary seafloor units. In our example, seafloor features such as 5 to 10m wide trails of dumped oysters shells as well as sand ripple-scale variations could be resolved (Fig. 3.11). Acoustic variability of the oyster trails as captured by the Bayesian classification indicates that they express a variable degree of density within the dumping area. The variability of sediment types in the area of sand ripples can be explained by the fact that the area was a former estuary exposed to tidal activity. Following the establishment of the dam in 1971, the sand ripple troughs started to accumulate fine grained terrigenous material and phytodetritus in a gradual pattern based on the bathymetry (Fig. 3.11 lower). Consequently, this creates an acoustic contrast that is resolved by our classification technique. Because of our findings and as an analogous to spatial resolution we would like to introduce the term *geoacoustic resolution* to describe the scale at which different types of sediment can be resolved using a certain acoustic classification/characterisation technique. Key aspects of this concept are:

- 1) The backscatter measurements per beam; the beam footprint is in general at a scale relevant to seascape features.
- 2) The Gaussians (Fig. 4.3). They express the geoacoustic resolution in practice; the more separate the Gaussians are, the better the geoacoustic resolution.

The geoacoustic resolution can be measured in dB values and is related to the difference of the mean value between classes (Fig. 3.6). The within-class standard deviation of BS values defines the number of classes that can maximally be discriminated based upon the backscatter values and the range of each class. The smaller the resulting difference between the mean (central) BS values of each class the better is the geoacoustic resolution (given small standard deviation within class). The majority of literature includes regional seafloor mapping where MBES backscatter classification results can distinguish between major sedimentary facies with increased acoustic contrast (e.g. sand from gravel) but when

the transition from one sedimentary unit to the other becomes smoother in terms of grain size (e.g. silt to fine sand) the need for a higher geoacoustic resolution exists. The more similar (neighbouring) sedimentary classes an acoustic classification method can discern, the higher is its geoacoustic resolution.

Table 3.4: Major habitat types according to their spatial extent (from Greene et al., 2007).

Habitat	Dimensions	Map scale	Physiography
Megahabitat	a few km to 10s of km	$\geq 1:1000000$	Shelf, slope, abyssal plain
Mesohabitat	10s of meters to a few km	1:50000 - 1:250000	Semounts, canyons
Macrohabitat	1-10 meters	1:1000-1:50000	boulders, outcrops, reefs
Microhabitat	cm - 1 meter	up to 1:1000	individual reef, crevaces, cracks

A technique with increased geoacoustic resolution can provide valuable information about fine scale sediment dynamics and interactions of benthos with various grain sizes. This kind of information about fine scale sediment variability is crucial for habitat mapping at seascape scale and the geoacoustic resolution can be used as a measure of this achievement. According to our fine scale classification (Table 3.2) our geoacoustic resolution is high enough to discriminate different grades of silt mixed with sand, shells and shell fragments up to 25%.

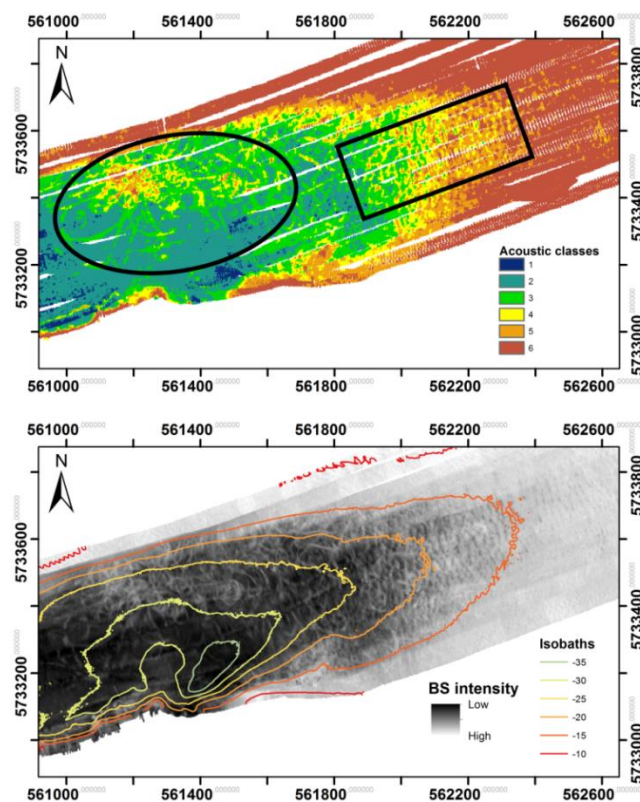


**Figure 3.11:**  
*Upper:* Acoustic classes with high geoacoustic resolution of fine scale sedimentary features such as trails of dumped oysters (ellipse) and sand ripples with low contrast in grain sizes due to terrigenous sedimentation (rectangle).  
*Lower:* Greyscale mosaic (2m bin) of backscatter intensities with bathymetric contours, to illustrate the comparability of acoustic classes above with fine scale seabed features

### 3.5 Conclusions

In this study we examined the capabilities of two unsupervised methodologies in acoustic classification of seafloor. Furthermore, we compared their results with grain size data in order to validate their performance. We can conclude that the Bayesian technique was more suitable for quantitative validation with ground truth given that it outputs acoustic classes that are related to dB values. We discovered that this method is capable to detect changes in relatively homogeneous sediments owed to minor fluctuations of the coarse fraction content. In addition, the produced acoustic classes express the effect of volume scattering. Another important finding is that the Bayesian technique provided acoustic classes for groups of neighbouring beams resulting in high spatial resolution of the final classification map. As a result we were able to resolve fine scale sediment variations of features such as dumped oysters trails and sand ripples.

These findings raise the necessity for discriminating sedimentary units with low acoustic contrast. Therefore we suggest the term geoaoustic resolution for describing the ability of an acoustic classification technique to resolve similar (neighbouring) sedimentary classes. We infer that mapping of macro and micro habitats requires not only high resolution MBES datasets but also processing techniques that better exploit these datasets and discriminate fine scale sedimentary features. Through high spatial and geoaoustic resolutions a map can inform decision makers on a scale comparable to that of the ground truth data.

This study demonstrates the efficiency of the Bayesian technique in discriminating fine unconsolidated sediments holding various percentages (up to 25%) of coarse-grained material (>500  $\mu\text{m}$ ). These types of sediment are comparable to pelagic sediments in terms of grain size composition. Hence we want to highlight the suitability of the method particularly for (AUV/ROV-based) deep sea studies where sediment sampling is significantly limited by time.

### Acknowledgements

We would like to thank the following people from the Royal Netherlands Institute for Sea Research (NIOZ), Prof. Filip Meysman and the captain and crew of RV Luctor for organising and ensuring the success of data acquisition surveys. Also we would like to thank Wim Versteeg (Flanders Marine Institute, VLIZ) for providing the underwater camera system for the surveys in July 2014. Additionally we would like to thank Rineke Gieles (NIOZ; Netherlands) and Dr. Christian Hass (AWI Sylt, Germany) for their support with grain size analyses.

#### 4. Multi-angle backscatter classification and sub-bottom profiling for improved seafloor characterization

This chapter was published in June 2017 in the Special Issue: “Seafloor backscatter from swath echosounders: technology and applications” of Marine Geophysical Research journal:

Alevizos E., Snellen M., Simons D.G., Siemes K., Greinert J., 2017, Multi-angle backscatter classification and sub-bottom profiling for improved seafloor characterization, Marine Geophysical Research , Special Issue "Seafloor backscatter from swath echosounders: technology and applications", pp.1-18, DOI:10.1007/s11001-017-9325-4

<b>Authors contributions (Elsevier standards)</b>	
Study conception and design:	Alevizos
Acquisition of data:	Alevizos, Greinert
Analysis and interpretation of data:	a) classification software development: Snellen, Siemes, Simons b) classification analysis and interpretation: Alevizos
Drafting of manuscript:	Alevizos
Critical revision:	Alevizos, Greinert

## Abstract

This study applies three classification methods exploiting the angular dependence of acoustic seafloor backscatter along with high resolution sub-bottom profiling for seafloor sediment characterization in the Eckernförde Bay, Baltic Sea Germany. This area is well suited for acoustic backscatter studies due to its shallowness, its smooth bathymetry and the presence of a wide range of sediment types. Backscatter data were acquired using a Seabeam1180 (180 kHz) multibeam echosounder and Sub-Bottom Profiler data were recorded using a SES-2000 parametric sonar transmitting 6 and 12 kHz. The high density of seafloor soundings allowed extracting backscatter layers for five beam angles over a large part of the surveyed area. A Bayesian probability method was employed for sediment classification based on the backscatter variability at a single incidence angle, whereas Maximum Likelihood Classification (MLC) and Principal Components Analysis (PCA) were applied to the multi-angle layers. The Bayesian approach was used for identifying the optimum number of acoustic classes because cluster validation is carried out prior to class assignment and class outputs are ordinal categorical values. The method is based on the principle that backscatter values from a single incidence angle express a normal distribution for a particular sediment type. The resulting Bayesian classes were well correlated to median grain sizes and the percentage of coarse material. The MLC method uses angular response information from five layers of training areas extracted from the Bayesian classification map. The subsequent PCA analysis is based on the transformation of these five layers into two principal components that comprise most of the data variability. These principal components were clustered in five classes after running an external cluster validation test. In general both methods MLC and PCA, separated the various sediment types effectively, showing good agreement ( $\kappa > 0.7$ ) with the Bayesian approach which also correlates well with ground truth data ( $r^2 > 0.7$ ). In addition, sub-bottom data were used in conjunction with the Bayesian classification results to characterize acoustic classes with respect to their geological and stratigraphic interpretation. The joined interpretation of seafloor and sub-seafloor data sets proved to be an efficient approach for a better understanding of seafloor backscatter patchiness and to discriminate acoustically similar classes in different geological/bathymetric settings.

## 4.1 Introduction

### Acoustic mapping of seafloor sediments

The applicability and effectiveness of multibeam echosounder systems (MBES) in mapping seafloor sediments has improved significantly in recent years. By characterizing the seafloor in terms of its geo-acoustic properties, several studies have mapped benthic habitats (e.g. Brown & Blondel, 2009; Brown et al., 2011). In general this approach exploits the affinity of benthic species for seafloor areas that exhibit certain sediment properties, particularly grain sizes or hardness of the sediment. These correlate to acoustic properties that correspond to particular backscatter intensity levels (Collier et al., 2004; Fonseca & Mayer, 2007; McGonigle & Collier, 2014). Other examples for habitat mapping using acoustic information are given e.g. in Blondel et al. (2006) who applied a multi-frequency approach to map deep sea corals; Ierodiaconou et al. (2007) combined video and image analysis with MBES data for mapping algae and invertebrate biotopes; Le Bas and Huvenne (2009) investigated various methods for processing acoustic data for benthic habitat mapping and Che-Hasan et al. (2012a,b and 2014) used Angular Response Analysis (ARA) for classifying the seafloor and link this to benthic habitats.

Additionally to studies using seafloor backscatter, others integrated backscatter with sub-bottom profiling (SBP) data as an approach for seafloor characterization. Sweeney et al. (2012) utilized MBES backscatter and high resolution CHIRP data for interpreting a low backscatter feature on the New Jersey (USA) continental margin, whereas Fakiris et al., (2014) combined side-scan sonar data with 3.5 kHz SBP data for benthic habitat mapping in the Lourdas Gulf (Greece). Siemes et al. (2010) used sub-bottom profiler data to investigate the reason for high seafloor backscatter data in areas with very fine sediment. The SBP data indicated the presence of gas in the area, which increase the measured seafloor backscatter strengths. Another example is given by Schneider von Deimling et al. (2013) who applied ARA on low frequency MBES data in conjunction with SBP data for identifying gas layers in the sediment of Eckernförde Bay (Germany). This shows that MBES and SBP datasets can complement each other for a better seafloor and sub-bottom property understanding. Acoustic seafloor classification results can be characterized further by correlating them to ground truthing but also SBP data if sub-seafloor reflectors have an expression on the seafloor, i.e. are partially exposed.

### Objectives

This study investigates the usefulness of within-angle and between-angle variability of MBES backscatter values for seafloor classification based on MBES backscatter data derived from high density seafloor soundings. We apply a Bayesian probability method on backscatter values for each incidence angle and we compare its results against classification results based on multi-angle backscatter layers using Maximum Likelihood Classification (MLC) and Principal Components Analysis (PCA). The Bayesian method uses the backscatter measurements per beam and classifies sediments at the resolution of the average beam footprint. Information about the backscatter angular response is not directly used; however the angular dependence (influence of the grazing angle) of the backscatter must not be removed from the data. In contrast to that, the traditional Angular Response Analysis (ARA)

matches the measured angular responses to a set of modelled angular response curves by varying the model input parameters until a maximum match is obtained. Traditional ARA results show only low spatial resolution since in most cases ARA is based on a fit of half of the swath of the MBES. In addition absolute backscatter strengths and thus well-calibrated MBES systems are needed for these backscatter measurements. In practice, backscatter measurements are often subject to imperfect calibration.

To counteract these drawbacks, we propose using empirical ARA (Beyer et al., 2005). This method is not dependent on absolute backscatter measurements and uses seafloor patches that are significantly smaller than half the swath width, which is considered a novelty in the field of backscatter processing and interpretation. The empirical ARA is based on stable, but not absolute backscatter measurements and is applied as an alternative to traditional ARA because of its insensitivity to systematic biases (Lurton & Lamarche, 2015) and thus offers better backscatter processing opportunities for seafloor classification. Hughes Clarke (1994) and Parnum (2007) highlight the necessity that data for ARA should ideally be derived from small scale homogeneous patches of the seafloor to better resolve sediment differences. The strategy most often used to maximize class separability in traditional ARA studies is to combine them with backscatter mosaic segmentation results (Fonseca et al., 2009; Che-Hasan et al., 2012a,b; Rzhano et al., 2012). Angular responses derived from segments representing homogeneous acoustic types are assumed to provide better discrimination capability. However, segmentation of backscatter mosaics relies on subjective settings selected by the user which has at the end implications for the selection of soundings belonging to a segment specific ARA response. In this study, we set the minimum dimensions of seafloor patches for extracting the ARA to 5x5 meters assuming that within these patches sediment variability is minimal/not existing. This selection is justified by the high density of soundings per seafloor unit.

By comparing the performance of the different backscatter classification approaches we aim to test their suitability in resolving a wide range of sediment types using only the raw backscatter data and their angular dependence. Classification results are being assessed and characterized using grain size and SBP data.

## 4.2 Methodology

### Study area

Eckernförde Bay (Eck Bay) has a diverse marine ecosystem and has in parts assigned a Site of Community Importance (SCI) under the Nature 2000 habitats directive. The study area has two basins with maximum depths of 20 to 30 m separated by the Mittelgrund area, a local elevation feature with a minimum depth of 8 meters. Approximately 99% of the slope values in the entire area range between 0-5 degrees, which translates into a smooth seafloor morphology. The entire area shows a high variability of sediment types, ranging from coarse sand with pebbles and boulders to silty clay. According to Jensen et al. (2002), Mittelgrund represents a relict morainic sill and is composed of glacial and marine sediments with variable thicknesses; predominantly Mittelgrund consists of glacial till and sands (Jensen et al., 2002).



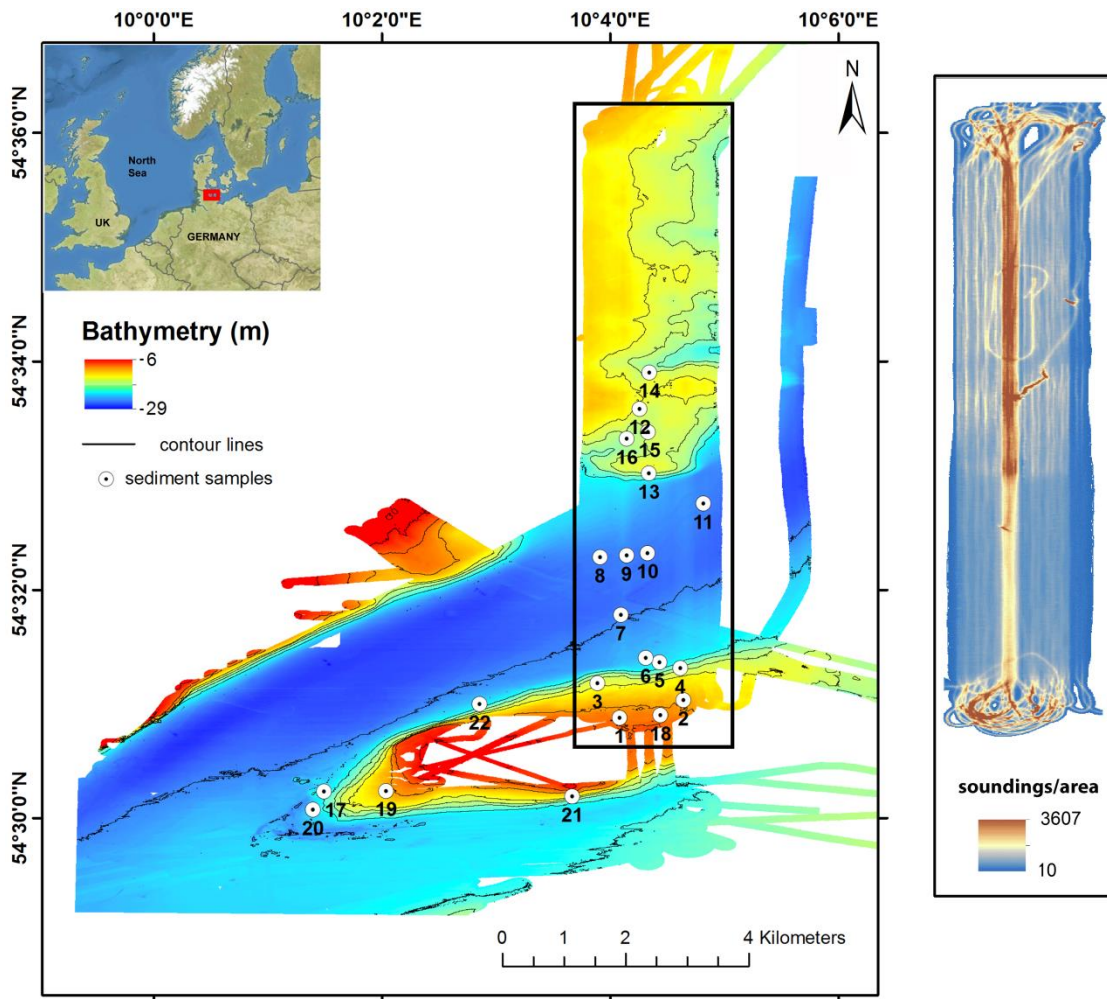


**Figure 4.1:** Overview map of the study area with bathymetry and contours, sediment samples locations, and the high density line-spacing survey (black rectangle). Soundings in the legend of the right image refer to a 5x5 meter area.

Earlier geological, geochemical and geophysical studies in the area showed that the marine continuation of a glacial sand aquifer is responsible for freshwater seepage at places where the overburden sediments are not sealing due to coarser grain sizes (Jensen et al., 2002; Müller et al., 2011). Whiticar (2002) realized that the presence of pockmarks in Eck Bay is caused by this freshwater seepage and not, as suggested for several other pockmarks, by methane ebullition (Hovland & Judd, 1988). In general, the southern part of the bay is formed by an incised channel filled with sediments of several meters of thickness whereas the northern part of the bay holds sediments with a vertical extent that could not be determined by the performed sub-bottom profiling because of gas blanking with free gas accumulating one to two meters below the seafloor (see also Jensen et al., 2002). The deeper parts of the bay contain finer sediments (mainly silt) under highly anoxic geochemical conditions due to high organic matter concentrations (Whiticar, 2002). Nittrouer et al. (1998) and Bentley et al. (2002) described the fine-scale stratigraphy of the deeper parts as areas in which most of the sediment consists of pelletized layers between 1 and 10 cm thickness alternating with slightly coarser (10% silt-sand) storm layers. Consequently, the study area contains a broad spectrum of seafloor sediment types, which

in conjunction with the smooth seafloor bathymetry offers a unique opportunity for dedicated MBES backscatter studies.

## Multibeam data

The study area was surveyed by MBES between 2012 and 2015 onboard RV Alkor and RV Littorina. On both vessels, an ELAC Seabeam 1180 MBES was used operating at 180 kHz. The surveys mainly covered the wider area of Mittelgrund whereas towards the west the data get sparser. In particular the 2012 surveys covered a narrow 1x10 km corridor from the northern part of Mittelgrund to the northernmost coast of Eck Bay with a dense line spacing (20-50 m) as part of a 3D seismic survey. This survey plan yielded dense soundings per seafloor area for various incidence angles (Fig. 4.1). The MBES data were corrected for sound speed and tidal effects using the ELAC-HDPPost software. The complete processed data were exported as ASCII data for further analyses in GIS software packages. In addition raw backscatter data for each beam were extracted from the sonar files. They were used for acoustic classification using two unsupervised and one supervised methodologies; these are described below. The bathymetry grid and the backscatter mosaic of the area were generated using a 2 by 2 meters cell size.

## Bayesian unsupervised classification based on individual beam angles

The raw backscatter data were processed in Matlab using the unsupervised Bayesian classification technique developed by Simons & Snellen (2009) and Amiri-Simkooei et al. (2009). This technique is based on the central limit theorem; applied to backscatter analysis, this means that the backscatter intensities of a specific type of seafloor will have a Gaussian distribution when examined at a single beam angle or a number of adjacent beam angles. This technique fits a number of Gaussian curves to the histogram of backscatter values recorded for the beam(s) under consideration over the entire study area. For areas with more than a single sediment type, the total backscatter histogram can be approximated by a number of Gaussian curves, each Gaussian corresponding to a certain sediment type. To find the number of Gaussians that are minimally needed to obtain the best possible agreement between the measured and the modelled histograms, the  $\chi^2$  criterion regarding the best fit to the entire histogram is considered. The minimum number of Gaussian curves that satisfy the  $\chi^2$  criterion, represents the optimum number of classes that can be discriminated based on the backscatter response (Amiri-Simkooei et al., 2009; Siemes et al., 2010; Snellen et al., 2013). For determining this number, outer beams at about 40° incidence angle are considered because the number of scatter pixels in the beam footprint is high, resulting in the best possible discrimination of sediment types. The derived number of Gaussian curves is then used to fit the histograms for all other incidence angles. Based on the resulting fits, acceptance regions of backscatter values are obtained for each incidence angle (or set of adjacent beams grouped as 'one' incidence angle) by applying the Bayes decision rule for multiple hypotheses. Each acceptance region corresponds to a certain acoustic class. The main advantages of this technique are: 1) that no absolute sonar

calibration is needed, 2) that it accounts for ping-to-ping variability, 3) that it can resolve different seafloor characteristics along the swath and 4) that it performs a statistical control on the optimal number of seafloor classes. A detailed description for applying the Bayesian approach to classify soft sediments can also be found in Alevizos et al. (2015). The final class assignment is performed for each beam and results can be exported as ASCII files and further analysed in GIS software packages.

## **Empirical Angular Response Analysis and MLC based on angular layers**

The angular dependence of seafloor backscatter varies with the physical properties of the substrate (Fonseca & Mayer, 2007) and this has been used in many studies providing semi-quantitative information on surficial sediment properties (Beyer et al., 2007; Lamarche et al., 2011; Rzhanoz et al., 2012; Huang et al., 2013). Although methodology constitutes a robust and physical model approach, it tends to lack sufficient spatial resolution when applied to most MBES datasets. Since half of the sonar swath is usually considered as a single measurement for ARA, the resulting classification patches are at least a few tens of meters in size, even in shallow water (in 10m water depth half of a 130° wide swath is 22m).

In addition, the traditional ARA approach requires MBES calibration. In the literature, approaches have been presented to compensate for these drawbacks; empirical approaches have been examined (Beyer et al., 2007) and strategies have been suggested to improve the spatial resolution of ARA (Fonseca et al., 2009). In this study, we follow an alternative approach that exploits the high sounding density of the used MBES surveys (Fig. 4.1) for extracting and utilizing the backscatter angular dependence without losing spatial resolution. The high density of the seafloor ensonification in most of the study area allowed the extraction of angular backscatter measurements from selected 5x5 m seafloor patches (training areas) which are assumed to have a homogeneous sediment cover. Each of these patches includes several hundreds of evenly spaced soundings (Table 4.1, appendix for chapter 4). The selection of seafloor patches was based on existing ground truth data (sediment samples) and the results of the Bayesian classification (Fig. 4.2). The high geo-acoustic resolution of the Bayesian approach (Alevizos et al., 2015) produces acoustic classes that discern minor differences between similar sediment types. In this regard, each extracted angular profile has a unique geometry representing different types of sediment (Fig. 4.2, Table 4.1 appendix for chapter 4).

Instead of the traditional ARA, where the full measured angular profile is used for a fit with a modelled angular profile, here we use the empirical ARA. The scheme for the resulting supervised acoustic classification was developed analogous to multispectral imagery classification. The measured backscatter intensity was gridded into individual layers, using the Inverse Distance Weighted (IDW) algorithm on the data points from individual beams at 20, 30, 40, 50 and 60 degrees of beam incidence angle (Fig. 4.2). In the end, five angular backscatter intensity layers with 5x5 m grid cell size were produced for the same area with small differences in overlap due to variable beam coverage. These layers were classified using the Maximum Likelihood Classification (MLC) algorithm implemented in ArcMap. The MLC considers that backscatter intensity values of a certain seafloor type

follow a Gaussian distribution. This applies for most of our training sample data (Table 4.1, appendix for chapter 4) given that they are derived from local homogeneous areas.

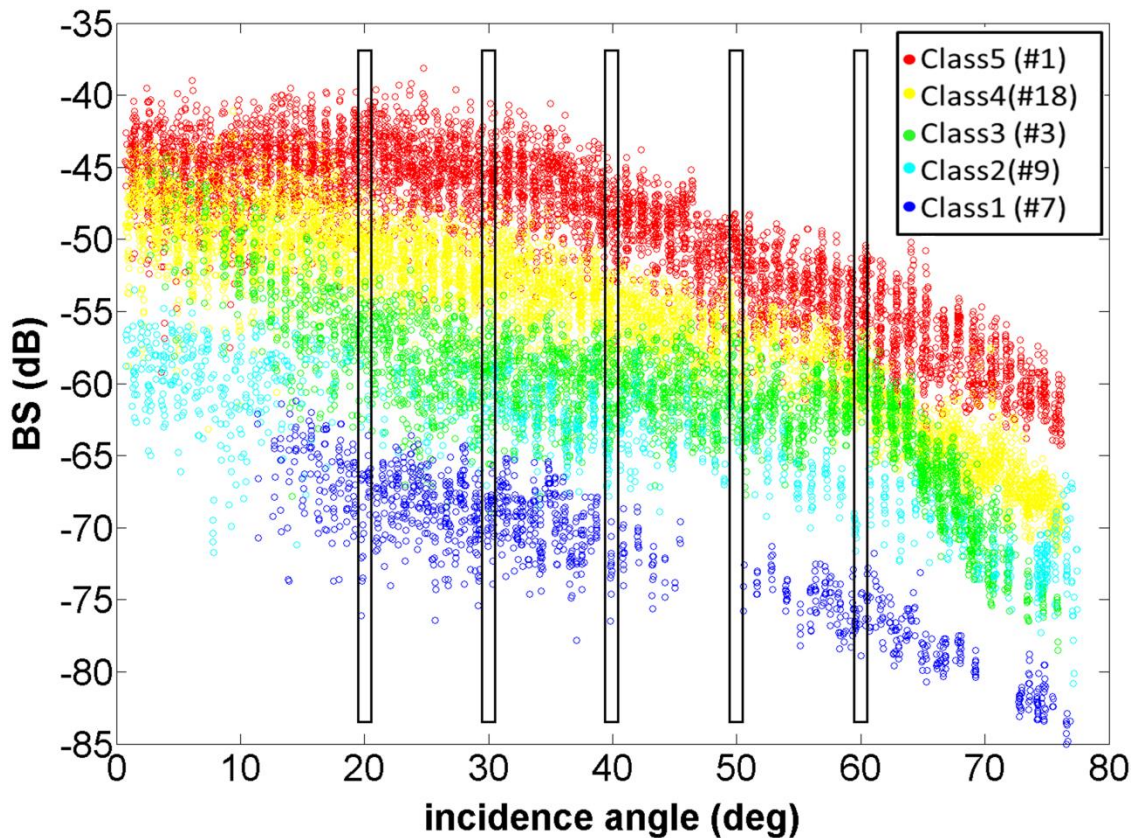


**Figure 4.2:** Angular responses plot of selected 5x5 m patches belonging to different acoustic sedimentary classes. Ground-truth sample number in brackets indicates from which locations the patches were extracted. These were used as training areas (a priori knowledge) for the MLC. Black rectangles indicate the selected angles for producing the angular layers.

The MLC algorithm is commonly used for multispectral satellite image classification and is also applied in seafloor mapping. Erdey-Heydorn (2008) and Calvert et al. (2014) applied MLC in order to classify benthic habitats using multiple layers of bathymetry, bathymetric derivatives and backscatter data. The supervised approach chosen in this study is similar to the approach described in Che-Hasan et al. (2012b) who used 71 individual angular response layers with a set of supervised algorithms including the MLC. They considered half of the sonar swath for the ARA whereas in this study angular data from 5x5 meters patches from training areas are used in the MLC as a priori knowledge.

Because data acquisition in 2012 and 2014-2015 took place with different sonar configurations, we performed a comparison before classification. The comparison (Fig. 4.3) was based on separate examinations of soundings from two seafloor patches (5x5 meters) with different sediment types that have been surveyed in 2012 and 2014-2015. These two patches were the only places sufficiently ensonified during all previous surveys. Although using two patches only may not be sufficient for statistical assessment of all ground truth locations, they provide an indication regarding the stability of the backscatter

measurements over the different years and surveys. After validating the backscatter stability for two different seafloor types (gravel and sand) we hypothesize that the stability also holds for other seafloor types in the study area.

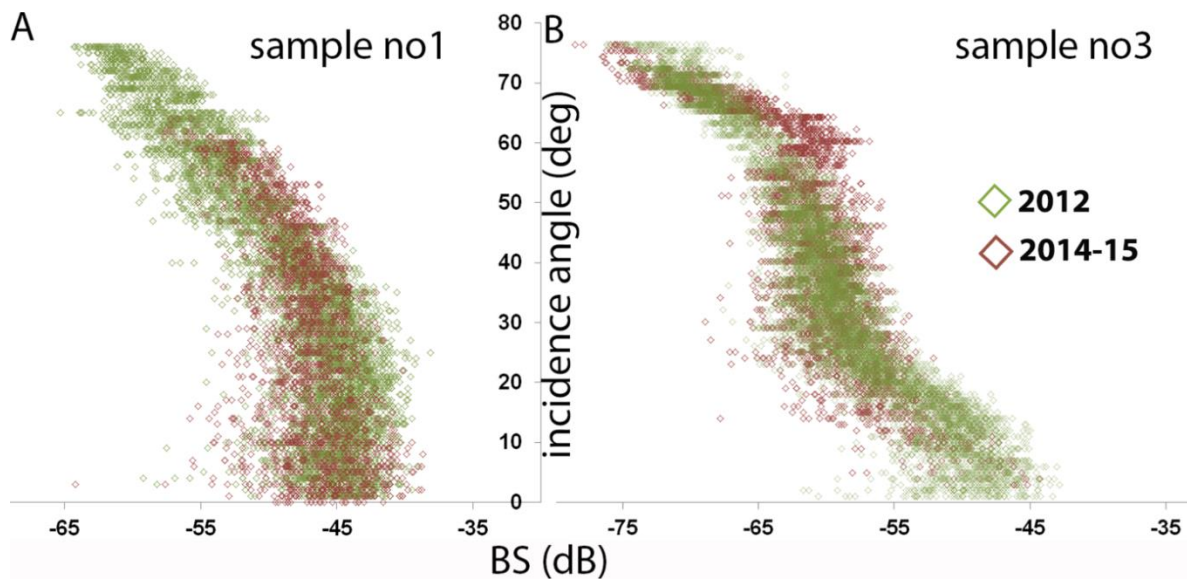


**Figure 4.3:** Comparison between soundings from seafloor patches at sediment sample locations investigated during different surveys (2012 mobile SeaBeam 1180 on RV Alkor; 2014-2015 fixed installed SeaBeam 1180 on RV Littorina).

## Principal Components Analysis using angular layers

This method is derived from satellite image analysis and allows for utilizing a dimensionally reduced dataset (fewer layers of information) to describe the data variability in a more effective way. The basic concept is to use a set of spatial layers as input and transform them into a new uncorrelated set of layers via orthogonal linear transformation of the initial set of layers. The transformed layers are fewer in number and represent an ordinal set of principal components. The first two principal components often account for the maximum in data variability and thus can be classified using a standard clustering algorithm such as k-means. The principal components do not contain the clusters themselves, but their combination has the potential for producing clustering patterns.

Before the use of k-means, a cluster validation test is performed to estimate the optimal number into which the principal components can be clustered. The Principal Component Analysis (PCA) has been repeatedly applied for seafloor classification using acoustic datasets. One example is the study of Preston (2009), who applied PCA to a set of textural layers produced from MBES backscatter. Other examples are from Amiri-Simkooei et al. (2011) and Eleftherakis et al. (2014), who applied PCA to a set of MBES bathymetry derivatives and backscatter statistics to discriminate riverbed sediments. In the present study we apply PCA to the set of five MBES backscatter angular layers described above and use the first two principal components in conjunction with the k-means clustering algorithm to classify the seafloor. Cluster validation was performed using the C-H criterion (Calinsky & Harabazr, 1974).



## Sub-bottom profiler data

A sub-bottom-profiler (SBP) survey in 2015 was designed to cover areas with variable seafloor backscatter responses seen in previous MBES surveys. The SBP survey was run with a SES-2000 system (Innomar) recording 12 kHz and 6 kHz simultaneously with the Innomar SIS<sup>®</sup> software. The system was mounted at the side of the vessel on a stable pole. The acquisition occurred during good weather conditions; in total 25 km of SBP data including two profiles along the minor and major axes of the Mittelgrund were acquired (Fig. 4.4A). Pre-processing included applying a bandpass filter along with stacking and smoothing based on two consecutive traces for data enhancement and gain adjustment. In another step, the bottom reflector, the acoustic basement reflector, and the top of an acoustic turbidity reflector were digitized and exported for further analysis using Fledermaus 3D viewer. The term 'acoustic basement' is here referred to as the continuous reflector beyond which the acoustic signal does not penetrate any further. The digitized reflectors were further analyzed using ArcGIS and EXCEL. In particular, we used the SBP navigation to extract the depth and acoustic class information from the Bayesian classification results for the two along and across Mittelgrund SBP lines (Fig. 4.4A). Visual interpretation of the sub-bottom was enhanced by draping the classification results on the SBP profiles.

## Sediment grain size analyses

Sample locations were selected by visual examination of the processed backscatter map (Fig. 4.4A) and acoustic classification results, with the aim of sampling as many different acoustic classes as possible for a robust validation. In total, 22 sediment samples were collected using a Van-Veen grab and a multi-corer. The samples were weighed and separated with 500 $\mu$ m, 2mm and 6.4mm sieves. The fine fraction <500 $\mu$ m was measured using a laser particle analyzer (Analysette-22 NanoTec, Fritsch<sup>®</sup>). We extracted the median and mode of each, the fine and total fractions and integrated the results of the particle analysis with the weight of the sieved fractions. This was achieved by converting the grain sizes of the fine fraction into weight assuming spherical particles.

## 4.3 Results

Backscatter analysis with the Bayesian approach indicates the existence of five acoustic classes (AC1-AC5, Fig. 4.4B,C). It is noteworthy that an intrinsic feature of the Bayesian classification is that it outputs sequential classes; here this means that an increasing class number represents increasing backscatter intensity. Based on this we correlated the Bayesian classes against the derived grain size parameters (Table 4.2). Bayesian classes were also used for comparison with the classification results of the other two approaches and for the interpretation of the SBP data.

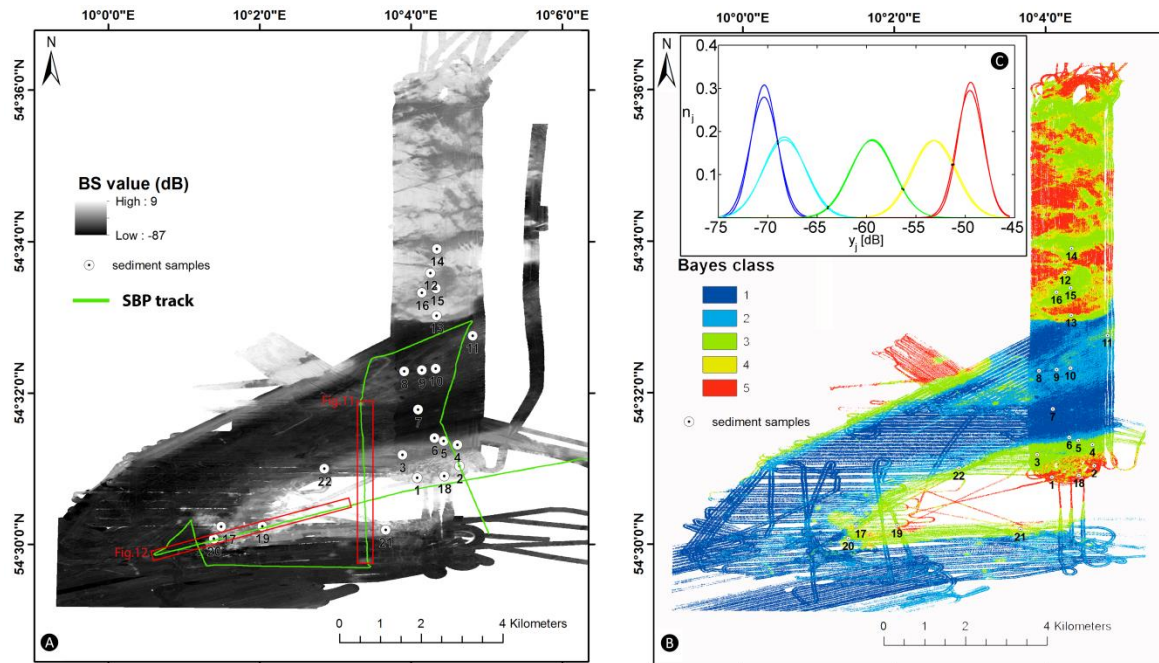


**Figure 4.4:** **A)** MBES backscatter mosaic of the study area (2012-2015 surveys) with sediment sample locations and SBP track lines (green). Red rectangles enclose the SBP profiles shown in the corresponding annotated Figures. **B)** Bayesian unsupervised classification map with locations of sediment samples. **C)** Density functions fitted to the MBES backscatter raw data from beams with incident angles 38 and 40 (port side) representing five major acoustic classes (curves are color-coded for their respective classes). Black squares indicate the intersection points of adjacent curves.

## Bayesian classification and correlation with ground truth data

The Bayesian method yielded five classes, expressed by Gaussian distributions holding a central dB value (Fig. 4.4C). The number of classes resulted from applying the  $\chi^2$  criterion for the Probability Density Functions (PDFs) fitted to the backscatter histograms of beams with incidence angles of  $38^\circ$  and  $40^\circ$ . Using these two neighboring beams simultaneously for class validation, the robustness of the optimum number of classes is increased with better  $\chi^2$  values and a better separation of the fitted PDFs (Fig. 4.4C). The suitability of incidence angles from the middle range of the swath is related to the significant different backscatter behavior of different sediment types in this range of incidence angles (for further explanation, see Discussion paragraph). The geo-acoustic resolution of the Bayesian classification (Alevizos et al., 2015) made it possible to map storm deposits within the upper ten centimeters of clayey/muddy sediment in the central area of the northern deep part of the Eckernförde Bay (samples 9, 10, 11, Fig. 4.4B) as the two separate acoustic classes AC2 and AC3. In general the sediments in the northern deep part have been described by Nittrouer et al. (1998) and Bentley et al. (2002) as sediments consisting of pelletized layers between 1 to 10 cm thickness alternating with slightly coarser storm layers (10% silt-sand).

Acoustic classes AC2 and AC3 (sediment samples 9 and 11) show only a small increase in coarse material (0.5 – 4 %) within a generally fine grained matrix (Table 4.3, appendix for chapter 4). We interpret these as storm deposits in which the coarse fraction produces the slightly stronger backscatter in the central deep part of the bay.

In an additional step, each class was correlated with different parameters of the grain size results (median, mode, and coarse fraction percentages, see Table 4.2) validating the acoustic clustering. In particular the percentage of the coarse sand fraction (2mm-500 $\mu$ m) along with the mode and the median grain size of the fine fraction (<500 $\mu$ m) show high correlation coefficients with the five classes (Table 4.2). However, the lower the class number (lower dB values) the greater is the ambiguity (class overlap between classes 1 and 2 in Fig. 4.4C).

*Table 4.2: Pearson's correlation coefficients for linear regressions of acoustic classes with grain size parameters.*

Grain size parameter	Correlation coefficient
median (<500 $\mu$ m)	0.71
mode (<500 $\mu$ m)	0.73
2mm-500mm percentage	0.75
6.3mm – 2mm percentage	0.67

## ARA-MLC and PCA classification using multi-angle layers

The MLC algorithm used the angular information from soundings of homogeneous training areas (Fig. 4.2). The data of these training samples partially satisfy the basic assumption of the MLC concept that a particular sediment type expresses a normal distribution of backscatter values (Table 4.1, appendix for chapter 4). Only samples from classes AC1 and AC2 show a different distribution, but these classes also hold much fewer data points. During the MLC processing, the mean vector (Fig. 4.5B) and the covariance matrix of all angular layers are estimated from the training set. This information is then used for assigning classes to the rest of the data.

The clear separation of the angular backscatter response curves in Fig.4.5B enhances the performance of the supervised classification, hence minimizing class overlap. The small standard deviation for class AC1 and AC4 might be responsible for the small areas assigned to these classes. It was found that AC4 occupies more small patches compared to the results of the two unsupervised methods (Fig. 4.5A, B) and shows a more abrupt transition from AC5 to AC3, particularly in the northern part of the bay. Data gaps in the final ARA-MLC classification map are due to unclassified pixels that did not hold sufficient overlap with all angular layers. The PCA results were clustered in five classes (as derived from the C-H criterion) using the k-means algorithm (Fig. 4.5C). Figure 4.5D shows these five classes in which the first two principal components of soundings from the 5 x 5 m patches of all sediment sample locations are plotted. The k-means clustering of the PCA results produced classes without ordinal character. It was observed that the spatial extent of each class corresponds very well with the spatial extent of the Bayesian classes that are ordinal. Hence the PCA and k-means classes were reclassified to correspond to the Bayesian ordinal classes order.



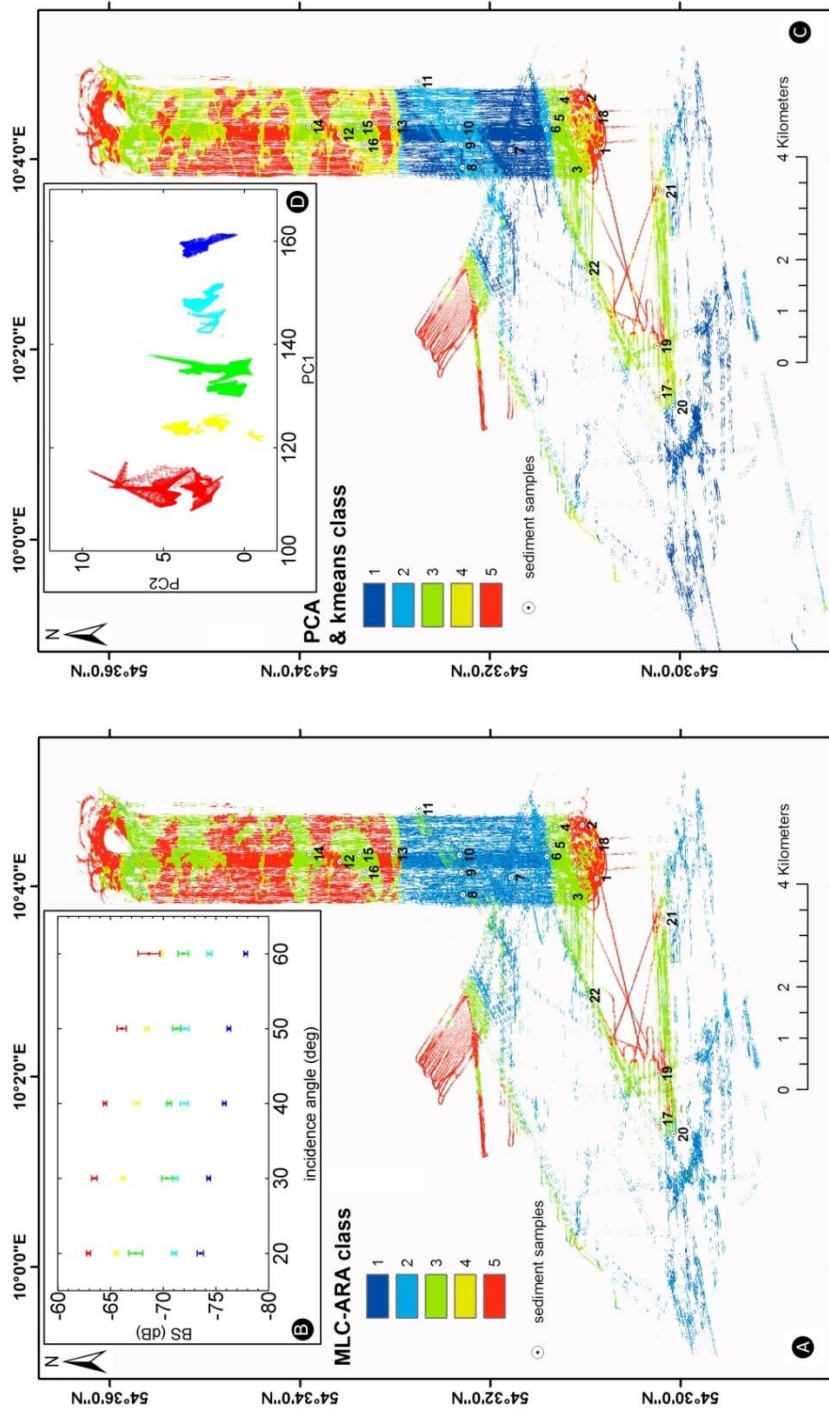


**Figure 4.5:** **A)** Classification map of the supervised ARA-MLC method with locations of sediment samples, **B)** Angular mean and standard deviation of backscatter values for each class of the training sample soundings. These data were derived from the “signature file” produced in ArcMap that is used by the MLC algorithm for assigning classes using the angular layers 20-60 degrees, **C)** Classification map of the PCA method clustered with the k-means algorithm including locations of sediment samples, **D)** Scatterplot of the first two principal components of soundings from all sediment sample locations. PC1 and PC2 resulted from the combination of five angular layers.

## Acoustic class description and sub-bottom interpretation

SBP data show an acoustic basement with a continuous high-amplitude reflector. The depth of this reflector is lowest on top of Mittelgrund where it corresponds to the seafloor surface; it increases to 1-2 meters along its slopes and rapidly deepens with increasing distance from the Mittelgrund (Fig. 4.6A). It is not possible to track the acoustic basement in the northern part of the bay because of gas blanking (Fig. 4.6A, symbol *g*), but we assume that acoustic basement lies several meters below the fine-grained sediment cover. Interpretation of the SBP data is supported by the Bayesian acoustic classes that correspond

with the proximity of the acoustic basement to the seafloor (Fig. 4.7, Table 4.4); the shallower the depth of acoustic basement, the higher the backscatter intensity. This is rather related to geological factors and not to the limited (<10cm) penetration of the high frequency (180 kHz) acoustic signal (Ferrini and Flood, 2006). Three distinct acoustic layers can be identified between the seafloor and the acoustic basement. The uppermost acoustically transparent layer of 0.5 – 1 meter thickness is found along the southern and northern flanks of Mittelgrund (Fig. 4.6A). Directly below, a 0.5 to 1m thick layer with chaotic reflectors can be observed. This layer reaches the seafloor mainly on the shoulder of Mittelgrund, where it is locally covered by the uppermost acoustically transparent layer (Fig. 4.6A, enlargement).

Table 4.4: Summary sedimentological and acoustic description of the Bayesian classes (mbs: meters below seafloor).

Bayes class	Central dB value	Backscattering factors	SBP units	% Coarse (>500µm)	Jensen et al., (2002)	Depth of acoustic basement (mbs)
1	-70.3	grain size	-	-	Littorina mud (with gas)	>>2
2	-68	grain size	-	<=1	Littorina mud (with gas)	>>2
3	-61	grain size, shells	uppermost transparent layer	1 - 4.1	Late Glacial sand (fine fraction)	0.5 - 2
4	-55.9	grain size, epibenthos, shells	chaotic layer, hyperbolae	15	Late Glacial sand (coarse fraction)	0 - 0.5
5	-50.9	grain size, epibenthos, shells	acoustic basement	>>20	<i>Subsurface:</i> Quaternary sand, <i>exposed:</i> Littorina sand & gravel / Till	0 ( or few cm)

Away from Mittelgrund, a more than two meters thick layer with parallel reflectors covers the northern and southern basins of the bay. In the north, this layer is blanked by free gas accumulations approximately 2 meters below the seafloor (Fig. 4.6A symbol *g*). Apart from continuous reflectors, sparse or dense hyperbolic reflectors were found as the uppermost acoustic layer in the westernmost part of Mittelgrund (Fig. 4.6B enlargement, symbol *h*). When overlaying the Bayesian acoustic classes on the sub-bottom profiles, AC3 mostly overlays the transparent uppermost layer on the Mittelgrund flanks (Fig. 4.6A, B). AC4 corresponds with the outcrop of the chaotic reflector layer at the southern flank of Mittelgrund (Fig. 4.6A). Away from the flanks, AC4 corresponds to hyperbolic reflector layers (Fig. 4.6B, symbol *h*). It is assumed that AC5 (highest backscatter intensity) covers a large portion of the shallowest part of Mittelgrund, which mainly consists of glacial till. There is no layering visible in the SBP data from this area due to the very hard reflection at the seafloor surface (Fig. 4.6A, B). It should be noted that AC3 away from the Mittelgrund also appears as patches within AC2 (Fig. 4.4B, 4.6A). AC1 covers the deeper parts of the area and locally alternates with AC2. The top of the acoustically opaque layer in the

northernmost part of the profile is highlighted in Fig. 4.6A. In the southern part, acoustic blanking occurs only locally in the deeper part of a paleo-channel (Fig. 4.6A).

In the following we present the characteristics of each Bayesian class along with their relationship to SBP interpretations and ground truth data following Folk's sediment classification (Folk, 1954):

**Acoustic class 1 (AC1) mud/clay:** According to two ground-truth samples this class represents the top of anoxic mud and clay deposits covering mainly the deep parts of the study area, where thick (> 2 meters) sediment accumulations exist with parallel reflectors in SBP data (Fig. 4.6A).

**Acoustic class 2 (AC2), gravelly/sandy mud:** Based on grain size analysis of five samples, this class represents muddy and clayey sediment, similar to AC1, but holds a small percentage (< 1%) of coarse grained material (including clasts, shells and shell fragments). This class is mainly found in the deep basin of the bay and at the foot of Mittelgrund.

**Acoustic class 3 (AC3), sand:** According to nine samples, this class consists of at least 80% fine sand (Table 4.4) with varying percentages (1-20%) of coarse sand and a small amount (<1%) of gravel-sized particles. Seafloor patches of this class are found in the deep basin, on the flanks of the Mittelgrund and within the pockmarks SW of Mittelgrund (Fig. 4.4B). According to the SBP data interpretation (Figs. 4.6A, B) class AC3 is characterized by the presence of a thin (up to 1m) transparent acoustic layer on both the northern and southern flanks of Mittelgrund. Grab samples from this class consistently recovered bivalves (*Macoma balthica*, *Astarte sp.*), numerous tubes of *Pectinaria* worms and several *Ophioura* specimens. This indicates that the backscatter character of AC3 might also be affected by the presence of macro-benthos.

**Acoustic class 4 (AC4), gravelly sand:** Sediments of this class (four samples) include a moderate amount (5-30%) of coarse sand, a small amount of gravel (1-8%) as well as shells and occasionally pebbles in a medium sand matrix (>50%). This class is related to a thin layer of chaotic reflectors outcropping at the southern part of Mittelgrund (Fig. 4.6A,B) and to the presence of hyperbolic reflectors at the westernmost slope of Mittelgrund (Fig. 4.6B, symbol *h*).

**Acoustic class 5 (AC5) sandy gravel:** Two sediment samples of this class are characterized by the coarsest sediments recovered from the study area, consisting of 30-40% medium sand, at least 60% coarse sand and 2-14% gravel. Shells and pebbles are also present in the samples and we assume that the top of Mittelgrund corresponds to the exposed acoustic basement (Fig. 4.6A, B).

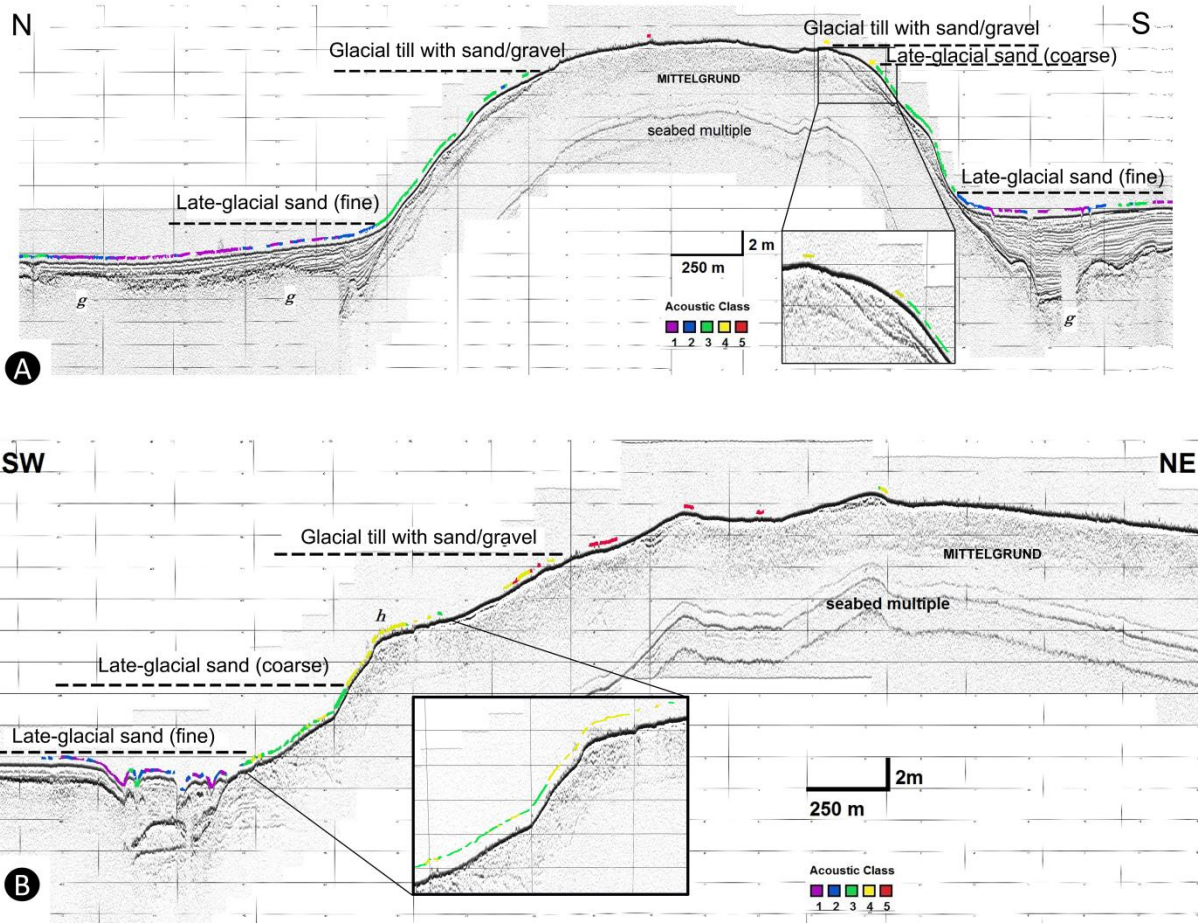


**Figure 4.6:** **A)** Sub-bottom profile (location on Fig.4.4A) crossing the minor axis of Mittelgrund. In the southern part the incised paleo-channel is clearly visible, filled with a well layered sediment package. In the northern part, gas trapped in the upper 1-2 m of sediment (g) prevents the signal from penetrating into the deeper sediment layers (Jensen et al., 2002). Acoustic class 3 dominates the Mittelgrund flanks, **B)** Sub-bottom profile (location on Fig.4.4A) along the western tip of Mittelgrund. Acoustic class 4 correlates to hyperbolic reflectors (symbol h, enlarged image).

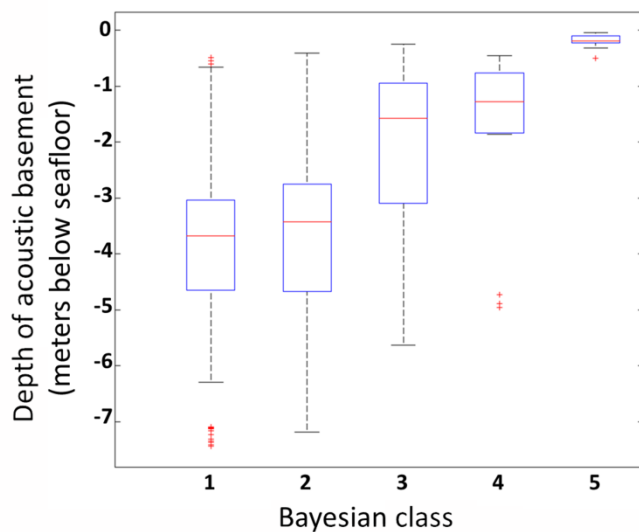


**Figure 4.7:** Boxplot illustrating the relation of Bayesian acoustic classes to the depth of the acoustic basement below the seafloor.

## 4.4 Discussion

### Angular response classification, comparison of single with multi-angle approaches

In this study we examine the within-angle and between-angles backscatter variability using different methods for defining seafloor acoustic classes with high spatial resolution. The Bayesian method is employed to estimate the optimum number of classes; this approach performs cluster validation before the final assignment of classes. This is an advantage compared to other unsupervised methods, which usually require some kind of external cluster validation tool (Verfaillie et al., 2009). However, the assumption of the Bayesian method—that the backscatter values within each seafloor type should have a Gaussian distribution—has been criticized because seafloor sediments or benthic habitats appear multi-modal by nature (Che-Hasan et al., 2012b). Sediment inhomogeneity in the study area is evident and different seafloor types can generate a similar backscatter response. For example, AC3 (sand) seems to be the same class as gravelly/sandy mud. The same is true for AC4; here the backscatter is the result of either boulders on the seafloor or coarse sediments from exposed layers. This ambiguity is also addressed in Eleftherakis et al. (2014). Therefore we suggest that combining various sensors such as MBES and parametric SBP along with sufficient ground truth data can offer a better discrimination of sedimentary classes.

In the study area the majority of the bathymetric surface has a slope of less than five degrees, so that no specific corrections of backscatter values are needed to account for the true grazing angle. This reduces pre-processing efforts considerably. The reference incidence angles used to drive the Bayesian classification lie in the mid-range of the MBES swath, this is in agreement with previous studies using the backscatter angular dependence (Lamarche et al., 2011; Hamilton & Parnum, 2011; Che-Hasan et al., 2014) and also with studies using the Bayesian approach (Alevizos et al., 2015). The selection of middle range beams is well suited for obtaining a realistic number of classes (best fit of five Gaussian curves according to the  $\chi^2$  criterion) and hence to reliably differentiate various seafloor types. The good performance of the Bayesian classification using incidence angles of  $38^\circ$  and  $40^\circ$  is also supported by Lamarche et al. (2011), stating that reliable backscatter measurements from angles closer to the nadir ( $<20^\circ$ ) are hindered by specular reflection that dominates the backscatter, whereas measurements in the outer range ( $>60^\circ$ ) are prone to strong angle dependencies and thus are less coherent.

Results from methods using angular layers (ARA-MLC and PCA) are compared to the Bayesian classification map which serves as reference, by examining their contingency matrices using Cohen's kappa as a measure of agreement. Usually contingency maps are produced by the combination of a classification map and a ground truth (reference) map for the same area. In this case the Bayesian classification map has the role of the reference map and is compared with the two multi-angle approaches. The relative agreement between the classes is assessed via the percentages of accurately classified pixels (Bayes\_acc, PCA\_acc and ARA-MLC\_acc; Table 4.5) for each method. For the PCA and ARA-MLC methods, PCA\_acc and ARA-MLC\_acc represent the respective percentage of pixels in agreement with the Bayesian class, while Bayes\_acc represents the reliability of this agreement. As an example from Table 4.5, 93% of the pixels classified as class AC1 by the PCA method are in agreement with the Bayesian results. As the Bayesian approach has 22% more pixels

identified as AC1, the Bayes\_acc value only gives 78% reliable agreement compared to the PCA classification for AC1. Additionally, the agreement between the three methods can be assessed using the classification results for each sediment sample location in Table 4.3 (Appendix). The contingency tables show that both the PCA and MLC approach produce comparable results with good agreement relative to the Bayesian method (Table 4.5). However, there are some fluctuations in the agreement between some acoustic classes. The highest overall agreement occurs between the unsupervised methods (Bayes and PCA). We observed that for classes AC5 and AC4, the PCA method generally agrees with the Bayesian approach, whereas there are minor differences regarding the percentage of pixels classified as classes AC1 to AC3 (Table 4.5). In contrast, the ARA-MLC approach shows a lower degree of agreement with the Bayesian map, particularly for classes AC1 and AC4. Despite these observations, the high Cohen's kappa values indicate that seafloor patches were classified consistently and that class assignments do not occur by chance.

The high sounding density allowed producing separate backscatter mosaics from selected angles. Between 20 to 60 degrees incidence angle there is little overlap between adjacent angular profiles, so beam angles from that range were selected to produce angular layers used by MLC and PCA. In this regard, the Bayesian classification was useful in quantifying the separation between the angular responses, hence maximizing the discrimination capability of the training set for the MLC. This highlights that Bayesian classification and ARA are a good complementary tool set. The Bayesian approach examines backscatter variability along a "narrow corridor" of middle range incidence angles quantifying the difference between angular responses in a statistically robust way.

The combination of empirical ARA with the MLC algorithm provides an automated sediment classification tool that depends on acoustic properties of the seafloor area under investigation. Sufficient ground truth information is required for both the classification and validation processes. In this study, applying empirical ARA to data from non-calibrated MBES was possible because the angular response profiles of the different sediments were sufficiently separated (Fig. 4.2, Fig.4.5B). The backscatter values for the areas of training samples 7 and 9 (for classes AC1 and AC2 respectively), are not normal distributed and considerably skewed (Table 4.1, appendix for chapter 4). The less good performance of the empirical ARA-MLC method for these two classes can be interpreted as a result of lack of normal distribution which is a prerequisite for the MLC method. Che-Hasan et al. (2012b) suggested that the MLC method does not work for sediments with a high degree of homogeneity. However, it has to be mentioned that they incorporated 71 different variables in their MLC, while it has been suggested that MLC is not suitable for data with high dimensionality and using only a limited amount of training data (Benediktsson et al., 1995).

Considering our data, it is not clear whether the low performance of the empirical ARA-MLC method is an algorithm shortcoming or if a poor data quality is the reason. Once more, if training samples with continuous angular backscatter responses can be used, the performance of the MLC for sediment differentiation can be more reliably evaluated. It is also suggested that future studies should make use of more than five angular layers in order to examine the capability of MLC to adequately classify (better discriminate) similar seafloor types.

The PCA and k-means approach, based on multi-angle layer information appears to discriminate the different sediment types in the study area efficiently (Fig. 4.5D). Although the five angular layers are highly correlated ( $r^2 > 92\%$ ), the resulting first two principal components are uncorrelated and describe more than 95% of the between-angle

backscatter variability. The spatial correspondence and agreement between the Bayesian and PCA classification maps can also be assessed by their contingency matrix.

Table 4.5: Contingency matrices showing the number of pixels classified and the relative accuracy percentages for the three methods (numbers in bold: Bayes\_acc, PCA\_acc, and ARA\_MLC\_acc).

Bayes and PCA (kappa=0.91)							
PCA map	Bayes map						
		Class 1	Class 2	Class 3	Class 4	Class 5	%PCA_acc
	Class 1	114642	9054	13	0	0	<b>93</b>
	Class 2	31990	64667	1769	2	0	<b>66</b>
	Class 3	109	8285	121610	27591	86	<b>77</b>
	Class 4	4	23	3607	62012	24605	<b>69</b>
	Class 5	0	2	13	5261	114517	<b>96</b>
	%Bayes_acc	<b>78</b>	<b>79</b>	<b>96</b>	<b>65</b>	<b>82</b>	
Bayes and MLC (kappa=0.76)							
MLC map	Bayes map						
		Class 1	Class 2	Class 3	Class 4	Class 5	%MLC_acc
	Class 1	41237	81878	592	0	2	<b>33</b>
	Class 2	26179	60997	11249	0	3	<b>62</b>
	Class 3	299	14081	134397	6182	2722	<b>85</b>
	Class 4	2	1843	15231	18247	54928	<b>20</b>
	Class 5	1	534	145	985	118128	<b>99</b>
	%Bayes_acc	<b>61</b>	<b>38</b>	<b>83</b>	<b>72</b>	<b>67</b>	

## Joint interpretation of sub-bottom structures and seafloor acoustic classes

Overlaying the Bayesian acoustic classes on SBP data and considering the results from Jensen et al. (2002) and Whiticar (2002) a good understanding of the wider Mittelgrund area stratigraphy can be supported. Acoustic class AC5 near Mittelgrund maps the exposed acoustic basement (Fig 4.6A,B) of glacial till or Littorina sand and gravel as described by Jensen et al. (2002) (Table 4.4). Other acoustic classes could be attributed to specific sub-bottom layers that pinch out at the seafloor, determining the seafloor backscatter (Table 4.4). Jensen et al. (2002) suggest that only one sediment type covers the glacial till on the Mittelgrund flanks, whereas the acoustic classification of this study could define two different seafloor types on the flank areas. These two classes (AC3 & AC4) can be linked to a finer and coarser fraction of Late Glacial sand as identified by Jensen et al. (2002). In this respect the layer with a chaotic character reaching the seafloor in the proximity of the Mittelgrund shoulder is related to AC4, representing the coarser fraction of Late Glacial sand (Fig. 4.6A, enlargement). AC3 which is related to the upper transparent reflector that covers large part of the Mittelgrund flanks probably represents finer material from Late Glacial sand deposits and seems to be an important substrate for the local benthic communities. Jensen et al. (2002) describe these deposits as laminated or massive fine sand and silt that



marks the transition into the basin. We assume that patches of AC3 in the deep basin (Fig. 4.6A) represent the coarser material of the storm deposits mentioned earlier (Nittrouer et al., 1998). AC3 also comprises the seafloor within the pockmarks SW of Mittelgrund (Fig. 4.6B) and vibrocore samples from within a pockmark in the same area (Jensen et al., 2002) confirm the existence of sand and gravel. Class AC1 can be simply characterized as Littorina mud (Jensen et al., 2002), but AC2 may be interpreted in two ways. Its occurrence at the foot of Mittelgrund is probably associated with deposits that are also characterized as Littorina mud whereas its appearance in the deep part of the basin possibly represents the finer fraction of sediments deposited during storms (Nittrouer et al., 1998).

Bayesian acoustic classes correlate with the maximum penetration depth of the SBP signal (the depth of the acoustic basement; Fig. 4.7). This paradoxical relationship between hydro-acoustic signals, with large difference in sediment penetration, highlights the connectivity of the two acoustic datasets in terms of their geological implications. It can be assumed that the depth of the acoustic basement is related to geological processes (e.g. transgressional erosion, sedimentation, reworking) that have taken place in the area and affect the coarseness of the surficial sediment. Accordingly, the variability in coarseness is reflected in the acoustic classification of the seafloor surface backscatter. It is inferred that areas with softer sediments allow a greater penetration of the SBP acoustic signal, which explains the relation between acoustic classes and acoustic basement.

## 4.5 Conclusions

Using gridded layers of MBES backscatter from various beam incidence angles proved useful for sediment class differentiation for both supervised and unsupervised approaches. These gridded layers were obtained from surveys resulting in high density soundings per seafloor area enabling to resolve acoustic classes in a higher spatial resolution than traditionally achieved. Single-angle analysis of raw backscatter data was performed using Bayesian statistics. This method performs cluster validation autonomously; the results correlated well with grain size analysis and provided a useful classification map for comparison with two multi-angle methods.

Combining multi-angle backscatter layers with empirical ARA-MLC gave promising results for discerning sediment classes at high spatial resolution. This is particularly interesting, as traditional ARA methods lack spatial resolution. The high density of soundings in the area supported the extraction of distinct angular backscatter responses from smaller seafloor patches; compared to other ARA studies described so far, the resulting maps are significantly more detailed. This is an advancement of the traditional half-swath and BS mosaic segmentation approaches, maximizing the between-class separation.

The applied empirical ARA method could be applied to uncalibrated sonar data once the extracted angular measurements were consistent for each seafloor class/type, and clearly separated from each other. PCA using multi-angle layers resolved the same number of classes as the Bayesian approach, highlighting the consistency of results between all three approaches. The incorporation of high resolution SBP data helped to characterize acoustic classes and added valuable information on the vertical and horizontal distribution of exposed stratigraphic layers. The acoustic classes representing fine sediments correlated with areas of a deeper SBP signal penetration. We can summarize that dense MBES backscatter measurements offer the advantage of extracting angular responses from fine-



scale seafloor patches without the need to perform backscatter mosaic segmentation. In this way, not only the spatial resolution of classification maps is improved but also the sedimentary classes are optimally separated. Future MBES survey planning may need to consider the acquisition of such high density of soundings per seafloor area, which would offer the possibility for accurate ARA-based seafloor classification on footprint-scale.

## **Acknowledgements**

We would like to specifically thank Sebastian Krastel (Institute of Geosciences, Christian-Albrechts-Universität, Kiel) and Christian Berndt (GEOMAR) for providing access to the MBES dataset collected in 2012. The SBP survey was supported by an Innomar Student Project which allowed us using the parametric SES-2000 sub-bottom profiler system with help by Peter Hümbts from Innomar. We would also like to thank, RV Littorina captain and crew, and Wärtsilä ELAC Nautik for providing a special pole for the SBP survey. Two anonymous reviewers are thanked as well as Dr. Geoffroy Lamarche for valuable comments and recommendations. We also thank Dr. Karin Meissner (Senckenberg) for providing the identification of macro-benthic organisms. Finally thanks go to Edna Hütten and Thomas J. Browning for providing valuable grammar and syntax corrections. This is publication 28 of the DeepSea Monitoring Group at GEOMAR.

## 5. Quantification of the fine-scale distribution of Mn-nodules: insights from AUV multi-beam and optical imagery data fusion

Part of this chapter has been presented at the GEOHAB 2017 (Halifax, Canada) conference:

Alevizos, E., Schoenning, T., Köser, K., Snellen, M., Greinert, 2017, Merging AUV-based multibeam and image data to map the small-scale heterogeneity of Mn-nodule distribution, GEOHAB 2017, Halifax, Canada, (oral presentation)

This chapter has been prepared in final form to be submitted for publication.

<b>Authors contributions (Elsevier standards)</b>	
Study conception and design:	Alevizos
Acquisition of data:	Greinert, Köser
Analysis and interpretation of data:	a) AUV image processing: Köser b) AUV image analysis: Schönning c) classification software development: Snellen d) classification analysis and interpretation: Alevizos
Drafting of manuscript:	Alevizos
Critical revision:	Alevizos, Greinert

## Abstract

Autonomous underwater vehicles (AUVs) offer unique possibilities for exploring the deep seafloor in high resolution over large areas. We highlight the results from AUV-based multibeam echosounder (MBES) bathymetry / backscatter and digital optical imagery from the DISCOL area acquired during research cruise SO242 in 2015. AUV bathymetry reveals a morphologically complex seafloor with rough terrain in seamount areas and low-relief variations in sedimentary abyssal plains which are covered in Mn-nodules. Backscatter provides valuable information about the seafloor type and particularly about the influence of Mn-nodules on the response of the transmitted acoustic signal. Primarily, Mn-nodule abundances were determined by means of automated nodule detection on AUV seafloor imagery and nodule metrics such as nodules  $m^{-2}$  were calculated automatically for each image allowing further spatial analysis within GIS in conjunction with the acoustic data. AUV-based backscatter was clustered using both raw data and corrected backscatter mosaics. In total, two unsupervised methods and one machine learning approach were utilized for backscatter classification and Mn-nodule predictive mapping. Bayesian statistical analysis was applied to the raw backscatter values resulting in six acoustic classes. In addition, Iterative Self-Organizing Data Analysis (ISODATA) clustering was applied to the backscatter mosaic and its statistics (mean, mode, 10<sup>th</sup>, and 90<sup>th</sup> quantiles) suggesting an optimum of six clusters as well. Part of the nodule metrics data was combined with bathymetry, bathymetric derivatives and backscatter statistics for predictive mapping of the Mn-nodule density using a Random Forest classifier. Results indicate that acoustic classes, predictions from Random Forest model and image-based nodule metrics show very similar spatial distribution patterns with acoustic classes hence capturing most of the fine-scale Mn-nodule variability. Backscatter classes reflect areas with homogeneous nodule density. A strong influence of mean backscatter, fine scale BPI and concavity of the bathymetry on nodule prediction is seen. These observations imply that nodule densities are generally affected by local micro-bathymetry in a way that is not yet fully understood. However, it can be concluded that the spatial occurrence of Mn-covered areas can be sufficiently analysed by means of acoustic classification and multivariate predictive mapping allowing determining the spatial nodule density in a much more robust way than previously possible.

## 5.1 Introduction

### Mn-nodules exploration

Research on Mn-nodules received increased attention in the last decade due to increasing prices for ores rich in Cu, Ni or Co, i.e. metal resources that are contained in Mn-nodules. In nature, the largest Mn-nodule occurrences are found in the deep sea, e.g. the equatorial Pacific between the Clarion and Clipperton fracture zone (CCZ), the Peru Basin as well as the Atlantic and Indian Ocean (Petersen et al., 2016). In the typically muddy sediments of the deep sea, Mn-nodules form an important hard substrate providing a habitat for deep sea sessile fauna such as sponges, corals and associated organisms (Vanreussel et al., 2016; Purser et al., 2016). Therefore, mapping Mn-nodule fields is a two-fold task, comprising not only the assessment of Mn-nodules and their density distribution for accurate resource assessment, but also the improved understanding of the natural habitat heterogeneity and its relation to the deep sea ecology. Knowledge about Mn-nodule habitats will support mitigation strategies for mining-induced impacts. Since an increasing number of countries move forward with exploitation plans for Mn-nodules in the CCZ, strategies for a detailed mapping of the deep sea Mn-nodule fields might become mandatory in order to proceed with licensing procedures prior to any mining activity.

Deep sea mining will cause substantial disturbances of the deep sea ecosystem since Mn-nodules, the primary hard substrate, will be removed and massive re-sedimentation of the top 20 to 30cm of sediment of the mined area will occur (Bluhm et al., 1995; Vanreussel et al., 2016). Thus, efforts have been made to investigate the effects of potential mining disturbances in the past (e.g. Thiel et al., 2001) and currently during the project “Ecological Aspects of Deep Sea Mining” as part of the Joint Programming Initiative Healthy and Productive Seas and Oceans (JPI Oceans). To study in detail the potential effects of a deep sea disturbance by Mn-nodule mining to benthic fauna, a plough-experiment was performed in 1989 in the Peru Basin as part of the DISturbance and reCOLonization project (DISCOL, [www.discol.de](http://www.discol.de)). A plough of 8m width was towed 78 times over a 2nmi wide circular area (February-March 1989) to generate dense and less dense impact sub-areas. Photographic surveys, sediment and biological sampling before and after the disturbance (September 1989, March 1992, February 1996), showed that the plough marks were well visible even after 26 years and that the benthic fauna did not recover to its initial state. The data used in this study were collected during the SO242-1 cruise to the DISCOL area during summer 2015, 26 years after the DISCOL experiment.

### The DISCOL study area

The DISCOL working area is situated 560 nmi SW of Guayaquil on the Pacific Oceanic Plate in the Peru Basin (Fig. 5.1) in about 4150 m water depth. The larger DISCOL area ranges from 3800m to 4300m water depth (Fig. 5.1B) and is characterized by N-S oriented graben and horst structures with a deep N-S elongated basin with water depths down to 4300m. An 11 km wide seamount complex in the NE along with a second seamount complex to the SW and three higher mounds to the NW clearly show that the DISCOL area is not located on a flat and homogenous deep seafloor.

The ploughed DISCOL Experimental Area (DEA) itself is located on a relatively smooth, slightly elevated part of the seafloor with a central valley of about 20m depth that dips southward (Fig. 5.2A). When inspecting the bathymetry data generated by the autonomous underwater vehicle (AUV) in more detail, the central part of the area shows a 20m deep valley, the floor of which is comprised by low-relief N-S trending ridges giving the impression of a braided river system (Fig. 5.2A). Despite the rich morphological features in the study area, it does not contain steep slopes and represents a rather smooth seafloor (<5 degrees).

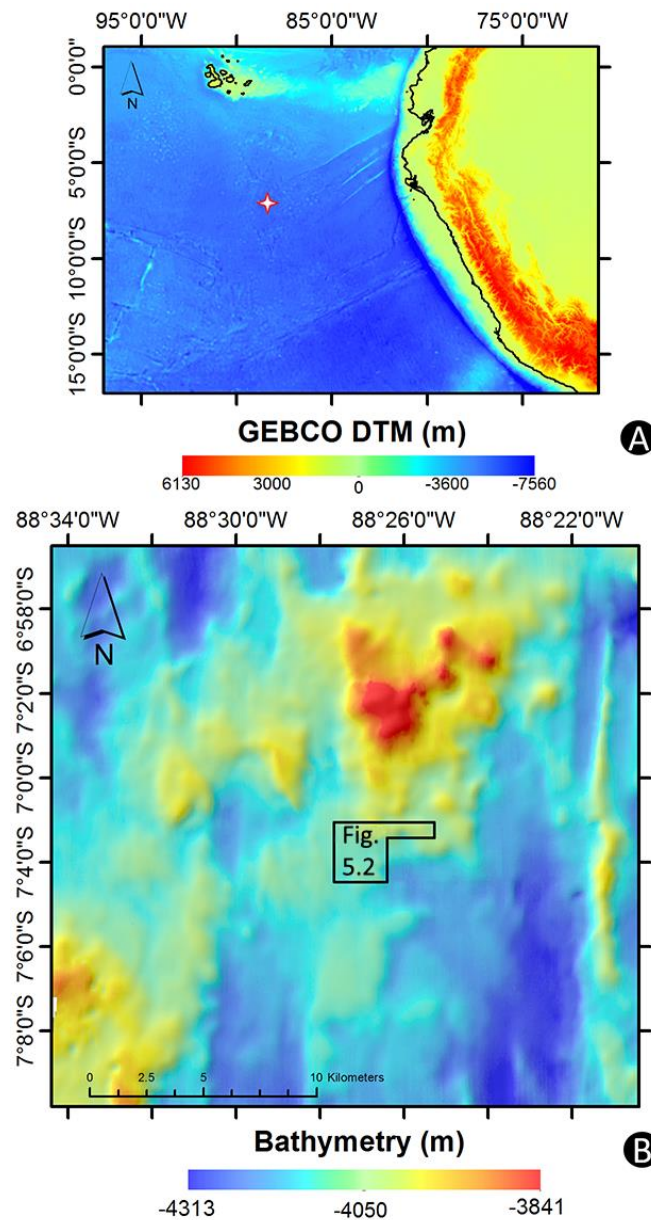


**Figure 5.1:** A) The DISCOL area location in the Peru Basin (red star). B) Ship-based, shaded bathymetry of the wider DISCOL area with 40 m pixel size. The black rectangle represents the boundaries of the AUV MBES dataset used in this study (Fig.5.2).

## Acoustic mapping of Mn-nodules and study objectives

Acoustic mapping has proved to be a useful tool for supporting deep sea mineral resource assessments. The initial studies mentioned below, showed promising results for Mn-nodule detection and quantification, however, progress in more detailed and meaningful method development and data processing capabilities has remained slow, mainly due to fluctuations in the global interest of deep sea mining. The majority of surveys performed for Mn-nodule mapping purposes rely on acoustic remote sensing and near-bottom photography (de Moustier, 1985). The applicability of acoustic methods is based on the clear acoustic contrast of at least 11 dB between the background deep sea soft sediment and the nodules (de Moustier 1985). Weydert (1985) found that the nodule size is proportional to the average backscatter strength for low frequency signals (<30 kHz). In addition, Weydert (1990) concluded that it is possible to map the percentage of seafloor covered by nodules based on backscatter measurements of sonar frequencies higher than 30 kHz, whereas for a frequency of 9 kHz it is possible to use the backscatter response to determine whether the nodule diameter is greater than 6 cm or smaller than 4 cm. Masson and Scanlon (1993) suggested that lower sonar frequencies produce a much weaker acoustic contrast between nodules and surrounding sediments for nodules of given size. They concluded that on a seafloor covered with mixed-size nodules larger nodules will have a greater impact on the backscattered energy than smaller ones. They also suggested that minor differences of nodule coverage will have a considerable effect in backscatter values. A more recent study by Chakraborty et al. (1996) suggested that the nodule coverage is proportional to the backscatter strength and that for low frequency (15 kHz; wavelength ca. 10 cm) the main type of scattering is Rayleigh scattering (wavelength/10 < nodule size) for nodules and coherent scattering for fine sediments.

During one of the first deep sea studies for acoustic mapping of Mn-nodules, de Moustier (1985) utilized a multi-beam echo-sounder (MBES) sonar combined with near-bottom acoustic measurements and photographs from a deep towed camera system to infer nodule coverage. He managed to obtain high agreement between relative backscatter intensity classes and three types of nodule coverage as interpreted from seafloor imagery (dense, intermediate and bare). At that time, his results highlighted the great potential of MBES technology in deep sea mineral prospecting. In more recent years Lee and Kim (2004) utilized side-scan sonar (SSS) to examine the relation of regional nodule abundance with geomorphology. According to their qualitative analysis, lower backscatter values are related with abyssal troughs whereas increased backscatter values are related to abyssal hills. Additionally, Ko et al. (2006) attempted to examine the relation between MBES bathymetry and slope with nodule density in the equatorial Pacific without identifying a solid pattern. Most recently, Okazaki and Tsune (2013) utilized AUV-based MBES, SSS and image data for Mn-nodule abundance assessment and its relation to deep sea micro-topography.

More recent projects regarding resource assessment of Mn-nodules at large scales (0.1' by 0.1' grid cell size) have been based on various spatial modelling and decision making techniques (ISA, 2010). Most commonly, the kriging method has been applied on sparse ground truth data (obtained by physical box-corer sampling) while logistic regression and fuzzy logic algorithms were applied in multivariate data sets of Mn-nodule-related environmental variables such as sediment type, sea surface chlorophyll and Ca Compensation Depth (CCD) (Agterberg & Bohnam-Carter, 1999, Carranza & Hale, 2001).

In this study we analyse AUV-based MBES and image data for quantitative mapping of Mn-nodule densities in the Peru Basin. Particularly, we utilize local ground-truth information (Mn-nodule measurements from AUV photographs) in order to investigate a) its relation to acoustic classification maps and b) its potential use for predictive mapping of Mn-nodules in wider areas where only hydro-acoustic information is available. Therefore, we apply two unsupervised methods (Bayesian probability and ISODATA) for seafloor acoustic classification and a machine learning algorithm (Random Forest) for Mn-nodule density predictions beyond the areas that were optically imaged using the AUV.

By applying different algorithms for unsupervised classification, we aim at comparing their results against quantitative ground truth data of nodule metrics from automated analyses on AUV imagery. This way, we will assess the ability of classification methods in discriminating areas with distinct nodule densities. To our knowledge, this is the first time the Random Forest algorithm is applied for predictive mapping of Mn-nodule densities. Therefore, we examine its performance and the influence of various AUV MBES data on the Mn-nodule prediction results.

## 5.2 Methodology

### AUV MBES data acquisition and processing

The data in this study were collected using the AUV “Abyss” (built by HYDROID Inc.) from GEOMAR, during cruise SO242-1 where various AUV missions were flown. The AUV is equipped with a RESON Seabat 7125 MBES sensor with 200 kHz operating frequency, 256 beams with 1 by 2 degree opening angle along and across track, respectively. From the original PDS2000 sonar data, files backscatter snippet data were extracted into s7k format whereas bathymetry data were extracted into GSF format. Prior to exporting, MBES bathymetric data were filtered within the PDS2000 software.

Bathymetry data from different AUV dive-missions were jointly used for interpolating one single grid of bathymetry and backscatter (Fig.5.2). Latency and roll-related artefacts affected bathymetry in places due to a none-constant time delay for roll values creating uncorrectable artefacts in the resulting grid. Therefore, the bathymetry was smoothed by applying a Gaussian filter with a 10 m x 10 m rectangular window with 3 and 5 standard deviations as smoothing factors in SAGA GIS. Filtered bathymetry was visually inspected for artefacts using the hill-shade function in SAGA GIS, giving satisfactory results. Vertical differences between the smoothed grid with the originally processed surface were everywhere less than 1 m, highlighting that the filtering did not cause significant smoothing and removal of finer details. The filtered bathymetric grid was used for calculating a variety of derivatives listed in Table 5.1. The MBES backscatter data were processed in two ways. First, the s7k/GSF pairs were automatically corrected (for radiometric and geometric bias) and mosaicked in QPS FMGT (Fig. 5.2B). In addition, backscatter mosaic statistics were calculated and exported as GEOTIF files using a 10 m x 10 m neighbourhood. The raw snippets data were exported prior to any processing using a combination of in-house conversion software and QPS DMagic for merging beam data with ray-traced easting and northing. The raw snippets data were transformed from 16-bit amplitude units to dB using the formula in Eq. (5.1):

$$\text{Backscatter (dB)} = 20 * \log_{10}(\text{amplitude}) \quad [5.1]$$

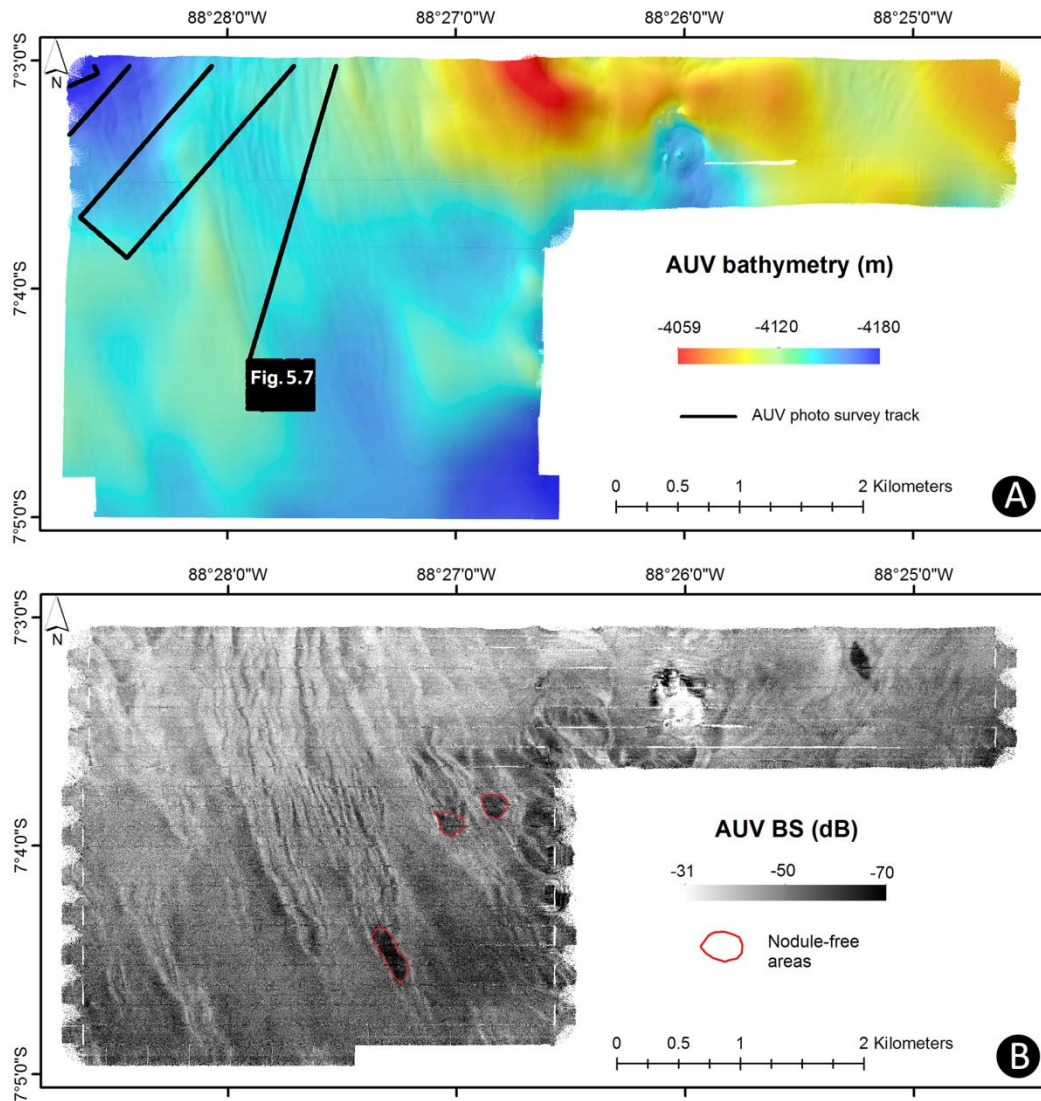


**Figure 5.2:** A) AUV MBES bathymetry with black lines indicating the tracks of the AUV image survey. Closely spaced track lines covering a rectangular area in the lower part of the image correspond to the areas shown in Fig. 5.7. B) AUV backscatter mosaic. The polygons delineated in red represent nodule-free areas as observed from underwater video data.

Raw backscatter data were processed by applying the Bayesian approach on certain beams as described in Alevizos et al. (2015 and 2017) whereas the gridded data were analysed with Random Forest (RF) regression trees and ISODATA clustering (see section below). An overview of the software used to process and classify each type of dataset is presented in Table 5.2.



Table 5.1: Description of MBES features (bathymetric derivatives and backscatter statistics) that are used as explanatory variables in random forests predictions.

Explanatory variables	Description
<b>From bathymetry</b>	<b>Scale: 6 m cell size</b>
Depth	AUV MBES, smoothed with Gaussian filter ( $5\sigma$ )
Slope	ArcGIS slope algorithm in percent units
BPI	Relative position of pixels compared to their neighbors. Inner radius 10m, outer radius 100 m (Iwashahi and Pike, 2007) SAGA GIS terrain analysis toolbox
LS factor	The integrated slope length and inclination, formula from Moore et al. (1991), SAGA GIS terrain analysis toolbox
Terrain Ruggedness Index (TRI)	Measure of the irregularity of a surface in 5m radius neighborhood (Iwashahi and Pike, 2007), SAGA GIS terrain analysis toolbox
Concavity	Measure of negative curvature of a surface (Iwashahi and Pike, 2007), SAGA GIS terrain analysis toolbox
<b>From backscatter</b>	<b>Scale: 10x10 m neighborhood, 6 m cell size</b>
mean	Average dB value of pixels falling within the neighborhood (FMGT module)
mode	Most frequent dB value of pixels falling within the neighborhood (FMGT module)
10% quantile	Value of neighborhood pixels describing the lower 10% of the total dB distribution (FMGT module)
90% quantile	Value of neighborhood pixels describing the 90% of the total dB distribution (FMGT module)

## Seafloor imagery and automated image analysis

AUV surveys were undertaken for collecting close-up images from the seafloor using a camera system recently described by Kwasnitschka et al. (2016). In this system the camera is mounted behind a dome port along with a 15mm fish-eye lens that produces extreme wide-angle images. This type of lens and dome port configuration induces significant distortions to the image which need to be corrected prior to any image analysis processing. Surveying at altitudes of 4-8m above the seafloor and using the novel state-of-the-art LED flash system, the AUV collected several hundred-thousand seafloor images at a 1Hz interval. The respective AUV surveys were designed to cover a large part of the study area with a single-track dive pattern and also to focus on two selected areas running track lines 5m apart for dense 2D image mosaicking (Fig. 5.2A). Each image was individually georeferenced using the AUV navigation and altitude data. This way, each pixel of the AUV imagery is translated to an actual portion of the seafloor.

Table 5.2: Datasets and methods applied in this study.

	Hardware		
	AUV RESON 7125		DeepSurveyCam (Kwasnitschka et al., 2016)
Software	MBES bathymetry	MBES backscatter (snippets)	Imagery
Processing	PDS2000 (sonar data), SAGA GIS (xyz, grids), ArcMap (grids)	Matlab (raw data), Fledermaus FMGT (corrected BS and mosaicking)	in-house software, ArcGIS
Classification / prediction	Random Forests (MGET)	Bayesian (raw data), ISODATA, Random Forests Mosaic and statistics	Random Forests (MGET)

For the automated image analyses (e.g. Mn-nodule counting), all images were smoothed by a Gaussian filter to remove noise and then converted to grayscale for computational speedup. Following, the images were corrected for inconsistent illumination due to the varying AUV altitude using the fSpice method described by Schoening, et al. (2012). The central (sharpest, best illuminated) region of each image was cropped and thresholded by an automatically tuned intensity limit before contours in the resulting binary images were detected and fused to blobs of pixels that served as nodule candidates. Each nodule candidate was finally fitted with an ellipsoid to account for potentially buried parts of the nodule. The sizes of these ellipsoids constitute the nodule size distribution within one image from which descriptive parameters were derived. This kind of automated image processing resulted in quantitative information such as: image area (square meters), number of nodules ( $n$ ), percentage of seafloor covered by nodules (amount of nodule pixels divided by total amount of image pixels), and the threshold sizes (estimated 2D surface) of 1, 25, 50, 75 and 99 percent quantiles of the nodule size distribution (comparable to a particle size analysis). A detailed publication on the nodule delineation algorithm can be found in Schoenning et al. (2017), while the source code is available online as Open Source (<https://doi.pangaea.de/10.1594/PANGAEA.875070>).

In this study, we considered the number of Mn-nodules per square meter as a normalized measure of nodule density in order to avoid overestimation of Mn-nodules due to multiple-detections between overlapping images. This metric is derived from the ratio of the number of nodules detected to the area ( $m^2$ ) of the image footprint (the size of the central 'good' part of the image). Therefore the results of the predictive mapping are presented with 6 m x 6 m resolution which is representative for the majority of image footprint sizes.

## Seafloor classification and prediction methods

Three different approaches were applied for a predictive Mn-nodule mapping. The first approach is an unsupervised method based on Bayesian statistics applied on raw snippet data. It examines the within-beam backscatter variability in the entire area in order to estimate the optimum number of seafloor classes. The output acoustic classes can then be validated with available ground-truth data. The second approach, is based on the

ISODATA algorithm (an unsupervised method as well), applied on gridded backscatter data. This algorithm can automatically adapt the number of classes to the data for given minimum and maximum values set by the user. Finally, a supervised machine learning method was applied on gridded bathymetric and backscatter data. This method requires a training set in order to model the complex relationship between the Mn-nodules occurrences and the bathymetry, bathymetric derivatives and backscatter information. The algorithm outputs a prediction grid for Mn-nodule densities and also estimates the importance of each input variable in accurately predicting Mn-nodule densities.

## **Bayesian probability on beam backscatter**

The raw backscatter data were classified by applying the Bayesian methodology developed and implemented by Simons and Snellen (2009) and Amiri-Simkooei (2009) and applied by Alevizos et al. (2015). In order to enhance the method's performance, strong outliers in the raw data were filtered by using a variance threshold set to 100 (i.e. 10 standard deviations). Thus, beams with a snippet data variance greater than 100 were disregarded from the classification process. The remaining snippet data were averaged for each beam for obtaining the mean relative backscatter intensity. The Bayesian method is based on the central limit theorem and the assumption that acoustic backscatter measurements of a homogeneous seafloor type would express normal distribution when derived from a certain incidence angle. Therefore all backscatter values were grouped per beam angle and their histograms were examined separately. At first, a number of Gaussian curves were fitted to each histogram and the goodness of fit was assessed by the  $\chi^2$  criterion. The minimum number of Gaussian curves that fitted well the overall distribution pattern of the histogram values (i.e.:  $\chi^2$  is less than 2), was considered as the optimum number of classes. Not all beam angles provided the same number of Gaussian curves; therefore it was important to identify those beam angles that gave consistent results about the number of classes. Usually the mid-range incidence angles provided the most consistent results (Alevizos et al., 2015) regarding the Gaussian fitting; hence beams from this range were utilized as reference in order to derive the optimum number of classes. Once the reference beams were identified, the mean and standard deviations of each Gaussian curve were used as conditions for classifying the backscatter values for the rest of the beams.

The Bayesian technique does not require the MBES to be calibrated and allows for class assignment per beam, thus maximizing the spatial resolution of the final map. The most important aspects of the Bayesian technique are the internal cluster validation based on  $\chi^2$  criterion and the increased geo-acoustic resolution, allowing for maximal acoustic discrimination of similar seafloor types (Alevizos et al., 2015).

## **ISODATA classification for grids**

The ISODATA classification was applied to the backscatter mosaic and its derived statistics (Table 5.1) using the ISODATA algorithm implemented in SAGA GIS. ISODATA stands for Iterative Self-Organizing Data Analysis and has been applied in several marine mapping studies involving backscatter information (Diaz, 1999; Hühnerbach et al., 2008; Blondel and Gomez-Sichi, 2009). The fundamentals of ISODATA processing are described in detail by Dunn (1977) and Memarsadeghi et al. (2007). A particular advantage of this method apart from its fast execution is that it estimates a suitable number of classes by

dividing clusters with large standard deviations and by merging similar clusters at the same time (Diaz 1999). This is done automatically and the user only defines an empirical minimum and maximum number of classes.

## Random Forest predictive mapping for grids

To exploit the full range of MBES gridded data and for comparison purposes, supervised classification was applied to the bathymetry, bathymetric derivatives and backscatter statistics (Table 5.1). Applying a machine learning algorithm was encouraged due to the abundant ground-truth data (nodule metrics from automated image analysis) and the high resolution of the various MBES layers. The Random Forest algorithm as implemented in the MGET toolbox for ArcGIS was used (<http://mgel2011-kvm.env.duke.edu/mget>). Initially developed by Breiman (2001) it has shown good results in marine predictive habitat mapping (Stephens and Diesing, 2014; Lucieer et al., 2013; Che-Hasan et al., 2014). The algorithm requires a training data set with the response variable (here: nodule density from AUV imagery analysis results) and a set of explanatory variables (here: bathymetry, bathymetric derivatives, backscatter) as inputs in order to model the relationship between them. The training set provides the required “knowledge” about the response variable and its corresponding explanatory variable’s values. At the next stage, an ensemble procedure based on several regression trees of random subsets of the explanatory variables is iteratively applied for classifying/predicting Mn-nodule density per grid-cell using a-priori information from the training sample. The prediction at a certain grid-cell is defined by the majority votes of all random subsets of trees (Gislason et al., 2006).

During the iterative processing, the Random Forest will reserve randomly selected parts of the training sample for internal cross-validation of the results (out-of-bag sample). During each iteration, one explanatory variable is neglected and its importance score is calculated according to its contribution to the resulting prediction error. The variable importance calculation is considered one of the main advantages of the Random Forest algorithm. An important step prior to Random Forest application is data exploration. With data exploration it is possible to identify which explanatory variables are capable to discriminate patterns of nodule density in the study area better. A standard approach is to explore the probability density function of the response variable with each of the other gridded variables (e.g. slope, BPI, etc.). These plots give first indications about the distribution type of the response variable for a given explanatory variable. The explanatory variables presented in Table 5.1 were chosen as good descriptors of nodule density in the area based on the probability density functions of arbitrarily chosen classes of nodule density (Fig. 5.3, appendix of chapter 5). The arbitrary classes were based on the quantiles method for classifying the nodule density histogram. It has to be noted that the arbitrary classes were used only for data exploration and not for the prediction of nodule densities.

All descriptor-grids were resampled to 6 m x 6 m pixels in order to be compatible with the average effective area of the AUV images upon which nodule metrics were computed. An appropriate selection of training samples is fundamental for modelling the relationship between the response variable and the gridded descriptor data. Particularly, the training samples need to span the entire range of the study area capturing most of the data variability. They have to contain as diverse values as possible regarding both the nodule density and the corresponding gridded descriptor data.

## 5.3 Results

### Automated nodule detection from AUV images

The automated nodule detection algorithm results for nodule density (number of nodules  $\text{m}^{-2}$ ) are shown in Fig. 5.4. The dense point cloud offers a detailed view of the nodule spatial distribution which can significantly enhance the interpretation of nodule density in conjunction with MBES bathymetry. In Fig. 5.4 the nodule density fluctuates in a pattern of alternating bands. By coloring the seafloor surface and the bathymetric profile cross-section according to nodule density values, it can be seen that higher nodule densities appear on smooth slope features where the seafloor appears locally concave or terraced and also on the foot of these slopes which appear relatively lower compared to the surrounding area. By colouring the AUV bathymetry according to the nodule density it became clear that MBES derivatives may be useful for quantifying the nodule distribution in the entire study area. We thus calculated bathymetric derivatives such as BPI, concavity, slope and slope-related derivatives (LS factor, TRI) to be included in predicting nodule densities.

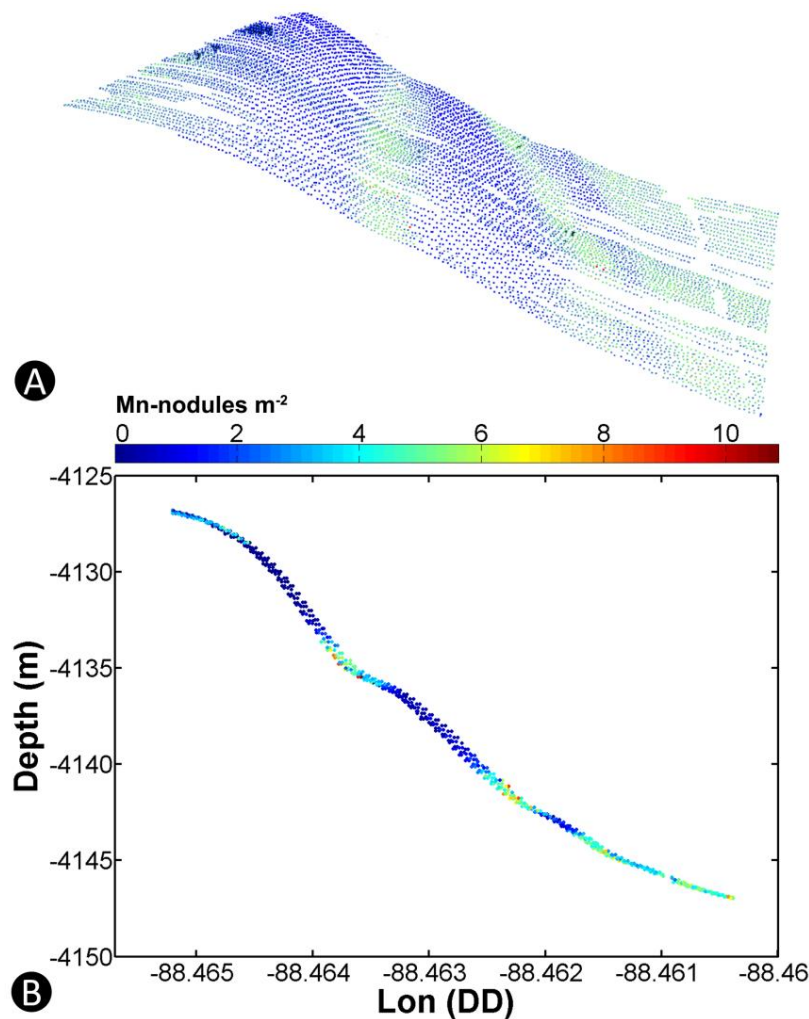


**Figure 5.4:** A) Points with nodule measurements derived from automated nodule detection, draped on AUV bathymetry, showing Mn-nodules per square meter from perspective view, B) Longitudinal section of bathymetric profile from same area highlighting the local scale morpho-bathymetry of Mn-nodule fields.

## Bayesian acoustic classification of raw BS data

The Bayesian method identified six classes based on the analysis of beams with incidence angles between 38 and 42 degrees (Table 5.3). Despite the variance-based filtering, it was not possible to compensate for the remaining effects on beam incidence angles in the middle range and towards the nadir. We believe that these effects are responsible for the stripe-like classification at the outer part of the swath. The selection of six classes resulted from the agreement between two adjacent beams (Table 5.3) and the relative lower overlap of the Gaussian curves. The finally derived classes are ordinal; meaning that from class 1 to class 6 there is an increase in backscatter intensity. The spatial distribution of the acoustic classes expresses a gradient of high to low backscatter classes in the N-S direction (Fig. 5.5A). The nodule-free areas holding lowest backscatter values are captured clearly.

*Table 5.3: Averaged central dB values of the Gaussians derived from reference beam angles on both sides of the AUV MBES.*

Acoustic class	PORT: (38° & 40°) central value (dB)	STARBOARD: (40° & 42°) central value (dB)
1	-60.7	-61.2
2	-59.4	-59.7
3	-57.4	-58.1
4	-56.3	-56.3
5	-54.8	-54.8
6	-52.8	-52.7

## ISODATA applied to BS data

The ISODATA algorithm was applied to the mean, mode, 10% and 90% quantiles of the backscatter mosaic. These datasets are considered more suitable than the raw backscatter data, as they hold a more realistic representation of backscatter spatial variability and they are slightly correlated (correlation coefficients: 0.5-0.9) with the mean backscatter. The ISODATA algorithm was set to produce an optimal number of clusters for different ranges of cluster amounts (minimum number of clusters from 2 to 5; maximum number of clusters from 6 to 10). The results for all possible pairs regarding the minimum and maximum clusters were divided, indicating five or six clusters as optimal. To have comparable results with the Bayesian method, six clusters were selected for further analyses. Although the algorithm does not output classes with ordering, the ISODATA classes were reclassified based on their nodule statistics to be comparable with Bayesian results (see discussion section). The classes show a decreasing amount of nodules from north to south with the nodule-free areas being sufficiently demarcated.



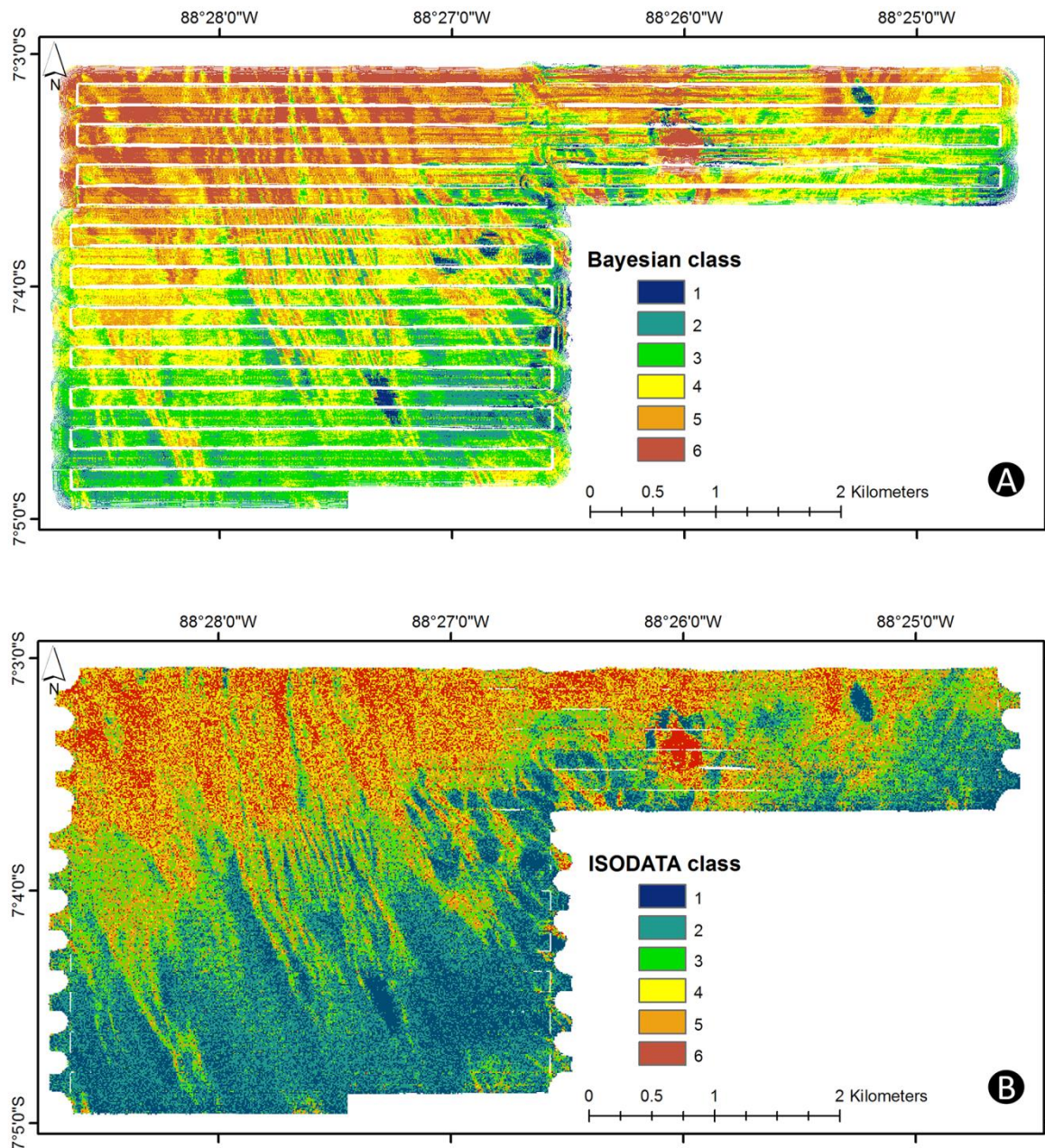


**Figure 5.5:** A) Bayesian classification map based on AUV backscatter beam data, B) ISODATA classification map based on AUV backscatter neighbourhood statistics (mean, mode, 10<sup>th</sup> Q and 90<sup>th</sup> Q, see Table 5.1).

## Random Forest predictions using bathymetry derivatives and BS data

The RF was performed in two steps: the training and the prediction step. First a sensitivity test was carried out using different percentages of training samples (Fig. 5.6B) and fitting models with 200 and 1000 trees. This test is essential for examining the optimal settings prior to applying a predictive model. It also helps in quantifying the stability of results (given the random character of the process) by running the model with optimal

settings repeatedly. For quantifying the model accuracy we used the percentage of variance explained by the out-of-bag samples (RF algorithm output report) whereas for assessing the prediction results, calculation of  $R^2$  was applied for measuring the correlation between the predicted and measured nodule density. According to the sensitivity analysis, a training set with 30% of the total amount of images with Mn-nodule statistics was sufficient to explain more than 70% of the variance of the out-of-bag sub-sample when training 200 trees.

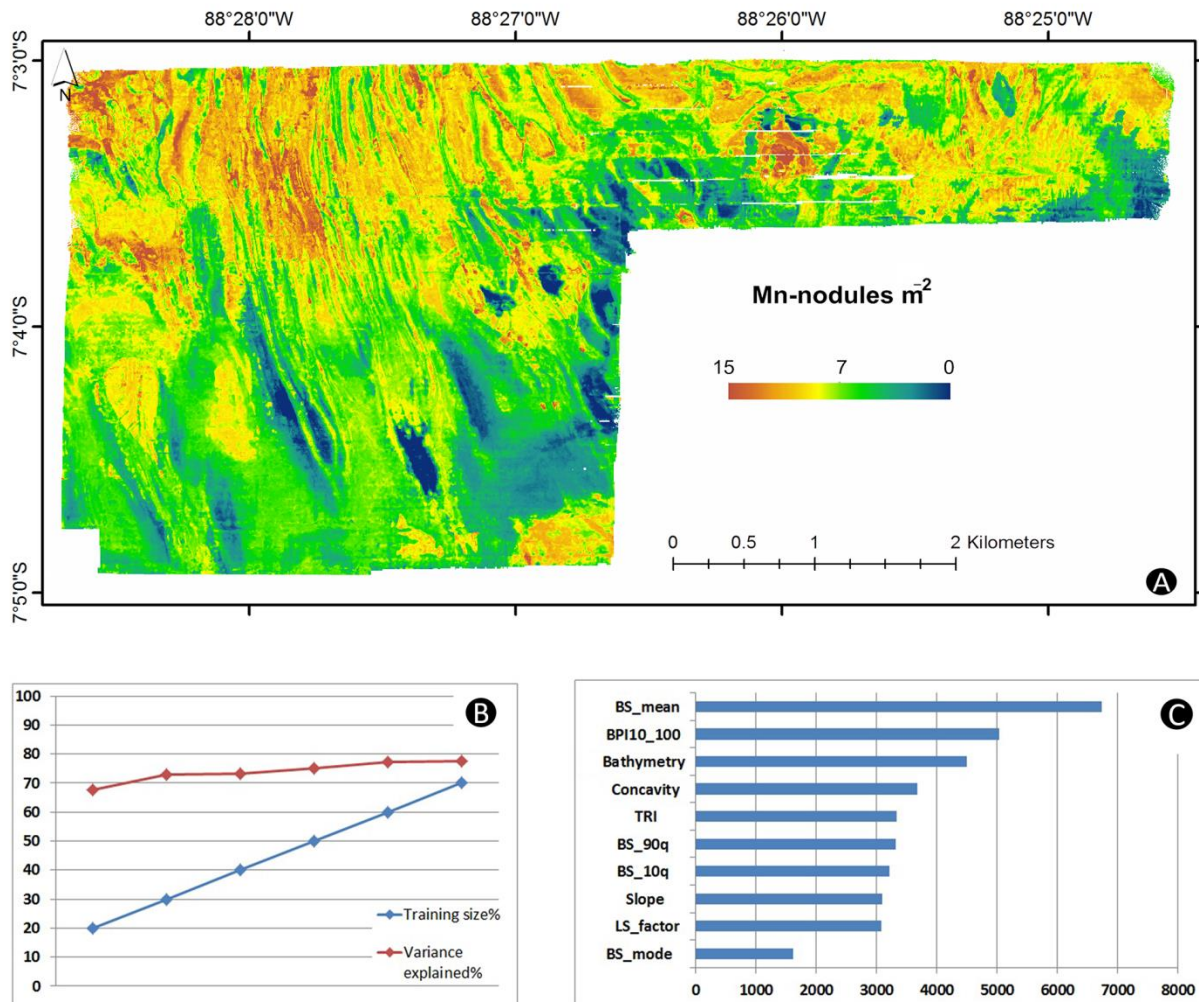


**Figure 5.6:** A) Random forests prediction map of Mn-nodules densities, Sensitivity analysis results: B) Percentage of training sample size and performance of RF model in terms of percentage of variance explained (out-of-bag). C) Importance scores of MBES explanatory variables, based on average percentage increase of mean prediction error from ten model runs.

It was also found that this accuracy value is not improving significantly when increasing the training sample size (Fig. 5.6B). By maintaining the same amount of training samples (30% of the total images acquired, ca. 2700 images) while using ten different parts of the data as training sample (ten-fold cross-validation), the model performance was relatively consistent (69-72%) regarding the out-of-bag variance explained (Table 5.4). These results refer to the Mn-nodules  $m^{-2}$  analyses. In addition we tested the predictability of the 2D size of nodules using the 50% and 75% quantiles of 2D sizes in square centimetres. The resulting out-of-bag variance explained was found to be much lower (35-40%),



independently from the number of trees and the size of the training sample set. By using the results from the ten-fold cross-validation (or sensitivity test) we extracted the mean importance score of each bathymetry and backscatter parameter (Fig 5.6C). Considering the prediction of Mn-nodules  $m^{-2}$ , the mean backscatter data was found to be the most influencing variable which constantly scored first, followed by the BPI, bathymetry and concavity. After the sensitivity test an optimal model using 30% of all images as training data and growing 200 trees (1000 trees did not produce better results) was developed using the explanatory variables for prediction of nodule densities. The final results of the RF method express a gradient from higher to lower nodule densities from North to South (Fig. 5.6A). An independent subsample of nodule measurements was used for validating the prediction results. This validation sample consists of measurements selected at least six meters away from any training location, to avoid the introduction of autocorrelation effects on the validation process which could overestimate the performance of the model. The value of 6m was selected as the majority of images cover a 6 m x 6 m area on the seafloor. A comparison between the image-based Mn-nodule measurements and the averaged predicted values based on ten different RF runs show a good average correlation based on the  $R^2$  coefficient (Table 5.4). This implies that there is a correlation between Mn-nodule density and MBES data, although there is some degree of uncertainty that remains in the prediction model (see Appendix).

*Table 5.4: RF model performance for minimum optimal settings of training sample and number of trees regarding prediction of Mn-nodule densities.*

<b>Training set size: 30% (ca. 2700 images) Trees: 200</b>		
<b>Model run#</b>	<b>OOB variance explained%</b>	<b>Predicted/Measured correlation (<math>R^2</math>)</b>
1	72.5	0.69
2	73.0	0.69
3	70.6	0.68
4	70.2	0.70
5	72.2	0.70
6	72.6	0.71
7	69.3	0.69
8	71.1	0.71
9	72.9	0.68
10	70.6	0.71
average	71.5	0.7

## 5.4 Discussion

Our results show that AUV imagery is capable to provide detailed information about Mn-nodule densities hence assisting quantitative mapping of the Mn-nodule distribution on the seafloor. Consistency and repeatability of quantitative methods are fundamental factors in mapping studies and therefore automated image analysis is crucial in this regard. Expert assessments of several tens of thousands of images are practically not possible in a

reasonable time frame and include a high rate of subjectivity. Thus, automated analysis of imagery is regarded as a very suitable method for quantitative mapping of Mn-nodules. This however comes at the cost that usually AUV image surveys are spatially restricted due to the low altitude above the seafloor. For larger scale quantitative mapping of nodule fields, AUV imagery data need to get spatially linked with AUV hydro-acoustic data supporting with data from all regions of interest at the seafloor. Results from image analysis can then be used as alternative information for acoustic class validation and predictive mapping.

Although image analysis results do not constitute ground-truth information they are the best available data to correlate with acoustic classification and prediction results. By exploring the relationship between Mn-nodule data with bathymetry, bathymetric derivatives and acoustic backscatter, we aim to identify potential linkages that allow extrapolation of nodule information to larger areas to assess mineral resources, determine benthic habitats or learn about geological processes that might influence nodule growth. The following paragraphs discuss the performance of the applied classification and prediction methods highlighting the potential use of high resolution Mn-nodule density maps. The various sources of errors induced throughout the data analyses are considered in appendix of chapter 5.

## **Fine scale spatial variability of Mn-nodule density**

Both, the unsupervised classifications (ISODATA, Bayesian) and the random forest prediction results are largely comparable to the nodule detection measurements map (Fig. 5.7). Hence, both classification and prediction data, and nodule measurements reflect a similar spatial distribution pattern of nodule densities. The Mn-nodule densities seen in the imagery highlight a pattern of alternating high and low density bands on bathymetric slope features. According to studies on the fine scale (tens of meters) distribution of Mn-nodules as summarized by Margolis and Burns (1976) higher nodule densities are related to hilltops, slopes and the foot of slopes. The authors particularly highlighted that e.g. nodule sizes vary significantly over short distances; unfortunately there were no methods to capture this variability sufficiently at the time of this study. The correlation to the bathymetry is supported by the variable importance plot of the RF model (Fig. 5.6C). This plot shows that both bathymetry and backscatter features contribute significantly to the prediction of the Mn-nodule densities with variables such as mean backscatter intensity, fine scale BPI, and concavity as good predictors. The predictive potential of these variables needs to be validated in future studies using MBES data from different study areas.

Both unsupervised acoustic classes and the Random Forest prediction suggest a gradient of decreasing nodule densities from north to south while the RF quantitative map (Fig. 5.6A) shows more gradual changes regarding the fine-scale spatial distribution of Mn-nodules. The northern part of the MBES survey is located very close to, and partly within, a seamount area. According to towed camera video footage these seamounts comprise ancient volcanoes that are now covered with deep sea fine sediments. In addition, a few pillow-basalt outcrops were found along with basalt slabs being exposed on the seamount slopes. Greater nodule densities can be observed from these images suggesting that accumulated nodules or exposed basalt rocks may be assigned to the same acoustic class that represents higher acoustic intensities. In the random forest prediction, high nodule densities could be confused with basalt rock as well (Fig. 5.6A, black arrows). Video data can be used in order to differentiate these seafloor types in the acoustic classes. Greater nodule

densities in the vicinity of the seamounts area can be explained by the findings presented by Vineesh et al. (2009) and Sharma et al. (2013). These two studies propose that in the proximity of abyssal hills and slopes, abundant basalt fragments act as nodule nuclei that favour nodule development.

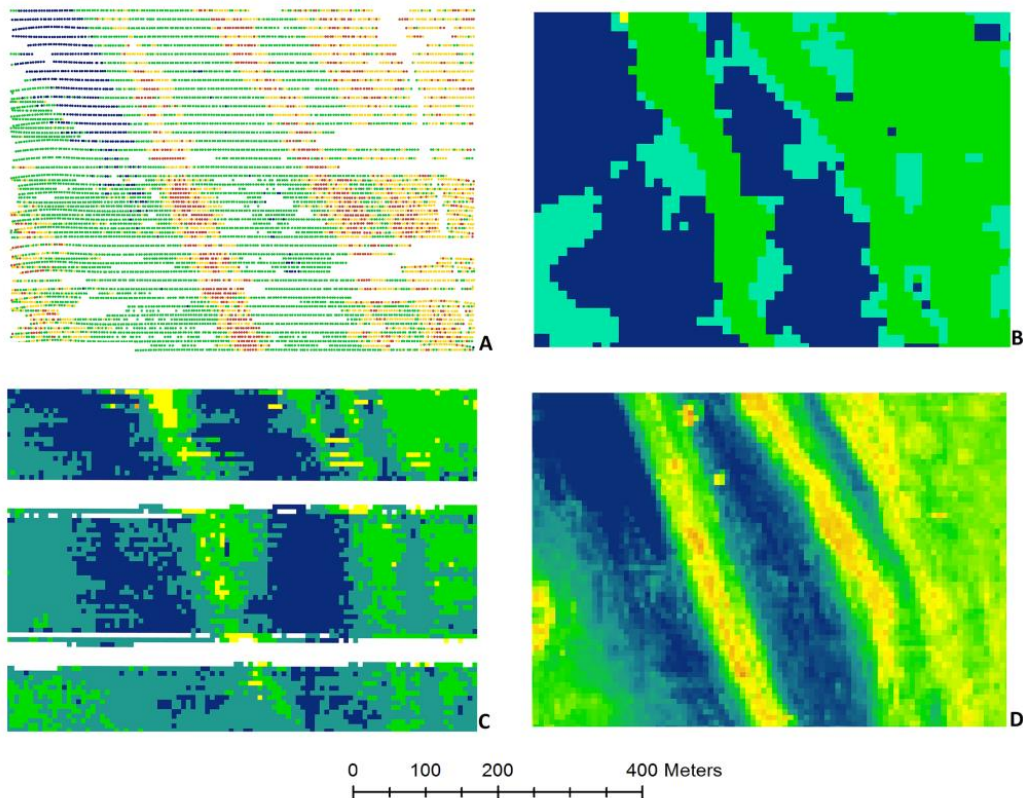


**Figure 5.7:** Inter-comparison of quantitative methods results from the same coverage area (Rectangle made by dense black lines in Fig. 5.2 A): A) Mn-nodules per image-point (automated nodule-detection from optical images), B) ISODATA classes (10m cell size), C) Bayesian classes (6m cell size), D) RF Mn-nodule density prediction map (6m cell size).

Away from the seamount area, the nodule density variations follow a banded pattern of high and low density alternations with localized depressions representing nodule-free areas (Fig. 5.2B). The band-pattern variation is not fully understood by the datasets available in this study; however, it is assumed that it is the result of a combination of the deep sea benthic boundary layer hydrodynamics, local sediment movement and active tectonics that impacts pore fluid migration. It is not clear why and how the nodule-free areas are formed and why we observe moderate nodule densities in broad deep plains of the area. Margolis and Burns (1977) suggest that bathymetric valleys are more influenced by sedimentation hence not favouring nodule growth, but that hill tops and bathymetric slopes are covered by a greater amount of nodules due to a lower impact of local sedimentation. Whether this explanation is also true for the described study area remains speculative. In any case, backscatter data clearly indicate where areas of higher and lower Mn-nodule densities exist, allowing for future investigations of the underlying factors.

## Assessing the Mn-nodule acoustic classification

To assess the performance of unsupervised classification methods in clustering homogeneous areas of Mn-nodules, we examined the within- and between-class variability of the Mn-nodules densities (nodules  $m^{-2}$ ). The assessment is based on the descriptive statistics of nodule measurements from each class (Table 5.5) and box-plots of nodules  $m^{-2}$  from each class (Fig. 5.8). The box-plots assist to better illustrate the separation between classes as well.

To evaluate the separation of Mn-nodule densities that fall within different acoustic classes (Bayesian and ISODATA), we performed a Welch ANOVA along with a Games-Howell test for testing whether the mean values between the classes differ significantly. This test was selected, because the Levene's test (Martin & Bridgmon, 2012) indicated that there is no homogeneity between the class variances for both classification methods ( $p < 0.05$ ).

Particularly the results of the Welch ANOVA for nodule populations belonging to the same Bayesian class ( $F(5,905)=700$ ,  $p < 0.05$ ) and ISODATA ( $F(5, 2520)=810$ ,  $p < 0.05$ ) support the finding that the mean values of Mn-nodules densities differ significantly between the different classes. This finding supports that classification results effectively resolve acoustically homogenous areas of nodule patches which are statistically distinct to each other.

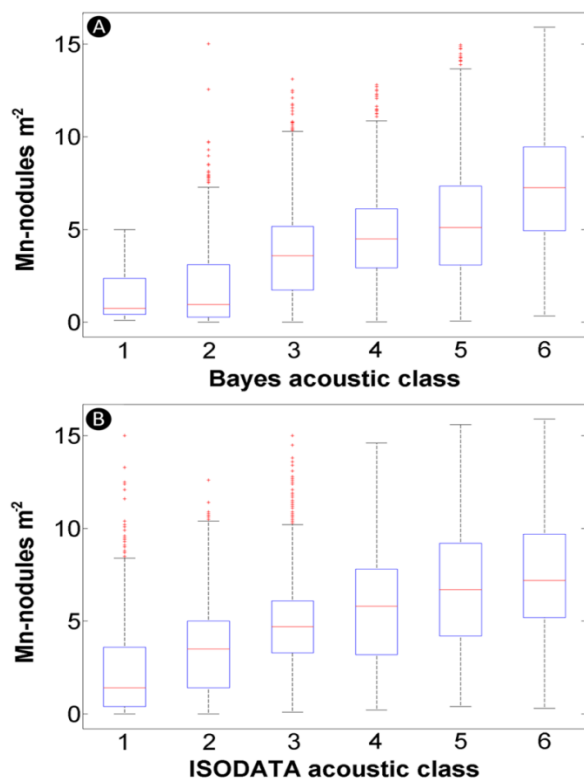
Regarding the Bayesian classification results, the ordinal type of the classes can be noticed both in the statistics and the box-plots (Table 5.5, Fig. 5.8A). The mean and median values of nodules  $m^{-2}$  are increasing with increasing class number suggesting that higher backscatter values are related to higher nodule densities. Class 1 represents the lowest nodule densities but without including samples of zero nodules, this would make this class more distinguishable with an even lower mean value. Some class overlap can be observed in the box-plot for the Bayesian classes; the within-class standard deviation is increasing with acoustic class number, suggesting larger ambiguity for areas with increased nodule density.

Table 5.5: Descriptive statistics highlighting the within-class variability of Mn-nodules for both classification methods.

Bayes – Mn-nodules $m^{-2}$					
Class	samples	mean	median	mode	St.dev.
1	91	1.4	0.7	0.4	1.4
2	1760	1.7	0.9	0.9	1.9
3	2200	3.6	3.6	3.6	2.4
4	2347	4.6	4.5	4.6	2.7
5	1500	5.5	5.1	4.9	3.4
6	756	7.5	7.3	6.4	3.6
ISODATA – Mn-nodules $m^{-2}$					
Class	samples	mean	median	mode	St.dev.
1	3468	2.2	1.4	0	2.3
2	2732	3.5	3.5	2.9	2.3
3	2800	4.8	4.7	4.7	2.4
4	570	5.9	6.1	4.9	3.2
5	628	7.0	6.9	5.2	3.6
6	964	7.7	7.3	6.6	3.6

Classes resulted from the ISODATA clustering hold similar standard deviations suggesting a similar degree of within-class variability. Overall, Mn-nodule density classes express high within-class variability with almost 50% of within-class measurements spanning in a wider range of values causing class overlap (Fig. 5.8). This can be attributed to few factors such as inaccurate navigation between the different AUV deployments, shortcomings of the image-based nodule detection algorithm and noise in the backscatter data (see Appendix). However, it can be inferred from the box-plots for each unsupervised method that seafloor areas of homogeneous Mn-nodule density can be discriminated by classifying the MBES backscatter information only.

No useful results were obtained for the 2D size of nodules (in  $\text{cm}^2$ ) when examining their descriptive statistics and box-plots with acoustic classes. This might be explained by limited interfering between acoustic wavelength and the nodules radii. The high frequency (200 kHz) MBES signal results in ca. 8 mm pulse-wavelength for  $1500 \text{ m s}^{-1}$  sound speed in seawater. This wavelength is significantly shorter than the average nodule size in the study area ( $>3 \text{ cm}$ ) suggesting that the dominant backscattering is sensitive to nodule density and not to nodule size. Early acoustic studies on Mn-nodules were based on low frequency sonars; therefore there is little or no information about the acoustic backscatter of nodules at high MBES frequencies ( $> 100 \text{ kHz}$ ). However, results from this study are in agreement with findings of Weydert (1985) according to which, frequencies higher than 30 kHz are more suitable for mapping the nodule density than the nodule size. This can be attributed to the fact that high frequency signals are more susceptible to surface roughness which is caused by fluctuating nodule densities. Therefore it is suggested that backscatter would increase with increased nodule density given that seafloor roughness increases as more nodules occur per seafloor area.



**Figure 5.8:** Box-plots of nodule densities grouped by acoustic class to illustrate the between-class variability. A) Variation of measurements, from samples belonging A) to the same Bayesian classes and B) same ISODATA classes. Blue rectangle bottom and top represent the 25% and 75% percentiles respectively whereas the red line indicates the median value. The whiskers extend to the minimum and maximum value of the samples that are not considered outliers (i.e.: they are no more than  $\pm 2.7\sigma$  apart). Outliers are marked with red crosses.

## Implications of acoustic mapping on Mn-nodule resource assessment and benthic habitat characterization

Obtaining high resolution seafloor acoustic classes and quantitative spatial predictions of the Mn-nodule density provides useful information for deep sea mining and impact management. The obvious application is a more realistic resource assessment (total tonnage of Mn-nodules per area) which can assist a better delineation of particular areas with mining interest on large and small scales. Resource assessment can be based on semi-quantitative information provided by acoustic classes that correspond to particular Mn-nodule densities or quantitative results from the RF predictive map. In addition, quantitative maps of Mn-nodule densities can be used to support extrapolations of benthic biota densities to seafloor areas where benthic information is not available. This is possible by considering the nodule substrate as surrogate for habitat mapping of certain biota. Surrogacy for mapping deep sea ecosystems has been incorporated in the study of Anderson et al. (2011); the authors point out, that geomorphic classes can be used for discriminating habitats in broad scales of tens to hundreds of kilometres. They also highlight that any surrogacy approach should be based on the correlation between the physical variables (e.g. bathymetry, backscatter) and the biological patterns that appear in the study area. In Vanreussel et al. (2016) and Amon et al. (2016) it is shown that seafloor covered with more Mn-nodules features higher epifaunal densities. This relation might be further evaluated to have a better and verified relationship between nodule and biota densities allowing estimating biota abundances in larger areas that have only been mapped acoustically.

### 5.5 Conclusions

AUV-based optical and acoustic mapping at high spatial resolution opens up new opportunities for mapping Mn-nodule fields. In this study, automated image analysis provided dense, quantitative information about Mn-nodules at fine scale. This information offers useful insights about the fine scale variability of Mn-nodule densities while it can be utilized for correlations with seafloor acoustic classes and predictive mapping. It was found that the Mn-nodule density within a 500 m x 500 m photo mosaic varies in a pattern of alternating bands (with denser and sparser amounts of nodules) according with smooth bathymetric slopes with a preference of increased nodule occurrence at concave seafloor morphologies. Areas with different nodule densities produced distinct backscatter classes that distinguished nodule populations with distinct mean density values. This suggests that Mn-nodule densities can be efficiently mapped with high resolution hydro-acoustic data. In addition, applying machine learning methodology showed great potential in quantitative predictive mapping of Mn-nodules through modelling the complex relation between image-derived nodule metrics with bathymetric derivatives and backscatter statistics. In essence, by using a relatively small amount of AUV images (ca. 2700) as the training set it was possible to obtain a 70% correlation between predicted and measured Mn-nodule densities.

High quality and spatial resolution AUV hydro-acoustic and optical data can provide a fast and less costly mean for Mn-nodule mapping. This has three major implications in deep sea studies: 1) it raises questions about what causes the Mn-nodules to follow the fine scale bathymetric morphology, 2) it assists in better resource assessment of Mn-nodules and provides the information needed for planning the optimal mining path and 3) it provides more accurate information about Mn-nodule substrate as a benthic habitat, hence it can be

utilized for better understanding the deep sea ecology and ecological impact of potential Mn-nodule mining.

## **Acknowledgements**

This study was based on data acquired during cruise SO242-1 which is part of the JPIO initiative. We thank Marcel Rothenbeck and Anja Steinführer for pre-processing of the AUV MBES data and providing them in various formats. In addition we thank Anne Peukert and Dr. Inken Preuss for their useful comments in proof-reading the manuscript.

## 6. The Hyper-Angular Cube concept for improving the spatial and acoustic resolution of MBES backscatter angular response analysis

This chapter has been based on a study that was presented as poster at GEOHAB 2017 (Halifax, Canada) conference:

Alevizos E., 2017, An object-based seafloor classification tool using recognition of empirical angular backscatter signatures, GEOHAB 2017, Halifax, Canada, DOI: 10.13140/RG.2.2.10257.84324

<b>Authors contributions (Elsevier standards)</b>	
Study conception and design:	Alevizos
Acquisition of data:	Greinert
Analysis and interpretation of data:	Alevizos
Drafting of manuscript:	Alevizos
Critical revision:	Alevizos, Greinert



## Abstract

This study presents a novel approach that is based on high dimensional data, for improving the performance of angular response analysis (ARA) on multibeam backscatter data in terms of acoustic class separation and spatial resolution. This approach is based on the Hyper-Angular Cube (HAC) data structure which offers the possibility to extract one angular response from each cell of the cube. The HAC consists of a finite number of backscatter layers, each one representing backscatter values corresponding to single incidence angle ensonifications. The construction of the HAC layers can be achieved either by using dense soundings from highly overlapping multibeam surveys (iHAC) or by producing several backscatter mosaics each one being normalized at a different incidence angle (synthetic HAC). The latter approach is considered here for the first time and it can be applied on multibeam data with standard overlap, thus minimizing the cost for data acquisition. The synthetic HAC is as efficient as the iHAC produced by actual soundings, providing distinct angular responses for each seafloor type. The HAC data structure increases acoustic class separability between different acoustic features. Moreover, the results of angular response analysis are applied on fine spatial scale (cell dimensions) offering more detailed acoustic maps of the seafloor. Considering that angular information is expressed through high dimensional backscatter layers, we further apply three machine learning algorithms (random forest, support vector machine and artificial neural network) and one pattern recognition method (sum of absolute differences) for supervised classification of the HAC, using a limited amount of ground truth data (one sample per seafloor type). Results from supervised classification are compared with results from an unsupervised method for inter-comparison of the supervised algorithms. It was found that all algorithms (regarding both the iHAC and the synthetic HAC) produced very similar results with good agreement ( $>0.5$  kappa) with the unsupervised classification. Only the artificial neural network required the total amount of ground truth data for producing comparable results with the rest of the algorithms.

## 6.1 Introduction

Seafloor acoustic mapping with multibeam echosounders (MBES) faces the emergence of new data acquisition styles, which also trigger the development of new data processing and interpretation approaches. Acquiring MBES datasets using multiple frequencies (Hughes-Clarke et al., 2015) or acquiring backscatter dedicated MBES surveys (Augustin & Lamarche, 2015; Alevizos et al., 2017) has enormously increased the volume of data per seafloor area, leading to increased dimensionality of MBES datasets. At the same time, novel data processing methods appeared for improving the accuracy and detail of geo-information about the seafloor. Although sparse in number, there are studies that have paved the way for more advanced seafloor mapping. Particularly, those techniques which incorporate the angular dependence of the seafloor are considered more robust and preferable for seafloor classification. This is due to the fact that angular dependence of backscatter is a physical property of the seafloor which has been validated both by model and in situ data (APL, 1994; Fonseca et al., 2009).

Combination of angular response analysis (ARA) with modern remote sensing methods such as object based image analysis (OBIA) and machine learning algorithms are considered state-of-the-art in the field of seafloor mapping. Recent studies have incorporated these techniques and have produced some promising results. For instance, Che-Hasan et al. (2012) applied various supervised classification techniques integrating backscatter measurements from 71 incidence angles for benthic habitat mapping. Furthermore, Che-Hasan et al. (2014) utilized the random forest algorithm in conjunction with ARA features (such as skewness and kurtosis of angular curves) and bathymetric features for benthic habitat mapping, while Rzhhanov et al. (2012) employed ARA and pattern recognition methods for classifying sediment types. Both studies (Che-Hasan et al., 2014; Rzhhanov et al., 2012) applied object based image analysis (OBIA) for backscatter mosaic segmentation. Similarly, Huang et al. (2013) combined bathymetric features and angular response curves using a neural network model for mapping seafloor sediments.

In most cases two major issues arise in traditional ARA of MBES backscatter data. These issues are related to the spatial resolution of ARA results and the separability of angular responses. The issue of spatial resolution occurs because angular responses are usually extracted from coarse seafloor patches with the size of half of the MBES swath. In addition, the separability of backscatter responses has an impact on discrimination of various seafloor types. Another problem considered in the studies of Che-Hasan et al. (2012) and Alevizos et al. (2017) is the performance of traditional supervised classifiers using a restricted amount of ground truth data along with high dimensional spatial datasets. The first two issues are highlighted by Hughes-Clarke et al. (1994), Parnum (2007) and Fonseca et al. (2009). They propose that ARA should be based on backscatter measurements from homogeneous seafloor areas in order to better discriminate their angular responses. In addition, Huang et al. (2013) and Rzhhanov et al. (2012) raise the necessity for calculating an  $n$ -dimensional backscatter matrix ( $n$  is the number of incidence angles) using the measurements from each incidence angle, for extracting angular responses per cell and thus increasing class separation and the spatial resolution of the classification map. The idea of such a matrix has been presented first by Hughes-Clarke et al. (1994) and initially implemented by Parnum (2007) using only sparse soundings. According to their concept, the cells of a matrix should be densely populated with backscatter values from multiple incidence angles (yielded by MBES surveys with high degree of overlap  $\gg 100\%$ ) which result in dense soundings per seafloor area. Despite the practical limitations of such

surveys, the advantages of the resulting datasets are significant regarding discrimination of acoustic classes. Additionally, the resulting classification maps can be constructed with a spatial resolution comparable to that of ground truth data and the MBES footprint (meters scale); a fact that increases their validity and usefulness for the end-users (McGonigle et al., 2009). Since the implementation of Parnum (2007) the above concept of an n-dimensional backscatter matrix has only later been employed again, in the studies of Alevizos (2017) and Alevizos et al. (2017) where they took advantage of the high density of MBES soundings resulted from a backscatter dedicated survey with >100% overlap. Interpolation of backscatter values from individual incidence angles was used for producing angular backscatter layers which then are stacked together to form the so called Hyper-Angular Cube matrix (HAC) that is presented here (Fig.6.1).

## Study objectives

Considering that extracting angular responses from the lowest level of acoustic elements (i.e.: the grid-cells of a backscatter layer/mosaic) is the way forward in improving the performance of ARA and that the HAC provides this possibility in a solid way, we focus the scope of this paper on utilizing a HAC from MBES data with high overlap and alternatively from MBES data with standard overlap. We present a new method to construct a HAC from MBES data with standard overlap in order to overcome the practical limitations of backscatter dedicated surveys, thus minimizing the time and cost of the fieldwork. This method has not been considered in literature according to our knowledge until now. In addition we examine and compare the performance of four supervised machine learning classifiers in terms of class separation and how to deal with a restricted amount of training data along with the high-dimensional HAC dataset. Building a high resolution HAC from MBES data of standard overlap and exploiting a small amount of ground truth samples for classification will have an impact on future backscatter studies by decreasing the cost of data collection but at the same time maximizing the usability and quality of acoustic and ground-truth datasets.

## 6.2 Methodology

### The Hyper-Angular Cube matrix

The hydro-acoustic dataset was obtained in 2012 using an ELAC 1180 MBES sonar at 180 kHz. The survey track lines have varying spacing from 15 to 40 m resulting in dense ensonifications per seafloor area (Fig.6.2B). Accordingly we produced 23 interpolated backscatter layers for separate incidence angles in the range of 10 to 65 degrees in steps of 2 degrees in the middle range beams and 3 degrees for the beams close to nadir and outer range. Interpolation for each of the 23 backscatter layers was performed using the IDW algorithm with 10 meters search radius and output cell size of 5 meters. Stacking of all layers defines a hyper-angular cube structure (interpolated HAC or iHAC hereafter) for which an angular signature per cell can be extracted.

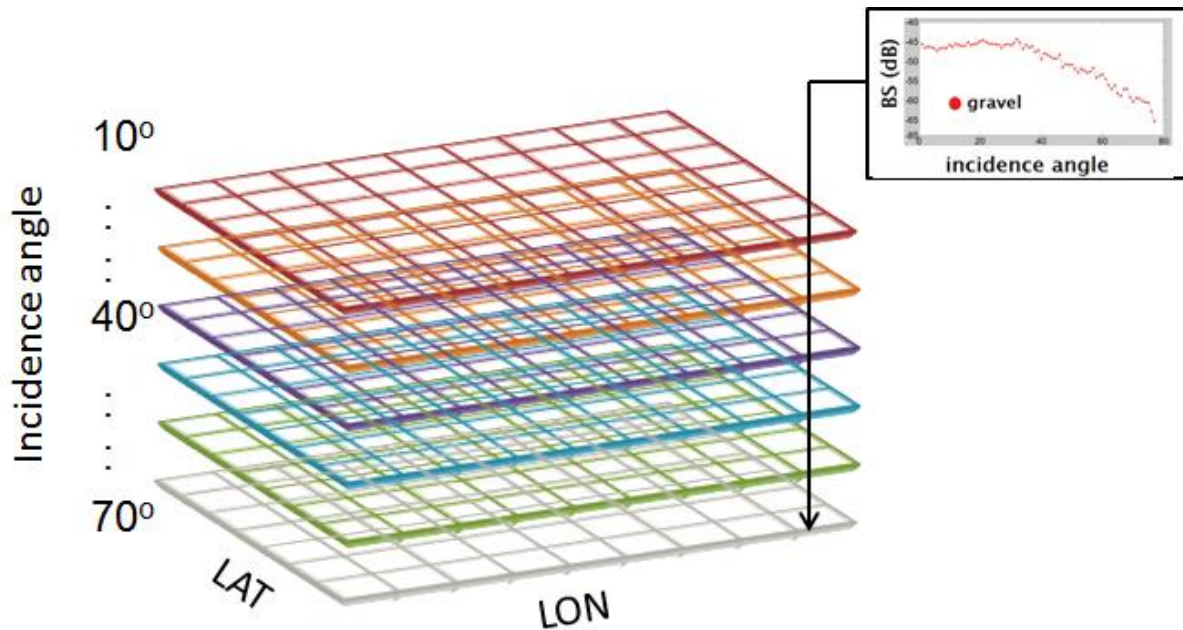


**Figure 6.1:** Example graph of the HAC matrix showing the stack of angular layers and an angular response derived from a single cell.

This approach requires dense soundings per seafloor area. However since collection of such data increases the ship-time and total cost of the MBES survey it is not always the most suitable option to follow. Alternatively we examine a method for obtaining a HAC matrix efficiently and without the costs of a backscatter dedicated survey (i.e.: with >100% overlap). Our approach is based on producing backscatter mosaics (using MBES data with normal overlap) each one being normalized with different reference angle values. Usually, a backscatter mosaic is produced by normalizing the backscatter intensities falling within a sliding window according to the value of middle range incidence angles (e.g.: 30°, 40° or 40°-60° average). Using the middle range incidence angles as reference for normalizing the backscatter values (removing the angular dependence) is a standard practice which has been supported by the study of Lamarche et al. (2011). They suggest that the backscatter intensity from the 45 degrees incidence angle can be used as a useful proxy for correlations with geological features, and that it has the potential for discriminating more seafloor types than the backscatter from the near and far range incidence angles. Thus, in most software packages for backscatter processing there is no option for selecting the reference angle for angle-normalization. One exception is MB Systems which was utilized in this study for producing 23 backscatter mosaics (using selected MBES lines with less than 100% overlap) each one being normalized at different reference angle (same as the number of iHAC layers). By stacking these mosaics we obtain a synthetic version of the HAC from which we can extract a full angular response from each individual cell.

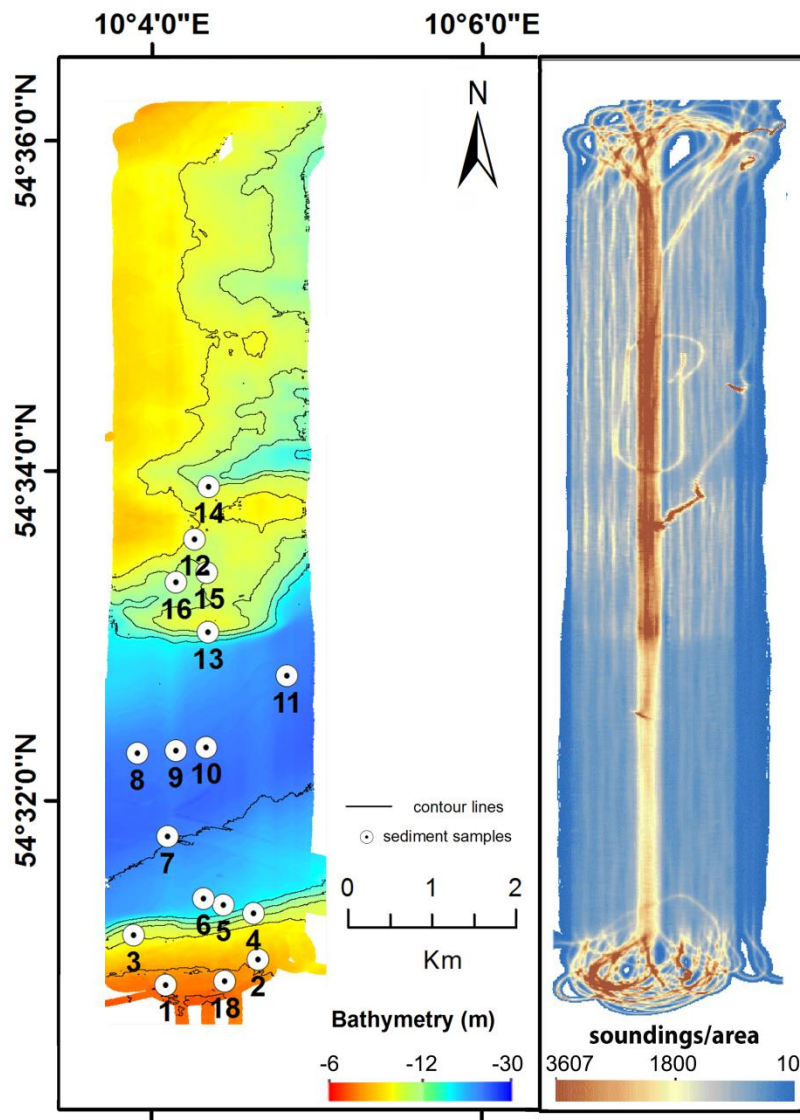


**Figure 6.2:** A) Bathymetry of the study area with locations of sediment samples. B) Sounding density map with area referred to a 5x5 m area.

It has to be noted that for obtaining useful angular responses, the MBES sonar should record backscatter intensity in a stable and linear way (Lurton and Lamarche 2015). Importantly, the original data should be geometrically (seafloor slope, footprint area) and radiometrically (beam pattern, TVG) corrected so it represents changes only depending on the seafloor type variations. In this study it was not necessary to apply seafloor slope corrections to the data as the study area has a very smooth bathymetry ( $\ll 5$  degrees for the majority of slopes).

## Supervised machine learning algorithms

Soundings from within matrix cells corresponding to ground-truth locations shown in Table 6.1 (appendix of chapter 6) were utilized as training data in the following supervised classifiers: a pattern recognition approach (SAD), random forest (RF), support vector machine (SVM) and an artificial neural network (ANN). Each algorithm was applied on both

types of HAC matrices i.e.: the one made of interpolated backscatter layers (iHAC) and the one made from angle-normalized mosaics (synthetic HAC). These algorithms were selected since traditional supervised classification with the MLC method has some limitations regarding the quality and quantity of training samples and the dimensionality of the backscatter data (Benedickson, 1999).

In supervised classification the training data provides the “knowledge” regarding each defined class that assists the algorithm in classifying the rest of the (unknown) data. The “knowledge” consists of a set of input data including the angular responses of each incidence angle and the corresponding seafloor type value (categorical). In this study we use the term “descriptors” to refer to the angular layers of the iHAC or the synthetic HAC from which the angular responses were obtained.

The pattern recognition approach used here is described in Alevizos (2017) where it was initially implemented. The method compares the 2D shape of known angular signatures with unknown ones. A similarity assessment is used for comparison of both signatures which are treated as 2D vectors. The level of similarity with each of the reference signatures determines the acoustic class membership of the unknown angular signatures. An adaptation of the sum of absolute differences algorithm (SAD) for 2D data is used for testing the similarity of angular signatures.

The SAD algorithm was initially developed for video compression and it is widely used for object recognition tasks (Dawoud et al., 2011). In our implementation, the algorithm calculates the difference between reference and unknown backscatter values of corresponding incidence angles. Then, similarity criteria are applied to the sum of differences for each class assignment. It is implied that the lower the values of the sum of absolute differences the higher is the similarity between the 2D objects (angular signatures) under examination. The user has to set only two criteria that will influence the similarity assessment hence the final classification results. These criteria include the standard deviation offset and the majority criterion. The standard deviation offset criterion controls the maximum acceptable absolute differences between known and unknown angular signatures. It is obtained by means of data exploration of soundings falling within the ground-truth cells (Table 6.2, appendix of chapter 6). Soundings forming the angular signature of known seafloor types hold particular standard deviation for each seafloor. This information helps in defining tolerance boundaries for the mean backscatter values of each seafloor type. The standard deviation offset can be used for strict or fuzzy class membership. The majority criterion controls the number of incidence angles, the difference values of which, are falling within the acceptable standard deviation offset. Accordingly, the majority criterion needs always to be set as large as possible (>80%) for more robust matching. It should be adjusted only if backscatter information is missing for certain angles.

The random forest (RF) is a machine learning algorithm that has been widely applied in image analysis and predictive seafloor mapping studies (Lucieer et al., 2013; Diesing et al., 2014). The training process is based on “growing” several (user defined) classification trees using random subsets of the training sample as a-priori information. This information is then compiled into a non-parametric model for classifying the grid-cells of the input layers. The prediction at a certain grid-cell is defined by the majority votes of all random subsets of trees (Gislason et al., 2006). Growing of classification trees is iterative, so each time (during the training) the RF will reserve randomly selected parts of the training sample (out-of-bag sample) for internal cross-validation of the results. With each iteration, one descriptor value is neglected and its importance score is calculated according to its contribution to the

resulting prediction error. Descriptor importance is considered one of the main advantages of the RF algorithm. The RF approach has been initially applied together with ARA by Che-Hasan et al. (2012, 2014). They used angular responses extracted from half swath measurements within objects (groups of cells) derived by automated segmentation of the backscatter mosaic. In this study we apply the RF on the grid-cells of layers building up the HAC matrices described above. The algorithm can identify non-linear relationships that underlie between backscatter values and the seafloor types. In addition, it outputs a rating with the importance scores for each angular layer indicating their influence in predicting a certain seafloor type.

The SVM is a machine learning algorithm which is particularly used for supervised classification of terrestrial multispectral data and recently for seafloor acoustic mapping (Che-Hasan et al., 2012; Stephens and Diesing, 2014). Che-Hasan et al. (2012) applied SVM on backscatter mosaic objects whereas in this study we apply the algorithm on cells of the HAC layers. SVM maximizes the separation of classes in a high dimensional dataset by fitting a hyper-dimensional plane (or just hyperplane) to the data feature space. The hyperplane is produced using a kernel function when the data cannot be linearly separated in feature space. The selection of a particular type of kernel function depends on the data separation pattern (in feature space) and will have a strong effect on classification. SVM has the ability to identify non-linear relations within the data and does not require normal distribution of the training backscatter values from within each acoustic class.

Finally, an artificial neural network (ANN) approach is examined in this study. ANNs are mimicking the functionality of biological neurons and they are extensively used in speech/face recognition but also in landscape classification studies (Coleman 2008, van Leeuwen 2012). They possess a number of advantages that distinguish them from common algorithms whereas they also hold some disadvantages. Regarding the merits of ANNs these include that they do not make any assumptions about the data (e.g.: normal distribution of training data is not a prerequisite for data analysis), they are able to identify non-linear relationships in high dimensional data and most importantly, they acquire learning without the input of physical models that describe data variability. However ANNs are considered as black boxes regarding input-output of data plus they require several trial-and-error iterations for optimally tuning of algorithm settings. In this study two training sets were used to support the ANN classification. The main concept of a supervised ANN is that an input of variables is examined in a combinatorial way regarding the production of certain outputs. The combination of variables leading to acceptable outputs (according to the training set) is determined by weight factors that strengthen the relationship between the input and output. Learning occurs when the ANN modifies the weight factors via a back-propagation technique in order to minimize a user-defined error rate value. The trained ANN applies then its "knowledge" to the rest of the data set for classification of unknown elements. ANN has been applied to backscatter angular responses initially by Huang et al. (2013) producing promising results. However they used seafloor patches generated from a half swath sliding window to extract the angular responses. This fact had an effect on the homogeneity of the angular responses and hindered class separability in their study.

## Training set selection

In this study we tested all classifiers using a training set with fixed size meaning that angular responses from only five representative ground-truth locations were utilized (Fig.6.3C, Table 6.1, appendix of chapter 6). The sediment samples of Table 6.1 (appendix of chapter 6) were collected using a multi-corer and a Van-Veen grab. The selection of the training set was based on grain size analysis results and information from an unsupervised classification (Alevizos et al., 2017). The unsupervised method applied in Alevizos et al. (2017) yielded an optimum number of five classes therefore it was considered as guiding information for the supervised training in this study. The small amount of training set was chosen to fit the purpose of the study in assessing the ability of machine learning classifiers to perform adequate classification using a restricted amount of training set. Only the ANN method required the total number of ground-truth data during training for producing results comparable to the rest of the classifiers.

## 6.3 Results

### Comparison of angular responses from dense soundings with interpolated and synthetic ones (HAC)

In this study we extracted the angular responses of five different seafloor types in three different ways. First we extracted the original soundings from within 5x5 m rectangular patches corresponding to the five ground-truth locations (Fig.6.2A, Table 6.1 appendix of chapter 6). These resulted in multiple backscatter values for all incidence angles and each seafloor type being represented by a distinct cloud of measurements. In addition, we extracted angular responses from the cells of the two matrices (iHAC and synthetic HAC) corresponding to the five ground-truth locations. In the first instance the iHAC consists of a set of 23 backscatter layers resulted from interpolation of original dense backscatter measurements. In the second instance the synthetic HAC consists of backscatter mosaics resulted from angle-normalization using 23 different incidence angles as reference each time. It is observed that all three sets of extracted angular responses represent the five seafloor types individually and clearly apart from each other (Fig.6.3). Each angular response follows a hierarchical plan from coarser to finer material, meaning that angular responses of coarse seafloor types hold higher dB values than those of the fine types at all instances. It appears that the angular responses derived from the cells of iHAC correspond close to the mean dB values of the original angular response cloud. The angular responses derived from the cells of the synthetic HAC appear smoother than those derived from the iHAC and with positive offset between 1 to 3 dB. In general, angular responses derived from both interpolated and synthetic HACs are suitable for seafloor classification using ARA since they hold continuous and distinctive information for each of the five seafloor types. Considering the suitability of the above angular responses for seafloor mapping we applied the following supervised classifiers on interpolated and synthetic HAC data for classifying the seafloor of the study area. The classification maps resulted from the HAC with the interpolated angular mosaics are shown in Fig.6.4.



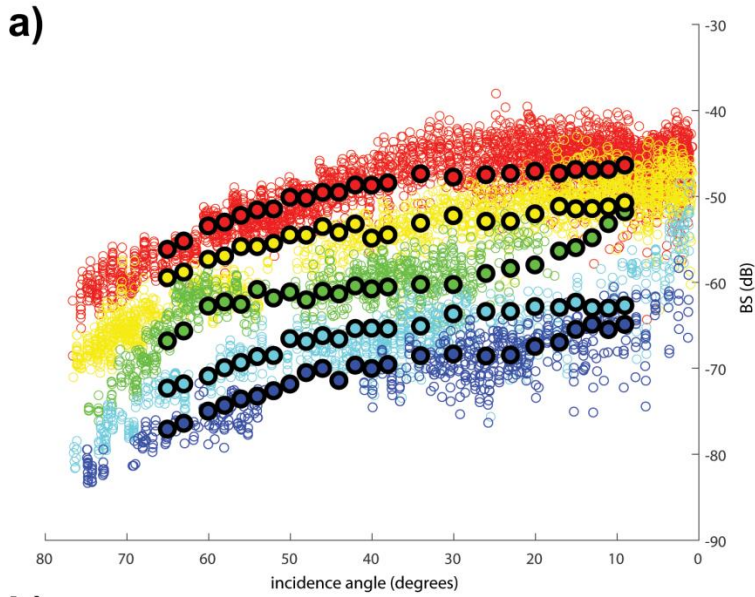
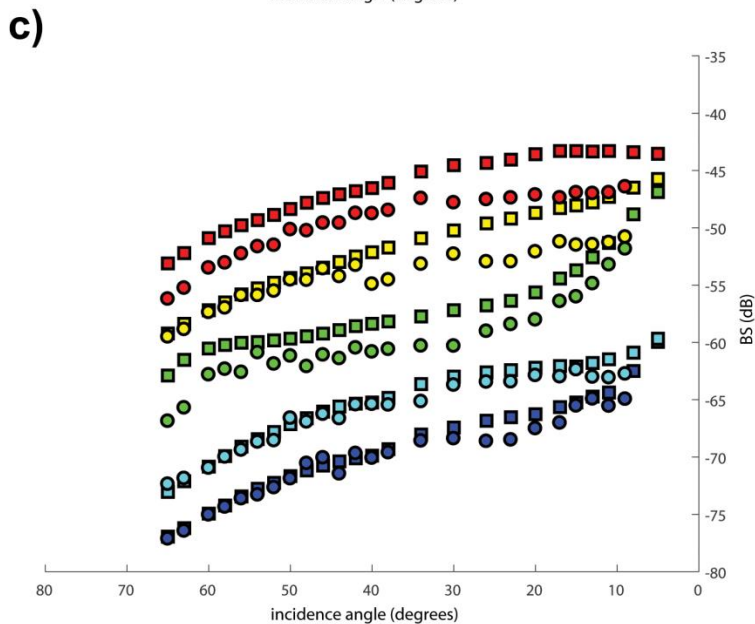
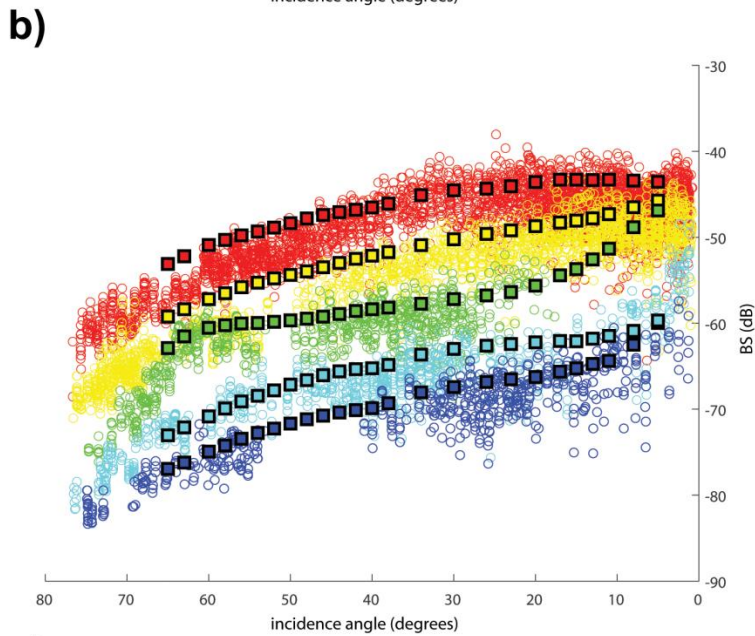


**Figure 6.3:** Angular responses of original soundings overlaid by: a) angular responses derived from cells of the iHAC, b) synthetic HAC, c) iHAC and synthetic HAC angular responses superimposed. Colors symbolize each acoustic class that has been characterized by ground truth data in Table 6.1 (appendix of chapter 6).



LEGEND		CLASS				
		1	2	3	4	5
ARA	original soundings	•	•	•	•	•
	interpolated angular mosaics	•	•	•	•	•
	normalized angular mosaics	■	■	■	■	■
	angular mosaics	■	■	■	■	■

**SAD:** The SAD algorithm uses a set of reference angular signatures representing a known seafloor type (class) (Fig.6.3C) for comparison with unknown signatures extracted from each grid cell of the HAC. Matching is based on criteria set by the user (st. dev. offset, majority) and each cell is assigned with the class represented by the successfully matched reference signature. In this study the offset value was selected according to the standard deviation of dB values from each angular signature, thus different offsets were applied for each class (Table 6.2, appendix of chapter 6). The majority threshold was set to 90% of the total number of incidence angles. Some cells could be matched with up to two adjacent angular signatures and receive double class assignment. In this regard class overlap was quantified and it was found to affect class boundaries of neighboring classes (Fig.6.4). Cells without continuous angular signatures or cells that did not conform to the majority criterion remained unclassified. This algorithm is implemented in Matlab code and is described in Alevizos (2017).

**RF:** The training sample for RF consists of several hundreds of angular backscatter values derived from five ground-truth locations (Fig.6.3AB, Table 6.1, appendix of chapter 6). We fitted models using 50, 100, 200, 500 and 1000 trees and found that all of them produce a zero out-of-bag error rate (OOB). This is an indication that the training sample is particularly effective and produces consistently correct results regardless of the number of trees used to fit the model. Additionally it was found that regarding variable importance some differences occur when fitting was done using a low (50) and high (500) number of trees. When the model is fitted with 50 trees almost half of the angular layers score with much higher importance values for predicting all classes. On the other hand when 500 trees are used for model fitting, the importance scores are much lower for the majority of angular layers regarding prediction of all classes. The individual class importance scores vary for each class and for the number of trees as well. In general, for the model fitted with 50 trees, the importance scores vary individually for each class while angular layers of 50 and 60 degrees incidence received consistently the lowest scores (zeros). When a model with relative higher amount of trees (500) is applied, the importance scores tend to differentiate more clearly two groups of classes. Meaning, that prediction of classes 1 and 2 is influenced more by a few angular layers from the near range (11, 13, 15, 17 degrees), a few angular layers from the middle range (40, 44 and 48 degrees) and a few angular layers from the outer range (54, 63, 65 degrees). In contrast, prediction of classes 3 to 5 was found to be equally influenced by all angular layers. For this application the MGET software (<http://mgel2011-kvm.env.duke.edu/mget>) was used.

**SVM:** Polygons corresponding with the grid-cells of five reference ground-truth locations were used as training areas. The SVM requires a user-defined kernel function for fitting a hyperplane to separate the acoustic classes. In this study we tested a number of kernel functions and it was found that linear, polynomial ( $C_0=1$ ,  $deg=0.5$ ,  $gamma=1$ ) and histogram-intersection functions provided the most convincing classification results (Fig. 6.4). In contrast, radial basis, sigmoid and exponential- $x^2$  kernel functions produced poor to non-realistic classification results. The effectiveness of the above kernel functions is related to the separation pattern of angular backscatter values in feature space. Therefore a suitable kernel function is one that fits better the class boundaries in the hyper-dimensional feature space. The SVM used in this study was implemented in the OpenCV library provided by SAGA GIS.

**ANN:** We run ANN using a) the polygons holding the five reference ground-truth locations and b) all polygons holding ground-truth information (18 locations) (Fig.6.2A, Table 6.1 appendix of chapter 6). The classification results show a more realistic appearance when the total amount of ground-truth data was used for training. One single layer was chosen for model simplicity and a Gaussian function ( $\alpha=1$ ,  $\beta=1$ ) was applied as activation function that adjusts the weight factors of model outputs during the learning process. An activation function is fundamental for ANN learning and its selection is not related to the features of the training set. The Gaussian function was chosen because it was the only one to produce reasonable classification results that are comparable to the results of the three classifiers applied. The number of neurons was set to 18, the same as the number of training areas (Huang et al., 2013). The ANN used in this study was implemented in the OpenCV library provided by SAGA GIS.

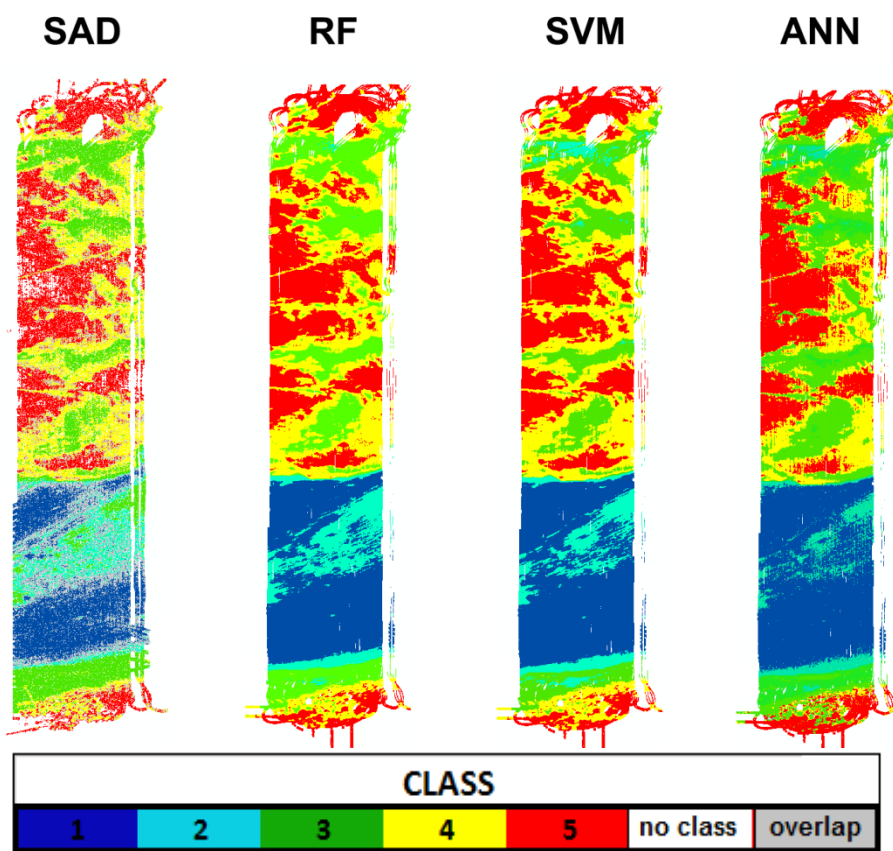


**Figure 6.4:** Supervised classification maps using the angular responses from five ground truth locations corresponding to the cells of the iHAC as training data (Table 6.1, appendix of chapter 6). For the ANN map all 18 ground truth locations needed for training.

## Validation

All classifiers produced very similar classification results (Fig.6.4, Table 6.3) and thus show great potential in automated supervised seafloor classification using high dimensional MBES backscatter datasets with a limited amount of ground truth data for training. Only the ANN classifier required a greater amount of training data (threefold) for producing classification results comparable to the other classifiers. The final classification maps express an agreement in the areal percentage per class but also it can be seen that all classes cover comparable geographical areas among each of the maps. Table 6.3 shows results of each supervised classification map when compared to the classification map of

Alevizos et al. (2017). This map is considered to represent sediment variability in a more objective way, since it has been produced by an unsupervised method that performs cluster validation. The comparison was done with the Map Comparison Kit implemented in (Visser and de Nijs, 2006, <http://mck.riks.nl/>) and agreement was quantified using kappa, kappa\_histogram and kappa\_location coefficients. The kappa coefficient is a standard measure of agreement between two categorical maps while kappa\_histogram expresses the agreement regarding the amount of cells belonging to each class and kappa\_location expresses the agreement of class assignment by location (i.e.: high kappa\_location score means that all areas have been classified similarly between the two maps). All scores suggest strong agreement between each classification map and the Bayesian classification map of Alevizos et al. (2017) with minor fluctuations. The scores of the classification maps produced using the synthetic HAC appear slightly lower than the scores of the classification maps produced using the interpolated HAC, but this difference is not statistically significant (i.e.: both iHAC and synthetic HAC scores in Table 6.3 belong to the highest ranking of agreement). This difference occurs because the backscatter mosaics of the synthetic HAC contain some noise in the nadir and outer range which was not possible to remove from the data, leading to misclassification of a small number of cells.

Table 6.3: Agreement scores between classification maps produced with the iHAC and the synthetic HAC data and the \*Bayesian classification map from Alevizos et al. (2017), calculated using the Map Comparison Kit.

HAC (interpolation)	Agreement scores with Bayesian classification map*			synthetic HAC (normalization)	Agreement scores with Bayesian classification map*		
	Kappa	K_Loc	K_Hist		Kappa	K_Loc	K_Hist
Machine learning classification map				Machine learning classification map			
SAD	0.61	0.70	0.86	SAD	0.53	0.66	0.83
RF	0.73	0.86	0.86	RF	0.61	0.67	0.81
SVM	0.68	0.84	0.81	SVM	0.54	0.66	0.82
ANN	0.68	0.77	0.88	ANN	0.55	0.69	0.81

## 6.4 Discussion

### Effectiveness of the HAC matrix for improving spatial and acoustic resolution of ARA

Until now, the main approach to overcome the problem of acoustic class homogeneity in ARA studies was by segmenting the backscatter mosaic into objects (groups of cells) using algorithms requiring several user-defined parameters. Then angular responses were extracted from soundings falling within each object, assuming that they better discriminate the corresponding seafloor types. The concept examined in this study takes ARA one step forward by introducing the HAC matrix.

The HAC matrix allows for extraction of angular signatures from the lowest level of spatial constituents (i.e.: the grid-cells of the HAC layers) eliminating the need for backscatter mosaic segmentation. Angular signatures derived from fine scale homogeneous seafloor areas (grid-cells similar to the average MBES footprint size) are relevant to the scale of ground-truth data, supporting highest possible separation of seafloor types. In this way, along swath seafloor variations can be resolved and acoustic classes can be assigned for each grid cell and not coarse seafloor patches. These two facts are expected to advance seafloor mapping by offering more detailed acoustic classification results that are consistent with seafloor acoustic properties (i.e.: angular dependence of backscatter). Highly detailed seafloor classification maps can effectively depict fine-scale variations of sediments on the seafloor and provide valuable input to benthic habitat and other studies that rely on effective separation of seafloor sediments.

The layers building the HAC matrix may result either from interpolation of spatially dense backscatter values of each incidence angle (iHAC) or by producing normalized backscatter mosaics using different incidence angle for reference each time (synthetic HAC). The iHAC requires backscatter dedicated MBES surveys with more than 100% overlap for obtaining dense soundings per seafloor area. Since backscatter dedicated MBES surveys are time-consuming (thus costly) the synthetic HAC is a useful alternative. The shape of angular responses yielded from the iHAC may appear less smooth than those derived from the synthetic HAC. This occurs because the cell values of the iHAC reflect the effects of the natural seafloor variability from actual soundings values while the synthetic HAC cell values represent angular variability based on calculation of average local backscatter intensity.

The HAC concept is an objective way to derive homogeneous angular responses in contrast to applying backscatter mosaic segmentation. Mosaic segmentation requires expert knowledge which can be subjective and by varying the segmentation parameters, different angular responses may be obtained. Considering the results of this study we suggest that future backscatter studies should either rely on dense backscatter soundings (for using the iHAC ) or on MBES surveys with conventional overlap but producing several backscatter mosaics normalized for different incidence angle each time that are used to generate the synthetic HAC. In addition a small amount of highly overlapping lines may/should be collected over known seafloor for validation purposes.

## **Suitability of machine learning algorithms for advanced seafloor mapping using the HAC**

Testing the performance of the four applied machine learning classifiers (SAD, RF, SVM, ANN) has revealed valuable information about new capabilities for automated MBES backscatter interpretation. A particular aspect in this study is the application of these algorithms on the HAC matrix. This type of data structure allows for exploiting the angular dependence of backscatter within a new processing concept while preserving the high spatial resolution of angular backscatter layers. One important finding is that the majority of the above classifiers produce valid classification results by using only a small but representative amount of ground truth training data. Thus, careful selection of ground-truth information is crucial for the performance of machine learning classifiers. It is suggested that each seafloor type should be represented by at least one training area. This implies that

even the minimum amount of ground truth data (one sample per seafloor type) is enough for classification, as long as the data come from acoustically and geologically distinct areas.

As a result, careful planning of ground truth sampling prior to classification should take place and it should consider variations in backscatter data as well. In case that the training set consists of polygon cells (for e.g.: SVM, ANN) the cell size should be set at the same size as the grid-cell size of the HAC layers. This affects the quality of angular responses considered and will have an impact on the class separation when the sediment variability is high within a few meters. It is implied that very large cell sizes will result in more mixed angular signatures and may produce inconsistent classification results. The same holds for the case when the training data are points (for e.g.: SAD, RF). Angular responses of reference seafloor types should be continuous and sufficiently separated from each other.

Backscatter values that are encompassed by either training areas or points are not required to have normal distribution when the described classifiers are used. Performing accurate seafloor classification by using high dimensional acoustic data even with a small training set is a very common situation in the field of seafloor mapping. The above algorithms in conjunction with the HAC structure will decrease the time and cost for ground-truth data collection, by using effectively a smaller but representative amount of seafloor samples.

## 6.5 Conclusions

In this study the concept of the HAC matrix was considered for improving the application of ARA using multiple angular backscatter layers. There are two ways of constructing the HAC layers. One that is based on interpolation of actual soundings (iHAC) from single incidence angles (i.e.: from backscatter dedicated surveys with high overlap). The other is to produce backscatter mosaics using a different normalization angle each time (synthetic HAC). Both HAC types yield comparable angular responses per cell that is the finest element of the matrix layers. This guaranties that angular responses come from naturally homogenous areas of the seafloor hence no backscatter mosaic segmentation is required. In addition, acoustic classes are assigned per cell, increasing the spatial resolution of the classification map. Acoustic maps of the seafloor with high resolution are more informative and provide trustworthy comparisons with the ground truth data.

The synthetic HAC provides the possibility to collect MBES data with standard overlap and obtain angular responses per cell as efficiently as with using an iHAC. Thus, the synthetic HAC minimizes the costs of backscatter dedicated surveys and seems as a promising alternative in ARA classification. The high dimensionality of the HAC matrices makes them ideal inputs to machine learning algorithms for advanced supervised seafloor classification by incorporating the angular backscatter information. Machine learning algorithms require the input of ground truth data for training. Practical limitations are usually responsible for collecting small amount of ground truth data and this consists of another challenge in seafloor mapping. In this study we tested the performance of four machine learning algorithms using the HAC layers and only one sample per seafloor type for classification. All four algorithms produced very comparable results that were in agreement with classification results from an unsupervised method (reference). The SAD, the RF and the SVM algorithms produced very comparable results using only one training sample per

seafloor type. In contrast, the ANN algorithm utilized three times the amount of ground truth data for producing similar classification results. The HAC approach described here shows potential in future ARA studies by maximizing acoustic class homogeneity and providing improved class separability. The use of machine learning algorithms in conjunction with high dimensional angular backscatter layers provides a reliable tool for fast, automated seafloor classification that integrates angular backscatter information.



## 7. CONCLUSIONS

### 7.1 Acoustic class separation

Effective identification of seafloor types using ASC methods requires that the acoustic characteristics of seafloor show some uniqueness which can be measured. Examining the acoustic characteristics of various seafloor types using statistical tools is essential for objective and repeatable results in ASC. Bayesian methodology applied on various hydro-acoustic data sets (chapters 3, 4 and 5) has led to important conclusions about the suitability of this unsupervised approach in revealing the dominant acoustic characteristics contained in backscatter data and how they are linked to geological seafloor types.

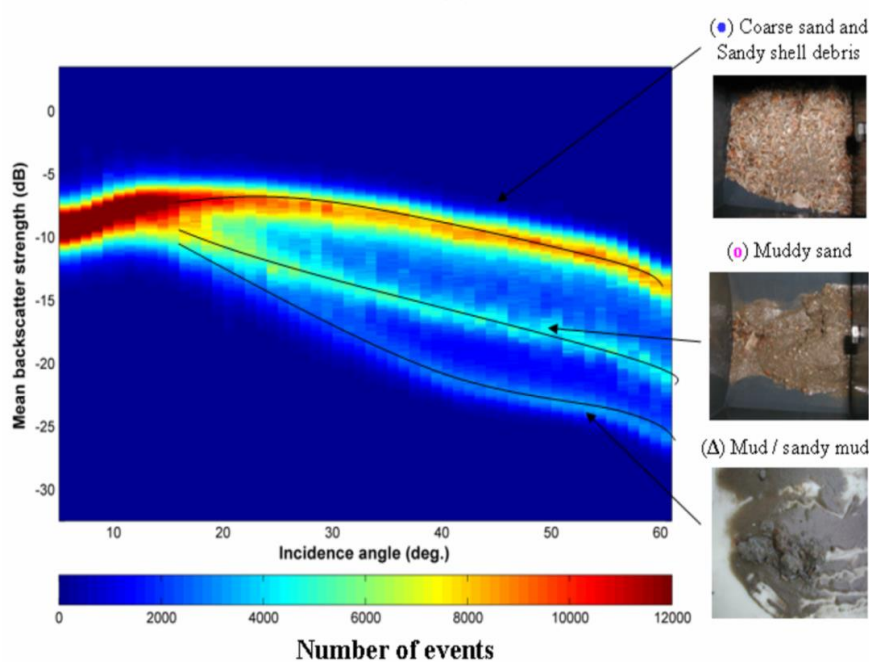


**Figure 7.1:** Plot of a 2D histogram from Parnum, (2007) with dominant angular responses of major seafloor types.

#### 7.1.1 Quantification of class separation – coupling of Bayesian method with ARA

Case studies and model results have indicated that the backscatter from middle range beams (20 – 60 degrees) or the so called “plateau regime” of angular backscatter responses has greater potential in differentiating acoustic classes. This happens because backscatter values representing various seafloor types occur mainly within well-defined ranges, the boundaries of which are more separated in the range of these beams. Lamarche et al. (2011) suggest that backscatter values from 40 to 45 degrees incidence angles are a robust proxy for geological interpretations. In addition, case studies in chapters 3, 4 & 5 show that backscatter values from 38 to 44 degrees incidence angles are more suitable for calculating the optimal number of acoustic classes according to the  $x^2$  criterion. Therefore these incidence angles were used as reference for producing a valid number of Gaussian curves for fitting the histogram of backscatter values resulted from all beams. More information about the suitability of the middle range angles for seafloor classification can be found in section 2.2). It has been further demonstrated, that the middle range angles are more



susceptible to seafloor roughness variations and also to subsurface geological features since they show better penetration potential. These facts offer these angles the ability to provide more detailed backscatter information covering a wider spectrum of backscatter responses.

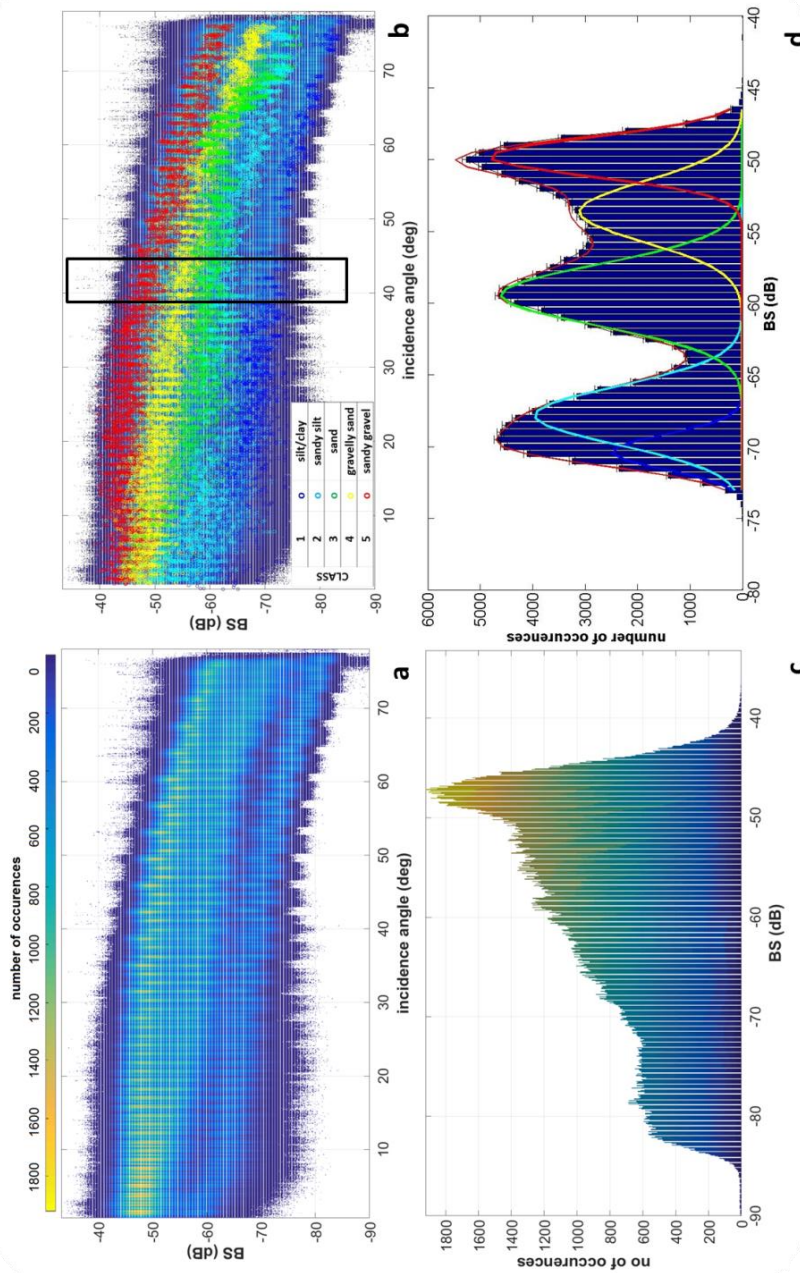


**Figure 7.2:** a) Plot of a 2D histogram using the entire dataset from Chapter 4, b) histogram of plot (b) overlaid with soundings at ground truth locations that have been classified by the Bayesian method, c) Profile view about the Y-Z plane of histogram in plot (a), d) Normalized Gaussian curves fitted on the histogram derived from the black rectangle in plot (b).

Consequently, basing the Bayesian method on backscatter values from middle range angles is a robust statistical approach for differentiating major acoustic classes which are defined by a set of dominant angular responses. The notion of dominant angular responses is derived from representation of backscatter data as a density plot which is essentially a 2D histogram representation of angular backscatter data. To illustrate the density plot better, we consider one example plot from Parnum (2007) (Fig.7.1). In his density plot he identified manually three dominant angular responses which are correlated with distinct seafloor types. In Fig.7.1 not all angular responses may be represented by the same density of

backscatter measurements. The same is true for Fig.7.2a,b where a total number of five Bayesian classes are identified and a manual classification is not possible to be made.

Angular responses of major seafloor types occur along dense patterns whereas other seafloor types may not appear distinctively (Fig.7.2a,c). Although sufficient ground truth data can provide useful information for empirical differentiation of angular responses, it is advisable that a density plot of angular responses should be objectively clustered by means of unsupervised classification.

Thus, we consider the Bayesian classification as an effective tool for identifying local maxima (from middle range angular backscatter) on density histograms (Fig.7.2b,d). These maxima are indicated by the Gaussian curves the mean values of which represent the backscatter values with maximum density along a “narrow corridor” of middle range incidence angles (Fig.7.2b,d). At the same time, the standard deviation value of each Gaussian curve delineates the boundaries between the dominant angular responses. Fundamentally, the Bayesian method links within- and between-angle backscatter variability in a statistically sound way, comprising a useful tool for identifying indirectly the dominant angular responses in the whole dataset.

### 7.1.2 The concept of geo-acoustic resolution

In every task that involves acoustic classification, there is a need for defining acoustic class separability. In short, there is a question about how much “apart” neighboring classes are and what is the minimum seafloor type difference, which can be resolved by means of ASC. These ideas form part of the discussion in chapter 3. Since Bayesian classes are ordinal categorical variables it is implied that there is a degree of similarity between consecutive classes. Therefore, the minimum seafloor type difference that acoustic classes can capture (e.g.: sandy gravel vs gravel) defines the so called geo-acoustic resolution of the method.

The geo-acoustic resolution is considered as an essential parameter since it is a measure of performance of an ASC method. It is perceived as an analogous to radiometric resolution for satellite multispectral imagery although geo-acoustic resolution applies on processed data. The geo-acoustic resolution can be expressed through different statistical tools that measure class homogeneity or the “distance” between classes depending on the type of output classification results. The geo-acoustic resolution can be assessed in two ways: first by examining the statistical significance of the acoustic class differences (cluster validation) and also by using ground truth information (chapters 3, 4, 5).

The geo-acoustic resolution is a measure of the strength of an algorithm to discern natural acoustic variability of similar seafloor types. Thus it is implied that the concept of geo-acoustic resolution is only applicable in unsupervised methods since they don’t make use of a predefined number of classes.

In the Bayesian method the optimal number of classes is defined by the  $\chi^2$  criterion. This criterion has also been referred as the goodness of fit between the Gaussian curves and the histogram curve of backscatter values from selected incidence angles. Theoretically an increasing number of Gaussian curves would approximate better the histogram curve thus leading to an ever increasing number of optimal classes. In practice it is important to identify the optimal number of classes; i.e.: the minimum number of Gaussians that satisfy the  $\chi^2$  criterion. This is because an increasing number of classes may still be valid in terms of

distinguishing even more homogenous seafloor classes however the differences between the classes may not be statistically significant. In essence, if an increasing number of classes do not improve class separation in terms of seafloor types then they should not be considered. The output Bayesian classes are characterized by Gaussian curves holding mean and standard deviation values (in dB) which can be used for expressing the geo-acoustic resolution quantitatively. The difference between the mean values of two adjacent acoustic classes is considered as the minimum acoustic difference that the algorithm can discern. Moreover, the mean backscatter or the categorical values of each class can be correlated with ground truth data for assigning a seafloor type to each acoustic class.

In case study of chapter 3 the Bayesian classes are compared against grain size analysis information. The most important finding is that the method identified seafloor types the differences of which are due to changes in the skewness of the grain size distribution (i.e.: percentage of coarse grained sediments) although the mean grain size values in general appear to be similar. In case study of chapter 4 the seafloor sediments comprise great variability spanning from silt/clay to gravel. Thus the Bayesian classification method discerned acoustic classes representing sediment classes with varying mean grain sizes. However, there was one acoustic class that it was represented by two different types of sediments. Apparently, these two types had an indistinguishable acoustic behavior. In case study of chapter 5 the Bayesian acoustic classes represent substrate types which are defined by different nodule density per seafloor area. However it was not possible to discern the highest nodule density class from nearby areas covered with basalt boulders.

Based on these findings, it can be concluded that there is a great diversity of natural factors that affect backscatter responses when a given sonar type and frequency is used. Thus, the geo-acoustic resolution will be influenced by such factors and the sonar characteristics. The most efficient way to overcome the difficulties of unsupervised classification (that may not resolve similar seafloor types) is with using a sufficient amount of ground truth data for characterization of each acoustic class or for applying supervised classification, given that all seafloor types are appropriately represented by the ground truth data. If there is redundant ground truth data for each class, class homogeneity can further be evaluated with the correlation coefficient and the ANOVA method. In chapter 5, we took advantage of the volume of image analysis results about nodule density and examined the statistical difference of nodule densities belonging to each acoustic class. The most important finding in this study was that each Bayesian acoustic class included samples with statistically different nodule density. In general, the greater the number of optimal classes the finest the geo-acoustic resolution is, suggesting sufficient between-class differences, greater within-class homogeneity and thus more acoustic seafloor types can be resolved.

## **7.2 Improvements of angular response analysis**

### **7.2.1 The hyper-angular cube matrix: spatial resolution, class separation, machine learning**

The hyper-angular cube provides an excellent opportunity for studying the angular dependence of seafloor backscatter in unprecedented detail. Chapters 4 and 6 explain the Hyper-Angular Cube matrix that consists of stacked backscatter layers, resulted from interpolated or normalized backscatter values yielded by different incidence angles. The

significance of the HAC is related with improving the separation between angular responses thus maximizing acoustic discrimination of seafloor types. This is because angular backscatter responses can be extracted from each cell of the HAC matrix instead of half the sonar swath that it is usually the case. Since the size of the HAC cells, is dictated by the size of the average sonar footprint, it is inferred that angular responses derived from single cells would represent naturally homogenous seafloor. This is because seafloor complexity that exists at scales finer than the sonar footprint cannot be resolved. As a result, homogenous angular responses will enhance the separation of mixed seafloor types and allow for more precise classification results. Acoustic homogeneity is generally an issue in ASC studies and traditional approaches of ARA do not offer convincing solutions so far, thus the HAC seems as a promising tool for revealing the homogeneity of distinct seafloor types.

So far in literature the construction of the HAC layers required data from backscatter dedicated surveys with significant swath overlap for yielding dense soundings for each angle per seafloor area. This kind of data acquisition significantly increases the duration of MBES survey and thus its total cost.

Considering that the concept of a high resolution HAC is the way forward in backscatter ARA, there is a need for minimizing/avoiding the time and cost limitations associated with backscatter dedicated surveys. By applying mosaic normalization for constructing the HAC layers (chapter 6) we obtain angular responses that are comparable to those responses derived from actual soundings. We consider this approach as a novelty in backscatter interpretation which is going to significantly improve the quality of ARA results without demanding the cost for backscatter dedicated surveys. It is further suggested that MBES backscatter processing software, should allow user-defined values regarding the angle of normalization for the generation of backscatter mosaics.

The HAC matrix introduces hydro-acoustic data to a novel sense of processing and interpretation. With the HAC, dimensionality of data is increased allowing for description of seafloor backscatter from multiple aspects. In this way, specific seafloor types can be emphasized in particular angular layers (e.g.: seafloor with volume heterogeneity is expected to be more distinguishable in layers of middle and towards the outer swath incidence angles). The HAC matrix can be seen as analogous to a hyper-spectral data cube. Therefore the more angular layers, the better the discrimination capability of various seafloor types. The HAC is suitable for introducing new concepts in backscatter classification and particularly it interconnects ARA with image-based processing. In addition, the HAC can be ideally combined with ground truth data for applying either ARA inversion or empirical ARA models using advanced supervised classification approaches. This is particularly interesting since the dimensions of the HAC cells (from which angular responses are extracted) are similar to the scale of ground truth data (a few square meters area on the seafloor). The great variety of seafloor and sediment types that exist naturally cannot always be modelled by the generic seafloor types that geophysical ARA models produce. Alternatively, empirical ARA models produced by data belonging to the specific study areas, can describe seafloor variability more efficiently. In this regard the HAC layers may be utilized for supervised learning, thus incorporating angular information to empirical relationships for specific seafloor types.

It has been found that supervised classification methods such as the MLC may perform well with small amount of input layers however it is not suitable for large number of layers (Benedickson et al., 1995). In addition the MLC requires that ground truth information from each training sample has normal distribution, fact that further restricts the capability for

adequate classification. Accordingly, high dimensional data (such as the layers of the HAC) require algorithms that can handle large amount of input layers and make use of small but effective amount of ground truth data which do not necessarily follow a normal distribution. Supervised learning algorithms such as those described in chapter 6, appear promising in automated backscatter angular response analysis using high resolution angular backscatter layers. All the tested algorithms in chapter 6 produced very comparable results for five major acoustic classes. This was also found to be in agreement with the unsupervised Bayesian classification results. An additional advantage is that these algorithms require a small amount of training samples for producing adequate classification results (chapter 6).

The emergence of the HAC matrix using MBES data with standard overlap along with the availability of sophisticated algorithms that utilize effectively a reduced amount of training samples is going to have a major impact in future backscatter studies. Through these developments, angular response analysis will be applied on high resolution backscatter layers producing seafloor classification maps that capture fine scale sediment variability without the need for increasing the cost for more data collection. Detailed geo-acoustic maps of the seafloor will drastically revise the way of integrating MBES information with other data, offering great opportunities for more precise estimations of geologically-related quantities such as benthic habitats, geomorphological structures and geochemical fluxes.

## REFERENCES

- Agterberg, F. P., and Bonham-Carter, G.F., 1999, Logistic regression and weights of evidence modeling in mineral exploration, Proc. 28th Interna. Symp. Computer Applications in the Mineral Industries, Golden, Colorado, 483-490.
- Alevizos E, Snellen M, Simons DG, Siemes K, Greinert J, 2015, Acoustic discrimination of relatively homogeneous fine sediments using Bayesian classification on MBES data. *Mar Geol* 370:31–42. doi:[10.1016/j.margeo.2015.10.007](https://doi.org/10.1016/j.margeo.2015.10.007), ISSN 0025-3227
- Alevizos E., 2017, An object-based seafloor classification tool using recognition of empirical angular backscatter signatures, GEOHAB 2017, Halifax, Canada, DOI: 10.13140/RG.2.2.10257.84324
- Alevizos E., Snellen M., Simons D.G., Siemes K., Greinert J., 2017, Multi-angle backscatter classification and sub-bottom profiling for improved seafloor characterization, *Marine Geophysical Research*, Special Issue "Seafloor backscatter from swath echosounders: technology and applications", pp.1-18, DOI:10.1007/s11001-017-9325-4
- Amiri-Simkooei A.R., Snellen M., Simons D.G., 2011, Principal Component Analysis of Single-Beam Echo-Sounder Signal Features for Seafloor Classification. *IEEE Journal of Oceanic Engineering*, 36, 259,272, doi:10.1109/JOE.2011.2122630
- Amiri-Simkooei A.R., Snellen M., Simons D.G., 2009, River bed sediment classification using MBES backscatter data. *Journal of the Acoustic Society of America* vol. 126, no. 4, 1724–1738.
- Amon, D. J., Ziegler, A. F., Dahlgren, T. G., Glover, A. G., Goineau, A., Gooday, A. J., Wiklund, H., Smith, C. R., 2016, First insights into the abundance and diversity of abyssal megafauna in a polymetallic-nodule region in the eastern Clarion-Clipperton Zone, *Sci Rep* 6:30492. doi:10.1038/srep30492.
- Anderson, J.T., Van Holliday, D., Kloser, R., Reid, D.G., and Simard, Y., 2008, Acoustic seabed classification, Current practice and future directions. *ICES Journal of Marine Science*, 65(6): 1004-1011
- Anderson, T.J., Nichol, S.L., Syms, C., Przeslawski, R., Harris, P.T., 2011, Deep-sea bio-physical variables as surrogates for biological assemblages, an example from the Lord Howe Rise, *Deep Sea Research Part II: Topical Studies in Oceanography*, 58, 979-991.
- APL-UW, 1994, High-Frequency Ocean Environmental Acoustic Models Handbook (APL-UW TR 9407). Seattle, WA: Applied Physics Laboratory, University of Washington.
- Augustin J-M., Lamarche G., 2015, High redundancy multibeam echosounder backscatter coverage over strong relief, *Proceedings of the Institute of Acoustics*, Vol.37, Pt.1
- Beaudoin, J., Hughes Clarke, J.E., van den Aamele, E. and Gardner, J., 2002, Geometric and radiometric correction of multibeam backscatter derived from Reson 8101 systems. *Canadian Hydrographic Conference 2002*, Toronto, Canada.
- Beaudoin J., Hughes Clarke J., Doucet M., Brown C., Brissette M., Gazzola V., 2016, Setting the Stage for Multi-Spectral Acoustic Backscatter Research, *GeoHab2016*, Winchester UK, May 3-5.
- Benediktsson JA, Sveinsson JR, Arnason K, 1995, Classification and feature extraction of AVIRIS data. *IEEE Trans Geosci Remote Sens* 33(5):1194–1205
- Bentley SJ, Nittrouer CA, Sommerfield CK, 1996, Development of sedimentary strata in Eckernförde Bay, southwestern Baltic Sea. *Geo-Mar Lett* 16:148–154. doi:[10.1007/BF01204502](https://doi.org/10.1007/BF01204502)
- Bergem, O., Pouliquen, E., Canepa, G., Pace N.G., 1999, Time-evolution modeling of seafloor scatter. II. Numerical and experimental evaluation, *J. Acoust. Soc. Am.* 105(6), 3142-3150
- Beyer A, Chakraborty B, Schenke HW, 2007, Seafloor characterization of the mound and channel provinces of the Porcupine Seabight: an application of the multi-beam angular backscatter data. *Int J Earth Sci.* doi:[10.1007/s00531-005-0022-1](https://doi.org/10.1007/s00531-005-0022-1)
- Blondel P., 2009, *The Handbook of Sidescan Sonar*, Springer, DOI10.1007/978-3-540-49886-5

- Blondel, P., Gomez Sichi, O., 2009, Textural analyses of multibeam sonar imagery from Stanton Banks, Northern Ireland continental shelf. *Applied Acoustics*, 70, 1288–1297.
- Blondel, P., Huvenne, V. and Huehnerbach, V., 2006, Multi-frequency acoustics of deep-water coral habitats and textural characterisation. In, Jesus, S.N. and Rodriguez, O.C. (eds.) *Proceedings of the 8th European Conference on Underwater Acoustics*, 12-15 Jun 2006. 8th European Conference on Underwater Acoustics Carvoeiro, Portugal, ECUA Secretariat, 379-384
- Bluhm, H., 1994, Monitoring megabenthic communities in abyssal manganese nodule sites of the East Pacific Ocean in association with commercial deep-sea mining. *Aquatic Conservation, Marine and Freshwater Ecosystems* 4, 187–201
- Breiman, L., 2001, *Random Forests*. *Mach. Learn.* 45, 5–32.
- Brown CJ, Blondel P, 2009, The application of underwater acoustics to seabed habitat mapping, *Appl Acoust* 70(10):1241. doi:[10.1016/j.apacoust.2008.09.006](https://doi.org/10.1016/j.apacoust.2008.09.006), ISSN 0003-682X
- Brown CJ, Smith SJ, Lawton P, Anderson JT, 2011, Benthic habitat mapping: a review of progress towards improved understanding of the spatial ecology of the seafloor using acoustic techniques. *Estuar Coast Shelf Sci* 92:502–520. doi:[10.1016/j.ecss.2011.02.007](https://doi.org/10.1016/j.ecss.2011.02.007)
- Calinski T., Harabasz J., 1974, A dendrite method for cluster analysis. *Communications in Statistics*, 3, 1–27
- Calvert J, Strong JA, Service M, McGonigle C, Quinn R, 2014, An evaluation of supervised and unsupervised classification techniques for marine benthic habitat mapping using multibeam echosounder data. *ICES J Mar Sci*. doi:[10.1093/icesjms/fsu223](https://doi.org/10.1093/icesjms/fsu223)
- Campbell, J.B. 1996, *Introduction to Remote Sensing*. Taylor & Francis, London
- Canepa, G., Pautet L., Pouliquen E., 2005, Manual of BORIS-SSA: Bottom response from inhomogeneities and surface using small slope approximation, NURC Memorandum M-0152, La Spezia, Italy.
- Canty, M.J., 2007, *Image Analysis, Classification and Change Detection in Remote Sensing with Algorithms for ENVI/IDL*. CRC Press, Taylor & Francis Group, Boca Raton.
- Carranza, E. J. M., and Hale, M., 2001, Geologically constrained fuzzy mapping of gold mineralization potential, Baguio district, Philippines, *Natural Resources Research* 10, 125-136.
- Chakraborty, B., Pathak, D., Sudhakar, M. and Raju, Y. S., 1996, Determination of Nodule Coverage Parameters Using Multibeam Normal Incidence Echo Characteristics: A Study in the Indian Ocean, *Marine Georesources and Geotechnology*, 15, 33–48., doi: [10.1080/10641199709379933](https://doi.org/10.1080/10641199709379933).
- Che-Hasan R, Ierodionou D, Laurenson L, 2012a, Combining angular response classification and backscatter imagery segmentation for benthic biological habitat mapping. *Estuar Coast Shelf Sci* 97:1–9
- Che-Hasan R, Ierodionou D, Laurenson L, Schimel A, 2014, Integrating multibeam backscatter angular response, mosaic and bathymetry data for benthic habitat mapping. *PLoS ONE* 9(5):e97339. doi:[10.1371/journal.pone.0097339](https://doi.org/10.1371/journal.pone.0097339)
- Che-Hasan R, Ierodionou D, Monk J, 2012b, Evaluation of supervised learning methods for benthic habitat mapping using backscatter from multi-beam sonar. *Remote Sens* 4:3427–3443
- Clements A. J., Strong J. A., Flanagan C., Service, M., 2010, Objective stratification and sampling-effort allocation of ground-truthing in benthic-mapping surveys. *ICES Journal of Marine Science*, 67: 628–637, doi: [10.1093/icesjms/fsp280](https://doi.org/10.1093/icesjms/fsp280).
- Coleman A. M., 2008, *An adaptive Landscape classification procedure using geoinformatics and artificial neural networks*, MSc thesis, Vrije Universiteit, Amsterdam, Netherlands.
- Collier JS, Brown CJ, 2005, Correlation of sidescan backscatter with grain size distribution of surficial seabed sediments. *Mar Geol* 214(4):431–449. doi:[10.1016/j.margeo.2004.11.011](https://doi.org/10.1016/j.margeo.2004.11.011)
- Dawoud NN, Samir BB, Janier J, 2011, Fast template matching method based optimized sum of absolute difference algorithm for face localization. *Int J Comp Appl* 18(8).



- de Moustier, C., 1988, "State of the Art in Swath Bathymetry Survey Systems", International Hydrographic Review. 901.<http://scholars.unh.edu/ccom/901>
- de Moustier C. and Alexandrou D., 1991, Angular dependence of 12-kHz seafloor acoustic backscatter. *Journal of the Acoustic Society of America*, vol. 90, no. 1, 522–531, 1991.
- de Moustier, C., 1985, Inference of manganese nodule coverage from Seabeam acoustic backscattering data. *Geophysics*, 50, 989–1005.
- Díaz, J. V. M., 1999, Analysis of Multibeam Sonar Data for the Characterization of Seafloor Habitats, MEng Thesis, University of New Brunswick, pp. 153.
- Diesing M., Green S.L., Stephens D., Lark R.M., Stewart H.A., Dove D., 2014, Mapping seabed sediments: Comparison of manual, geostatistical, object-based image analysis and machine learning approaches, In *Continental Shelf Research*, Volume 84, Pages 107-119, ISSN 0278-4343
- Dolan, M.F.J., Grehan, A.J., Guinan, J.C., Brown, C., 2008. Modelling the Local Distribution of Cold-Water Corals in Relation to Bathymetric Variables: Adding Spatial Context to Deep-sea Video Data. *Deep-Sea Research Part I: Oceanographic Research Papers* 55, 1564-1579.
- Dunn J.C., 1973, A fuzzy relative of the isodata process and its use in detecting compact well separated clusters. *Journal of Cybernetics*. 28, 32–57.
- Dunn, D.C., Halpin, P.N., 2009, Rugosity-based regional modeling of hard-bottom habitat. *Marine Ecology Progress Series* 377, 1-11.
- Durand S., Legendre P., Juniper S.K., 2006, Sonar backscatter differentiation of dominant macrohabitat types in a hydrothermal vent field. *Ecological Applications*, 16, 1421-1435.
- Eleftherakis D, Snellen M, Amiri-Simkooei A, Simons DG, Siemes K, 2014, Observations regarding coarse sediment classification based on multi-beam echo-sounder's backscatter strength and depth residuals in Dutch rivers. *J Acoust Soc Am* 135(number 6):3305–3315
- Eleftherakis D., 2013, Classifying sediments on Dutch riverbeds using multi-beam echo-sounder systems, PhD Thesis, TU Delft
- Eleftherakis D., Amiri-Simkooei A.R. Snellen M., Simons D. G. 2012. Improving riverbed sediment classification using backscatter and depth residual features of multi-beam echo-sounder systems. *Journal of the Acoustical Society of America*, 131, 3710-3725, DOI:<http://dx.doi.org/10.1121/1.3699206>.
- Eleftherakis D., Snellen M., Amiri-Simkooei A.R., Simons D., 2014, Potential of multi-beam echo-sounder backscatter strength and depth residuals as classifying parameters for very coarse riverbed sediments, *Journal of the Acoustical Society of America*, Volume 135 (number 6), 2014, pp. 3305-3315.
- Erdey-Heydorn MD, 2008, An ArcGIS seabed characterization toolbox developed for investigating benthic habitats. *Mar Geodesy* 31(4):318–358. doi:[10.1080/01490410802466819](https://doi.org/10.1080/01490410802466819)
- Estomata M. T. L., Blanco A. C., Nadaoka K., Tomoling E. C. M., 2012, Extraction of benthic cover information from video tows and photographs using object-based image analysis. *International Archives of Photogrammetry and Remote Sensing*, XXXIX-B8, 539-544, doi:[10.5194/isprsarchives-XXXIX-B8-539-2012](https://doi.org/10.5194/isprsarchives-XXXIX-B8-539-2012).
- Etter R.J., Grassle F.J., 1992, Patterns of species diversity in the deep sea as a function of sediment particle size diversity. *Nature*, 360, 360-576.
- Fakiris E, Zoura D, Ferentinos G, Papatheodorou G, 2014, Towards joint use of side scan sonar and subbottom profiler data for the automatic quantification of marine habitats. Case study: Lourdas gulf, Kefalonia isl., Greece, UA2014 2nd international conference and exhibition on underwater acoustics
- Ferrari, R., McKinnon, D., He, H., Smith, R., Corke, P., Gonzalez-Rivero, M., Mumby, P., Upcroft, B., 2016, Quantifying Multiscale Habitat Structural Complexity: A Cost-Effective Framework for Underwater 3D Modelling. *Remote Sensing*, 8(2), 1-21, <http://dx.doi.org/10.3390/rs8020113>



- Ferrini VL, Flood RD , 2006, The effects of fine-scale surface roughness and grain size on 300 kHz multibeam backscatter intensity in sandy marine sedimentary environments. *Mar Geol* 228(1–4):153–172. doi:[10.1016/j.margeo.2005.11.010](https://doi.org/10.1016/j.margeo.2005.11.010)
- Folk RL, 1954, The distinction between grain size and mineral composition in sedimentary-rock nomenclature. *J Geol* 62:344–359
- Fonseca, L., and Calder, B. ,2006, Geocoder: An Efficient Backscatter Map Constructor, Center for Coastal and Ocean Mapping, University of New Hampshire, Durham.
- Fonseca L, Brown C, Calder B, Mayer L, Rzhanov Y, 2009, Angular range analysis of acoustic themes from Stanton Banks Ireland: a link between visual interpretation and multibeam echosounder angular signatures. *Appl Acoust* 70:1298–1304. doi:[10.1016/j.apacoust.2008.09.008](https://doi.org/10.1016/j.apacoust.2008.09.008)
- Fonseca L., Mayer, L. A., 2007, Remote estimation of surficial seafloor properties through the application Angular Range Analysis to multibeam sonar data. *Marine Geophysical Researches*, vol. 28, 119-126, 2007.
- Foubert A., Huvenne V.A.I., Wheeler A., Kozachenko M., Opderbecke J., Henriot J.-P., 2011. The Moira Mounds, small cold-water coral mounds in the Porcupine Seabight, NE Atlantic: Part B. Evaluating the impact of sediment dynamics through high-resolution ROV-borne bathymetric mapping. *Marine Geology*, Volume 282, Issues 1–2, 65-78, <http://dx.doi.org/10.1016/j.margeo.2011.02.008>.
- Gardner, J. V., Dartnell, P., Mayer, L. A., & Hughes Clarke, J. E., 2003, Geomorphology acoustic backscatter and processes in Santa Monica Bay from multibeam mapping. *Marine Environmental Research*. New York, NY, USA: Elsevier
- Gislason, P.O., Benediktsson, J.A., Sveinsson J.R., 2006, Random Forests for land cover classification, *Pattern Recognition Letters*, Volume 27, Issue 4, 294-300, ISSN 0167-8655, <http://dx.doi.org/10.1016/j.patrec.2005.08.011>.
- Greene H.G., Bizzarro J.J., O’Connell V.M., Brylinsky C.K., 2007, Construction of digital potential marine benthic habitat maps using a coded classification scheme and its applications. in Todd, B.J., and Greene, H.G., eds. *Mapping the Seafloor for Habitat Characterization: Geological Association of Canada, Special Paper 47*, pp.145-160.
- Greene H.G., Yoklavich M.M., Starr R., O’Connell V.M., Wakefield W.W., Sullivan D.L., MacRea J.E., Cailliet G.M., 1999, A classification scheme for deep-water seafloor habitats. *Oceanologica Acta*, 22, 663-678
- Greinert, J., McGinnis, D., Naudts, L., Linke, P. and De Batist, M., 2010, Atmospheric methane flux from bubbling seeps: Spatially extrapolated quantification from a Black Sea shelf area. *Journal of Geophysical Research - Oceans*, 115 . C01002. DOI 10.1029/2009JC005381.
- Hamilton L. J., I. M. Parnum, 2011, Acoustic seabed segmentation from direct statistical clustering of entire multibeam sonar backscatter curves. *Continental Shelf Research* 31: 138-148
- Hammerstad, E. ,2000, EM Technical Note: Backscattering and Seabed Image Reflectivity. Horten, Norway: Kongsberg Maritime AS. Technical note, 5pp.
- Haralick RM, Shanmugam K, Dinstein IH, 1973, Textural features for image classification. *IEEE Transactions on Systems, Man and Cybernetics* SMC-3: 610–621
- Hellequin, L., Boucher, J.M., and Lurton, X., 2003, Processing of high-frequency multibeam echo sounder data for seafloor characterization. *IEEE Journal of Oceanic Engineering*, 28(1): 78-89.
- Holmes K.W., Van Niel K.P., Radford B., Kendrick G.A., Grove S.L., 2008. Modelling distribution of marine benthos from hydroacoustics and underwater video. *Continental Shelf Research*, Volume 28, Issue 14, 1800-1810, <http://dx.doi.org/10.1016/j.csr.2008.04.016>.
- Hovland M, Judd AG, 1988, Seabed pockmarks and seapages, impact on geology, and the marine environment. *Graham and Trotman*, London, p 293.
- Huang Z, Siwabessy J, Nichol S, Anderson T, Brooke B, 2013, Predictive mapping of seabed cover types using angular response curves of multibeam backscatter data: testing different feature analysis techniques. *Cont Shelf Res* 61–62:12–22. doi:[10.1016/j.csr.2013.04.024](https://doi.org/10.1016/j.csr.2013.04.024)
- Huetten E., Greinert J., 2008, Software controlled guidance, recording and post-processing of

- seafloor observations by ROV and other towed devices: the software package OFOP. *Geophysica* Research Abstracts, 10, EGU2008-A-03088.
- Hughes Clarke, J.E., 2015, Multispectral Acoustic Backscatter from Multibeam – Improved Classification Potential. U.S. Hydrographic Conference 2015, National Harbor MD
- Hughes Clarke, J.E., 1994, Toward remote seafloor classification using the angular response of acoustic backscattering: a case study from multiple overlapping GLORIA data: *IEEE Journal of Oceanic Engineering* v.19, no.1, p.364-374
- Hughes Clarke, J.E.; Danforth, B.W.; Valentine, P., 1997, Areal seabed classification using backscatter angular response at 95kHz. *High Frequency Acoustics in Shallow Water*, NATO SACLANT Undersea Research Centre, Lerici, Italy, 30 Jun-4 Jul 1997. Vol.Series CP-45: 243-250.
- Hühnerbach, V., Blondel, Ph., Huvenne, V., Freiwald, A., 2008, Habitat mapping on a deepwater coral reef off Norway, with a comparison of visual and computer assisted sonar imagery interpretation. In: Todd B, Greene G, editors. *Habitat mapping*. Geological association of Canada special paper, vol. 47. 297–30.
- Ierodiaconou D, Burq S, Laurenson L, Reston M, 2007, Marine habitat mapping using multibeam data, georeferenced video and image classification techniques: a case study in southwest Victoria. *J Spatial Sci* 52(1):93–104
- Ierodiaconou D., Monk J., Rattray A., Laurenson L., Versace V.L., 2011, Comparison of automated classification techniques for predicting benthic biological communities using hydroacoustics and video observations. *Continental Shelf Research*, 31 (2 SUPPL.), S28-S38, DOI: 10.1016/j.csr.2010.01.012.
- Innangi S., Barra M., Di Martino G., Parnum I.M., Tonielli R., Mazzola S., 2015, Reson SeaBat 8125 backscatter data as a tool for seabed characterization (Central Mediterranean, Southern Italy): Results from different processing approaches, *Applied Acoustics*, Volume 87, Pages 109-122, ISSN 0003-682X, <https://doi.org/10.1016/j.apacoust.2014.06.014>
- ISA, 2010, A Geological Model of Polymetallic Nodule Deposits in the Clarion-Clipperton Fracture Zone. Technical Study: No. 6, International Seabed Authority, Kingston, Jamaica. <http://www.isa.org.jm/files/documents/EN/Pubs/GeoMod-web.pdf>
- Iwahashi, J., and Pike, R.J., 2007, Automated classifications of topography from DEMs by an unsupervised nested-means algorithm and a three-part geometric signature. *Geomorphology*, 86, 409–440.
- Jackson, D.R., and Briggs, K.B., 1992, High-frequency bottom backscattering: Roughness versus sediment volume scattering. *Journal of the Acoustical Society of America*, 92(2): 962-977.
- Jackson, D., Richardson, M., 2007, *High Frequency Seafloor Acoustic*. Springer, N.Y.: 616 pp.
- Jackson, D.R., Ishimaru, A., and Winebrenner, D.P., 1986, Application of the composite roughness model to high frequency bottom backscattering. *Journal of the Acoustical Society of America*, 79(5): 1410-1422.
- Jensen JB, Kuijpers A, Bennike O, Laier T, Werner F, 2002, New geological aspects for freshwater seepage and formation in Eckernförde Bay, western Baltic. *Cont Shelf Res* 22:2159–2173. doi:[10.1016/S0278-4343\(02\)00076-6](https://doi.org/10.1016/S0278-4343(02)00076-6)
- Kinsler, L.E., Frey, A.R., Coppens, A.B., and Sanders, J.V., 1999, *Fundamentals of Acoustics*, 4th. John Wiley, New York.
- Ko, Y., Lee, S., Kim, J., Kim, K.,H., Jung, M.,S., 2006, Relationship between Mn nodule abundance and other geological factors in the northeastern Pacific: application of GIS and probability method, *Ocean Sci. J.* 41(3),149-161.
- Kostylev V.E., Courtney R.C., Robert G. Todd B.J., 2003, Stock evaluation of giant scallop (*Placopecten magellanicus*) using high-resolution acoustics for seabed mapping. *Fisheries Research*, 60, 479–492

- Kumar RM., Sreekumar K., 2014, A Survey of Image Feature Descriptors. *International Journal of Computer Science and Information Technologies*, Vol. 5(6).
- Kwasnitschka, T., Köser, K., Sticklus, J., Rothenbeck, M., Weiß, T., Wenzlaff, E., Schoening, T., Triebe, L., Steinführer, A., Devey, C., Greinert, J., 2016, DeepSurveyCam—A Deep Ocean Optical Mapping System, *Sensors* 16 (2),164
- Lamarche G, Lurton X, Verdier A-L, Augustin J-M, 2011, Quantitative characterisation of seafloor substrate and bedforms using advanced processing of multibeam backscatter-application to Cook Strait, New Zealand. *Cont Shelf Res*, 31(2 suppl):S93–S109. doi:[10.1016/j.csr.2010.06.001](https://doi.org/10.1016/j.csr.2010.06.001)
- Le Bas TP, Huvenne VAI, 2009, Acquisition and processing of backscatter data for habitat mapping: comparison of multibeam and sidescan systems. *Appl Acoust* 70(10):1248–1257. doi:[10.1016/j.apacoust.2008.07.010](https://doi.org/10.1016/j.apacoust.2008.07.010), ISSN 0003-682X
- Lee, S.,H., Kim, K.,H., 2004, Side-scan sonar characteristics and manganese nodule abundance in the Clarion-Clipperton Fracture Zones NE equatorial Pacific, *Mar. Georesour. Geotech*, 22, 103-114.
- Lucieer V., Lamarche G., 2011, Unsupervised fuzzy classification and object-based image analysis of multibeam data to map deep water substrates, Cook Strait, New Zealand. *Continental Shelf Research*, 31 (11), 1236-1247, DOI: [10.1016/j.csr.2011.04.016](https://doi.org/10.1016/j.csr.2011.04.016).
- Lucieer V., Lucieer A., 2009, Fuzzy clustering for seafloor classification. *Marine Geology*, Volume 264, Issues 3–4, 230-241, <http://dx.doi.org/10.1016/j.margeo.2009.06.006>.
- Lucieer, V., Hill, N.A., Barrett, N.S., Nichol, S., 2013, Do marine substrates ‘look’ and ‘sound’ the same? Supervised classification of multibeam acoustic data using autonomous underwater vehicle images. *Estuarine Coastal Shelf Sci*.117, 94–106.
- Lundblad E., Wright D. J., Miller J., Larkin E. M., Rinehart R., Naar D. F., Donahue B. T., Anderson S. M., Battista T., 2006, A Benthic Terrain Classification Scheme for American Samoa. *Marine Geodesy* 29(2):89–111
- Lurton, X., Dugelay, S., and Augustin, J.M., 1994, Analysis of multibeam echo sounder signals from the deep seafloor. *IEEE 1994*, Brest, France: 213-218.
- Lurton, X., 2002, An introduction to underwater acoustics: principles and applications, Springer, ISBN 978-3-540-78480-7
- Lurton, X., 2010, An Introduction to Underwater Acoustics. Principles and Applications. 2nd edition. Springer Praxis Books & Praxis Publishing, UK: 346 pp.
- Lurton, X., Lamarche, G. (Eds), 2015, Backscatter measurements by seafloor-mapping sonars. Guidelines and Recommendations. 200p. <http://geohab.org/wp-content/uploads/2014/05/BSWGREPORT-MAY2015.pdf>
- Marcon Y., Sahling H., Allais A.G., Bohrmann G., Olu K., 2014, Distribution and temporal variation of mega-fauna at the Regab pockmark (Northern Congo Fan) based on a comparison of videomosaics and geographic information systems analyses. *Marine Ecology*, 35, 77–95. doi: [10.1111/maec.12056](https://doi.org/10.1111/maec.12056)
- Margolis, S. V., Burns, R. G., 1976, Pacific deep-sea manganese nodules: their distribution, composition and origin. *Annual Review of Earth and Planetary Sciences*, 4, 229-263.
- Martin, W. E., Bridgmon, K. D., 2012, Quantitative and statistical research methods: from hypothesis to results. New Jersey: John Wiley & Sons, ISBN: 978-0-470-63182-9.
- Masson, D. G., Scanlon, K. M., 1992, Fe-Mn Nodule Field Indicated Gloria, North of the Puerto Rico Trench, *Geo-Marine Letters*, 208-213.
- Mayer, L., Fonseca, L., Pacheco, M., Galway, S., Martinez, J. V. and Hou, T., 1999, “The STRATAFORM GIS CD,” U.S. Office of Naval Research distribution.
- McGonigle C, Collier JS ,2014, Interlinking backscatter, grain size and benthic community structure. *Estuar Coast Shelf Sci* 147:123–136. doi:[10.1016/j.ecss.2014.05.025](https://doi.org/10.1016/j.ecss.2014.05.025)

- McGonigle C., Brown C., Quinn R., Grabowski J., 2009. Evaluation of image-based multibeam sonar backscatter classification for benthic habitat discrimination and mapping at Stanton Banks, UK. *Estuarine, Coastal and Shelf Science*, 81, 423-437, DOI: 10.1016/j.ecss.2008.11.017.
- Memarsadeghi, N., Mount, D.M., Netanyahu, N.S., Moigne, J.L., 2007, A fast implementation of the isodata clustering algorithm. *International Journal of Computational Geometry and Applications* 17, 71–103.
- Moore, I.D., Grayson, R.B., Ladson, A.R., 1991, Digital terrain modelling: a review of hydrological, geomorphological, and biological applications. *Hydrological Processes*, 5, 3 – 30.
- Mopin, I., Lurton, X., and Le Bouffant, N. ,2012, Intensity calibration of Multibeam-Echosounders: issues and possible solutions. *ICours Advances in Seafloor Mapping, SeaTechWeek 2012, Brest, France.*
- Mulder J.P.M., Louters T., Hallie F.P., Postma R., Craeymeersch J.A., Hamerlynck O., 1991, Integrated coastal research in the SW Netherlands. *Proceedings of the 26th International Coastal Engineering Conference*, 3, 2984-2997.
- Müller H, von Dobeneck T, Nehmiz W, Hamer K ,2011, Near-surface electromagnetic, rock magnetic, and geochemical fingerprinting of submarine freshwater seepage at Eckernförde Bay (SW Baltic Sea). *Geo-Mar Lett* 31(2):123–140. doi:10.1007/s00367-010-0220-0
- Naudts, L., Greinert, J., Artemov, Y., Beaubien, S. E., Borowski, C. and De Batist, M., 2008, Anomalous sea-floor backscatter patterns in methane venting areas, Dnepr paleo-delta, NW Black Sea. *Marine Geology*, 251 . pp. 253-267. DOI 10.1016/j.margeo.2008.03.002
- Neves B.M., Du Preez C., Edinger E., 2014, Mapping coral and sponge habitats on a shelf-depth environment using multibeam sonar and ROV video observations: Learmonth Bank, northern British Columbia, Canada. *Deep Sea Research Part II: Topical Studies in Oceanography*, 99, 169-183, <http://dx.doi.org/10.1016/j.dsr2.2013.05.026>.
- Nittrouer CA, Lopez GR, Wright LD, Bentley SJ, D’Andrea AF, Friedrichs CT, Craig NI, Sommerfield CK, 1998, Oceanographic processes and the preservation of sedimentary structure in Eckernförde Bay, Baltic Sea. *Cont Shelf Res* 18(14–15):1689–1714. doi:10.1016/S0278-4343(98)00054-5, ISSN 0278-4343
- Novarini, J. C., Caruthers, J. W., 1998, “A simplified approach to backscattering from a rough seafloor with sediment inhomogeneities,” *The Journal of Oceanic Engineering* 23 (3), 157-166.
- Okazaki, M., Tsune, A., 2013, Exploration of Polymetallic Nodules Using AUV in the Central Equatorial Pacific, *Proc. of the ISOPE Ocean Mining Symposium, Szczecin, Poland, 22-26 September 2013*, 32-38.
- Parnum IM, 2007, Benthic habitat mapping using multibeam sonar systems. PhD thesis, Curtin University, Perth, p 208
- Petersen, S., Krätschell, A., Augustin, N., Jamieson, J., Hein, J. R. und Hannington, M. D., 2016 , News from the seabed – Geological characteristics and resource potential of deep-sea mineral resources, *Marine Policy*, 70 , pp. 175-187. DOI 10.1016/j.marpol.2016.03.012
- Peukert A., 2015, Correlation of ship-and AUV-based multibeam and side scan sonar analyses with visual AUV-and ROV-based data: studies for Mn-nodule density quantification and mining-related environmental impact assessments. Master thesis, Christian-Albrechts-Universität Kiel/GEOMAR
- Pouliquen, E., Bergem, O., Pace, N.G., 1999, Time-evolution modelling of seafloor scatter. I. Concept, *J. Acoust. Soc. Am.* **105**(6), 3136–3141.
- Preston J., 2009, Automated acoustic seabed classification of multibeam images of Stanton Banks. *Appl Acoust* 70(10):1277–1287.doi:10.1016/j.apacoust.2008.07.011
- Purser, A., Marcon, Y., Hoving, H.J.T., Vecchione, M., Piatkowski, U., Eason, D., Bluhm, H., Boetius, A., 2016, Association of deep-sea incirrate octopods with manganese crusts and nodule fields in the Pacific Ocean, *Current Biology*, 26, Issue 24, 2016, R1268-R1269, ISSN 0960-9822, <http://dx.doi.org/10.1016/j.cub.2016.10.052>.

- Reid, D. 2007, Accounting for spatial and temporal scales and interpolation in ASC surveys. ICES Cooperative Research Report, 286:77–100
- Rengstorf, A. M., Yesson, C., Brown, C. and Grehan, A. J., 2013, High-resolution habitat suitability modelling can improve conservation of vulnerable marine ecosystems in the deep sea. *J. Biogeogr.*, 40: 1702–1714. doi:10.1111/jbi.12123
- Roberts, J.J., Best, B.D., Dunn, D.C., Treml, E.A., Halpin, P.N., 2010, Marine Geospatial Ecology Tools: An integrated framework for ecological geoprocessing with ArcGIS, Python, R, MATLAB, and C++. *Environmental Modelling & Software*, 25, 1197-1207. doi: 10.1016/j.envsoft.2010.03.029.
- Rooper C.N., Zimmermann M., 2007, A bottom-up methodology for integrating underwater video and acoustic mapping for seafloor substrate classification. *Continental Shelf Research*, Volume 27, Issue 7, 947-957, <http://dx.doi.org/10.1016/j.csr.2006.12.006>.
- Rzhanov Y, Fonseca L, Mayer L, 2012, Construction of seafloor thematic maps from multibeam acoustic backscatter angular response data. *Comput Geosci* 41:181–187. doi:10.1016/j.cageo.2011.09.001
- Savini A., Vertino A., Marchese F., Beuck L., Freiwald A., 2014, Mapping Cold-Water Coral Habitats at Different Scales within the Northern Ionian Sea (Central Mediterranean): An Assessment of Coral Coverage and Associated Vulnerability. *PLoS ONE* 9(1), doi:10.1371/journal.pone.0087108
- Schoening, T., Kuhn, T., Nattkemper, T.W., 2012, Estimation of poly-metallic nodule coverage in benthic images, Proc. of the 41st Conference of the Underwater Mining Institute (UMI).
- Schoening, T., Jones, D. O., and Greinert, J., 2017, Compact-morphology-based poly-metallic nodule delineation, *Scientific Reports*, 7, 13 338, doi:10.1038/s41598-017-13335-x.
- Sharma, R., Khadge, N.H., Sankar, S.J., 2013, Assessing the distribution and abundance of seabed minerals from seafloor photographic data in the Central Indian Ocean Basin, *International journal of remote sensing*, 34 (5), 1691-1706.
- Siemes K, Snellen M, Amiri Simkooei A, Simons DG, Hermand JP, 2010, Predicting spatial variability of sediment properties from hydrographic data for geoacoustic inversion. *IEEE J OceanicEng* 35(4):766–778
- Siemes K., Snellen M., Simons D. G., Hermand J.P., 2009, Using MBES backscatter strength measurements for assessing a shallow water soft sediment environment. *IEEE OCEANS Conference Proceedings*.
- Simons D.G., Snellen M. & Ainslie M.A., 2007, A multivariate correlation analysis of high frequency bottom backscattering strength measurements with geo-technical parameters. *IEEE Journal of Oceanic Engineering*, Volume 32 (number 3), 640-650
- Simons D.G., Snellen M., 2009, A Bayesian technique to seafloor classification using multi-beam echo-sounder backscatter data. *Applied Acoustics*, Volume 70, 1258-1268, <http://dx.doi.org/10.1016/j.apacoust.2008.07.013>
- Snellen M, Eleftherakis D, Amiri-Simkooei A, Koomans RL, Simons DG, 2013, An inter-comparison of sediment classification methods based on multi-beam echo-sounder backscatter and sediment natural radioactivity data. *J Acoust Soc Am* 134(2):959–970. doi:10.1121/1.4812858
- Stephens D., Diesing M., 2014, A Comparison of Supervised Classification Methods for the Prediction of Substrate Type Using Multibeam Acoustic and Legacy Grain-Size Data. *PLoS ONE*, doi:10.1371/journal.pone.0093950.
- Summers-Morris E., Iampietro P., Kvitek R., 2004, Geographic Information Systems (GIS) analysis of high-resolution multibeam bathymetry and remotely operated vehicle data to model rockfish habitat preference. *The Journal of the Acoustical Society of America*, 116, 2486-2486, DOI:<http://dx.doi.org/10.1121/1.4784927>
- Sweeney EM, Gardner JV, Johnson JE, Mayer LA, 2012, Geological interpretation of a low-backscatter anomaly found on the New Jersey continental margin. *Mar Geol* 326–328:46–54. doi:10.1016/j.margeo.2012.08.007, ISSN 0025-3227



- Tesei A, Canepa G, Zampolli M, 2009, Measurements and modelling of high-frequency acoustic scattering by a rough seafloor and sea surface, Proceedings of the 3rd International Conference and Exhibition on Underwater Acoustic Measurements: Technologies and Results, 21-26 June, 2009, Nafplion, Greece
- Thiel, H., 2001, Evaluation of the environmental consequences of polymetallic nodule mining based on the results of the TUSCH Research Association, Deep Sea Research Part II: Topical Studies in Oceanography, 48, (17–18), 3433-3452. doi: [http://dx.doi.org/10.1016/S0967-0645\(01\)00051-0](http://dx.doi.org/10.1016/S0967-0645(01)00051-0)
- Tibshirani R, Walther G, Hastie T., 2001, Estimating the number of clusters in a data set via the gap statistic. *J R Stat Soc - Series B: Stat Methodology.*;63:411–423
- Urick, R.J., 1983, Principles of Underwater Sound (3rd edn). McGraw-Hill, New York.
- van Leeuwen, B., 2012, Artificial neural networks and geographic information systems for inland excess water classification. Ph.D. dissertation, University of Szeged, Hungary
- Vanreusel, A., Hilario, A., Ribeiro, P. A., Menot, L., and Arbizu, P. M., 2016, Threatened by mining, polymetallic nodules are required to preserve abyssal epifauna. *Sci. Rep.* 6:26808. doi: [10.1038/srep26808](https://doi.org/10.1038/srep26808)
- Verfaillie E, Degraer S, Schelfaut K, Willems W, Van Lancker V, 2009, A protocol for classifying ecologically relevant marine zones, a statistical approach. *Estuar Coast Shelf Sci* 83(2):175–185. doi:[10.1016/j.ecss.2009.03.003](https://doi.org/10.1016/j.ecss.2009.03.003), ISSN 0272-7714
- Vineesh, T. C., Nath, B. N., Banerjee, R., Jaisankar, S. and Lekshmi, V., 2009, Manganese Nodule Morphology as Indicators for Oceanic Processes in the Central Indian Basin, *International Geology Review*, 51, 27–44.
- Visser H. , de Nijs T., 2006, The Map Comparison Kit. *Environmental Modeling & Software* 21, 346-358.
- von Deimling JS, Weinrebe W, Tóth ZS, Fossing H, Endler R, Rehder G, Spieß V, 2013, A low frequency multibeam assessment: spatial mapping of shallow gas by enhanced penetration and angular response anomaly. *Mar Petrol Geol* 44:217–222. doi:[10.1016/j.marpetgeo.2013.02.013](https://doi.org/10.1016/j.marpetgeo.2013.02.013), ISSN 0264-8172
- Weiss, A.D., 2001, Topographic Position and Landforms Analysis. Poster presentation, ESRI User Conference, San Diego, CA.
- Welton, B., Beaudoin, J., Weber, T.C., Lanzoni, C., and Rice, G.A., 2013, Development of a Method for a Relative Backscatter Field Calibration using Reson 7125 Multibeam Sonar Systems. US Hydrographic Conference 2013, New Orleans, LA, USA.
- Weydert, M., 1990, Measurements of the acoustic backscatter of selected areas of the deep seafloor and some implications for the assessment of manganese nodule resources, *J Acoustical Society of America*, 88, 350–366.
- Weydert, M., 1985, Measurement of acoustic backscattering of the deep seafloor using a deeply towed vehicle. A technique to investigate the physical and geological properties of the deep seafloor and to assess manganese nodule resources, Ph.D thesis, San Diego: University of California.
- Whiticar MJ, 2002, Diagenetic relationships of methanogenesis, nutrients, acoustic turbidity, pockmarks and freshwater seepages in Eckernförde Bay. *Mar Geol* 182:29–53. doi:[10.1016/S0025-3227\(01\)00227-4](https://doi.org/10.1016/S0025-3227(01)00227-4)
- Williams K. L., Jackson D. R., Thorsos E. I., Tang D., Briggs K. B., 1998, “Acoustic backscattering experiments in a well characterized sand sediment: Data/model comparisons using sediment fluid and Biot models,” *IEEE J. Ocean. Eng.* 27, 376–387
- Wilson, M.F.J., O’Connell, B., Brown, C., Guinan, J.C., Grehan, A.J., 2007, Multiscale terrain analysis of multibeam bathymetry data for habitat mapping on the continental slope. *Marine Geodesy* 30, 3-35

- Wright, D. Report of HURL Cruise KOK0510: Submersible Dives and Multibeam Mapping to Investigate Benthic Habitats of Tutuila, American Samoa. Technical Report, NOAA's Office of Undersea Research Submersible Science Program, Hawaii Undersea Research Lab, Honolulu, HI, <http://dusk.geo.orst.edu/djl/Samoa/hurl/k.kO510cruisereport.pdf>
- Wright, D.J., Pendleton, M., Boulware, J., Walbridge, S., Gerlt, B., Eslinger, D., Sampson, D., and Huntley, E., 2012, ArcGISBenthic Terrain Modeler (BTM), v. 3.0, Environmental Systems Research Institute, NOAA Coastal Services Center, Massachusetts Office of Coastal Zone Management

## APPENDICES APPENDIX OF CHAPTER 3

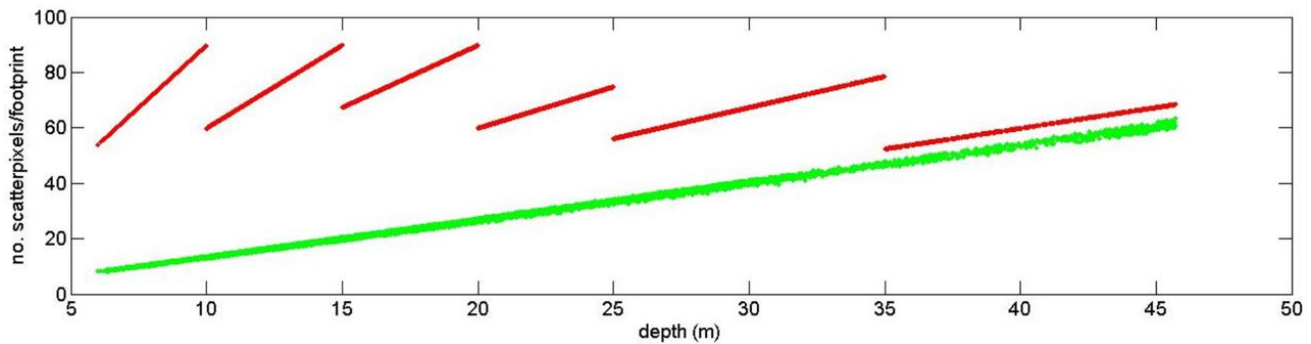


**Figure 3.2.** An example of the theoretical (red) and estimated (green) scatter pixels for beam with incidence angle 50 degrees of the port side versus depth.

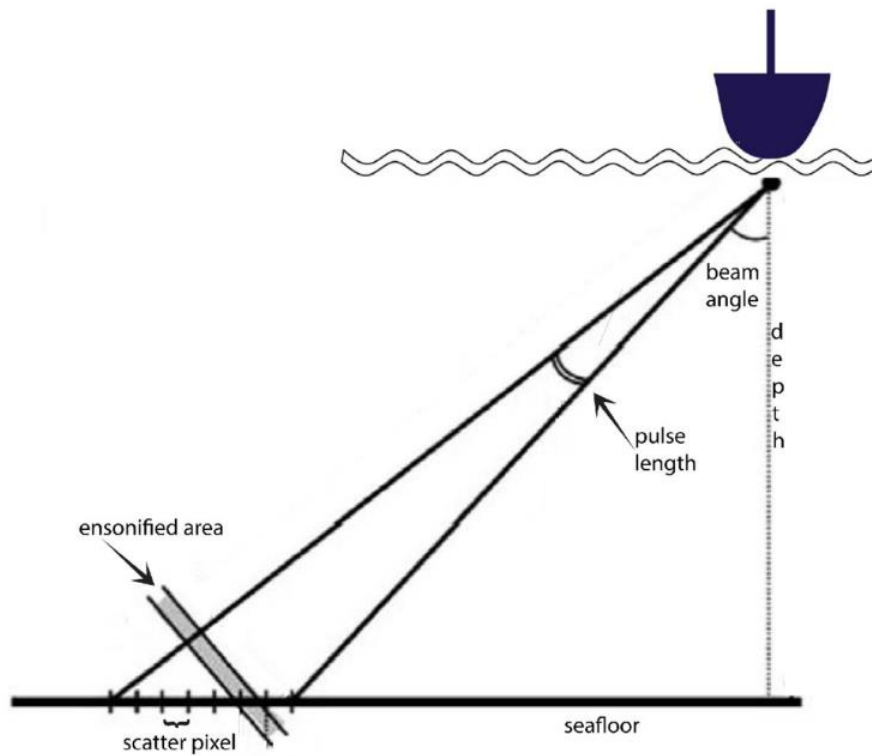


**Figure 3.3:** Graphical representation of the scatter pixels concept (modified after Simons & Snellen, 2009).

$$N_{\theta} = \frac{dA}{da} = (H\theta_T / \cos^2\theta) (2\sin(\theta) / c\tau) \quad [3.1]$$

Where:  $N_{\theta}$  = number of scatter pixels,  $dA$  = depends on waterdepth  $H$  and the beam opening angle  $\theta_T$ . Whereas  $da$  depends on the water column sound speed  $c$  and the pulse length  $\tau$ .



## APPENDIX OF CHAPTER 4

Table 4.1: Population statistic features and frequency distributions (x axis: backscatter (dB), y axis: frequency) of soundings from five sediment sample locations (5x5m patches)

Training areas (5x5 meters)	
<p><b>Sample_No: 1</b></p> <p>Acoustic class : 5                      Type: sandy Gravel                      Number of soundings: 1517                      Mean dB: -48.1</p>	<p style="text-align: center;"><b>Distribution</b></p> <p style="text-align: center;">Frequency Distribution</p> <p style="text-align: center;">-63.8 -60.8 -57.7 -54.7 -51.6 -48.6 -45.5 -42.5 -39.5</p>
<p><b>Sample_No: 18</b></p> <p>Acoustic class : 4                      Type: gravelly Sand                      Number of soundings: 1442                      Mean dB: -53.9</p>	<p style="text-align: center;">Frequency Distribution</p> <p style="text-align: center;">-70.6 -67.3 -64.0 -60.8 -57.5 -54.2 -50.9 -47.7 -44.4</p>
<p><b>Sample_No: 3</b></p> <p>Acoustic class : 3                      Type: Sand                      Number of soundings: 782                      Mean dB: -61.8</p>	<p style="text-align: center;">Frequency Distribution</p> <p style="text-align: center;">-76.2 -73.1 -69.9 -66.8 -63.7 -60.6 -57.4 -54.3</p>
<p><b>Sample_No: 9</b></p> <p>Acoustic class : 2                      Type: (gravelly/sandy) Mud                      Number of soundings: 312                      Mean dB: -64.4</p>	<p style="text-align: center;">Frequency Distribution</p> <p style="text-align: center;">-76.1 -73.0 -69.8 -66.7 -63.5 -60.4 -57.3</p>
<p><b>Sample_No: 7</b></p> <p>Acoustic class : 1                      Type: Mud &amp; Clay                      Number of soundings: 287                      Mean dB: -71.7</p>	<p style="text-align: center;">Frequency Distribution</p> <p style="text-align: center;">-83.4 -80.5 -77.6 -74.8 -71.9 -69.0 -66.1</p>

Table 4.3: Percentages and grain size statistics of the coarse and fine grain fractions, presence of shells from sieved data measurements and classifications results.

sample	W% >6.3mm	W% 2-6.3mm	W% 2mm-500µm	W% <500µm	Shells/pebbles	d50 (<500µm)	Mode (<500µm)	D50 all (µm)	mode all (µm)	Bayes class	ARA-MLC class	PCA class
1	14.59	20.17	34.12	31.12	1/1	240.0	246.0	2600	1000	5	5	5
2	2.23	30.89	21.96	44.91	1/1	220.0	246.0	1800	4000	5	5	5
3	0.00	0.65	14.49	84.86	1/0	170.0	197.0	210	180	3	3	3
4	0.00	0.49	2.56	96.95	1/0	151.8	191.5	200	180	3	3	3
5	0.00	0.69	3.28	96.03	1/0	41.3	73.0	100	90	2	3	2
6	0.00	0.00	0.00	100.00	0/0	23.0	44.3	50	40	2	1	2
7	0.00	0.00	0.00	100.00	0/0	23.0	43.5	50	40	1	2	1
8	0.00	0.00	0.00	100.00	0/0	26.3	43.0	50	40	1	1	1
9	0.00	3.39	0.74	95.87	0/0	20.8	41.0	40	40	3	2	2
10	0.00	0.00	0.72	99.28	0/0	21.0	43.8	40	40	2	2	2
11	0.00	0.72	0.24	99.04	0/0	20.5	42.0	50	40	2	-	-
12	0.00	0.42	15.36	84.21	1/1	197.0	236.0	320	250	4	5	4
13	0.00	0.27	7.89	91.84	1/0	157.0	270.0	290	250	3	3	3
14	0.00	0.38	21.87	77.76	1/1	192.0	216.0	280	180	3	3	3
15	0.00	0.40	4.08	95.52	1/0	206.0	236.0	220	130	3	3	3
16	0.00	0.07	7.94	92.00	1/1	236.0	246.0	460	350	3	3	4
17	0.00	8.06	18.38	73.57	0/1	84.0	188.0	210	180	4	3	4
18	0.00	1.41	31.15	67.44	1/0	282.0	270.0	270	350	4	4	4
19	0.00	0.00	7.93	92.07	0/0	226.0	236.0	310	250	3	3	3
20	0.00	0.13	5.90	93.97	0/0	56.0	258.0	280	250	3	2	3
21	0.00	1.10	3.87	95.04	0/0	112.0	150.0	150	130	4	4	4
22	0.00	0.00	1.31	98.69	0/0	50.8	109.0	110	90	2	3	2

APPENDIX OF CHAPTER 5

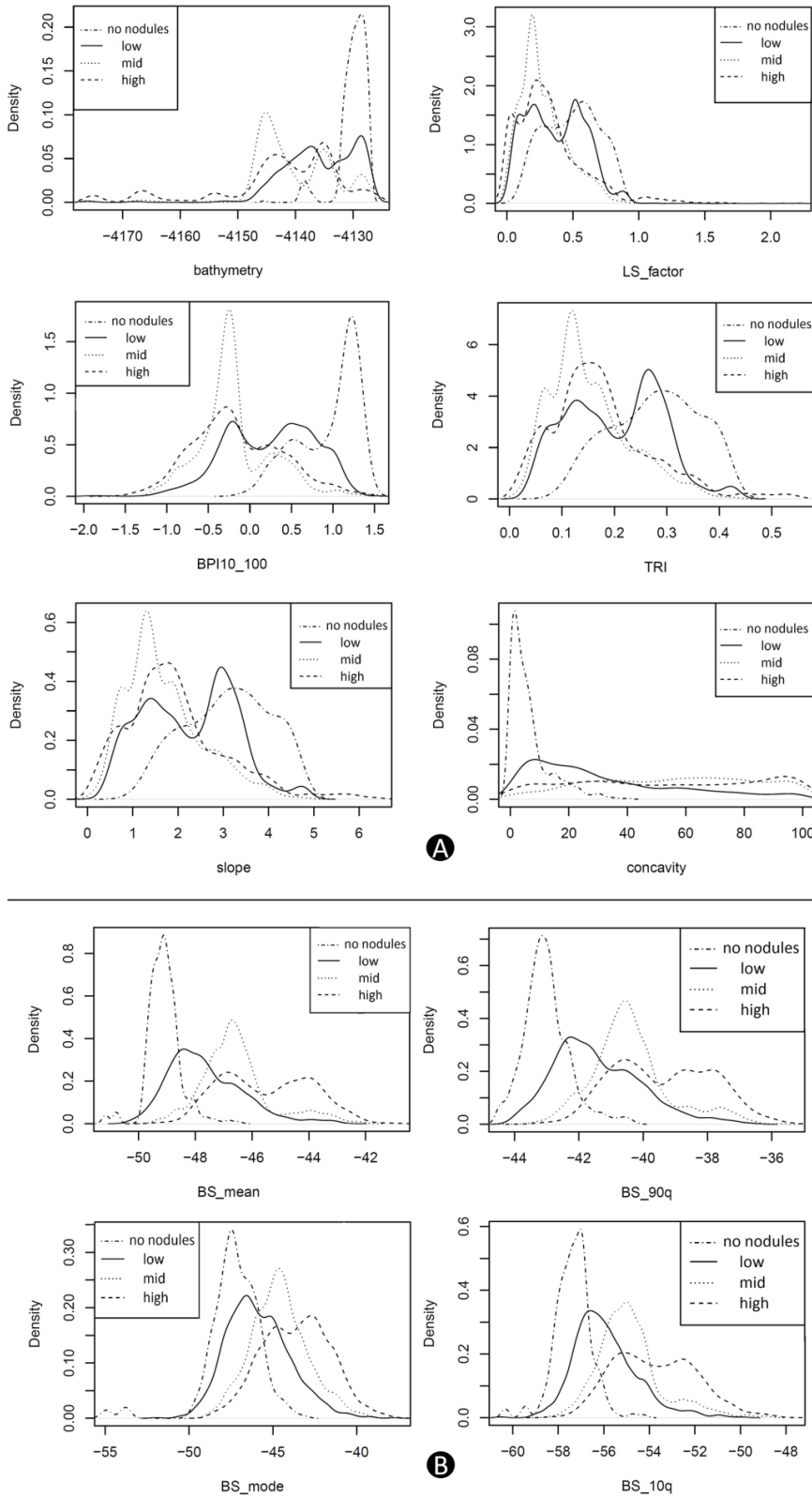


**Figure 5.3:** Data exploration results showing probability density functions for arbitrary classes of nodules per image (<10: no nodules, 10-184: low, 185-270: mid, >270: high) for A) bathymetry and derivatives and B) Backscatter and neighbourhood statistics.

### Error sources in quantitative Mn-nodule mapping

A few error sources need to be considered when performing seafloor classification and nodule density estimates with optical and acoustic data acquired during multiple AUV deployments.

1. *Noisy backscatter data*: Since the Bayesian approach uses the raw backscatter data, any final classification is susceptible to the effects of noise. Hence, beam incidence angles less than 20 degrees were discarded due to extreme nadir noise effects. The ISODATA classification was based on the backscatter mosaic and its statistics which are also affected mainly by nadir specular noise. It is thus strongly recommended that backscatter data are properly corrected for geometric and sensor-related effects during pre-processing and grids are also filtered/smoothed before the final classification.
2. *AUV navigation*: As exact underwater navigation in 4 km water depth is generally a difficult task, relative misalignments of data from different deployments are very common. Differences in absolute positioning between two deployments can easily amount to 100 m. Thus correlating image based nodule densities from one deployment with backscatter values from another dive might introduce correlation errors that also impact predictability. Although the large scale spatial pattern of classes is well defined, these misalignments can slightly alter the position of class boundaries causing disagreement with the nodule density measurements in places. A correct and verified re-navigation of all AUV-tracks is important for all subsequent analyses. This was done during this study, but slight misalignments remain.
3. *Nodule sediment blanketing*: The effect of Mn-nodules being blanketed by sediment needs to be considered as a source of error here as the individual nodule size and thus the seafloor coverage might be underestimated by automated annotation. Apart from natural sedimentation, the re-deposition of the plume cloud caused by ploughing during the first disturbance experiment (conducted in 1989), has covered certain parts of the nodule field which might lead to a lower nodule densities in those areas. This effect can artificially reduce the correlation between acoustic classes and Mn-nodule densities given that backscatter is not affected by sediment blanketing.

## APPENDIX OF CHAPTER 6

Table 6.1: Grain size analysis data and Bayes class (Alevizos et al., 2017) for sediment samples 1-18 shown in Fig.6.2A. Green cells indicate the five samples used for deriving the different angular responses in Fig.6.3.

sample	W% >6.3mm	W% 2-6.3mm	W% 2mm-500µm	W% <500µm	Shells/pebbles	d50 (<500 µm)	Mode (<500 µm)	D50 all (µm)	mode all (µm)	Bayes class
1	14.59	20.17	34.12	31.12	1/1	240.0	246.0	2600	1000	5
2	2.23	30.89	21.96	44.91	1/1	220.0	246.0	1800	4000	5
3	0.00	0.65	14.49	84.86	1/0	170.0	197.0	210	180	3
4	0.00	0.49	2.56	96.95	1/0	151.8	191.5	200	180	3
5	0.00	0.69	3.28	96.03	1/0	41.3	73.0	100	90	2
6	0.00	0.00	0.00	100.00	0/0	23.0	44.3	50	40	2
7	0.00	0.00	0.00	100.00	0/0	23.0	43.5	50	40	1
8	0.00	0.00	0.00	100.00	0/0	26.3	43.0	50	40	1
9	0.00	3.39	0.74	95.87	0/0	20.8	41.0	40	40	3
10	0.00	0.00	0.72	99.28	0/0	21.0	43.8	40	40	2
11	0.00	0.72	0.24	99.04	0/0	20.5	42.0	50	40	2
12	0.00	0.42	15.36	84.21	1/1	197.0	236.0	320	250	4
13	0.00	0.27	7.89	91.84	1/0	157.0	270.0	290	250	3
14	0.00	0.38	21.87	77.76	1/1	192.0	216.0	280	180	3
15	0.00	0.40	4.08	95.52	1/0	206.0	236.0	220	130	3
16	0.00	0.07	7.94	92.00	1/1	236.0	246.0	460	350	3
17	0.00	8.06	18.38	73.57	0/1	84.0	188.0	210	180	4
18	0.00	1.41	31.15	67.44	1/0	282.0	270.0	270	350	4

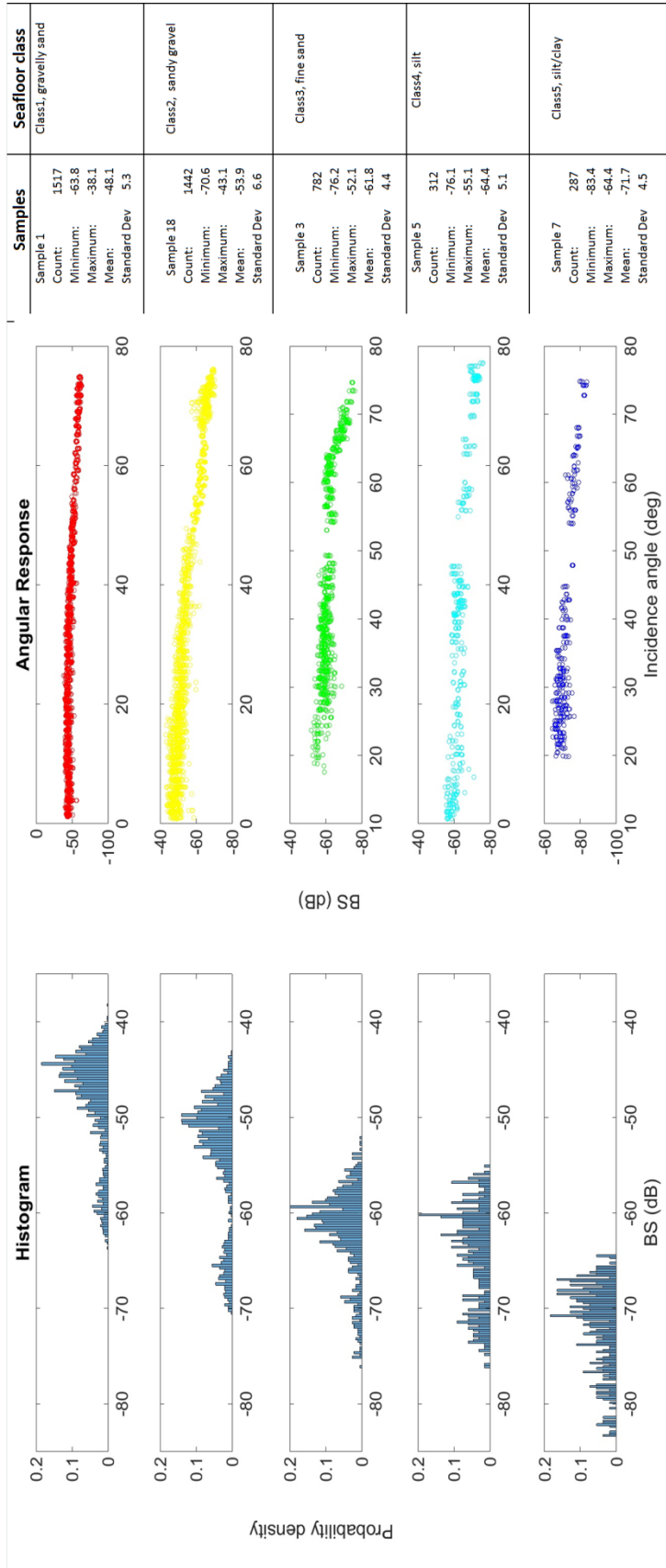


**Table 6.2:** Descriptive statistics of soundings (belonging to each acoustic class) which have been used for training of the RF classifier along with the histogram and angular response of each training sample.